Relationship between Microstructure, Durability and Performance of CEM X Composite Cements

Samuel Adu-Amankwah

Submitted in accordance with the requirements for the degree of
Doctor of Philosophy

The University of Leeds
School of Civil Engineering

October 2016

The candidate confirms that the work submitted is his/her own, except where work which has formed part of jointly-authored publications has been included. The contribution of the candidate and the other authors of this work has been explicitly indicated below. The candidate confirms that appropriate credit has been given within the thesis where reference has been made to the work of others.

The pore solution data included in Chapter 5 was supplied by Dr Barbara Lothenbach of EMPA and Dr Maciej Zajac of Heidelberg Technology Centre. Dr Zajac also provided the Mercury Intrusion Porosimetry data included in Chapters 5 and 6. The nano-indentation data reported in Chapter 6 was performed by Dr Jiri Nimecek of the Czech Technical University, Prague. The author, Samuel Adu-Amankwah was responsible for the remainder of the work and the interpretation of the data.

This copy has been supplied on the understanding that it is copyright material and that no quotation from the thesis may be published without proper acknowledgement.

The right of Samuel Adu-Amankwah to be identified as author of this work has been asserted by him in accordance with the Copyright, Designs and Patents Act 1988.

© 2016 The University of Leeds and Samuel Adu-Amankwah

Acknowledgements

This research project was funded by a scholarship from the School of Civil Engineering, University of Leeds for Samuel Adu-Amankwah. Heidelberg Technology Centre GmbH also provided additional funding and technical support for the project.

The research journey was long-winded but the support and guidance from my supervisor, Dr Leon Black kept me on course. Thank you, Leon! I would also like to express my heartfelt gratitude and appreciation to Maciej Zajac, Jan Skocek, Gerd Bolte and Christopher Stabler of Heidelberg Technology Centre for the technical support they provided to me throughout the project.

The useful discussions with colleague researchers and technicians in the materials group of the IRI are very much appreciated. Special thank you to Julia, Joe, Suma, Josh and Sola for the regular lab-chat about cement.

Thank you to my wife Vida and our son Evangel for their amazing support and understanding throughout my PhD. Finally, I wish to dedicate this thesis to my mum Yaa Akoto and to the memories of my late sisters Barbara and Hagar.

Abstract

Cement production is a major contributor to anthropogenic CO_2 emissions. Composite slag cement is one way of reducing the clinker factor, and hence emissions. Synergies between limestone and slag have been suggested to enhance the performance of such cement. The synergistic effect on mechanical performance has been ascribed to the carboalumination formation, which in turn prevents the conversion of ettringite to mono sulphoaluminate. Whilst the benefits of the synergy are documented, causation factors are not fully understood. In order to maximise the synergy, a clear understanding of the relationship between composition and the carboalumination-ettringite balance and how this impacts on performance is essential. Consequently, this study focused on the kinetics of reaction, microstructure and the implications on strength development and the freeze-thaw durability.

The QXRD/PONKCS method proposed elsewhere has been extended to monitor the residual slag contents in ternary blended systems. The slag phase was modelled from the x-ray diffraction pattern of a 100 % slag specimen. The model was then calibrated on a 50:50 mixture of slag and corundum using the internal standard method. The measurement accuracy was found to be ± 2 % following implementation of the calibrated slag phase on simplified slag-corundum mixes of varying proportions. In hydrated cement systems, however, the accuracy established from the comparison between the results from QXRD/PONKCS and SEM/IA analysis was ± 6 %. The investigated hydration stopping methods except freeze-drying had minimal impact on the results as long as the mass attenuation coefficient (MAC) was accurately quantified. For implementing the QXRD/PONKCS method, freshly ground non-hydration stopped sample preparation is recommended. This method presented the least challenge in calculating the MAC and also preserve the other hydrates particularly the AFt/AFm phases. However, if hydration stopping cannot be avoided, a double solvent exchange regime using isopropanol and diethyl ether is recommended. The residual slag content is overestimated from freeze-dried samples.

Multiple techniques including the QXRD/PONKCS method, SEM/IA, isothermal conduction calorimetry, chemical shrinkage and thermal analysis were subsequently used to investigate the kinetics of hydration. These revealed that

limestone accelerates slag and clinker hydration. Alite hydration is accelerated by the supplementary cementitious materials including slag and quartz. However, while belite hydration is retarded in the binary slag mix, this is not the case in limestone ternary blends. Calcium carbonate also reacts with additionally dissolved aluminates instead of the latter converting ettringite to mono sulphoaluminate. Therefore, the synergy between limestone and slag is not only due to preserved ettringite but the additional hydrates and pore structure modification. The carboaluminate content is higher in the presence of limestone but the home to mono carboaluminate balance shifts with the limestone content. The aluminates available for incorporation into other hydrates and in the pore solution are lowered by carboaluminate formation.

The pore structure and pore solution chemistry were analysed in order to further investigate the mechanisms for the accelerated dissolution of slag and the major clinker phases. The overall pore volumes as measured by MIP were similar in the slag containing mixes with or without limestone. Evaluation of the free water content at the end of experiment also indicated excess free water thus indicating that the pore structure and capillary pore water are not the limiting factors for slag hydration in the investigated mixes. The identified drivers behind the role of limestone in the synergy are the nucleation and dilution effects in the case of clinker, while for slag hydration pore solution effects are important. The incorporation of alumina into carboaluminates and C-S-H lowers the alumina in the pore solution and consequently promote slag dissolution.

The freeze-thaw resistance of the ternary blends at the investigated 0.5 water/binder ratio is low compared to the CEM I 42.5 R concrete. Decalcification through carbonation during conditioning and leaching during freeze-thaw is identified to be the dominant microstructural difference between degraded and non-degraded samples. A chemo-mechanical degradation mechanism, which is similar to the glue-spall mechanism, is hypothesised for surface scaling during freeze-thaw. By this, freeze-thaw damage in concrete is caused by decalcification and spalling of successive layers under induced stresses of ice growth.

Table of Contents

Acknowledgements ..... **iii**
Abstract ..... **iv**
Table of Contents ..... **vi**
List of Tables ..... **xi**
List of Figures ..... **xiii**
List of abbreviations ..... **xix**
1. Chapter 1 Introduction **1**
1.1 Background 1
1.2 Literature overview 2
1.3 Methodological gaps 3
1.4 Scope of research 6
1.5 Organisation of thesis 7
2. Chapter 2 Literature review **9**
2.1 Sustainability of Portland cement 10
2.2 Low CO_2 cements 11
2.3 Hydration of Portland cement clinker 13
2.3.1 Overview 13
2.3.2 Tricalcium Silicate (Ca_3SiO_5) polymorphism 16
2.3.3 C_3S hydration and microstructure 16
2.3.4 The mechanism of C_3S hydration 18
2.3.5 Dicalcium Silicate (Ca_2SiO_4) polymorphism 21
2.3.6 C_2S hydration and microstructure 22
2.3.7 The mechanism of C_2S hydration 23
2.3.8 Tricalcium aluminate polymorphs, $Ca_3Al_2O_6$ 25
2.3.9 C_3A hydration and microstructure 27
2.3.10 Mechanism of C_3A hydration 29
2.3.11 Tricalcium aluminium- ferrite, C_4AF 31
2.4 Hydration of composite cements 32
2.4.1 Hydration of composite clinker – slag cements 33
2.4.2 Impact of slag on clinker hydration 33

2.4.3 Hydration of slag 36
2.4.4 Microstructure of composite clinker- slag cements 38
2.4.5 Hydration of clinker – limestone composite cements 39
2.4.6 Hydration of clinker - Slag - limestone composite cements 41
2.5 Relationship between composition, microstructure and carbonation resistance of slag-limestone containing cements 43
2.5.1 Mechanism of carbonation 44
2.5.2 Factors affecting carbonation 45
2.5.3 Effect of carbonation on microstructure 47
2.6 Relationship between composition, microstructure and freeze-thaw resistance of slag containing cements 48
2.6.1 Evidence of freeze-thaw attack on concrete 48
2.6.2 Mechanisms of freeze-thaw attack on concrete 50
2.6.3 Factors affecting freeze-thaw resistance 57
2.7 The relationship between microstructure and freeze-thaw resistance 58
2.7.1 Clinker composition 58
2.7.2 Slag cements 59
2.7.3 Limestone 61
2.7.4 Effect of carbonation on freeze thaw resistance of slag-limestone containing cements 63
2.8 A review of techniques for characterization 64
2.8.1 Isothermal Conduction Calorimetry 65
2.8.2 Chemical shrinkage 68
2.8.3 Quantitative XRD and the PONKCS method 70
2.8.4 Scanning Electron Microscopy (SEM) 77
2.8.5 Porosity determination 79
2.9 A review of freeze-thaw testing methods 82
2.10 Summary of key literature and approach to address gaps 85
3. Chapter 3 Materials and methods 87
3.1 Materials 87
3.2 Formulation of mixes 91
3.3 Sample preparation 93
3.3.1 Hydration and microstructure characterisation 93
3.3.2 Samples for freeze-thaw testing 94
3.4 Hydration stopping 97

3.4.1 Freeze-drying 99
3.4.2 Solvent exchange 100
3.5 Techniques for hydration studies 101
3.5.1 Isothermal conduction calorimetry 101
3.5.2 Chemical shrinkage 103
3.6 Freeze-thaw monitoring 115
4. Chapter 4 Development and validation of the PONKCS Method 118
4.1 Mixes considered 118
4.2 Implementation of the method in synthetic mixes 119
4.3 Implementation of the method in anhydrous cements 122
4.4 Quantification of the slag content in composite cements 125
4.5 Accuracy of the PONKCS Method 139
4.6 Recommendations for implementing the PONKCS method 142
5. Chapter 5 Hydration and microstructure of limestone ternary blends 143
5.1 Mixes investigated 143
5.2 Overview of hydration 145
5.2.1 Influence of slag and limestone on the kinetics 152
5.2.2 Influence of limestone content and constituent fineness on the kinetics of hydration 156
5.2.3 Impact on the hydration of the major clinker phases 160
5.2.4 Impact on slag reaction 164
5.2.5 Impact on limestone reaction 169
5.2.6 Effect of slag and limestone on the hydrates formed 172
5.2.7 Effect of slag and limestone on the pore structure 180
5.2.8 Effect of limestone on the pore solution chemistry 184
5.2.9 Implications of the synergy on compressive strength evolution 186
5.2.10 Summary of hydration and microstructure studies 189
6. Chapter 6 Freeze-thaw resistance of limestone ternary blends .. 191
6.1 Samples investigated 191
6.2 Fresh properties of concrete 192
6.3 Compressive strength evolution 194
6.4 Effect of conditioning on the capillary suction 196
6.4.1 Early stage capillary suction 196
6.4.2 Long term capillary suction in concretes 198

6.5 Freeze-thaw performance of composite cements 199
6.5.1 Methodological remarks 199
6.5.2 Effect of composition on the freeze-thaw performance 202
6.6 Microstructure before freeze-thaw 210
6.6.1 Effect of carbonation 210
6.6.2 Effect of capillary suction on the microstructure 213
6.7 Microstructural response to freeze-thaw of composite slag cements 217
6.7.1 Freeze-thaw of cement paste samples 218
6.7.2 Effect of freeze-thaw on hydrated phase assemblages 219
6.8 Mechanism of freeze-thaw damage of composite cements in deionized water 224
6.9 Correlation between microstructure and freeze-thaw resistance of composite cements 231
7. Chapter 7 Discussions, Conclusions and recommendations for further studies 232
7.1 The PONKCS Phase in the Rietveld refinement 232
7.2 Effect of limestone on hydration in ternary blends 233
7.3 Effect of limestone on the microstructure of in ternary blends ...234
7.3.1 Hydrated phase assemblages 234
7.3.2 Pore structure 235
7.4 Mechanisms behind the synergy in limestone ternary blends 235
7.4.1 Nucleation effect 235
7.4.2 Dilution effect 237
7.4.3 Pore fluid composition-based mechanisms 239
7.5 Relationship between hydration, microstructure and compressive strength 240
7.6 Relationship between hydration, microstructure and freeze-thaw resistance in deionized water 242
7.6.1 Microstructure on freeze-thaw 242
7.6.2 The mechanism of freeze-thaw 244
7.7 Conclusions 244
7.8 Recommendations for further studies 247
8. List of References 249
1. Appendices 275
A.1.1 Data extraction from Chemical shrinkage images 275

A.1.2 Scoping results 276
A.1.3 Rietveld Refinement/PONKCS 278
A.1.4 Backscattered SEM images and thresholding for quantitative analysis 284
A.1.5 Pore solution composition during hydration 295
A.1.6 Phase assemblage changes due to freeze-thaw 296

List of Tables

Table 2-1 Stages of cement hydration [88] **15**

Table 2-2 Solubility and densities of calcium carbonate polymorphs and Portlandite [238] **47**

Table 2-3 Standardised methods for assessing the internal structural damage during freeze-thaw **84**

Table 3-1 List of materials and Blaine and their fineness for composite cements **87**

Table 3-2 Oxide composition of raw materials (%wt.) **88**

Table 3-3 Mineralogical compositions of the CEM I 42.5 R [C1] and CEM I 52.5 R [C2] (%wt.) **88**

Table 3-4 Mineralogical compositions of supplementary materials (%wt.) **88**

Table 3-5 Properties of aggregates **91**

Table 3-6 Proportioning and nomenclature of cements for preliminary study (% wt.) **92**

Table 3-7 Instrument parameters which were fixed for calibration and refinement **107**

Table 3-8 Structures for Rietveld refinement from ICSDS **108**

Table 4-1 Composite cements for assessing the robustness of the calibrated slag phase **119**

Table 5-1 Mixes for investigating hydration and microstructure of limestone ternary blends **144**

Table 5-2 Experimental matrix for the samples under investigation **144**

Table 5-3 Effect of slag and limestone interaction on the composition of the C-S-H and the slag rim (± 0.02) **179**

Table 6-1 Composite cements investigated for freeze-thaw resistance **192**

Table 6-2 Mix design to yield a cubic metre of concrete **192**

Table 6-3 Fresh properties of composite cements compared to CEM I **193**

Table 6-4 ‘Apparent’ sorptivity of concretes samples **197**

Table 6-5 Water absorbed by the concrete samples compared to initial sorptivity and porosity of the paste **199**

Table 6-6 Equivalent lime from portlandite and calcite due to carbonation compared to complementary non-exposed samples **213**

Table 6-7 Effect of conditioning and pre-freeze thaw capillary suction on the bound water contents. **216**

Table 6-8 Effect of freeze-thaw on the Young’s modulus (GPa) of the C-S-H in CEM I and composite cements **230**

Table 7-1 The unbound water contents (%) after 180d **237**

Table 1-1 Concentrations in the pore solution (mM) with hydration time**... 295**

List of Figures

Figure 2-1 CO_2 emissions in the clinker production chain; arrow thickness is indicative of CO_2 concentration [57] **10**

Figure 2-2 Compositional map of cementitious materials (A) and probable products (B) [10] **13**

Figure 2-3 Illustration of the stages of hydration **15**

Figure 2-4 C_3S polymorphs as a function of temperature [93] **16**

Figure 2-5 Influence of polymorphism on the kinetics of C_3S hydration [99] **18**

Figure 2-6 C_3S-hydrate interfacial region **20**

Figure 2-7 Characteristic reflections and microstructure of (a) cubic C_3A and (b) SO_3 stabilised orthorhombic C_3A [150]. **26**

Figure 2-8 Effect of slag and filler on the rate of reaction of composite cements [143] **35**

Figure 2-9 Isothermal calorimetry of PC-slag-LL ternary blends [225] **43**

Figure 2-10 Secondary electron image of a tobermorite 11-A before carbonation [247] **47**

Figure 2-11 Secondary electron image of a tobermorite 11-A after carbonation 30 days at 10%CO_2 and 75%RH [247] **47**

Figure 2-12 BSE of non-carbonated BFS cement showing magnesium rich hydrated rim [250] **48**

Figure 2-13 SEI of BFS cement carbonated at 3%CO_2; insert is the stretched interfacial zone [250] **48**

Figure 2-14 Illustration of the glue-spall mechanism of freeze-thaw damage as a function of the thickness of the ice layer [261] **55**

Figure 2-15 Relationship between degree of hydration and internal damage [25] **60**

Figure 2-16 Illustrative heat of reaction and cumulative heat of CEM I and composite cement **67**

Figure 2-17 Backscattered SEM images with corresponding grey-level histogram [325] **77**

Figure 3-1 Particle size distribution of the investigated clinkers as determined by laser granulometry **89**

Figure 3-2 Particle size distribution of the investigated slags as determined by laser granulometry **89**

Figure 3-3 Particle size distribution of constituent materials **90**

Figure 3-4 Particle size distribution of aggregates **90**

Figure 3-5 Arrangement of lateral PTFE and splitting of samples for freeze-thaw test **95**

Figure 3-6 Programme for characterization of paste samples during freeze-thaw **96**

Figure 3-7 Illustrative grid and indent for evaluating changes in the mechanical properties of the C-S-H. **97**

Figure 3-8 Setup for the acquisition of heat of reaction data **103**

Figure 3-9 Accessories and setup for recording the chemical shrinkage of cements **104**

Figure 3-10 Illustration of filler effects and slag hydration on chemical shrinkage **105**

Figure 3-11 X-ray diffraction pattern of 100 % GGBS and the modelled PONKCS phase. **107**

Figure 3-12 The calibrated slag phase in hydrated cement **109**

Figure 3-13 Illustration of porosity and area of residual slag extraction. ... **111**

Figure 3-14 TG and DTA curves and extraction of CH **113**

Figure 3-15 Setup for freeze-thaw testing **116**

Figure 4-1 Plots of the diffraction patterns of binary slag-corundum mixes showing the variation of the halo intensity on the slag content. **120**

Figure 4-2 Refined phases in a binary slag and corundum mix. **121**

Figure 4-3 Relationship between actual and measured slag content **122**

Figure 4-4 Effect of cement composition and fineness on the XRD background and impact on quantification. **123**

Figure 4-5 Refinement of 1:1 binary slag – C-S-H mix **126**

Figure 4-6 DTG of CEM I 52.5 R as a function of hydration stopping after 1 and 28 days **128**

Figure 4-7 DTG of CEM I 52.5 R + slag + 10% limestone as a function of hydration stopping after 1 and 28 days **129**

Figure 4-8 Effect of dehydration methods on the AFt/AFm and portlandite content in CEM I (C2) **129**

Figure 4-9 Effect of dehydration methods on the AFt/AFm and portlandite content in ternary slag/limestone cement (C2S1-10L) **130**

Figure 4-10 Effect of dehydration method on the contents of ettringite and portlandite from QXRD of C2S1-10L **130**

Figure 4-11 Effect of dehydration method on the XRD diffractogram of composite slag cements after 1 and 28 days. **132**

Figure 4-12 Mass absorption co-efficient for neat and composite cements pastes as a function of dehydration method and hydration time **134**

Figure 4-13 Scale factor of slag in mixes C2S1 and C2S1-10L after 1 day as a function of dehydration technique. **136**

Figure 4-14 The degree of hydration of clinker as a function of hydration stopping technique. **137**

Figure 4-15 The degree of hydration of slag as a function of hydration stopping technique **139**

Figure 4-16 Comparison between the degree of hydration of slag by PONKCS method and SEM/IA **141**

Figure 5-1 Evolution of chemical shrinkage in limestone ternary blends, normalised to the CEM I content. **145**

Figure 5-2 Effect of slag, limestone and CEM I fineness on the chemical shrinkage of ternary blends. **147**

Figure 5-3 The influence of slag, limestone and fineness on the evolution of portlandite, by TGA **148**

Figure 5-4 The influence of slag, limestone and fineness on the bound water contents of ternary blends, by TGA **152**

Figure 5-5 The influence of slag and inert filler on the rate of reaction **153**

Figure 5-6 The influence of limestone and added sulphate on the rate of reaction of ternary blended cements. **155**

Figure 5-7 The influence of limestone content, slag and CEM I fineness on the rate of reaction of ternary blended cements. **157**

Figure 5-8 Influence of slag, limestone and inert filler on the hydration of the major clinker phase, as determined by QXRD **161**

Figure 5-9 Influence of slag, limestone and constituent fineness on the degree of hydration of clinker. **164**

Figure 5-10 Chemical shrinkage due to slag reaction in composite slag cements. **165**

Figure 5-11 Effect of limestone and inert filler on slag hydration of composite cements. **167**

Figure 5-12 Comparison between DoH as quantified by QXRD/PONKCS BSEM/IA and chemical shrinkage. **168**

Figure 5-13 Consumption of limestone in the ternary blends **169**

Figure 5-14 Degree of reaction of limestone in composite cements compared to the neat cement **170**

Figure 5-15 DTG of paste samples hydrated for 1 and 180 days. **173**

Figure 5-16 Effect of slag and limestone interaction on the sulphate and carbonate-bearing phase assemblages after 1, 28 and 180 days hydration. **174**

Figure 5-17 Effect of limestone content, slag and clinker fineness on the evolution of ettringite and carboaluminate assemblages. **176**

Figure 5-18 Effect of slag and limestone interaction on the C-S-H composition as analysed by SEM/EDS. **178**

Figure 5-19 Representative SEM image for compositional analysis of hydrates **179**

Figure 5-20 Microstructures of composite slag-limestone cements after 180d **180**

Figure 5-21 Effect of slag and limestone interaction on the pore structure of composite cement as determined by MIP after 1, 7, 28 and 180 days.**182**

Figure 5-22 Effect of the slag-limestone interaction on porosity (BSEM/IA)**184**

Figure 5-23 Effect of limestone on the pore solution chemistry during hydration. **185**

Figure 5-24 Effect of limestone on the compressive strength evolution between 1 and 180d days. **188**

Figure 5-25 Relationship between compressive strength, porosity and degree of hydration **189**

Figure 6-1 Compressive strength of concrete before and after exposure at 20 °C and 65 % RH for 21 days **195**

Figure 6-2 Initial water absorption before saturation for freeze-thaw testing**197**

Figure 6-3 Comparison between the internal structural damage measured on CEN TR/15177 (Ref) and an extended freezing rate (Test) freeze-thaw profiles **200**

Figure 6-4 Comparison between the scaled matter measured on CEN TR/15177 (Ref) and extended freezing rate (Test) freeze-thaw profiles**201**

Figure 6-5 Effect of cement composition on the internal structural damage in concretes. **203**

Figure 6-6 Effect of cement composition on the scaling resistance of concretes. **204**

Figure 6-7 Water uptake during freeze-thaw as a function of cement composition. **205**

Figure 6-8 Comparison of the test surfaces after 56 freeze-thaw cycles showing the effect of slag. **206**

Figure 6-9 Effect of limestone content on the scaling resistance of concrete after 56 freeze-thaw cycles. **207**

Figure 6-10 Effect of CEM I and slag fineness on the scaling resistance of concrete after 56 freeze-thaw cycles. **209**

Figure 6-11 Effect of conditioning on C-S-H/AFt, portlandite and calcite contents compared to samples cured under sealed conditions for 7 and 28 days **211**

Figure 6-12 Effect of the 21 d conditioning and saturation on the portlandite content compared to the CH content in non-exposed samples cured for 7 and 28 days. **212**

Figure 6-13 Pore distribution of hydrated cements before drying at 65 %RH and 20 ◦C. **214**

Figure 6-14 Effect of saturation on the AFt/AFm contents relative to portlandite loss.....216

Figure 6-15 Effect of cement composition on freeze-thaw: Cement pastes observations. 218

Figure 6-16 Effect of freeze-thaw on the microstructure of surface and core of cements in the neat cement, C 221

Figure 6-17 Effect of freeze-thaw on the microstructure of surface and core of cements in the binary mix, CS 222

Figure 6-18 Effect of freeze-thaw on the microstructure of surface and core of cements in the binary mix, CS-2L. 222

Figure 6-19 Susceptibility of the investigated cements to decalcification of portlandite 225

Figure 6-20 Leaching of calcium ions during freeze-thaw.....226

Figure 6-21 Effect of freeze-thaw on the microstructure of composite cements 227

Figure 6-22 C-S-H composition of mixes C (left) and CS-2L (right) after 0 and 25 FT. 228

Figure 6-23 Effect of freeze-thaw on the C-S-H 229

Figure 6-24 Illustrative frequency density plots of the effect of freeze-thaw on the Young's modulus of the C-S-H for mixes C and CS-2L 230

Figure 7-1 Effect of slag and limestone on the pore volume as determined by MIP 238

Figure 7-2 The relationship between Al concentration in the pore solution and chemical shrinkage and degree of hydration of slag. 240

Figure A-1 Steps for automatic extraction of shrinkage data from images.275

Figure A-2 Cumulative heat, chemical shrinkage and strength development in CEM I 42.5R composite cements.....276

Figure A-3 Cumulative heat, chemical shrinkage and strength development in CEM I 42.5R ternary slag blends as a function of fineness and limestone content.....277

Figure A-4 Observed pattern for mix C2S1-10L hydrated for 1 day. 278

Figure A-5 Refined pattern for mix C2S1 279

Figure A-6 Refined pattern for mix C1S1-10L.....280

Figure A-7 Refined pattern for mix C2S1-10L.....281

Figure A-8 Refined pattern for mix C2S1-20L.....282

Figure A-9 Refined pattern for mix C2S2-20L.....283

Figure A-10 Typical B-SEM images and thresholding for mixes C2 and C2Q1 285

Figure A-11 Typical B-SEM images and thresholding for mix C2S1.....287

Figure A-12 Typical B-SEM images and thresholding for mix C1S1- 10L . **289**

Figure A-13 Typical B-SEM images and thresholding for mix C2S1-10L .. **290**

Figure A-14 Typical B-SEM images and thresholding for mix C2S1-20L .. **292**

Figure A-15 Typical B-SEM images and thresholding for mix C2S2-20L .. **294**

Figure A-16 Comparison between the surface and the core of mix C after 11 freeze-thaw cycles **296**

Figure A-17 Comparison between the surface and the core of mix C2S1 after 11 freeze-thaw cycles **296**

Figure A-18 Comparison between the surface and the core of mix C2S1-10L after 11 freeze-thaw cycles **297**

Figure A-19 Comparison between the surface and the core of mix C2S1-20L after 11 freeze-thaw cycles **297**

List of abbreviations

Cement Nomenclature:

A = Al_2O_3	K = K_2O
C = CaO	M = MgO
C = CO_3	N = Na_2O
F = Fe_2O3	S = SiO_2
H = H_2O	s = SO_3

Clinker Phases and Hydrated assemblages

Alite		$3CaO.SiO_2$
Belite		$2CaO.SiO_2$
Tricalcium Aluminate		$3CaO.Al_2O_3$
Tetracalcium alumino- ferrite		$4CaO.Al_2O_3.Fe_2O_3$
Gypsum		$CaSO_4.2H_2O$
Portlandite/ CH		$Ca(OH)_2$
Calcium Silicate Hydrate		$CaO\text{-}SiO_2\text{-}H_2O$
Calcium Aluminate Silicate Hydrate		$CaO\text{-}Al_2O_3\text{-}SiO_2\text{-}H_2O$
Ettringite / AFt		$3CaO.Al_2O_3.3CaSO_4.32H_2O$
Monosulfoaluminate / Ms	AFm	$3CaO.Al_2O_3.CaSO_4.12H_2O$
Hemicarboaluminate / Hc	AFm	$3CaO.Al_2O_3.0.5Ca(OH)_2.0.5CaCO_3.11.5H_2O$
Monocarboaluminate / Mc	AFm	$3CaO.Al_2O_3.CaCO_3.11H_2O$
Stratlingite		$2CaO.Al_2O_3.SiO_2.8H_2O$
Hydrotalcite / Ht[1]		$Mg_6Al_2(OH)_{16}.CO_3.{}_4H_2O$

[1] This denotes the pure hydrotalcite phase. However, typical composition in hydrated cements, has Mg/Al closer to 2.

Techniques

BSEM	Back Scattered Electron Microscopy
DTG	Differential Thermogravimetry
EDS	Energy Dispersive X-Ray Spectroscopy
FT	Freeze-thaw
ICC	Isothermal Conduction Calorimetry
IC	Ion Chromatography
ICP-OES	Inductively Coupled Plasma Optical Emission Spectroscopy
MIP	Mercury Intrusion Porosimetry
PONKCS	Partial or No Known Crystal Structure
SEM/IA	Scanning Electron Microscopy Image Analysis
STA	Simultaneous Thermal Analysis
TGA	Thermogravimetric Analysis
w/s	Water to solid ratio
w/c	Water to cement ratio

Chapter 1
Introduction

1.1 Background

One of the major challenges confronting the cement industry is satisfying the increasing demand for cement-based infrastructure in the midst of a global clamour for the industry to reduce its CO_2 footprint. Significant strides towards plant efficiency coupled with increasing utilisation of alternative fuels have been made by the cement industry. However, ~ 60% of the 0.8-1.0 tonnes of CO_2 emitted per tonne of clinker produced are inherently associated with calcination of limestone into quicklime [1]. Clinker replacement is a popular and feasible alternative approach for a sustainable cement future.

Slag and pulverised fuel ashes have found extensive industrial applications, frequently for durability purposes. However, availability of slag and useful fly ash as cement supplements are limited [2, 3]. Utilisation of alternative additives is necessary. These should however not compromise the mechanical and durability performance. It is in this regard that, finely ground limestone has become a popular ingredient. Up to 35% of finely ground limestone, is permitted in binary OPC-limestone cements but durability is worsened beyond 15% limestone contents [4-6].

Potential routes to maximise the uncalcined limestone content in cement must be explored. To achieve this, the impact of composition on hydration, phase assemblages, microstructural evolution and engineering performance must be understood in order to optimise the composition of such systems.

1.2 Literature overview

Ternary blended Portland cement (PC)–slag and limestone has attracted considerable research attention recently [7-9]. The hydration mechanisms and performance of PC-slag and PC-limestone binary cements are well understood [6, 10-12]. Slag is latently hydraulic while limestone is a non-pozzolanic SCM, yet they both influence clinker hydration physically and chemically. Physically, they provide nucleation sites for C_3S and C_3A hydration as well as enhanced packing density [4, 13]. Regarding hydration products, coexistence of ettringite and carboaluminates have been reported in limestone-containing Portland cement-slag composite cements [14, 15]. In such systems, hemi-carboaluminates form initially but gradually converts into mono-carboaluminate as additional limestone is consumed. Incorporation of carbonates from limestone into cement hydrates is enhanced in high C_3A containing cements [16]. Synergies have also been reported between limestone and aluminate containing pozzolans or latently hydraulic SCMs [9, 17, 18]. Pertinent questions remain as to what is the origin of the synergy and what are the factors that drive this?

The interaction between limestone and aluminates is favourable for strength development [7] and durability [19-21]. Despite the advantageous effect of limestone content (though up to 15%) on hydration and mechanical properties, contradictory results have been reported in the literature regarding freeze-thaw resistance [22, 23]. Scaling resistance of non-air entrained concretes produced with binary cements of slag or limestone with Portland cement is lower compared to CEM I cements [24, 25]. This is often attributed to the slow reactivity of slag or the dilution effect of limestone, and hence susceptibility to carbonation. In

composite Portland cement-slag-limestone cements, compressive strength, freeze-thaw resistance and carbonation have also been reported to correlate inversely with the limestone content [26]. Comparison of mixes with similar compressive strengths rather than *w/c* ratios is suggested to present a fairer basis for comparing the durability of concretes formulated from different types of cement [27]. It is therefore anticipated that, at equivalent strengths, concretes produced from different cement compositions should exhibit similar freeze-thaw resistance. It is in this respect that relating freeze-thaw resistance to microstructure for composite cements becomes vital.

1.3 Methodological gaps

Quantification of the reactivity of SCMs is important for maximising their use in composite cements. Selective dissolution, SEM/IA and inferences from isothermal calorimetry, chemical shrinkage and the bound water content have been explored in the literature [12, 28-30] to follow the reaction of SCMs. However, most of the above methods to quantify the reactivity of GGBS are inaccurate [12, 30] or labour intensive [28, 29, 31].

The PONKCS method [32, 33] has the capability to monitor different amorphous phase contents in cementitious materials. The technique has been employed to study synthetic systems of different amorphous SCMs and simplified hydrated cements [33]. However, hydrated ternary cements present a more complex system particularly due to multiple amorphous constituents. Additionally, water in the sample due to the requirement to preserve poorly crystalline hydrates further complicates the challenge. The robustness of the method to simultaneously

quantify hydrated phase assemblages and the residual slag content needs to be assessed particularly for different dehydration methods. Furthermore, comparison of the results from PONKCS with other independent methods is also lacking. These need resolving for widespread adoption of the technique for studying composite cements.

Freeze-thaw damage in concretes may manifest as internal structural damage or scaling of the surface matter. Some authors suggest similar mechanisms control scaling and internal damage [34-36]. The suggested mechanisms include hydraulic and osmotic pressure, microscopic ice lens, crystallisation pressure and glue-spall. Some of these mechanisms are inter-related and consider different factors which may interact during the freezing of water in the capillary pores or on the surface of the concrete. For example, the hydraulic pressure theory [37] attributes freeze-thaw degradation to the expansion associated with ice formation in the capillary pores. The osmotic pressure [38] and crystallisation pressure [35, 39, 40] consider the effect of ionic species in the solution and attribute freeze-thaw damage to either the drawing of water from adjacent pores by osmosis or pressure acting on the pore wall.

Despite differences in how freeze-thaw may manifest and the potential mechanisms, there is a consensus that adequately air-entrained concretes have better freeze-thaw resistance [38, 41, 42]. However, a recent review [36] noted that air entrainment is only effective for improving the resistance scaling in the presence of de-icing salts. This implies, the microstructural phenomenon dictating the resistance to internal structural damage is dependent on cement composition

rather than the applied air entraining agent. However, this line of enquiry has not been investigated previously.

Some of the suggested freeze-thaw mechanisms also consider scaling and internal damage as independent manifestations of freeze-thaw and hence controlled by different mechanisms. That is, scaling occurs following freeze-thaw in the presence of de-icing agents and internal damage without de-icing agents [34, 35]. Consequently, unrelated mechanisms such as glue spalling for scaling and crystallisation pressure for internal damage have been suggested [35, 36]. The simultaneous observation of internal damage and scaling even without de-icing salts is indicative of the lack of insights into the controlling mechanisms. A microstructural-based approach, therefore, adopted to investigate the factors which control the freeze-thaw resistance of composite cement concretes.

Influencing parameters such as the degree of saturation of concrete, the rate of freezing and thawing, ice formation and growth in concrete among others have been rigorously evaluated elsewhere [43]. However, the approach has predominantly been a macro-scale investigation. The primary assessment technique for internal structural damage is the dynamic elastic modulus [22, 44]. The technique which theoretically identifies microstructural changes in concrete is flawed in two ways: First is the assumption that the mass and geometry of the concrete specimen under investigation remains unchanged over the duration of the test [45]. This assumption does not always hold due to the potential alterations in mass and dimensions over the duration of the freeze-thaw testing. Despite knowledge of cement hydration evolving with time, neither ultrasonic pulse velocity nor length measurements are uniquely capable of decoupling progressive

hydration from microstructural changes due to aggressive exposures. Secondly, cement hydration is exothermic and may induce micro-cracks in the mortar phase of concrete. These may falsify the extent of damage due to the progressing ice growth.

The microstructural approach to investigating hydration and durability has gained significant research attention in the past two decades [46]. Despite the informative nature of microstructural-based investigations and their suitability for freeze-thaw resistance investigation [47], methods employed in the literature are not devoid of shortfalls. From the literature reviewed so far, the only attempt to relate microstructure to the macro-scale evidence of freeze-thaw degradation is an inference of pore structure based on mercury intrusion porosimetry (MIP) data [48]. Adoption of complementary techniques to understand the deterioration mechanism is thus essential for extracting useful information for cement mix design as well as predicting the service performance.

1.4 Scope of research

The aim of the project was to investigate the impact of limestone on the hydration, microstructure, compressive strength development and freeze-thaw resistance of composite slag cements.

Pursuant to the above aim, a scoping study based on compressive strength testing of 22 mixes was carried out. The objective was to identify the relationship between the cement composition and compressive strength. Based on preliminary results, six mixes were identified for detailed characterisation of hydration, microstructure evolution and durability with a focus on freeze-thaw resistance. This allowed the

effect of limestone content, plus the fineness of slag and clinker to be evaluated. Consequently, the following objectives were pursued:

1. To establish the effect of limestone on the kinetics of clinker and slag hydration in ternary slag cements.
2. To identify the drivers for the synergy between limestone and slag in ternary cements.
3. To analyse the relationships between hydration, microstructure and compressive strength.
4. To identify the relationship between microstructure and freeze-thaw resistance of limestone ternary blends.

In pursuit of objective 1, different methodologies for determining the hydration of slag were analysed. One such method which has been proposed recently is the PONKCS method [32, 33, 49]. The method was further extended to evaluate the residual slag content in ternary slag cements.

1.5 Organisation of thesis

This thesis is organised into 7 chapters

Chapter 2 presents a review of the relevant and up to date literature on developments towards a sustainable cement industry; hydration and microstructure of clinker phase assemblages and their polymorphs; hydration and microstructure of ternary blended slag-limestone cements; mechanisms and freeze-thaw performance of composite cements. Finally, a methodological review for hydration and microstructure as well as freeze-thaw testing is provided.

Chapter 3 describes in detail the materials and methods used in this project.

Chapter 4 develops and validates the PONKCS method for monitoring slag hydration. The impact of different dehydration methods on the quantification of the evolved phase assemblages and importantly the residual clinker and slag content are examined.

Chapter 5 presents the results and discussions on the hydration and microstructure of limestone ternary blends.

Chapter 6 presents the results from freeze-thaw testing. The results are discussed in terms of the microstructure and phase assemblage modifications during freeze-thaw

Chapter 7 draw relationships between the different results, then summarise the main conclusions. The chapter also makes recommendations for future studies.

Chapter 2
Literature review

Specification of concretes produced with composite cements has become a common practice. This presents technical, environmental and economic benefits [50]. Cements containing supplementary cementitious materials are however associated with slow hydration rate [51-53] and develop microstructures which differ from conventional Portland cement [17, 31, 54, 55]. The degree of reaction and microstructures of hardened concretes are particularly important with respect to resistance to carbonation and freeze-thaw durability.

This review focuses on the relevant literature on the kinetics and mechanisms of hydration, microstructure evolution and freeze-thaw resistance of ternary slag-limestone composite cements. The effects of the physical and chemical composition of materials on the hydrated phase assemblages, microstructure and implications for durability are also reviewed.

Kinetics and mechanisms of hydration, microstructure and freeze-thaw plus the methodologies for assessing these constitute the scope of the review. The chapter is grouped into the following sub-topics:

1. Sustainability of Portland cement and alternatives
2. Kinetics of hydration of clinker (C_3S, C_2S, C_3A and C_4AF), slag and limestone and implications on and microstructure
3. Effect of slag and limestone on freeze-thaw resistance of concrete
4. A review of characterization techniques and methodologies for freeze-thaw testing

2.1 Sustainability of Portland cement

Globally, the usage of concrete is only second to water, with a projected upsurge in demand especially in developing countries [56]. Portland cement clinker (PCC), produced from calcining limestone and clay, is the most common binding component in concrete. During manufacturing, limestone is calcined into quicklime and at ~1450°C, fuses with silica and aluminates to give the different clinker phases. The production chain illustrated in Figure 2-1 shows the CO_2 emissions at different stages of cement clinker production.

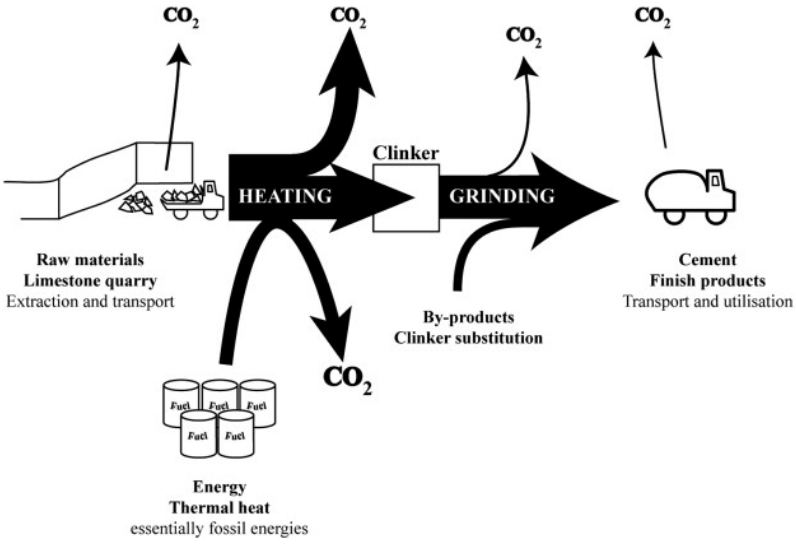

Figure 2-1 CO_2 emissions in the clinker production chain; arrow thickness is indicative of CO_2 concentration [57]

Per unit weight produced, concrete may be a comparatively lower CO_2 emitter than other construction materials such as steel and timber [58]. However, the aggregated effect of the over 3.4 billion tonnes of clinker produced globally per annum is substantial; accounting for approximately 5% of human-related CO_2 emissions.

Habert *et al.* [57] reviewed the production chain and reported 0.53t of CO_2 from decarbonisation of limestone; 0.39t from fuels while grinding contributed 0.1t CO_2 per tonne of clinker produced. Consequently, the production chemistry and the heat requirements constitute the main areas to focus in order to reduce the carbon footprint of cement significantly. Moreover, the decarbonisation related CO_2 have been shown to be independent of the kiln type and efficiency [50]. Therefore, realistic emission targets with conventional Portland cement clinker is limited to 35% of current levels since only heating efficiency can be improved unless CO_2 capturing technologies are implemented at industrial scale.

Gartner [50] reported 1800MJ/t as the theoretical minimum energy required to produce a tonne of C_3S from limestone and clay. However, none of the production technologies at present [57] operates at this efficiency. As a matter of fact, despite improvements in cement kiln technology [1, 50, 57], the respective emissions from decomposition reactions and fuels seem to have plateaued over the last 30 years [1, 59]. Consequently, reducing the clinker content of cements through SCMs, engineered concrete mix designs [60, 61], or cements with different production chemistry to Portland cement clinker [62] among others present viable alternatives to minimising the environmental impact of the cement industry.

2.2 Low CO_2 cements

Geopolymer, magnesia, sulfoaluminate and composite cements are suggested alternatives to clinker based cements [63-65]. The merits and demerits of these have been reviewed elsewhere [66]. However, these are yet to be standardisation as well as long-term durability concerns will stifle commercialization of these in the

short term. Consequently, cements with compositional matrices and hydrated phase assemblages similar to those in Portland cement [10, 62, 67] are appealing to manufacturers and users alike.

Notwithstanding the drawbacks, non-conventional cements offer some environmental and technical advantages [66, 68-70]. For example, the calcium contents in calcium aluminate (CAC) and calcium sulpho-aluminate (CSA) cements are considerably lower than that in clinker [62]. This implies less limestone is calcined hence lower CO_2 emitted in the process. However, the calcination temperature for CAC is about 1500 ~ 1600°C and five times more expensive than PCC [70-72]. Calcium sulpho-aluminate cements, on the other hand, are produced at slightly lower the calcination temperature 1200 ~ 1350°C [73]. However, a high fraction of water is incorporated into ettringite, the main reaction product and hence lower overall degree of hydration at longer hydration times [73]. This has implications for the carbonation resistance of the resulting microstructure [74]. Gypsum is formed upon carbonation but this has the tendency to form expansive ettringite upon re-saturation (i.e. delayed ettringite formation). A further alternative to PC is geopolymer or alkali-activated binders [63, 75]. These are synthesised from industrial wastes such as fly ash or slag with an activator [76-79] and hence has no requirement for calcination. Consequently, the savings in CO_2 emissions compared to PCC could be up to 64% [80]. However, classification of the feedstock as wastes and hence negligible CO_2 penalty means the low greenhouse emissions may be fictional. Therefore, despite the attractions of geopolymer, their dominance over PCC as the binding phase in concrete may be a mirage in the foreseeable future.

Blended cements with higher clinker replacement levels is a realistic opportunity to reduce the clinker factor. In fact, such cements have been shown to present the least global warming potential [81]. A guide to the development of such cements and the predicted products of reaction have also been suggested elsewhere [10] and reproduced in Figure 2-2. Compared to PC, commonly used SCMs (slag and PFA) lead to a lowering of the calcium content but increases the alumina and silicate contents. This leads to a lower Ca/Si ratio while Al intake into the C-S-H is increased [82]. Consequently, the alumina available to form expansive ettringite is reduced and thus improve the resistance to aggressive environments such as sulphates.

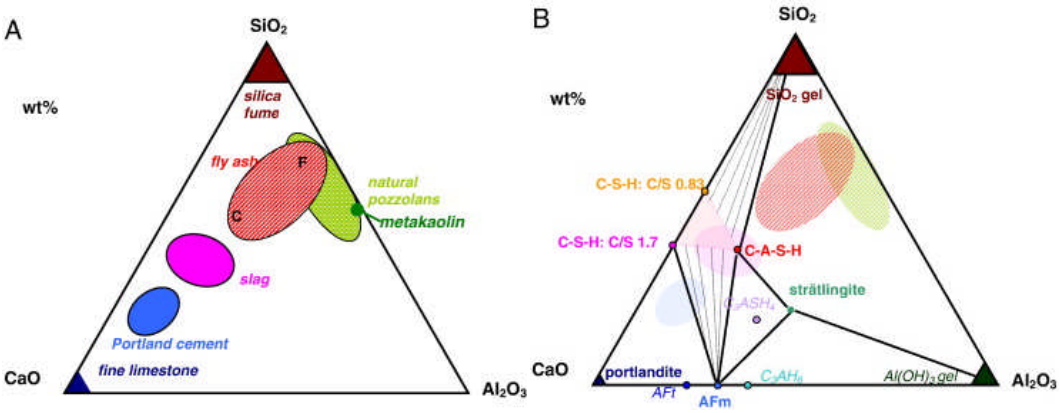

Figure 2-2 Compositional map of cementitious materials (A) and probable products (B) [10]

2.3 Hydration of Portland cement clinker

2.3.1 Overview

Anhydrous Portland cement clinker phases, mainly tri-calcium aluminate (C_3A), alite (C_3S), belite (C_2S) and tetra-calcium alumino-ferrite (C_4AF) react upon contact

with water at different rates, but inter-dependently. The kinetics of hydration (see Figure 2-3) in conventional cements are fairly well understood [83, 84]. Cement hydration consists of a series of endothermic and exothermic reactions. The kinetics and suggested reactions accounting for them are summarised in Figure 2-3 and Table 2-1. Some evidence suggests simultaneous dissolution of C_3S during the initial surface wetting [85]. The initial wetting and or dissolution is followed by an induction period, accelerating stage, deceleration stage and post-deceleration or steady stage hydration.

Whilst there is general agreement regarding the kinetics of hydration [86, 87], a divergence of opinions persists over the mechanism(s) responsible for the induction and subsequent stages of hydration. Of significance to the present study is the influence of SCMs on the hydration of the major clinker phases and reaction of the SCMs themselves. Slag is latently hydraulic and its reaction depends on the alkalinity of the hydrating environment. The hydration of C_3S produces calcium hydroxide which raises the pH to the levels required for slag hydration. Calcite from limestone, on the other hand, reacts with aluminates from C_3A and slag upon depletion of sulphates to form hemi or mono carbo-aluminate. Hydration of the major clinker phases and the impact of slag and limestone on the kinetics of hydration are subsequently reviewed.

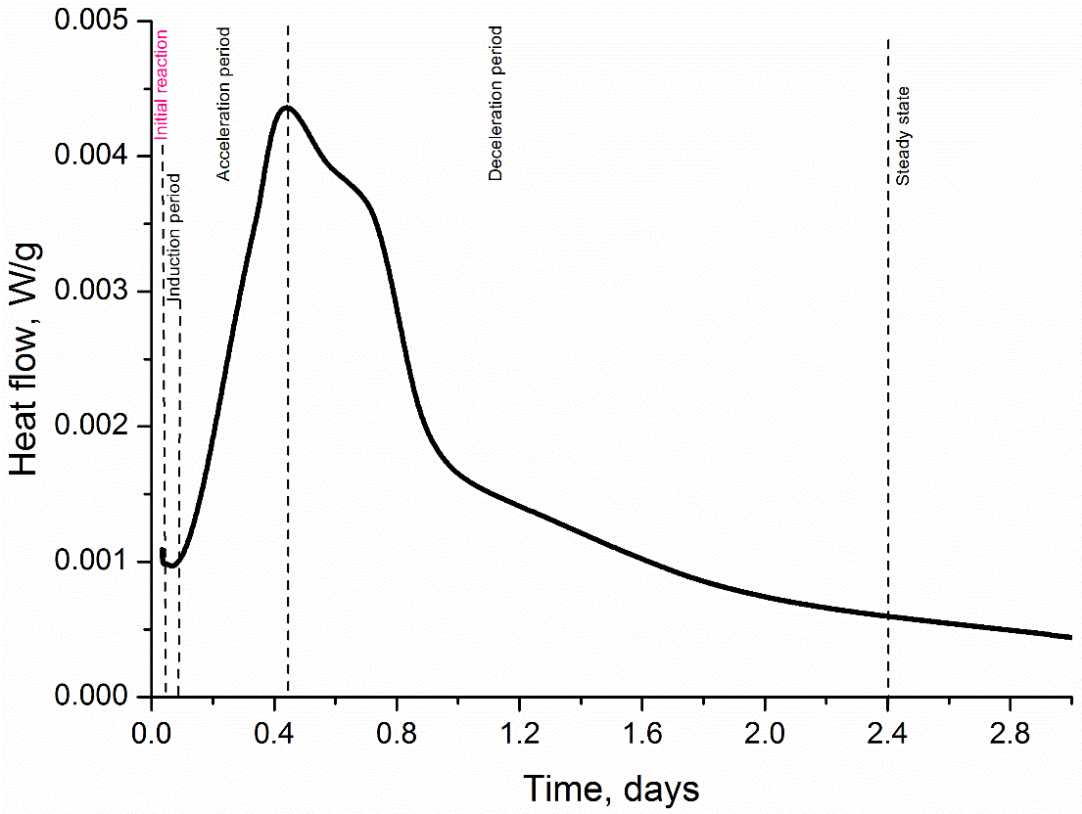

Figure 2-3 Illustration of the stages of hydration

Table 2-1 Stages of cement hydration [88]

Stage	Characteristics	Kinetics	Chemical process	Effect on cement properties
I	Initial hydrolysis	Chemical control	Initial hydrolysis, dissolution of ions	
II	Dormant stage	Nucleation control	Continued dissolution	Initial set
III	Acceleration	Chemical control	Initial formation of hydrates	Final set and initial hardening
IV	Deceleration	Chemical and diffusion control	Continued formation of hydration products	Early strength gain
V	Steady state	Diffusion control	Slow formation of hydration products	Later strength gain

2.3.2 Tricalcium Silicate (Ca_3SiO_5) polymorphism

Tri-calcium silicate (C_3S) is perhaps the most investigated clinker phase owing to its relative proportion in clinker (≈60%) and the influence on early age and long-term mechanical properties. The C_3S in PCC is not pure but contains impurities, as a result of which it is known as alite. The structure varies with temperature and together with impurities can modify the crystal structure (i.e. the lattice parameters) [89]. The modifications as a function of temperature have been investigated by several authors [90-92]. There are seven possible polymorphs namely T1, T2, T3, M1, M2, M3 and R. The M3 polymorph has only been reported following observations under high-temperature light microscopy [93] and hence often discounted when considering the phase transitions. The alite phase as a function of temperature is shown in Figure 2-4.

$$T1 \xleftrightarrow{620\,^{\circ}C} T2 \xleftrightarrow{920\,^{\circ}C} T3 \xleftrightarrow{980\,^{\circ}C} M1 \xleftrightarrow{990\,^{\circ}C} M2 \xleftrightarrow{1060\,^{\circ}C} M3 \xleftrightarrow{1070\,^{\circ}C} R$$

Figure 2-4 C_3S polymorphs as a function of temperature [93]

2.3.3 C_3S hydration and microstructure

Foreign ions modify the crystal structure of C_3S as pointed out already and consequently influence the hydraulic activity of alite.

When in contact with water, C_3S undergoes initially rapid reaction but this reaction slows very quickly. Depending on the cement composition, a 1 – 4 hour period of inactivity (i.e. the induction period) is observed. The extent of dormancy is influenced by the alite polymorph [94]. Particularly, the effects of MgO, Al_2O_3, and Fe_2O_3 on kinetics have been reported elsewhere [89, 95, 96]. Where influential, the oxides generally tend to modify the early reaction rates [89, 96]. Valenti *et al.*

[97] doped triclinic C_3S with 1% of MgO, Al_2O_3, or Fe_2O_3 and found a lower degree of C_3S hydration in the presence of all foreign ions. The extent of retardation increased in the order of MgO, Fe_2O_3, or Al_2O_3. Stephan *et al.* [96] varied the dosages of the three oxides and found that MgO affected C_3S hydration minimally, except a slight acceleration of silicate dissolution at early ages [89, 96]. However, the impact was insignificant below 1.0% doping [98]. There is some convergence over the retarded C_3S hydration when doped with either Fe_2O_3 or Al_2O_3. In either case, the retardation increased with the dopant concentration [89]. The effect of multiple oxide doping has been shown to be additive [96] with MgO being least influential. The retardation of alite hydration when doped is consistent with Stewart and Bailey [99]. However, that MgO doped monoclinic was more retarded than the Al_2O_3 doped trigonal C_3S as shown in Figure 2-5 is inconsistent with the already reviewed literature [95-97]. In fact, the monoclinic (i.e. MgO doped) could even be more reactive than the pure triclinic C_3S on the basis of Mg having a smaller ionic radius than Ca with a potential to destabilise the C_3S structure. This is in agreement with the data reported elsewhere [100]. However, differences in reactivity also exist within the monoclinic group, such that, M1 has been reported to be more reactive than M3 [101]. ZnO stabilises the triclinic C_3S at room temperature. It is well documented that ZnO improves silicate dissolution without necessarily accelerating the reaction [98, 100]. Nucleation favouring reactions in the presence of ZnO have been suggested to explain the enhanced silicate dissolution.

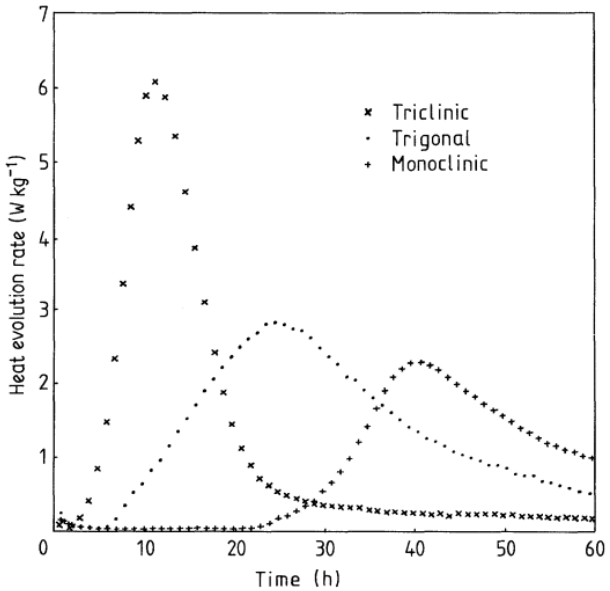

Figure 2-5 Influence of polymorphism on the kinetics of C_3S hydration [99]

The products of C_3S hydration are C-S-H and calcium hydroxide. The hydrates are intermingled with pores of varying sizes as a relic of residual water. Foreign ions modify the nature and distribution of hydrates. It has been shown that Al, Mg and Fe can be incorporated into the C-S-H. However, the levels of Mg are comparatively low [102] and mostly end up in the inner product C-S-H [103]. Al on the other may be incorporated into the inner or outer product C-S-H. Richardson *et al.* [104] showed that Al can substitute for Si in the bridging sites of the C-S-H structure. There is also evidence that external sources of foreign ions [105] can influence the composition and porosity of the C-S-H formed from alite hydration.

2.3.4 The mechanism of C_3S hydration

It is worth emphasising that the main hydration peak is attributed to silicate reaction, which at early stages may be limited to C_3S [106, 107]. Most of the available data on C_3S hydration focus on the pure triclinic polymorph [100, 108-110]. Thomas *et al.* [111] proposed a two-step reaction kinetic, i.e. fast initial

reaction and slow-diffusion controlled reactions. During the fast initial reaction stage, Ings *et al.* [108] observed a thick layer around the reacting C_3S particle. Further C-S-H precipitation eroded the initially formed protective layer instead with a secondary acicular C-S-H evolving after longer hydration times as illustrated in Figure 2-6. Based on proton NMR, Pustovgar *et al.* [112] identified a layer of hydroxylated silicate but unpolymerized silicate species in proximity to the reacting surface during the induction stage. This is supportive of a meta-stable barrier mechanism for the slowed silicate dissolution.

This membrane is believed to restrict water and ion mobility to and from the reacting particle and persists until the membrane is destabilised [113]. Postulated hypotheses for termination of the induction include C-S-H phase transformation, osmotic pressure, supersaturation, crystallographic defects, and nucleation-growth mechanism. A study by Juilland *et al*. [114] however highlighted crystallographic defects which were related to the quenching rate as most influential. Differences in the C-S-H composition with hydration time and also the bulk matrix and at the product/C_3S interface [115] suggests an equilibrium driven mechanism for rapturing the protective barrier [116]. This implies that dissolution is facilitated by the need to restore equilibrium between the interface and the bulk as hydration progresses.

The disappearance of the initially formed metastable barrier [108] corresponds to the renewed C_3S hydration hence acceleration of the rate of reaction. This agrees with the formation of dimers and oligomeric silicate species, Q^1 and Q^2 respectively as reported elsewhere [110, 112]. The mechanism, therefore, involves polymerization and formation of C-S-H with longer silicate chain lengths. This is

consistent with the erosion of short chained protective layers [108] as shown in Figure 2-6.

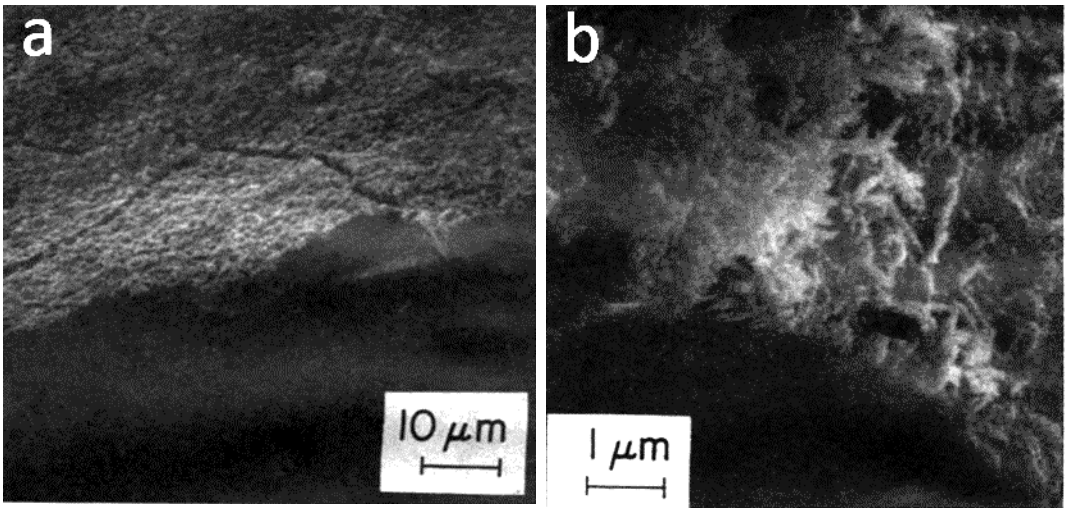

Figure 2-6 C_3S-hydrate interfacial region
after (a) 30mins of hydration with 5µm thick precipitated and; (b) eroded protective layer after 60mins with 0.1 µm thick acicular morphology [108]

Calorimetric studies [96, 99] and microstructural observations [108] show a further barrier. The lowered reaction rate arising from the continuous acicular layer around anhydrous C_3S is the basis for this barrier [86, 117, 118] and coincides with the deceleration stage. An inhibited hydration arising from precipitated C-S-H [119], impinged growth [120, 121], C-S-H densification [122] and C-S-H polymerization [112] are suggested reasons for the deceleration stage. These mechanisms are somewhat inter-related such that longer silicon chain lengths directly increase density and similarly reduce the available space for further growth. Reductions in the size of the anhydrous particle over the course of hydration also imply smaller reacting surface area hence lower monomeric silicate (i.e. Q^0) concentration. Consequently, there are fewer species available for polymerization. This mechanism may also account for the diffusion controlled steady-stage reactions.

2.3.5 Dicalcium Silicate (Ca_2SiO_4) polymorphism

Belite is the second most abundant crystalline phase in Portland cement clinker. The formation temperature ≈1200°C is lower than that for alite. The potential savings in clinkering energy has resulted in a number of studies focusing on high belite-content cements [123-125].

Belite can exist in several polymorphs including α, α'_H, α'_L, β and γ-C_2S. C_2S polymorphism depends on the chemistry of the constituent raw materials, stabilising agents and processing temperature [126-128]. The phase transitions as a function of temperature and the implications on the lattice parameters of the crystal structures are reported elsewhere [127].

An intermediate polymorph (?-C_2S) was identified by Ishida *et al.* [129] following thermal treatment of α-C_2SH. The morphology and XRD patterns of this phase were, however, similar to that of the least reactive γ-C_2S. A recent study [125] also identified an amorphous belite and X-C_2S as two other polymorphs. The latter were synthesised by α-C_2SH autoclaving at 200°C for 16 hours. The X-ray reflection of the X-C_2S was closely related to the γ-C_2S. It, therefore, seems that the ?-C_2S in [129] is the same phase referred to as amorphous belite in [125].

Similar to alite, incorporation of foreign ions as detailed elsewhere [126, 130, 131] can also stabilise the other polymorphs at room temperature. Generally, most common foreign ions in cement apart from Mg^{2+} [132] preferentially incorporate into belite. For example, higher SO_3 doses during clinkering increased the formation temperature for C_3S and hence promoted β-C_2S [132]. These ions reduce the Gibbs free energy [128] such that at room temperature, the transition phases (polymorphs) are thermodynamically stable. However, the resulting phase

transitions also depend on the processing temperature profile. For example, higher foreign ion concentrations [133] can stabilise α-C_2S when the melt (> 1250°C) is rapidly cooled. Cooling same slowly, however, stabilises α'_H-C_2S instead. Manipulation of the belite polymorphs with the view to improving early age reactivity is the subject of further pursuit. However, for cement clinkers, β-C_2S is the dominant phase but traces of α'_H-C_2S may co-exist. A range of foreign ions can stabilise β-C_2S in cement clinker and have been reviewed elsewhere [128]. It is noteworthy that, the stabilising agent and concentration can significantly influence the hydraulic activity of the belite polymorph [134, 135].

2.3.6 C_2S hydration and microstructure

Belite hydrates at a slower rate compared to alite but the polymorphs exhibit different hydration behaviours [130, 136]. This is partly related to the lattice configurations as well as crystallographic defects, and particle grading among others.

Jelenic and Bezjak [134] reported an initially faster rate of reaction of α-C_2S such that, the degree of hydration was even better than alite at the very early stages of hydration. The trend however reversed after 5 hours. Compared to other C_2S polymorphs, the degree of α-C_2S hydration was consistently higher than the β-C_2S. Similar observations were made by Trettin *et al* [136] who compared the early hydration of three belite polymorphs. Irrespective of the polymorph, the major changes according to the specific surface area occurred in the first 30 mins where three peaks were observed in the α-C_2S mix as opposed to two in β and γ-C_2S. In addition, the heat flow measurements indicated a single exothermic peak which occurred in the first 10 minutes in all mixes with a slightly higher peak intensity in

the α-C_2S while the β and γ-C_2S were similar. In the presence of phosphorous oxide, Fukuda and Taguchi [137] however noticed better hydraulic activity in β-C_2S compared to α'-C_2S. This was attributed to the twin boundaries in the β-C_2S crystal fragmentation during cooling (α'_L to β-C_2S). This provided active centres for reaction with water.

In contrast, Cuberos *et al.* [138] found β-C_2S to be inert in the first 90 days of hydration while γ-C_2S began to react after 1 year. The newly identified belite polymorphs are however more reactive than the α', β and γ-C_2S. For example, the ?-C_2S polymorph [129] reacted completely after 1 day. Similarly, Link *et al.* [125] reported complete hydration of the amorphous and x-C_2S after 40 hours while the γ-C_2S was inert within the same time range; hydration of the amorphous C_2S was found to precede the x-C_2S. Larger particle surface area, as well as the presence of protons in the structure, were two suggested reasons for the rapid early age reaction.

The more reactive belite have implications for the hydration of other clinker phase assemblages and mechanical property evolution. However, these are not yet available in commercial cement clinkers. Notwithstanding, the slowly reacting β-C_2S may still have useful implications and will be reviewed under the mechanism of belite hydration in the next section.

2.3.7 The mechanism of C_2S hydration

β-C_2S is the dominant belite polymorph in cement clinker. The hydration mechanisms of such are consequently reviewed.

C_2S reacts with water to form C-S-H and portlandite. The portlandite content [134] and the composition of the C-S-H [136] undergo tremendous changes from the

early stages of hydration. First, calcium ions evolved in solution and the concentration increased sharply in the first 10 mins but decreased afterwards; becoming stable from 30 mins onwards. The Ca/Si ratio of the C-S-H followed a similar trend. Considering that Si levels in the pore solutions are generally low [139], the Ca^{2+} concentration may be the most influential factor controlling silicate dissolution. Indeed, the adsorption of Ca^{2+} ions onto the hydrates has been suggested elsewhere [136]. A similar experiment in the presence of saturated lime solution [136] also noted that belite hydration was favoured by the removal of Ca^{2+} ions from the bulk solution. This has been confirmed by Nicoleau *et al.* [139]. The inhibited β-C_2S was consequently attributed to the formation of a calcium rich barrier around the anhydrous particle.

It is firmly established that, the presence of Ca^{2+} generally reduces silicate dissolution [86, 113, 114, 140] and that, dissolution of belite in ordinary cements does not proceed until such a time when the calcium ion concentration in the pore solution has significantly dropped. However, the precipitation of calcium rich C-S-H around hydrating belite particle as reasons for the retarded hydration seems counter-intuitive. If the Ca^{2+} concentration influences silicate dissolution [141], then lowering of Ca^{2+} by absorption onto hydrates or precipitation of C-S-H should theoretically favour C_2S dissolution unless the precipitated Ca-rich C-S-H was localised to belite. The existence of such is not known for C_2S except for alite [142]. Moreover, the C-S-H composition around hydrating clinker in neat cements have been shown to be virtually unchanged at longer hydration times [143, 144] except in [145]. Consequently, a calcium-rich barrier mechanism may not fully account for the retarded belite reaction.

The dilution effect [67] has been shown to modify the hydraulic activity of belite. This has been previously investigated and found beneficial for suspended mixes for β-C_2S [136, 139] and Portland cement [146]. Nicoleau *et al.* [139] noted that belite hydration was more affected by dilution than alite. The beneficial effect of dilution on belite hydration was attributed to the formation of calcium deficient C-S-H [136]. Indeed, variations in the C-S-H as a function of the w/c ratio has been reported elsewhere [145]. An equilibrium driven mechanism [139] where the concentration of ionic species in the pore solution at early age depends largely on the composition of C_3S and precipitated phases has also been suggested.

Differences in solubility [147] and the available space for hydrate growth provide further insight into the retarded belite hydration. The dilution effect reviewed above constitutes the basis of this hypothesis. Higher effective w/c ratio implies that negative pore pressure which would otherwise inhibit silicate dissolution is averted. Additionally, a smaller volume of C-S-H compared to reactants (hence chemical shrinkage) leads to additional space which can promote silicate dissolution in the long term [51, 67, 86].

2.3.8 Tricalcium aluminate polymorphs, $Ca_3Al_2O_6$

$Ca_3Al_2O_6$ abbreviated C_3A is an important phase in cement clinker. In the pure form, C_3A has a cubic structure [148, 149] with suggested unit cell dimensions a=b=c=7.263 Å [148] or 15.263 Å [149]. However, C_3A occurs as an impure compound in cement clinkers where MgO, Na_2O or K_2O may substitute for CaO or Fe_2O_3 for Al_2O_3.

Impurities in raw materials and from combusting fuels can induce polymorphism of C_3A. The effect of Na_2O is well documented [83, 150]. The cubic structure is

maintained in the presence of up to 2.4% Na_2O; 2.4-3.6% Na_2O stabilises orthorhombic C_3A and then the monoclinic C_3A between 4.6- 5.7% [83]. K_2O can also stabilise the orthorhombic and monoclinic C_3A [150, 151]. Ordinarily, K^+ does not enter the C_3A lattice due to differences in ionic radii, i.e. Ca^{2+} (0.99 Å) and K^+ (1.33 Å). In addition, K_2O has a tendency to form arcanite (K_2SO_4) during clinkering. Na_2O, K_2O or K_2SO_4 can exert the physical influence of expanding the lattice and consequently stabilising polymorphs other than the cubic. This was confirmed by Gobo *et al.* [150, 151] who found a correlation between the orthorhombic C_3A and the SO_3 content as well as a visibly expanded microstructure in SO_3 stabilised polymorph as in Figure 2-7. Additionally, the cooling rate has also been suggested to induce phase transitions in C_3A [152].

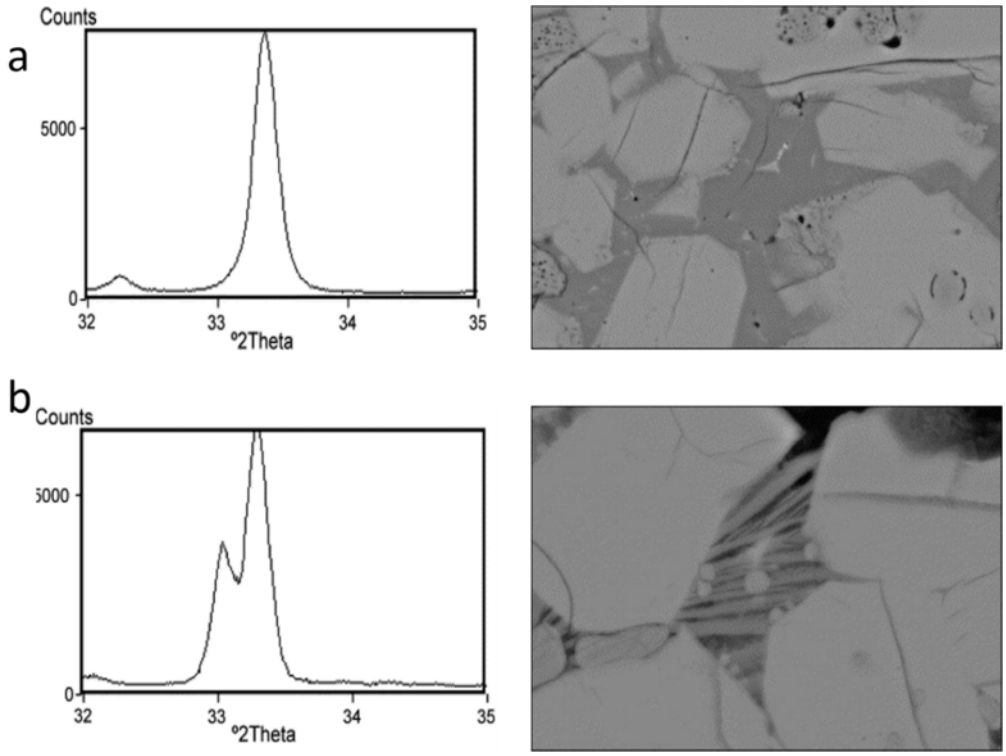

Figure 2-7 Characteristic reflections and microstructure of (a) cubic C_3A and (b) SO_3 stabilised orthorhombic C_3A [150].

2.3.9 C_3A hydration and microstructure

Polymorphism in C_3A has been discussed in the preceding section. The C_3A in ordinary cements is, however, cubic, orthorhombic or their combination. The only exception is the case in [151] where monoclinic C_3A in commercial cement was reported. Different levels of alkalis in the C_3A polymorphs have implications on the hydration kinetics.

In the presence of water, C_3A dissolves rapidly. At room temperature and low w/s ratio, Breval [153] noticed hydrogarnet (C_3AH_6) as main reaction product within minutes of contact with water. In diluted reaction media, however, intermediate products (C_2AH_8 and C_4AH_{13}) were formed but transformed into hydrogarnet subsequently. The hydrogarnet initially evolves as an amorphous gel-like product [154, 155] but crystallises into a cubic structure with hydration time. Meredith *et al.* [156] showed that this product precipitates on the anhydrous C_3A surface. Ciach and Swenson [157] observed hydroxy aluminate and portlandite in addition to hydrogarnet. It was not however clarified as to whether these evolved from the decomposition of C_3AH_6 or renewed C_3A hydration. Irrespective of the mechanism, these phase assemblages are noteworthy with regards to the interaction with SCMs and also carbonates. Indeed, hydration of C_3A in the presence of CO_2 at the early stages inhibit hydrogarnet formation [153]. Carbonates also react with additionally dissolved aluminates and portlandite to form carbo aluminates [155] and consequently stabilise ettringite.

The effect of various foreign ions fused at high temperature [158] or blended [155, 159] on the hydration of C_3A is well documented. Stephan and Wistuba [158] showed that K_2O accelerated while Fe_2O_3 always retarded C_3A hydration with or without sulphates. The effect of Na_2O, MgO and SiO_2 depended on the presence

of sulphates; with Na_2O exerting an acceleration effect in the presence of sulphates. The acceleration was assigned to the existence of potentially amorphous by-products which may have formed at the high temperature rather than the modified C_3A.

C_3A hydration is known to cause flash setting in cements [160, 161]. A three-stage reaction kinetic comprising of simultaneous dissolution and precipitation, steady-stage dissolution and eventually precipitation of hydrogarnet accompanied by saturation of calcium in the pore solution [162] had been suggested. Without sulphates, Black *et al.* [154] observed the formation of C_4AH_{16} and eventually hydrogarnet while ettringite formed at the expense of C_4AH_{16} when sulphate was present. It, therefore, seems that prevalence of hydrogarnet or hydro-aluminates may be responsible for the flash setting accompanying C_3A hydration. Minard *et al.* [163] found that sulphates did not impact on the initial C_3A dissolution but controlled the intermediate reactions. Based on XRD and SEM observations, the retarding effect of gypsum was neither ascribed to ettringite precipitation nor protective barrier [159]; rather adsorption of dissolved calcium or sulphate ions on the C_3A surface was hypothesised.

The microstructure arising from the hydration of the cubic and orthorhombic C_3A polymorphs largely depends on the chemistry of the reacting matrix, i.e. hydroxyl, calcium, sulphate and aluminate ion concentrations. For example, higher Al concentration at low pH favours large crystal-sized ettringite evolution [164] as opposed to the microcrystalline ettringite in portlandite saturated solutions [165]. Some studies have focused on the hydration and microstructure evolution in the C_3A polymorphs [166]. This is shown to be polymorph as well as w/s ratio

dependent. In the presence of sulphates and portlandite, the orthorhombic C_3A has a higher dissolution rate than the cubic with ettringite as the main reaction product. However, larger sized ettringite evolved from the orthorhombic C_3A compared to the cubic. The precipitation of microcrystalline ettringite from cubic C_3A hydration in the presence of sulphates and excess portlandite has been attributed to supersaturation of the less mobile hydroxyl-aluminate and calcium ions [166, 167]. The breaking of Na-O bonds at the expense of Ca-O and preferential release of Al^{3+} have been postulated for the type of ettringite formed by the orthorhombic C_3A.

2.3.10 Mechanism of C_3A hydration

The reaction of C_3A with water involves the destruction of the Ca-O and Al-O bonds. The reaction products precipitate on the reacting C_3A surface and in the presence of sulphates, the ettringite formed may be intermixed with hydrogarnet [156]. However, controlling the amount of precipitated hydrogarnet is useful in controlling flash setting in cements. Notwithstanding, the mechanism for the retardation and subsequently renewed C_3A hydration is still debated [168, 169].

The postulated mechanisms include the protective barrier [159], sulphate adsorption [170], aluminium inhibited dissolution [168] among others. The protective barrier mechanism attributes the retarded C_3A dissolution to the transitional phase assemblages which precipitate on the C_3A surface. In the presence of sulphates, the transitional hydrates (C_3AH_6, C_2AH_8 and C_4AH_x) gradually convert to ettringite (C_6AsH_{32}) which forms a dense layer on the C_3A surface and consequently act as a barrier to further C_3A dissolution [159]. Black *et al.* [154] however observed rapid ettringite precipitation without any intermediate assemblage(s). Notwithstanding, the retarded mechanism was proposed to

involve hydrates restricting diffusion of water to the reacting C_3A grain surface. An alternate view is that conversion of transitional phases into ettringite increases the calcium ion concentration on the product/grain interface [171] and hence suppressing aluminium dissolution. This protective barrier mechanism has been disputed on the basis that, the nature of ettringite puts into question the purported impervious barrier capable of inhibiting diffusion [165].

Skalny and Tadros [168] also suggested a mechanism based on restructuring of the C_3A reacting surface such that further dissolution was inhibited. By observing the concentrations of Ca^{2+} and Al^{3+}, and $SO4^{2-}$, it was argued that Ca-O dissolved more quickly from C3A, leaving an alumina-rich reacting surface. Upon dissociation of calcium and sulphates (n the presence of $CaSO_4$), ettringite forms initially with dissolved aluminates but then, the calcium ions adsorbed onto this aluminium-rich structure and consequently slows down further C_3A dissolution [141]. However, recent studies have not found evidence of the existence of such calcium-rich hydrate/grain interface [166, 167].

Anions other than sulphates may also affect C_3A hydration [155, 172]. In the absence of other components which can also react with dissolved aluminates, the renewed C_3A hydration upon depletion of sulphates converts ettringite ($Ca_6Al_2(SO_4)_3(OH)_{12}.26H_2O$) to mono-sulphate ($Ca_4Al_2(SO_4)(OH)_{12}.6H_2O$). It is noteworthy that, mono sulphoaluminate formation is not necessarily limited to sulphate depletion in the bulk system [163]. However, in cements containing calcium carbonates in addition to sulphates, ettringite ($C_3A.Ca(OH)_2.18H_2O$) forms initially but carbo-aluminates evolve with time [17, 155, 159, 173, 174] and co-exist with ettringite. This preserved ettringite by additionally dissolved aluminates

forming carbo aluminates instead [7]. It, therefore, follows that the C_3A content in cement has implications on the hydration of other cement constituents including silicate phase assemblages and SCMs.

The mechanisms and products of C_3A hydration are not only relevant from the mechanical property and durability point of view [175], they also impact on the hydration of other assemblages [9, 155, 176]. More importantly, in pozzolanic or latently hydraulic composite cements, the aluminate fraction in cement indirectly dictates the alumina-sulphate sink which must be stabilised. This is advantageous for early age strength development [11, 177, 178].

2.3.11 Tricalcium aluminium- ferrite, C_4AF

The C_4AF is one of the interstitial phases in Portland cement clinker. A typical for action in PCC can vary up to 10%. C_4AF does not show polymorphism but Al and Fe can substitute in the octahedral and tetrahedral sites [161]. In addition, Mg^{2+} and Si^{4+} can also be incorporated and consequently modify the crystal cell parameters.

Beaudoin and Ramachandran [179] examined the hydration and strength contribution from C_4AF in comparison to the other major clinker phase. It was reported that the compressive strength development in C_4AF exceeded that of alite in the first 10 days of hydration. Plowman and Cabrera [180] however showed that the rate constant for C_3A was about six times larger than that of C_4AF. This seems to suggest that the alumina to ferrite ratio is an important factor regarding the reaction of C_4AF. On the basis of the compressive strength versus porosity data presented in [179], it is reasonable to expect the microstructures of the hydrates formed from C_3A and C_4AF to differ.

Questions, however, persist regarding the destination of iron following the dissolution of C_4AF. The aluminates may incorporate into the C-S-H, ettringite or AFm phases while Ca may end up as portlandite or in the C-S-H. Whether Fe remains as hydroxy-iron or some other hydrate is a matter of ongoing debate. Theoretically, iron can substitute for aluminium in hydrogarnet. Rogers and Aldridge [181] reported about the temperature dependence of the hydrates from C_4AF. A solid solution of $C_3(A,F)H_6$ was suggested where the incorporation of ferrites into the lattice led to the conversion to portlandite, ferro-hydroxides and hydrogarnet at 21 °C and above. However, Dilnesa et al. [182] noted that only traces of iron substituted hydrogarnet (C_3FH_6) at room temperature. Instead, (C_3FH_6), portlandite and ferrohydrite were the dominant hydrates even in the presence of iron. The incorporation of iron into ettringite and AFm have also been reported elsewhere [183-185]. However, iron bearing AFm phase assemblages have crystal structures significantly different from the corresponding aluminium AFm [186].

2.4 Hydration of composite cements

Composite or blended cements use SCMs or their combinations with the view to reducing the Portland clinker factor of cements. EN 197-1 [187] specifies a range of formulations for these cement types with clinker contents varying from 20 - 94%. Permissible SCMs include slag, fly ash, limestone, pozzolana and burnt shale. Moreover, a combination of more than one SCM including aluminosilicates with limestone is also permitted under the Portland-composite cements category (i.e. CEM II/A-M and CEM II/B-M) however with not less than 65% clinker content. These SCMs may be hydraulic or pozzolanic; in that their reactivity commences

upon attainment of appropriate pH or directly reacts with $Ca(OH)_2$ formed from the hydration of clinker phases respectively. This influences hydration of different SCMs and consequently their impact on the hydration of clinker. This section, therefore, reviews the current knowledge with regards to hydration and microstructure of composite cements with emphasis on aluminosilicate-clinker and then ternary blends of such with limestone.

2.4.1 Hydration of composite clinker – slag cements

Binary clinker-slag cements can be prepared by intergrinding with clinker or blending separately ground slag and clinker. Separate grinding is preferred to intergrinding [188] due to differences in grinding kinetics of slag and clinker and energy efficiency. As a result, separately blended slag cements [8, 12] are most reported.

Slag is latently hydraulic therefore in composite clinker – slag systems, the clinker hydration (i.e. C_3S) is assumed to precede that of the aluminosilicate slag. The reaction of C_3S with water brings into solution calcium and silicate species. Upon supersaturation of these, calcium silicate hydrates (C-S-H) and calcium hydroxide precipitate [86, 189], thus establish the highly alkaline environment (pH≥12) required for slag hydration.

2.4.2 Impact of slag on clinker hydration

Calorimetry studies [29, 31, 190] show clear differences between the kinetics of hydration of neat CEM I and composite slag cements. As illustrated in Figure 2-8, the main stages of hydration are not altered by the presence of slag but the peak

intensities are modified in addition to the possible occurrence of additional peaks. These effects to a larger extent depend on the fineness of the CEM I and slag. For GGBS ground to 559m^2/kg Blaine fineness, Wu *et al.* [190] reported a certain degree of reaction within the first 24 hours and assigned the aluminate peak from calorimetry to slag reaction. Kocaba [143] and Whittaker *et al.* [31] made similar observations in binary slag mixes but attributed the second reaction peak to the filler effect of slag on the C_3A reaction. This assertion was upheld in the work of Berodier and Scrivener [51] who noted similar behaviour in binary slag or quartz mixes and as a result suggested that slag was inert within the reported period of 35 hours. Cetin *et al.* [191] also noticed higher silicate reaction peak intensity with increasing slag fineness. Lower intensity but broader peaks were reported for coarser slags.

The chemical composition of slag can also influence the secondary aluminate peak. Accelerated aluminate reactions in the presence of fillers are well documented [146, 192]. If slag merely exerted filler effects at an early age [51], then similarly graded slags must impact similarly on this peak. However, Whittaker *et al.* [31] demonstrated acceleration of the aluminate reaction peak as the alumina content of slag increased. The mechanism for this acceleration has not been clarified previously. In addition, the relative importance of the two mechanisms (i.e. filler versus chemical interactions) on clinker hydration, on the whole, has not been answered.

What is clear is the agreement that the presence of slag influences the kinetics of clinker hydration [10, 67] but divergent views persist over the hydration of slag at the very early stage [33, 67].

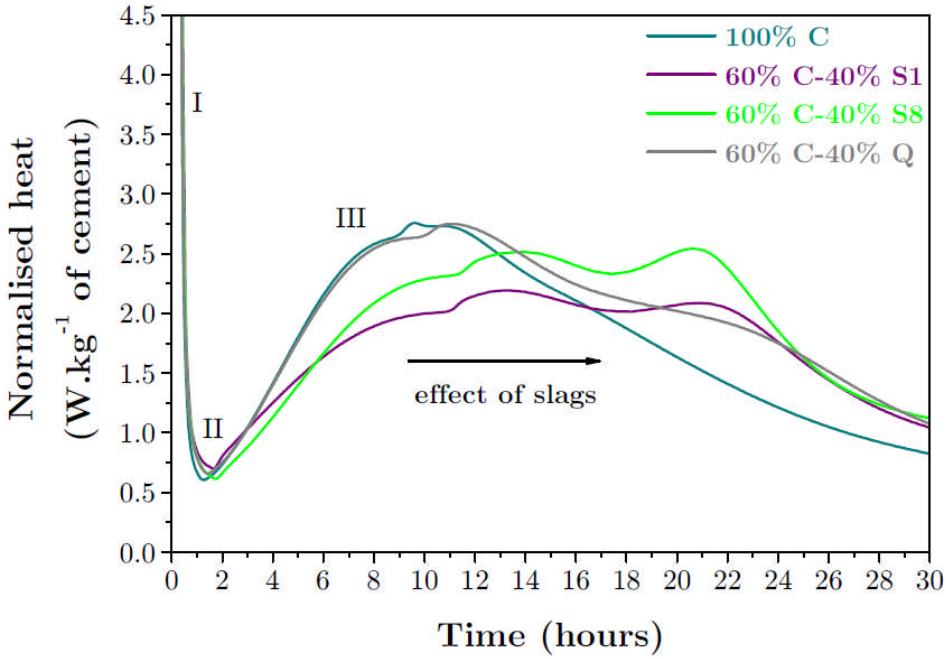

Figure 2-8 Effect of slag and filler on the rate of reaction of composite cements [143]

Note: C is CEM 1; S1 is low alumina but high amorphous; S2 is high alumina but high crystalline content; Q is quartz

Physically, slag provides nucleation sites for C-S-H growth. This accelerates the hydration of the alite phase. However, the nucleation effect is not peculiar to slag as similar results have been shown elsewhere for the inert filler, quartz [51]. In addition to nucleation, the rates of reaction of slag are much slower compared to clinker. Consequently, the effective water available for clinker hydration (i.e. the dilution effect) would be higher at an early age in slag cements. This has been shown to be most significant at higher slag replacement levels [54, 190].

Recent studies [31, 143] have shown retarded belite hydration in binary slag blends. Whereas the acceleration of aluminate and ferrite hydration have been ascribed to the filler effect [14] than a chemical interaction [143], detailed explanation of the mechanisms behind retarded belite reaction was not provided.

The concept of space-limiting kinetics for later stage clinker hydration has been suggested elsewhere [193].

2.4.3 Hydration of slag

The reaction of slag in composite cements involves hydrolysis of alumina and silicates followed by polymerisation of the silicates with C-S-H as the main hydration product. Some of the aluminium in slag may be incorporated into the C-S-H leading to higher C-S-H Al/Si ratio [31, 143, 194]. Richardson et al. [195] however found compositional differences between this Al-rich outer product (Op) C-S-H and the inner product (Ip) C-S-H upon hydration of slag. The latter is an intimate mixture of C-S-H and the hydrotalcite-like Al, Mg hydroxide phase. Mg was not incorporated into the Op but instead, remained in the Ip C-S-H.

Many authors have considered the kinetics in detail [12, 77, 196] and deduced the impact on clinker hydration and vice versa. Escalante-Garcia and Sharp [196] postulated slag reaction kinetics to be similar to Portland cement except for the timelines for the occurring chemical activities. Reactivity was observed to increase with curing temperature. At room temperature, the degree of reaction of slag was 40% after one month and remained significantly unchanged until one year where 60% reactivity was reported. Deduced reaction kinetics involved an initially intense reaction followed by a period of dormancy and renewed reaction. The stages of reaction were similar however the rate of reaction increased with curing temperature. Through selective dissolution, Luke and Glasser [30] investigated the effects of cement and slag composition plus fineness on hydration. It was shown that reactivity of slag increased with increasing hydraulic modulus (i.e. Ca+Al+Mg/Si) and fineness (to a slightly lesser extent). While reactivity expectedly

decreased with increasing slag content in the blend, the limited data on clinker type was inconclusive. It was also suggested that extra sulphates did not influence slag reactivity.

The impact of the cement fineness on slag hydration is well documented [197, 198]. Reactivity increases with fineness due to the accelerated dissolution of the clinker phases with portlandite as a hydrate. However, that of the cement chemistry in composite systems has not been reported; probably due to the narrow phase compositional ranges in the CEM I. The relevant constituents which may influence slag hydration include the Al_2O_3, CaO, SiO_2, MgO and added sulphate contents. This is because these are either present at significant levels in clinker and slag or form hydrates which may impact on slag. Presumably, the effects of the above oxides in Portland cements may be similar to those in slag except the latter dissolving slowly. On that premise, higher Al_2O_3 levels retard slag dissolution, but only at an early age [199]. For external aluminate sources, Ismail *et al.* [200] and Scholer *et al.* [201] found retarded slag hydration in the presence of fly ash which have significantly higher Al_2O_3 content than CEM I. However, for a given slag fineness, Whittaker *et al*. [31] noted enhanced slag reactivity at higher Al_2O_3 content. The prevalence of a conducive activating medium was suggested to be more influential than the alumina content. Considering an alkali-activated system, Ben Haha [202] found slag reactivity to increase with MgO content. This resulted in more hydrotalcite formation. This took up most of the aluminates and consequently reduced the available Al incorporated into the C-S-H. Less alumina in the C-S-H is proportional to the concentration in the pore solution. Therefore, all things being equal, slag reactivity would be influenced by the aluminate contents of the cement despite the latter dissolving quickly during hydration [141, 203]. The

effect of the SiO_2 is only reported for alkali-activated systems and even here the results contradict [204, 205]. SiO_2 in clinker exists as alite and belite and therefore forms C-S-H. The higher the C-S-H from clinker, the lower the space available for hydrates from slag hydrate to fill. This effect may, however, be marginal considering that the major hydrates, i.e. C-[A]-S-H intermixed with hydrotalcite [104, 206, 207] tend to be localised.

Sulphate in the form of gypsum, anhydrite or hemihydrate is added to control C_3A hydration as discussed already. The hydrates resulting thereof may be ettringite or mono sulphoaluminate depending on the SO_3/Al_2O_3 ratio. The activation of slag by sodium sulphate solution has also been reported elsewhere [208, 209] with ettringite and C-[A]-S-H and hydrotalcite as major hydrates. It is also well known that sulphate/aluminate imbalance transforms ettringite to mono sulphoaluminate. Excess sulphates, therefore, have the potential to activate slag reaction. This, however, was not confirmed in the study by Whittaker *et al.* [31].

Like belite, slag hydrates slowly and the lack of space for hydrates to fill could discourage dissolution. This effect underpins the increased GGBS reactivity with increasing w/c ratio and lower slag loading [12]. The recent study by Berodier and Scrivener [54] confirmed the importance of the available space but further suggested that the available water in the capillary pore network is equally important.

2.4.4 Microstructure of composite clinker- slag cements

In composite cements, the hydration of slag contributes C-[A]-S-H and a hydrotalcite-like phase to the microstructure in addition to the C-S-H and

portlandite from clinker. These are intimately mixed with unreacted slag and pores left over by water.

Richardson and Cabrera [207] reported about the microstructure of the C-S-H of slag-cement. The amorphous C-S-H had clearly defined inner and outer hydration products. However, the portlandite content decreased while the morphology changed from fibrillar to foil-like with increasing slag content. Portlandite consumption was expected considering that the Ca/Si ratio in the unreacted slag is significantly lower than that of the hydrated slag [207, 210, 211]. Indeed the Ca/Si ratio determines the morphology of C-S-H [212] and this has implications on the mechanical properties [213, 214].

At a given w/c ratio, the slower rate of reaction of slag leads to higher porosity at early ages. However, with slag contributing additional hydrates, the pore structure is refined as hydration progresses. Slag has been found to refine the pores more efficiently than other SCMs [54, 215].

2.4.5 Hydration of clinker – limestone composite cements

Limestone has physical and chemical implications on the hydration of clinker and other constituents in composite cements [4, 7, 13].

Physically, limestone exerts an accelerating effect on cement hydration [17, 216]. Some studies have concluded that limestone powders merely act as micro-fillers in cement systems [217]. Such arguments were underpinned by the enhanced effect on clinker with increasing fineness of limestone without corresponding new phase assemblages [218]. However, finely ground limestone composite cements led to the formation of carbo-aluminates [17, 219, 220]. These however influenced strength insignificantly with the impact on strength credited to stabilised ettringite

[177]. Concerning the kinetics of hydration, Poppe and Schutter [221] observed via isothermal conduction calorimetry a shortening of the induction period and evidence of an aluminate reaction plus intensified alite hydration in limestone-clinker binary blends. Replacing limestone with quartz, however, did not yield a similar shortening of the induction period. The shortening of the induction period has recently been attributed to limestone providing a better substrate for C-S-H nucleation [51].

The accelerating effect of limestone on the hydration of the major clinker phases has also been suggested to depend on the w/c ratio [4]. At low w/c, a fraction of clinker phases remains anhydrous thus acting as expensive filler material. At higher w/c ratios (≥ 0.42), sufficient space exists in the hydrating matrix for hydrate growth. The hypothetical spaces for hydrate growth and provision of nucleation sites account for the high early age strength [222]. However, increasing limestone content effectively reduce the volume of actively hydrating materials.

Bentz [216] integrated the physical influence of limestone on hydration (i.e. provision of nucleation sites for hydrate precipitation) and the chemical interaction between calcite and the calcium sulphoaluminate assemblages in a hydration model. Limestone acceleration of clinker hydration depends on the water/solid (w/s) ratio. Similar to the observations by Bonavetti *et al* [219], the accelerating effect was indiscernible above 0.434 w/s ratio. In the model, mono carboalumination formation became pronounced after depletion of sulphates. However, up to 180 days of hydration, only 5 out of the 20 % limestone substituting for clinker had participated in the hydration process.

In limestone composite cements, dissolved aluminates form carboaluminates instead of converting ettringite to mono sulphate [7, 17, 173, 174, 177]. Consequently, limestone does not only exert a filler effect on clinker hydration but interacts chemically. However, the aluminium and calcium concentrations in ettringite are significantly higher in carboaluminates compared to ettringite [17, 173, 174, 223]. Indeed, the presence of limestone in Portland or composite limestone cements has been suggested to lower the portlandite content [224]. This has been attributed to the formation of portlandite consuming products [7], i.e. carboaluminates. Despite the dissolution of calcite contributing additional calcium [51], there is more calcium in carboaluminates than that supplied by dissolved calcite [173, 174].

2.4.6 Hydration of clinker - Slag - limestone composite cements

Recently, ternary blends of clinker, slag or PFA and limestone have received considerable research focus [17, 18, 225].

Both slag and PFA predominantly comprise aluminate and silicate species. Participation of these in the hydration process, therefore, increases the aluminate fraction, and in the presence of carbonates, carbo-aluminates are formed [155]. This prevents the transformation of ettringite into mono sulphate [17, 155, 177].

Improved compressive strengths with up to 5% limestone addition in clinker-slag or PFA ternary blends have been reported in the literature [14, 17]. This has been attributed to the synergy between limestone and aluminates from the SCM which leads to the formation of additional pore refining calcium aluminate hydrates while calcium carboaluminates precipitate.

Mounanga *et al.* [225] showed that, at a given clinker to SCM ratio, altering the slag to limestone ratio had minimal influence on the heat flow (see Figure 2-9). The heat of reaction associated with the ternary blends was also higher than the corresponding binary blends. The independence of the heat flow on the slag/limestone loading is quite surprising taking into account differences in their nucleation effects [51]. At early stages of hydration, both slag and limestone provide nucleation sites for C-S-H growth and hence promote hydration of the major clinker phases [4, 12, 13]. Considering that hydration of slag also commences at a pH of ~12, it would be expected that the heat flow associated with the hydration of slag would vary with the slag content. Furthermore, the formation of carbo-aluminates which are deemed non-contributory to mechanical properties [218] would be associated with enthalpies which influence the heat flow data. It is, however, worth noting that limestone in this context was comparatively coarser than the slag and over the reported duration, the presence of calcite would rather promote sulphate reaction at the expense of calcite. Consequently, the chemical effect may not necessarily be evident.

In limestone ternary blends, synergies depend to a large extent on the CO_3^{2-}/Al_2O_3 ratio [226]. It is also possible that enhanced reactivity of SCMs in the ternary system arises from the accelerating effects of both limestone and slag on C_3S hydration (due to the provision of nucleation sites). Accelerated C_3S hydration implies high portlandite content which subsequently activates slag hydration at early ages.

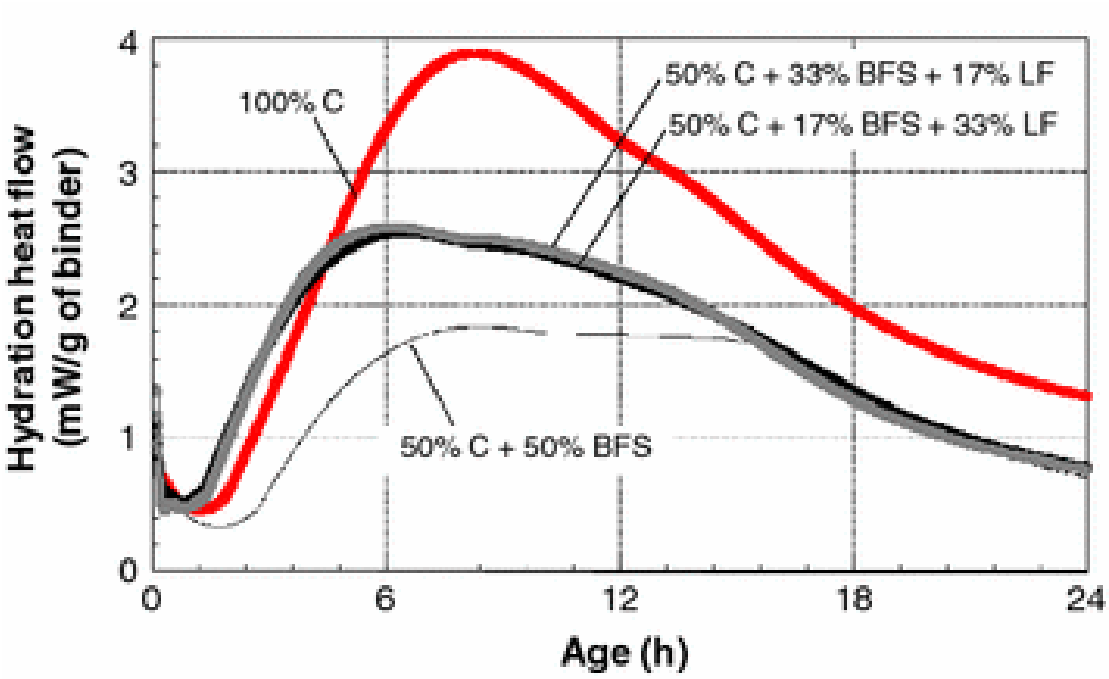

Figure 2-9 Isothermal calorimetry of PC-slag-LL ternary blends [225]

In addition to the carbonate/aluminate ratio, Matschei *et al.* [173] suggested that the sulphate to aluminate ratio is also imperative for predicting potential phase assemblages in limestone containing cements. That calcium sulphates (e.g. for 2.41g/L gypsum) are more soluble than corresponding carbonates (0.014g/L) is well established [227]. The initial sulphate-aluminate ratio, therefore, determines the point at which carbonates are incorporated into hydrates. Considering that dissolution of slag increases the aluminate concentration, there is a potential for higher levels of calcium carbonates (from limestone) to be incorporated.

2.5 Relationship between composition, microstructure and carbonation resistance of slag-limestone containing cements

Concretes exposed to aggressive environments may deteriorate. Normally deterioration is caused by a combined of mechanisms [27, 228-230]. Carbonation

and chloride-induced corrosion in concretes are well understood to arise from the loss of passivation around the reinforcing steel [231]. Carbonation can also increase the susceptibility to freeze-thaw induced damage [25, 232-234]. Consequently, the mechanisms for carbonation and freeze-thaw as a function of cement composition are reviewed.

2.5.1 Mechanism of carbonation

Slag containing cements are particularly susceptible to carbonation [235]. This is often attributed to the slow pozzolanic reaction of SCMs [236, 237]. When compared to Portland cement at early ages, the microstructure of composite cements are less developed and hence more permeable to atmospheric CO_2 ingress. Additionally, hydration products - ettringite, calcium hydroxide (CH) and C-S-H are also susceptible to carbonate. The reactions taking place during carbonation may be simplified in the equations below in equations 2.1 – 2.4 [238, 239]:

$H_2O(l) + CO_2(g)$ --------> HCO_3^{2-} ----------Equation 2.1

$Ca(OH)_2 + CO_2$ ----------> $CaCO_3 + H_2O$ ----------Equation 2.2

$C\text{-}S\text{-}H + CO_2$ ----------> $CaCO_3 + SiO_2 + H_2O$ ----------Equation 2.3

$3CaO.Al_2O_3.3CaSO_4.32H_2O + CO_2$ --------> $3CaSO_4.2H_2O + 3CaCO_3 + 2Al(OH)_3 + 23H_2O$ ---------- Equation 2.4

A significant number of investigations into the mechanism and effects of carbonation of slag containing cements have been reported in the literature.

Stark and Ludwig [25] noted the co-existence of calcite, aragonite and vaterite in slag containing cements while calcite was the dominant carbonation product in

Portland cement. Similar observations have been reported elsewhere [44]. In the latter, the metastable carbonates were, however, present in trace quantities. The products of carbonation depend on the carbonating phase – portlandite, C-S-H or ettringite as well as the relative humidity [240] and temperature [239]. With the C-S-H, Black *et al.* [241] showed increased susceptibility to carbonation at higher Ca/Si ratio due to structural disordering.

The products of carbonation vary in crystallinity. Following carbonation of a tobermorite-like system (C-S-H), the existence of vaterite as a carbonate polymorph is only transitional. Vaterite eventually recrystallizes into calcite [242]. A pseudo-morphosis mechanism was postulated; where calcite and its polymorphs are deposited within the tobermorite while maintaining the original shape-morphology.

Wowra [238] concluded from solubility and density data (see Table 2-2) that, recrystallization of aragonite to calcite was expansive while vaterite to calcite was compressive. Irrespective of the carbonate polymorph, carbonation of Portlandite can be considered expansive. The effect of this has been suggested to be more critical in blast furnace slag cements [243]. The latter may be due to the presence of magnesium favouring carbonate polymorphs other than calcite.

2.5.2 Factors affecting carbonation

Porosity, permeability, degree and products of hydration, as well as the exposure conditions including relative humidity, temperature and CO_2 concentration among others, influence the carbonation resistance of cementitious materials [229, 239, 240].

Concerning the formation of aragonite and vaterite, Stepkowska *et al.* [244] reported relative humidity history during hydration and cyclic wetting and drying as influencing factors. The carbonation rate is highest between 50 and 70 % relative humidity [245, 246]. Above 70 % RH, pores are generally saturated and inhibit the ingress of CO_2 while inadequate moisture may be available to dissolve CO_2 below 50 % RH. Outside, the carbonation favouring RH range, the phase transition of carbonated assemblages may still occur. For example, deposition of aragonite and vaterite was higher in specimens in which water was retained through changes in relative humidity (100% --> 95% -->50%). Specimens in which water was retained through absorption, however, showed the least levels of aragonite and vaterite [247].

The presence of magnesium in concrete or from an external source such as de-icing agents as well as organic additives has also been shown to facilitate the formation of aragonite and vaterite. In such systems, vaterite was only observed at early stages of hydration but later converted to aragonite or calcite [238]. Also, in the presence of magnesium salts, the potential for uncalcined limestone to form aragonite under atmospheric CO_2 has also been reported [248].

Despite hydrating at a slower rate, slag refines the pore structure of composite cements [11, 12]. Limestone in composite cements is suggested to increase pore volume hence densification of the microstructure [17, 173, 249]. Therefore, high permeability may only account for the susceptibility of slag cements to carbonation at early ages but the trend may reverse at longer hydration times [243].

2.5.3 Effect of carbonation on microstructure

Carbonation of CH decreases the pore volume hence the associated shrinkage. However, carbonation of C-S-H leads to a calcium deficient silica gel with a higher pore volume [238, 250].

Table 2-2 Solubility and densities of calcium carbonate polymorphs and Portlandite [238]

Modification	Calcite	Aragonite	Vaterite	Portlandite
Solubility(mol^{-1} at 20^{0}C	4.96*10^{-9}	4.62*10^{-9}	12.24*10^{-9}	4.68*10^{-9}
Density (g/cm3)	2.711	2.927	2.664	2.23

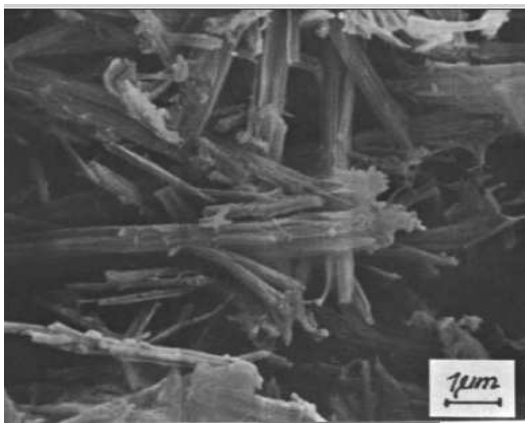

Figure 2-10 Secondary electron image of a tobermorite 11-A before carbonation [247]

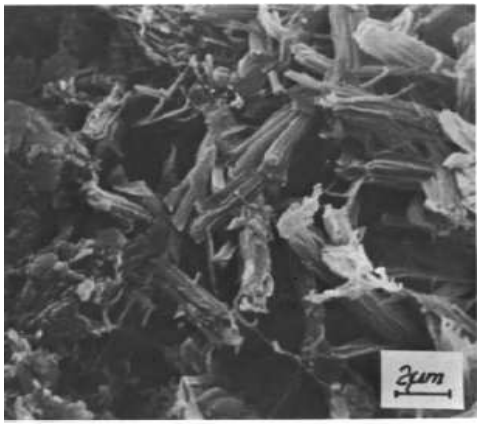

Figure 2-11 Secondary electron image of a tobermorite 11-A after carbonation 30 days at 10%CO_2 and 75%RH [247]

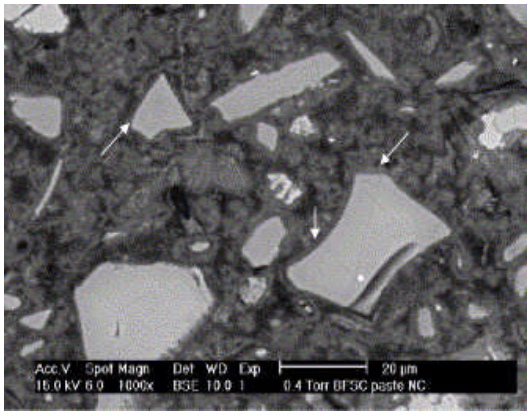

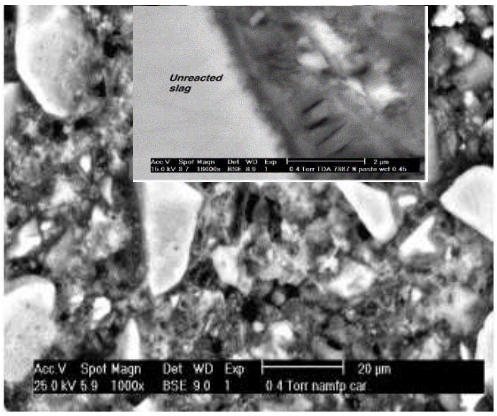

Figure 2-12 BSE of non-carbonated BFS cement showing magnesium rich hydrated rim [250]

Figure 2-13 SEI of BFS cement carbonated at 3%CO_2; insert is the stretched interfacial zone [250]

The effects may be compensatory in Portland cement mixes. However, partially replacing Portland cement with slag increases the C-S-H volume while decreasing the calcium hydroxide content. Therefore, carbonation of the C-S-H in such blends results in a coarsened microstructure.

Šauman [247] observed no significant changes in the rod and flat plate-shaped crystal morphologies in the tobermorite system at low relative humidity. However, increasing the CO_2 concentration and relative humidity to 100% resulted in thinning of the crystals (see Figure 2-10 and Figure 2-11) over longer exposure times. Based on inferences from the adsorption and desorption curves, Johannes and Utgenannt [251] concluded that carbonation effectively increased the proportion of finer pores in the microstructure. Furthermore, coarsening of the microstructure as well as stretched transition zones following carbonation of high slag cements (see Figure 2-12 and Figure 2-13) have been reported elsewhere [250].

2.6 Relationship between composition, microstructure and freeze-thaw resistance of slag containing cements

2.6.1 Evidence of freeze-thaw attack on concrete

Freeze-thaw related degradation may manifest itself through surface scaling; internal structural damage; or a combination of both.

Surface scaling, the commonly reported evidence of freeze-thaw action occurs where concrete subjected to cyclic freezing and thawing is in contact with water containing some form of salt. This is noticeable from the mass loss on the concrete surface and may not necessarily compromise performance. The generally held opinion is that some form of distress occurs in the cover-crete prior to spalling, hence the basis for suggestions that the same mechanism may be responsible for surface scaling and internal damage [34]. Scaling is perceived as the coupled effect of de-alkalination of the surface concrete through chloride interactions (which renders the microstructure porous) and ingress of the solution in contact with concrete [25]. Water in contact with concrete alone facilitates the build-up of freezable water through absorption while the coarsened microstructure provides a repository for water and eventually ice forming centres. Simple assessment for scaling resistance has been through an evaluation of the mass of scaled matter as well as characterising the scaled materials for composition.

Internal structural damage which may not show signs of distress on the outer appearance, however, compromises the structural integrity of concrete. This is observed in exposures where concrete is in contact with water even without saline or de-icing agents. The possibility of internal damage to develop even in exposures where concrete is not in direct contact with moisture has also been suggested [252].

High slag content composite cements are known to exhibit improved resistance to chloride ingress [253]. Carbonation resistance is, however, lower compared to neat clinker systems [230, 254]. In view of the above, pin-pointing scaling of surface material purely to freeze-thaw attack may be somewhat inaccurate.

2.6.2 Mechanisms of freeze-thaw attack on concrete

Expansion associated with the conversion of pore water into ice and crystallisation pressure arising from ice growth are the main paradigms from which a number of proposed freeze-thaw mechanisms spring. Among these are; hydraulic pressure theory [37]; osmotic pressure theory [38]; the closed container theory and the microscopic ice lens growth [252]. These are discussed in the subsequent sections.

2.6.2.1 Hydraulic pressure theory [37]

Capillary water absorption is inevitable for concrete in contact with water. Water saturation of the concrete is, however, heterogeneous (i.e. capillaries near the surface in contact with water is more saturated than those farther away). Assuming the direction of heat flow is from the concrete to the surrounding water, then at a freezing temperature, water outside the concrete would freeze initially. That in the pores may not necessarily freeze at such temperatures as the state of water and ionic concentrations may differ [255]. The ice in immediate contact with concrete provides a seal to further water ingress. Next to freeze is the capillary water in the saturated cover zone. The expandable volume of ice then forces unfrozen water into the less saturated regions. However, the pressure associated with expelling unfrozen water through the porous cementitious media translates into frictional resistance at the water/pore interfaces as well as the hydraulic pressure which are equal but opposite to the expulsive pressure. The magnitude of the pressure expelling the unfrozen water and the tensile strength of the porous media determine the extent of degradation arising from the progressing ice front. Whilst the expansive pressures associated with ice growth causes deterioration, the

mechanism of ice growth is not fully addressed by this mechanism. Beaudoin and MacInnis [256] suggested an internal migration based on the vapour pressure gradients in frozen and unfrozen pores. The suction of the water on the surface of has also been suggested elsewhere [257]. It is noteworthy that, the concept of air entrainment in concrete stemmed from this theory and have proven successful in combatting freeze-thaw induced damage.

However, the theory has some shortcomings in explaining some forms of freeze-thaw induced deteriorations in concretes. First, the fact that the theory considers the behaviour of ice/water interactions in the pores and subsequently the pressure on the pore walls implies that it does not explain freeze-thaw attack in saline environment (e.g. salt-induced scaling). Moreover, the pore solution in concrete contains ionic species and with ice being pure water, the fate of the species and the impact are not accounted for. It has been argued elsewhere [258] that expulsion of the ionic concentration in the pores is implicit following ice growth. Additionally, the observations of volumetric contraction at lower pore spacing [38], as well as continuous expansion (i.e. cryo-deformation) even when freezing has ceased in non-air entrained, concretes [38, 259] further questions the validity of the theory.

The validity of the hydraulic pressure theory in fully explaining the internal structural damage has also been questioned [35]. The pressure generated by the expulsion of water from the pores by was shown to be incapable of causing damage unless the pores are saturated beyond the 91% critical limit [252]. However, saturation above the critical limit is hardly the case in the bulk concrete. In addition, the pore solution is never pure water, therefore, the interface between the ice nucleus and

the pore wall would be a highly concentred ionic solution which will inhibit the complete occupation of the pores with ice [40].

2.6.2.2 Osmotic pressure theory [38]

This mechanism effectively addresses the influence of ionic species in the pore solution. The presence of ionic/molecular species in the pore solution alters the freezing characteristics; implying that, when ions are present in the pore solution, ice crystal formation and growth is selective. Ice is however pure water. This implies that surrounding the ice crystal in a pore is a film of the highly concentrated ionic solution with the pore wall acting as a semi-permeable membrane. The established concentration gradient causes the flow of unfrozen pore solution from the less concentrated region.

Powers and Helmuth [38] however argued that osmotic pressure may not be a primary internal damage mechanism as alkalis are present in trace levels. However, the threshold concentration of alkalis for osmotic pressure development or otherwise has yet to be reported. The theory may be dominant in scaling type of freeze-thaw attack where external alkalis may end up in pore solutions. Additionally, SCMs with significant alkali may theoretically be more susceptible. Experimental studies reported elsewhere [260, 261] show that maximum scaling occurs at about 3% salt concentration irrespective of the nature of the salt (i.e. it is a colligative property). This obviously deviates from the direct proportionality between solute concentration and the migration of water towards the freezing site and consequently fuelled suggestions of salt scaling being a physically than chemically controlled. The explanation for the 3% pessimism is two-fold. For NaCl solution, the tensile strength of the ice crystal was found to vary with the solute

concentration. Çopuroğlu and Schlangen [261] reported highest tensile strength of the crystal and hence the pressure exerted on the pore wall at 3% NaCl. The effect of high concentration is implicit in the second hypothesis, such that defective ice is formed due to the absorption of salts [35]. If scaling only arose in saline environments, the assertion of a physical mechanism may hold. However, surface scaling has long been reported in non-saline liquid exposures [262]. Therefore, if applicable, the osmotic pressure can be instigated by species other than that from the external environment. This is contrary to the suggestions by Valenza and Scherer [36] who argued that the external solution is more influential than the pore solution.

2.6.2.3 Closed container theory [252]

This theory assumes that hydrating cement matrix consists of closely packed individual unit cells. These cells have hollow spheres with impermeable walls. Evaporable water (i.e. freezable and non-freezable) is located within these spheres and if subjected to freezable temperature, water freezes in situ. At a given freezing temperature, pressures resulting from the ice/water phase are transferred to the walls as tensile stresses. The severity of the induced tensile stresses depends on the freezing temperature and the degree of saturation of individual pores. The degree of saturation exceeding 91% is suggested to be critical for freeze-thaw induced damage [252] because of the 9 % increase in volume when the state of water changes from liquid water to ice. Unlike the hydraulic pressure theory, the excessive pressure within individual pores is responsible for degradation.

2.6.2.4 Microscopic ice lens and growth theory [252, 263]

The hydraulic pressure mechanism neglects the potential of ice growing by drawing unfrozen water from its surroundings (including gel pores) which are normally the case. From entropies of water and ice at lower temperatures, water has high potential energy and freely migrates (by diffusion) to the capillary pores where they are attracted to the ice nucleus for growth. The growth in ice crystals consequently exerts pressure on the paste leading to expansion of the entire matrix. Additionally, drawing of unfrozen water from nearby pores has the potential of collapsing the draining pores.

2.6.2.5 Glue spall mechanism

This mechanism based on the tensile stress field generated at the interface between ice and the concrete surface has been suggested as the primary cause for surface scaling [36].

Under this mechanism, the source of degradation is the thermal response of the composite action between ice and concrete. The thermal conductivity of these is however different and hence the response to cooling or melting. For example, ice with thermal conductivity (~2.18 W/m.K) would expand at sub-zero temperatures while concrete or the pore wall (~1.7 W/m.K) contracts and vice versa. The effects would be cracks emanating from the interface but projecting into the individual materials. An illustration of this mechanism as a function of the thickness of ice on the freezing front is shown in Figure 2-14 from [261].

Valenza and Scherer [35, 36] the discussed the capabilities of this mechanism in addressing the existence of pessimum solute concentration, pore solution composition, nature of damage evidenced and the role of air entrainment. It was

argued that excess solutes weaken the mechanical properties of the ice layer which is consistent with the [261]. The possibility of increased compressive strength curtailing crystal growth has not been considered.

The mechanism is purely a surface based one and hence deemed applicable to scaling only. However, in [261] internal damage occurred in addition to scaling but independently. The fate of the ions which may be present in the freezing medium is not also dealt with under this mechanism.

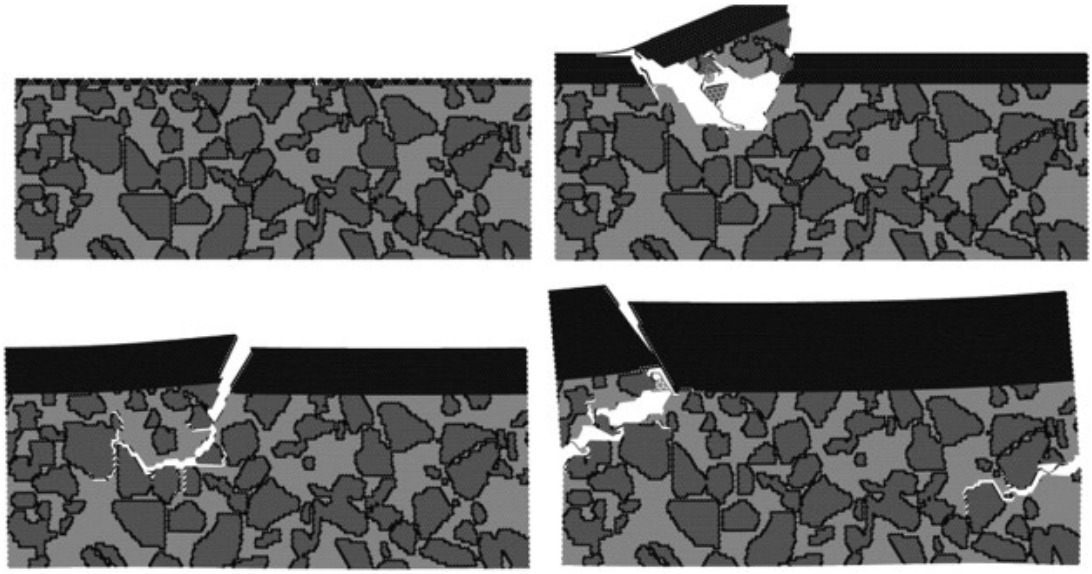

Figure 2-14 Illustration of the glue-spall mechanism of freeze-thaw damage as a function of the thickness of the ice layer [261]

It is conceivable that this would form a concentrated layer between the concrete/pore surface and ice. If this were the case, deterioration would not occur until this layer is forced into the concrete and by osmosis, water is rather withdrawn from the pores. Secondly, scaling is not as a result of internal damage since the spalling goes as far back as the crack propagates. However, ionic interaction between the test solution and pore solution have the potential to weaken concrete.

This is also not limited to the saline environment as carbonation and leaching can decalcify the underlying microstructure and induce internal damage.

2.6.2.6 Crystallisation pressure theory

This theory is a hybrid of the hydraulic and osmotic pressure theories [37, 38]. Similar to the osmotic pressure theory, this considers the pore wall to be permeable however the destructive pressure on the pore wall arises from the interface energies between the ice nucleus, unfrozen water and foreign particles or species in the pore solution [39].

Scherer [39] discussed ice formation and growth from melts and solutions and implications on the magnitude of the interfacial energies between ice/water/particles. It was suggested that a film of liquid always exists between the ice and the pore wall. For sustained ice growth, the ice/particle interfacial energy must exceed the sum of the energies existing between the interfaces of ice/water (liquid) and then water/particle [264]. Consequently, the particles/ionic species are repelled while water from the adjacent pores is drawn. Degradation could, therefore, arise from the pressure on the pore walls due to the rejected particles and or shrinkage due to the drawing of water. It must be said that the particle or ions could also be incorporated into ice depending on the magnitude of these forces.

Scherer [39] evaluated the van der Walls repulsive forces for some oxides which may coexist with water in the pores of hydrated cement. Between quartz, mica and alumina, it was shown that alumina possessed the highest tendency to induce interaction between the pore wall and the crystal (i.e. Hamaker constant). Thus water would be displaced by expulsion or incorporation into ice depending on the

chemical potential for the system. The van der Waals energy was also highest and negative suggesting that, the repulsion would be greater and consequently, the flow of water into the pore rather increases. However, this is also dependent on the pore size, pore morphology and the ice/surrounding film ratio including unfrozen particles and species. The severity of high crystallisation in individual pores has been questioned elsewhere [35, 36]. There is consensus however that, sustained ice growth occurring over regions which control the integrity of the concrete is the cause of deterioration [39, 40].

2.6.3 Factors affecting freeze-thaw resistance

The microstructure of cementitious materials comprises hydration products, pores and anhydrous materials. Pores exist as either gel pores within the C-S-H or capillary pores in locations originally occupied by water. Saturation of the capillary pores is the primary source of freeze-thaw related problems in concrete. In addition to the capillary pores, micro-cracks also act as a reservoir for freezable water and hub for expansion. Porous aggregates also act as repositories for freezable water [265]. For concretes made from freeze-thaw resistant aggregates, freeze-thaw related deterioration primarily concerns capillary pore water, water within the calcium silicate hydrate (C-S-H) gel and the pore distribution of concrete. The air-void sizes and their spacing within the microstructure are the most important parameters with respect to freeze-thaw durability [37].

There is a trend in the literature that slag containing cements have inferior freeze-thaw durability especially in the presence of de-icing salts [25, 44, 250, 266-269]. Among the reasons accounting for the lower freeze-thaw durability are: lower degree of hydration compared to Portland cement; carbonation of the surface layer

resulting in the formation of metastable calcium carbonates which may be soluble in sodium chlorides [25]; permeability of the cover-crete [238]; and disturbance of the air-void content in slag cements [44, 266]. These effects are however only valid at early ages where the degree of hydration of the slag may be low. Limestone addition also deteriorates freeze-thaw durability [24]. However, in either slag or limestone binary blends, the comparison was made to Portland cement and usually at the same w/c ratios. Also, the influence of limestone quality (i.e. the clay content) has not usually been highlighted.

2.7 The relationship between microstructure and freeze-thaw resistance

2.7.1 Clinker composition

The effect of clinker composition on the freeze-thaw durability has been reported elsewhere [270, 271]. There is a consensus that increasing C_3A content lowers the resistance to freeze-thaw. As discussed in previous sections, C_3A may form ettringite, mono-sulphate, carboaluminates or be incorporated into the C-S-H. Stark *et al.* [234] reacted synthetic C_3A with gypsum and assessed the freeze-thaw resistance of the reaction products after 28 days. Increased ettringite content during freeze-thaw was reported independent of the presence or otherwise of de-icing salt. The mechanism was attributed to re-precipitation of ettringite from mono-sulphate. The conversion was necessitated by the thermodynamic stability of mono-sulphate compared to ettringite [272]. Meanwhile, carbonation of ettringite could also lead to mono-sulphate formation [172, 272]. Taylor [271] also suggested an osmotic pressure based mechanism explain the lowered scaling

resistance with increasing C_3A content after testing samples according to ASTM C672. It was shown that the C_3A in question incorporated high fraction of alkalis which end up in the pore solution upon hydration. Consequently, gel-shrinkage due to the migration of water towards the ice-nucleus was facilitated.

Girodet *et al.* [270] found higher C_3S contents to be detrimental while the C_2S and C_4AF contents had beneficial effects on freeze-thaw resistance after testing samples aged 28 days. It is noteworthy that the poorly performing clinkers were the finest in terms of particle specific surface areas. The pore structure would hence differ. However, the chemical effects were explained in terms of the proportion of portlandite in the case of C_3S versus C_2S and the ettringite content for C_3A. A unit C_3S dissolved produces more portlandite compared to C_2S (see equations 2.5 and 2.6). On the other hand, for a given sulphate content, the ettringite content also increases with increasing C_3A content (see equations 2.7). While these are advantageous for strength development, their impact on the pore structure could be deleterious and hence the performance under freeze-thaw [273].

$$2C_3S + 6H \dashrightarrow C_3S_2H_3 + 3CH \quad \text{Equation 2.5}$$

$$2C_2S + 4H \dashrightarrow C_3S_2H_3 + CH \quad \text{Equation 2.6}$$

$$C_3A + CsH_2 + 10H \dashrightarrow C_3A.Cs.H_{12} \quad \text{Equation 2.7}$$

2.7.2 Slag cements

Generally, SCMs impact negatively on the freeze-thaw resistance, particularly scaling [274]. This in part depends on the SCM loading and the degree of reaction and consequently the microstructure at the time of exposure.

Stark and Ludwig [25] related the degree of hydration and the microstructure of slag containing cements to internal freeze-thaw damage and salt scaling. With respect to internal structural damage, freeze-thaw resistance was shown (reproduced in Figure 2-15) to be directly proportional to the degree of slag hydration. Above 50% degree of hydration, slag cement (over 55% slag content) showed superior freeze-thaw resistance compared to the Portland cement. However, the scaling resistance showed no direct relationship with the degree of hydration. The latter was rather identified to correlate with the extent of carbonation of the surface layer.

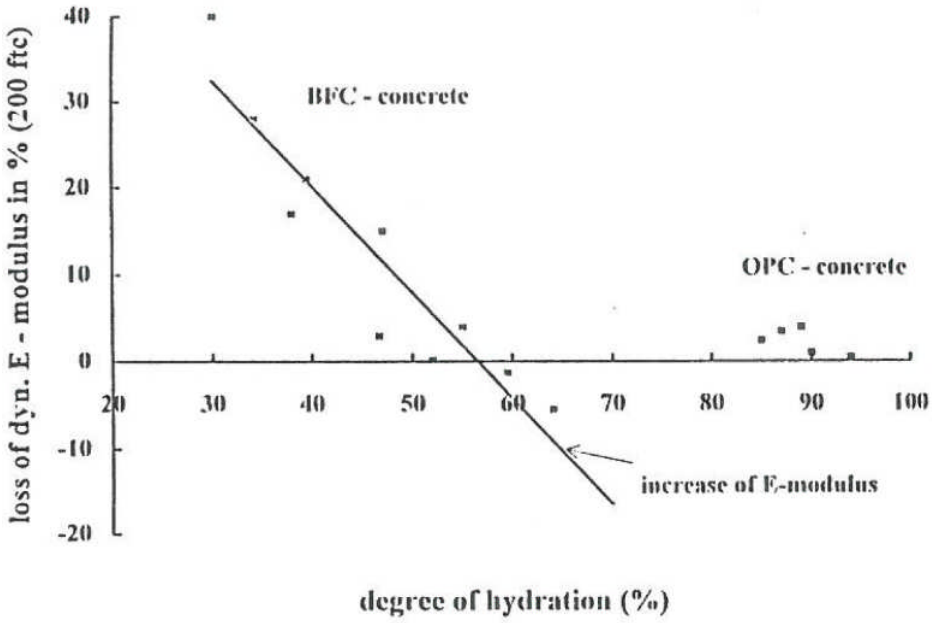

Figure 2-15 Relationship between degree of hydration and internal damage [25]

Chidiac and Panesar [275] however reported significantly improved scaling and internal damage resistance with increasing degree of slag hydration. The contradictory effects of the degree of slag hydration can be pinned to the preconditioning history of samples. In the work of Chidiac and Panesar [275], specimens were cured in a saturated lime solution for 14 days according to ASTM

C-672. However, the CIF method (7 days curing in water and 21days at 65%RH and 20°C) was used in [25]. The latter curing regime facilitates leaching and carbonation and hence at a given degree of saturation, the surface features may be significantly different and consequently the freeze-thaw resistance. Higher effective w/c ratio in composite slag cements due to slow hydration rate also increases susceptibility to carbonation. Consequently, the performance of slag cements with respect to internal damage and surface scaling depend on the pore structure as well as the nature of the test surface.

2.7.3 Limestone

Several factors including dosage, w/c ratio, fineness and air entrainment affect the performance of limestone containing cements subjected to freeze-thaw.

In Portland cement-limestone cements, no detrimental effects on freeze-thaw have been reported for limestone contents up to 15% [5, 6, 24, 276]. However, slight changes in the w/c ratio and higher levels of limestone can be quite damaging [24]. According to the data presented by Dhir *et al.* [24], higher w/c and limestone contents increased susceptibility to carbonation. The increased bleeding capacity at higher w/c and limestone contents explain the lower carbonation resistance and consequently poorer surface scaling resistance. This is consistent with the findings of Li *et al.* [277] who noticed increased loss to abrasion as the limestone content increased. It is noteworthy that in [277], limestone was used as fine aggregate. However, for particle size distribution with a D_{50} of ~15 µm, there is the likelihood of these interacting with other cement hydrates although no phase assemblages were reported by the authors.

The freeze-thaw resistance of clinker-alumino-silicate-limestone cement systems have been reported sparingly. Meddah *et al.* [276] examined quaternary system containing clinker, PFA, slag and limestone blended in proportions of 47.5: 25: 25: 2.5 respectively. The presence of limestone reduced the durability factor compared to a similar ternary system without limestone. The observation could not be explained in terms of carbonation of the surface layer as carbonation depth was similar with or without limestone. Espion *et al.* [278] assessed the internal damage and scaling resistance of ternary blends of varying slag and limestone loading and reported significantly improved performance compared to CEM I following prolonged curing for 91 days. The internal damage resistance was remarkable even when the clinker factor was reduced to ~20 % while the slag and limestone content increased to 50 and 30 % respectfully. The scaling resistance, however, decreased with a reduction in the slag/limestone loading. This is not surprising considering that the proportion of limestone which can react is limited as well as compared to clinker and slag. In addition, the aluminates dissolved from slag constitute the precursor for limestone dissolution [178]. Therefore, unreacted limestone in the hydrated matrix constitutes loosely bonded particles which may be removed following degradation of the surrounded hydrates. The high resistance to internal damage, on the other hand, may be associated with the increase in effective ratio such that, the other constituents react better and hence refining the pores. Furthermore, the increased porosity associated with higher limestone contents [276] can also provide relief centres for the built up pressures associated with ice formation. Whilst this may be advantages for internal damage resistance, it can also be detrimental to scaling as the increased porosity leads to the higher suction capacity of the surface layer.

2.7.4 Effect of carbonation on freeze-thaw resistance of slag-limestone containing cements

The effect of carbonation on the pore structures and carbonation products from Portland cement differs from a slag containing cements [229, 236, 238].

Battaglia *et al.* [279] showed that inadequate scaling resistance of slag cements was attributable to carbonation. This hypothesis was not fully supported by their data such that some non-carbonated samples also showed significant scaling. This was attributed to supersaturation of the samples, although the latter was only speculative. Espion *et al.* [278] reported that cements with high slag contents were more susceptible to carbonation. Direct correlations between carbonation and neither scaling nor internal damage could be found, even after normalising the data by the clinker content.

A number of studies have correlated indicators of carbonation resistance with the freeze-thaw durability particularly the scaling resistance. Basheer *et al.* [228] reviewed the freeze-thaw and carbonation performance indicators of OPC and slag blended concretes and reported a good correlation between water absorption, initial surface absorption test (ISAT) and air permeability. These indicators also correlated negatively with the carbonation resistance. Consequently, concretes with higher permeability may exhibit lower freeze-thaw resistance [269] due to the combination of carbonation of hydrates and saturation of pores.

Çopuro *et al* [280] systematically investigated the effect of preconditioning on the scaling resistance of CEM III/B with the slag content set at 68%. It was reported that the mass of scaled matter increased with carbonation at a given relative

humidity. Additionally, the specimens which were conditioned in demineralized water showed low scaling resistance but the magnitude was about 50 % of that associated with carbonation. However, preconditioning in lime saturated solution significantly reduced the mass of scaled material. The amount of leached Ca ions was found to be 135, 141.5 and 80 after conditioning in demineralized water, NaCl solution and in tap water respectively.

It, therefore, follows that the combined effects of carbonation and leaching impact greatly on the freeze-thaw durability, especially the scaling resistance. Given that calcium ions can influence the freeze-thaw performance and the likelihood of these being incorporated into hydrates in composite cements [31, 177], it is important to clarify their implications in ternary blends of limestone.

2.8 A review of techniques for characterization

Evaluation of the extent of hydration of the individual components in composite cements is vital in understanding the evolution of phase assemblages and pore structure, and consequently mechanical performance and durability. This section, therefore, reviews some of the methods available for studying the hydration and microstructure of composite slag cements and finally the freeze-thaw performance.

The explored methods for assessing hydration in composite cements include heat flow, the bound water and portlandite content, mass or volumetric changes, x-ray diffraction (XRD), scanning electron microscopy (SEM), thermogravimetric analysis (TGA), Nuclear Magnetic Resonance (NMR), FTIR among others [29, 31, 51, 52, 143, 177, 281]. The above techniques evaluate the degree of hydration directly or indirectly. For example, XRD and NMR can measure residual contents

of the individual phases present in clinker directly [29, 31, 178, 282]. By SEM image analysis, the bulk residual clinker content can be quantified. However, the individual clinker phases cannot be accurately resolved.

2.8.1 Isothermal Conduction Calorimetry

The phase assemblages in clinker react with water at different rates to form a host of hydration products. The steps involved in these reactions often involve an initial dissolution followed by precipitation and condensation of polymerised hydrates [283-285]. Isothermal conduction calorimetry (ICC) has been very useful in accurately characterising these reactions in cementitious materials [51, 107].

The calorimeter measures heat output as a function of time [286]. The operational principles involve the conversion of the aggregated temperature difference from sample and reference *(ΔT)* into a voltage difference *(ΔU)* through the Seebeck co-efficient *'E'* according to Equation 2.8.

$$E = N.\frac{\Delta U}{\Delta T} \quad \text{----------} \quad \text{Equation 2.8}$$

Where N is the number of sensors in the thermocouple plate.

$$\varepsilon = \frac{K}{E} \quad \text{----------} \quad \text{Equation 2.9}$$

The heat rate per voltage output *(ε)* is equipment dependent and often termed as the calibration co-efficient (units W/V); and denotes the ratio between the thermal conductance of the calorimeter (K) and the Seebeck co-efficient as shown in equation 2.9. This is, in fact, one of the three critical operational considerations to be taken into account in the interpreting calorimetric data [287]. Together with the baseline *(U_0)* and the time constant *(T_s)*, they determine the thermal power (also

the heat flow) which is computed from the voltage. The relationship between these parameters is illustrated in equation 2.10. The thermal power of a material 'c' is given by [287]:

$$P_c = \varepsilon(U - U_o) + T\frac{\partial[\varepsilon(U-U_o)]}{\partial t} \text{ ---------- Equation 2.10}$$

The extent to which any of the above parameters influences the thermal power depends on the data collection regime and the information to be extracted. Wadso [287] suggested that the calibration co-efficient and baseline are worth considering if the data of interest is the 7 days of reaction while the time constant needs to be accounted for if the early stage reaction kinetics are of interest. Wadso and Wadso [286] suggested up to ~ 5% residual error when a calorimeter was electrically calibrated. The authors rather proposed regular chemical calibration. In addition, the implementation of suitable control runs was recommended to minimise the errors associated with the baseline. Furthermore, careful proportioning of specimens of interest and the reference material taking into account their respective heat capacities (see equation 2.11) and their potential variations over the measurement period [287] can also help to minimise baseline drifts. However, this does not fully eliminate the baseline related errors since changes in the proportions of the individual components changes with hydration time.

$$m_R = \frac{C_c m_c + C_s m_s + C_w m_w}{C_R} \text{ ---------- Equation 2.11}$$

Where m is mass, C is specific heat capacity, c= cement, w is water, s is slag and R are reference material.

Isothermal calorimetry has been used to examine the influence of SCMs on clinker hydration kinetics [29, 51, 52] and estimated the degree of hydration of slag [29].

The heat of reaction (illustrated in Figure 2-16) is made up of an initial peak, a period of dormancy, the main reaction peak, a shoulder to the main peak and steady stage reaction.

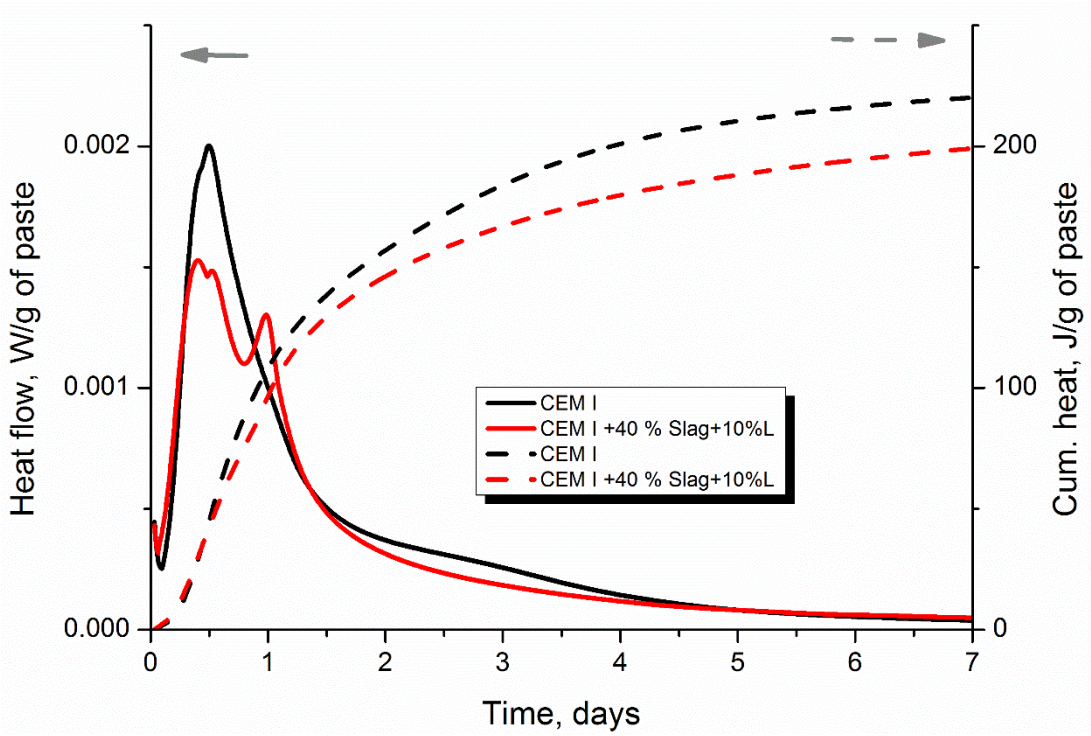

Figure 2-16 Illustrative heat of reaction and cumulative heat of CEM I and composite cement

The initial peak attributable to the particle surface wetting and is often discounted in the analysis of reaction kinetics. Jansen *et al.* [107] studied the kinetics of hydration of OPC by coupling isothermal calorimetry and QXRD. It was reported that the main reaction peak is attributable to silicate dissolution while the shoulder to this peak is indicative of aluminate reaction. The distinction of the two peaks is consistent with recently published data on alite hydration in which the aluminate reaction peak was absent [288]. Based on calorimetry, Berodier and Scrivener [51] found that limestone shortened the dormancy period and hence accelerated alite hydration, while slag exerted a dilution effect by increasing the effective w/c ratio.

This increased the intensity of the silicate reaction peak and was not different from the effect observed in a binary quartz blend. Consequently, it was suggested that slag was inert within the first 24 hours of hydration. The technique has also been used as a proxy for quantifying the degree of hydration of clinker [289] and slag [29, 31]. However, calibration is required either by estimating the anticipated cumulative heat for a given cement system or by comparing the results at a given age with an accurately quantified degree of hydration determined form either SEM, XRD or NMR [29, 143].

2.8.2 Chemical shrinkage

The hydrates of cements are denser than the initial combined density (water and cement) and hence give an indication of the progress of hydration. The changes may be followed by weight or volumetric monitoring system. The technique is standardised in ASTM C-1608-12 and two methods based on direct density or volume measurement are recommended [290]. Setter and Roy [291] utilised the model by Powers and Brownyard [292] as shown in equation 2.12 and estimated that the chemical shrinkage of a pure cement at complete hydration would be 6 cm^3 per 100g of cement. In the same study, the chemical shrinkage increased with increasing w/c ratio as well as in the presence of plasticisers and mineral admixtures.

$$V_t = V_w - B(V_w - V_d)\frac{W_n}{W_t} \text{ ---------- Equation 2.12}$$

Where V_t is the total specific volume (cm^3/g), V_w is the specific volume of water (1 cm^3/g), V_d is the specific volume of the compressed water (i.e. sum of gel, Wg and non-evaporable water, Wn), Wt is the weight of water in saturated hardened

cement paste and B being the sum of gel and non-evaporable water per unit non-evaporable water. This expression $B(V_w - V_d)$ takes the average value of 0.279 cm^3/g for common cements [292, 293].

Application of the dilatometry based technique for studying cements have increased since the earlier work of Geiker [281, 294] and Geiker and Knudsen [294]. During the developmental stages, the technique required manual recording at regular time intervals but automated measurements are now possible [29, 31]. Boivin *et al.,* [295] reported on the effects of sample size and suggested a 10mm optimum sample thickness with inaccuracies resulting from infiltration difficulties in larger samples. Sample sizes exceeding this resulted in artefacts which were dominant beyond 1 day. The effect was eliminated by using the weight based approach except that the setup requirements, in this case, being more complex. The impact of the w/c ratio on the measured shrinkage, however, contradicted those of Geiker and Knudsen [294] and Setter and Roy [291], with a reduction in the chemical shrinkage at higher w/c reported in [295, 296]. Clearly, there is divergence regarding the effect of w/c ratio of cements as measured by chemical shrinkage. Chemical shrinkage is also influenced by temperature. At a given w/c ratio, shrinkage increased with temperature [294, 297]. This was attributed to the enhanced hydration at a higher temperature and consequently the bound water content.

For a given w/c ratio, knowledge of the non-evaporable water content at infinite hydration time can be used to estimate the corresponding ultimate chemical shrinkage. This can then be used to quantitatively establish the degree of hydration. However, the matrix becomes complex for composite cements. In such

systems, calibration with complementary techniques then becomes essential. Parrot *et al.* [298] found direct correlation between chemical shrinkage and isothermal calorimetry as well as the degree of hydration of clinker as determined by QXRD. Whittaker *et al.* [31] and Kocaba *et al*. [29] also reported a correlation between the cumulative heat and chemical shrinkage of composite cements.

2.8.3 Quantitative XRD and the PONKCS method

To understand the hydration of composite slag cement, an assessment of the slag reaction is crucial, though difficult. Backscattered scanning electron image analysis and selective dissolution of the glassy phase are two commonly used techniques [12, 29-31, 299]. However, these approaches have their problems. Selective dissolution was found to overestimate slag hydration, with poor reproducibility [29]. BSEM/IA meanwhile is resource intensive, being a lengthy process, especially when considering very fine materials [28]. X-ray diffraction has been used to quantify the degree of hydration of cement clinker but has struggled with quantification of the glassy slag. The development of the PONKCS method [32, 33] enables quantification of amorphous phases, so offers an alternative to measuring slag hydration. The method also allows simultaneous evaluation of hydrates and non-hydrated phases, ideal for following hydration of cementitious materials.

2.8.3.1 Sample preparation and data collection

The data collection regime can influence the quality of the x-ray powder diffraction scan significantly and hence the results from the quantitative analysis. Factors including the geometry of the diffractometer, radiation type and wavelength, instrument alignment and sample preparation are some of the critical issues which can lead to errors in the scan. McCusker *et al.* [300] and Le Saoût *et al.* [301]

provide useful guidelines on sample preparation, data collection and the subsequent refinement. The volume of powder which can be detected in a diffractometer determines the count. However, this is influenced by the slits, nature of samples and more importantly the particle size. The latter directly dictates population of crystalline phases per unit volume of a specimen as well as the micro-absorption of x-rays. The options are using larger slits or significantly reducing the particle sizes. Mitchell *et al*. [302] compared reducing the particle sizes of commercial clinkers and noticed improved repeatability, particularly for the interstitials and minor phase assemblages. However, the effect of grinding further below 15 µm was small [301] and hence the recommendation to keep powdered samples at ~10 µm. Homogeneity in the particle grading is usually achieved by grinding in a solvent, for example in propan-2-ol [303]. This can, however, interfere with some phases especially in hydrated systems which can influence further analysis.

The preferred orientation of crystals can also occur while placing the ground powders into the specimen holders. Front loading of powders and subsequent pressing with a glass or plastic slide tends to promote cleavage along certain crystallographic planes. The effect is falsely increased peak intensities of the affected phases and hence errors in the quantitative analysis. The tendency for preferred orientation can be minimised through back-loading of specimen [301] which ensures a random distribution of crystals. However, the implementation of the March-Dollase pole-density function [304] or spherical harmonics [305] in common Rietveld refinement packages can model these effects. Notwithstanding, these have their limitations and still require good sample preparation to minimise artefacts.

2.8.3.2 Rietveld refinement method

The Rietveld refinement technique is essentially an optimisation process with the objective of minimising the difference between the experimental and simulated or calculated patterns. The goodness of fit is the residual weighted pattern, Rwp which is defined in equation 2.13 according to [300, 306] as the difference between the observed (Y_o)and simulated (Y_c) patterns.

$$Rwp = \sqrt{\frac{\Sigma w(Y_o - Y_c)^2}{\Sigma w(Y_o)^2}}$$ ---------- Equation 2.13

As discussed in the preceding sections, the anhydrous cement is a polycrystalline material but also contains some amorphous content. Following hydration, the crystalline phases are consumed with either crystalline or poorly crystalline hydrates evolving. Accurate determination of phases present in the anhydrous or hydrated cements relies on the model mixture of all phases present as well as the adopted background function [307-309]. The background can be fitted by interpolation, or one of the several predefined functions may be utilised. Adoption of a predefined background function has been recommended for polycrystalline materials [300]. Different background functions have been utilised from the literature. With regards to the background function, Snellings *et al.* [303] reported similar results from the Chebyshev and the polynomial functions. However, the polynomial order influence the background and consequently the amorphous content calculated. The amorphous content increased with the background while the goodness of fit worsened at low polynomial order. The effects of refinement parameters on the background and the calculated unknown or amorphous content

were also echoed by Jansen *et al.* [310] who concluded that no amorphous content actually exists in OPC if the background function is optimised.

Phase contents can be extracted through the relative intensity method [311, 312], internal standard [307] and external standard [313, 314] methods. The internal standard method requires that a known amount of a given material (i.e. standard) which is not present in the objective material is mixed and scanned together. In the work of Scrivener *et al.* [309], 10 % of corundum was used as the internal standard but blended with the cement prior to hydration with a view to ensuring homogeneity. This has been shown to influence the kinetics hydration [315]. Recent applications, therefore, blended the standard and material with phases to be quantified separately.

The weight fraction of a given phase α can be estimated using the refine scale factor, density and unit cell volume of the phase according to equation 2.14.

$$W_\alpha = \frac{s_\alpha \rho_\alpha V_\alpha^2}{\sum_p s_p \rho_p V_p^2} \text{---------- Equation 2.14}$$

Where s is scale factor, ρ is density and V is the unit cell volume, α is the phase of interest and ρ denotes all phases in the material.

The internal standard method, however, assumes all phases in the scanned material are crystalline. This is often not the case and hence correction factors [316, 317] must be implemented to account for any amorphous phases which may be present.

The external standard method originally described by O'Connor and Raven [318] overcomes the lapses of the internal standard method. With this, a scan of the reference standard or a mixture with a known quantity is separately obtained,

however under similar measurement conditions as the material whose phases are to be quantified. Differences in the absorption coefficients of the standard and material under investigation are also accounted for in the calculations. Based on the scale factor and unit cell densities of the standard, a calibration factor, K is derived. This is solely dependent on the instrument and data collection regime but not on the phases in the sample. Consequently, only amorphous components are not grossly included in the quantification. The relationship between the weight fraction of a given phase, W_a and the calibration constant is illustrated in equation 2.15.

$$W_a = \frac{s_a(ZMV)_a\mu_m}{K} \text{ ---------- Equation 2.15}$$

Where Z is the formula units, M and V are the unit cell mass and volume respectively of the given phase and μ_m is the mass absorption coefficient of the material which is determined from the oxide composition of the material.

Hydrated cements comprise of hydrated phases assemblages which may be crystalline or semi-crystalline, water and unreacted phases. Water dilutes the crystalline phases and hence must be accounted for both in the mass absorption coefficient and the calculated phase contents. A procedure for normalising the results was suggested in [319] and involves applying a factor of say 1.5 for 0.5 w/c ratio.

2.8.3.3 Methods to quantification poorly crystalline or amorphous phases

SCMs are increasingly used in cements for technical and environmental reasons as discussed already. Most of these are however predominantly amorphous and

tend to show a broad hump in x-ray diffraction patterns. The amorphous contents quantified using the any of the already discussed methods does not distinguish between those from hydrates and the unreacted SCMs. To do achieve this, the amorphous phase to be quantified must be accurately modelled [32, 33] and structural parameters assigned for inclusion in the Rietveld refinement of all other phases. This has the advantage of following the progress of hydration of SCMs simultaneously with that of clinker in composite cements as well as the evolution of phase assemblages.

The internal and external standard methods can indirectly quantify the amorphous content by scaling quantified phases to 100% and then assigning the deficit to the unknown content which includes the amorphous material. Kocaba [143] reported a 1:1 relationship between the amorphous contents estimated using the internal and external standards and crystalline phases. However, Scarlett and Madsen [49] and then Madsen and Scarlett [317] found overestimation from these methods and recommended direct methods including the linear calibration, partial or no known crystal structures (PONKCS) or degree of crystallinity methods. The bias calculated for the PONKCS method was 0.2 % (wt) which was about a 10th of that associated with the external standard method.

The PONKCS method relies on the internal standard method to calibrate the phase of interest which can also be a crystalline. A model of the phase is generated from a scan of the pure phase or a mixture in which the phase to be calibrated dominates. This can also be performed on a homogenised mix of the material with a reference standard in known proportions. The latter is preferred since it provides the unit cell parameters and together with the known weights of the standard and

the material of interest, a calibration constant can be determined for this material according to equation 2.16.

$$(ZMV)_a = \frac{W_a}{W_s}.\frac{S_s}{S_a}.(ZMV)_s$$ ---------- Equation 2.16

Where α is the phase to be calibrated, s is the standard, W is the known weights in the homogenized mix, Z is the formula units, M and V are the unit cell mass and volume respectively.

Following the calibration, the ZMV constant for the phase is assigned and the scale factor refined. This can then be implemented in the Rietveld refinement procedure together with the crystalline phases.

The adoption of this method for cements is evolving. Bergold *et al.* [288, 320] followed the evolution of the semi-crystalline C-S-H over the course of hydration of alite. The C-S-H, water and background contributions were modelled separately. The model was generated on a fully hydrated alite. In the refinement, a model for water was introduced to account for the free water contribution to the background. Snellings *et al*. [33] implemented the PONKCS method to follow the hydration of slag in hydrated and synthetic composite cements. The background was modelled with a first order Chebyshev polynomial function with a 1/2Θ term. The C-S-H contribution to the background was modelled from the scan of a fully hydrated white Portland cement using sets of pseudo-Voigt peaks. The slag phase was modelled similarly to the C-S-H. The method yielded consistent results for binary and ternary mixes with ± 2 wt. % bias reported. The composite cements were, however, hydration stopped prior to the XRD scan acquisition and hence the contribution of water to the background was not considered. The hydration stopping is known to

disturb the AFm phases in cements [321, 322]and it remains to be seen if the method yields accurate results in mixes which are not hydration stopped.

2.8.4 Scanning Electron Microscopy (SEM)

The use of backscattered SEM image analysis to follow cement hydration is well documented [28, 29, 31, 46]. The technique is capable of determining the area fractions of residual clinker, hydrates formed and the porosity [46, 323] and by assuming a unit thickness, the volume fraction can be calculated. These microstructural features are segregated based on the grey level histogram which is proportional to the atomic number of the phases contained in the image [324]. Typical BSE images and the associated grey level histogram are shown in Figure 2-17.

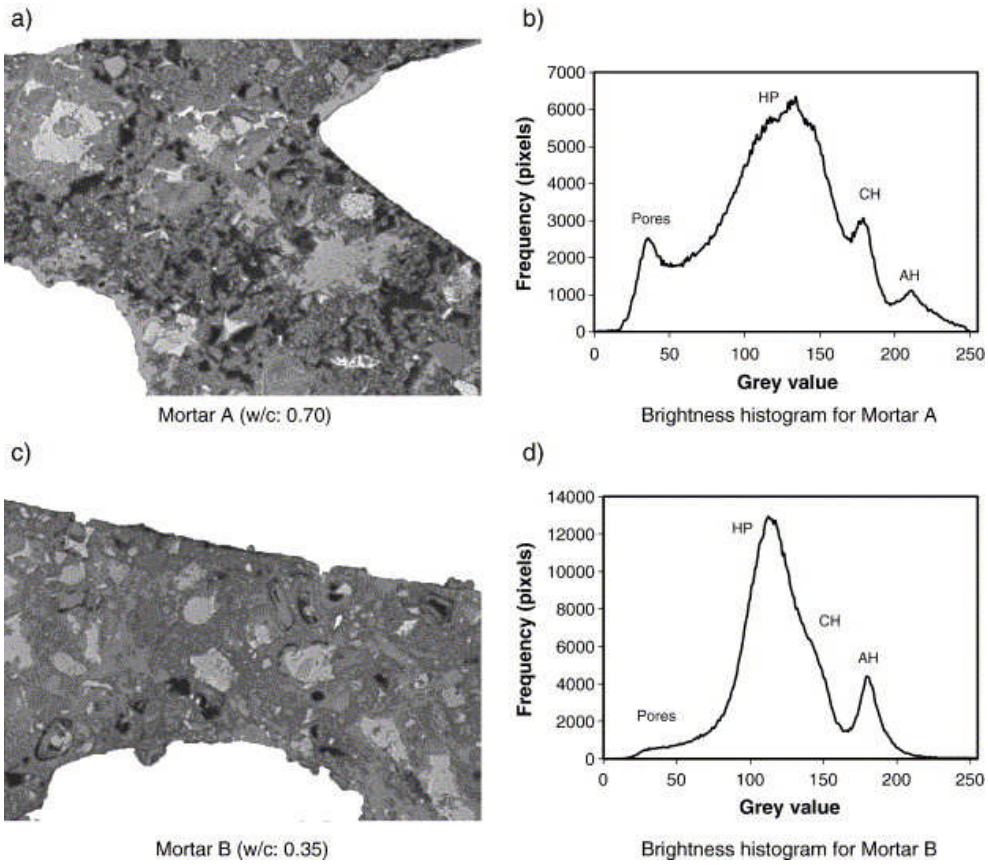

Figure 2-17 Backscattered SEM images with corresponding grey-level histogram [325]

It can be seen that the sharpness of the peak for the pores depends on the age and w/c ratio of in the mix. The threshold for the area fraction of pores is the inflexion point with hydrates [46, 325]. Quantification of the unreacted clinker is straightforward. The area fraction is calculated by thresholding for that region of the grey level histogram. The area fraction calculated from the grey-level histogram is 2-dimensional but the assumption of a unit thickness translates this to a 3-dimensional representation. The degree of hydration of is calculated from the residual and the original.

For SEMs equipped with EDX detector, compositional analysis can also be performed [29, 31, 207]. This is useful in adopting the technique to follow the hydration of supplementary cementitious materials.

Details of the image analysis procedures have been outlined elsewhere [28, 143, 144]. Scrivener *et al.* [323] recommended a minimum of 10 images at 400x magnification. Ben Haha *et al.* [28] performed the quantification on fly ash with 60 images collected at 1600x magnification while Kocaba [143] acquired 70 – 100 images at 800x magnification. The more recent work by Whittaker *et al*. [31] collected 50 images at 800x magnification and but showed that a further increase in the number of images only reduced the standard error without changing the mean.

Comparison between the degree of hydration as determined by SEM/IA and other independent methods have been reported. About 2 % over-estimation is reported [28, 31] due to the inability to resolve particles under ~2 µm. Lothenbach et al. [55] also reported overestimation of slag hydration from SEM/IA compared to the selective dissolution. Since the degree hydration scales the residual to the

originally added contents, lack of homogeneity in the blend could also influence the accuracy of the analysis. It is, therefore, imperative to verify the obtained results independently.

The application of the SEM point counting is an alternative method to image analysis. This technique uses only the electron image without the elemental maps and hence shorten the time dependence significantly. Feng *et al.* [326] quantified the degree of hydration of slag, PFA and clinkers using the technique. However, the degree of hydration based on the loss on ignition was used as the independent method to validate their data. Kocaba [143] compared the degree of hydration of neat cements from SEM point counting and XRD. A good agreement was reported but only for the anhydrous cements.

2.8.5 Porosity determination

The microstructure of aged cementitious materials contain pores in addition to hydrates. Gel pores are contained in the hydrates while the spaces originally occupied by water but are not filled with hydrates constitute the capillary pores. The pore sizes and distribution to a larger extent determines several properties of hardened cement [327] including strength development. The durability in aggressive environments also depends on the pore structure but more importantly to the permeability which is an indicator of the connectivity of the capillary pores. This influenced by the degree of hydration of the constituent materials, curing regime as the w/c ratio. It has been shown recently that, water-filled capillary pores influences the hydration of supplementary cementitious materials [54]. Powers [37, 327] argued that the freezing of pore water occurs only in capillary pores and consequently influences the freeze-thaw durability.

Accurate assessment of the porosity of composite cements is thus imperative in understanding the durability and mechanical property evolution. Methods explored for characterizing the pore structure include SEM [7, 143, 144], mercury intrusion porosimetry (MIP) [328, 329], 1H NMR [330] and computed tomography [331].

The MIP technique is based on the principle that a non-wetting liquid such as mercury can be incrementally forced into a porous media under pressure [332]. Based on the applied pressure (P), the contact angle of the intruded liquid (Ө) and surface tension of the liquid (γ), the entry diameter of the intruded pores can be calculated from the Washburn equation (Equation 2.17). The total pore volume is equivalent to the volume of mercury intruded while the differential of volume per unit pressure yields the pore size distribution.

$$P = \frac{-4\gamma cos\theta}{d}$$ ---------- Equation 2.17

It is to be remarked that, the diameters calculated from the Washburn equation is only the entry diameter and may differ significantly from the actual pores depending on the intruded pore geometry. Additionally, the contact angle of a liquid also depends to a large extent on the state of emptiness of the pores but this can vary considerably with different hydration stopping methods [333].

Diamond [329] and Abell *et al.* [328] compared the intruded pore volumes with those from backscattered SEM/image analysis. First, the capability of MIP to identify submicron sized pores as opposed to image analysis was indicated. Secondly, there is no basis to distinguish between air voids whether entrained purposely or not from pores formed through the hydration. The pore size distribution calculated from the derivatives of intruded volume and pressure was found to be wrongly assigned to the true of pores volumes in cement pastes. The

threshold diameter and intruded volumes were consequently suggested to reasonably reflect the acquired data.

Konecny and Naqvi [334] suggested solvent exchange in propan-2-ol as most effective dehydration technique for samples to be characterised by MIP. Berodier and Scrivener [54] however combined solvent exchange with a vacuum pump to remove remnants of the solvent from the sample. Whilst the data was consistent over the course of hydration, correlations with the microstructural observations were only qualitative.

Recently, Ma [335] examined the impact of sample preparation including sizing technique, particle sizes, hydration stopping among other factors on the results from MIP. Lower particle sizes have the advantage of raising particle surface area and hence larger accessible pores. Sample particle sizes below 5 mm were recommended however through sawing or drilling of cores. Micro-cracks were associated with crushed samples which interfered with the volume of pore sizes exceeding 0.1 µm [335, 336]. The solvent exchange was also recommended for hydration stopping.

Notwithstanding the shortcomings, the MIP technique still provides useful information about the microstructure of cements. It is reasonable to assume that, for the same batch of materials, similarly hydration stopped and measurement performed under same conditions, any errors and misallocations of pore sizes may be uniform and hence provide a basis for comparing the microstructures of cements.

2.9 A review of freeze-thaw testing methods

The freeze-thaw durability of concrete may be evident through scaling and or internal damage. Methodologies for assessing the resistance against these deterioration indicators differ and for scaling or internal damage. This section reviews the standardised methods according to ASTM C666/666M-03(2008) and CEN/TR 151177:2006 for internal damage and then ASTM C672/C672M-12 and CEN/TS 12390-9:2006 for evaluating the scaling resistance of concretes. It should be remarked that the objective of these standards is mostly conservative; in that, they provide a basis for determining the effect of concrete composition on the performance of any chosen test method. With the exception of CEN/TS 12390-9:2006 where a reference method is prescribed alongside alternatives, the choice of the test method is the preserve of individual laboratories. Sample sizes, pre-freeze-thaw conditioning, and test exposed (i.e. test surfaces) are as variable as the test temperature profiles. It is known that larger sizes are more susceptible to deterioration under freeze-thaw cycles [160]. Moreover, Fridh [43] showed that the amount of ice formed at any given temperature increases with a lowering of the freezing rate. Consequently, there is no basis for comparing even the internal structural damage caused by the cyclic freeze-thaw assessed with the different methods detailed in Table 2-3. Indeed the preamble to the scope of CEN/TR 151177:2006 clearly warns about the lack of basis for comparing the performance as measured by the other methods. Also worthy of note are the curing regimes recommended by the various test methods. The methods based on the ASTM provide for 14 days moist curing with curing in lime solution recommended for the internal damage test while the CEN standards recommend 7 days moist curing. Clearly, the additional 7 days of moist curing can make a lot of difference to the

microstructure [54] especially at the early age. For internal damage, ASTM C666/666M-03(2008) defines as 60% relative dynamic modulus or the modulus after 300 freeze-thaw cycles whichever occurs first. CEN/TR 151177:2006, on the other hand, does not define a failure limit but RILEM TC 176 [337] recommends an 80% limit.

Table 2-3 Standardised methods for assessing the internal structural damage during freeze-thaw

Reference		Specimen		Freeze-thaw			
Standard	Method	Size	Conditioning	Test media and profile	Cycles	Indicators	Failure criterion
ASTM C666/666M-03(2008) Standard Test Method for Resistance of Concrete to Rapid Freezing and Thawing	Procedure A: Rapid freeze-thaw in water	Moulded prisms or cylinders or sawn from hardened concrete; 75≤w,d, Θ≤125 mm; 275 ≤L≤405 mm	14 days curing in saturated lime water	Specimen in water for freezing and thawing; refresh water between cycles; test starts from 15 days; + 4 to -18 °C then -18 to +4 °C in 2 – 5 hours	300	Relative Dynamic Modulus of Elasticity (RDME); Durability factor; length; mass	RDME after 300 cycles or 60 % RDME
	Procedure B: Rapid freezing in air and thawing in water	Moulded prisms or cylinders or sawn from hardened concrete; 75≤w,d, Θ≤125 mm; 275 ≤L≤405 mm	14 days curing in saturated lime water	Freezing in air in the chamber; thawing in water; test starts from 15 days; + 4 to -18 °C in air then -18 to +4 °C in water for 2 – 5 hours	300	Relative Dynamic Modulus of Elasticity (RDME); Durability factor; length; mass	RDME after 300 cycles or 60 % RDME
CEN/TR 15177:2006 Testing the freeze-thaw resistance of concrete – Internal structural damage	Beam test	100 x 100 x 400 mm	24 hours in mould, wrapped in plastic for 6 days, 21 days in water at 20 °C	Test starts at 28 days; freezing in air from + 20 °C to -20 °C in 8 hours; thawing by flooding the chest with water or water bath at 13 ±8 °C for 4 hours	56	RDME, Mass change	-
	Slab test	Sawn slab from 150 x 150 x 150 mm cube	24 hours in mould, 6 days in water bath, 21 days in climate chamber	All sides except the sawn surface insulated; dyke filled deionized water and sealed to prevent evaporation; 72 hrs re-saturation before freeze-thaw test starts; temperature in freezing medium held above the test surface from + 20 °C to - 20 °C in 16 hours, then - 20 °C to + 20 °C in 4 hours	56	RDME, Length change	-
	CIF	150 x 150 x 150 mm cubes split into halves using PTFE plates as test surfaces	24 hours in mould, 6 days in water bath, 21 days in climate chamber	Lateral sides sealed with epoxy resin; test commences after 28 days; 7 days re-saturation in deionized water; cooling liquid temperature from + 20 °C to - 20 °C in 4 hours, held at - 20 °C for 3 hours and then - 20 °C to + 20 °C in 4 hours	56	RDME, Length change, water uptake	80 % RDME (RILEM TC 176)

2.10 Summary of key literature and approach to address gaps

Incorporation of higher levels of SCMs presents a viable alternative to minimising the carbon footprint of cement. The synergy between aluminates from slag and carbonates in limestone enhance mechanical properties derived from limestone ternary blends. The literature has demonstrated that components in composite cements affect the reactivity of each other. With regards to clinker reactivity, nucleation and dilution effects have been distinguished in the presence of both limestone and slag. However, the influence of impact of limestone on the alumina-silicate reaction and vice versa have not been addressed. The limits of constituents and impact of such synergies on durability have not also been addressed in the literature. The first step towards this is the ability to accurately quantify the reactivity of all components and subsequently examining the impact of varying the individual components on hydration and microstructure development.

A range of methods has been explored in the literature to follow hydration of GGBS. Backscattered scanning electron image analysis and selective dissolution of the glassy phase are two commonly used techniques [12, 29-31, 299]. However, these approaches have their limitations. Selective dissolution was found to overestimate slag hydration, with poor reproducibility [29]. BSEM/IA meanwhile is resource intensive, being a lengthy process, especially when considering very fine materials [28]. X-ray diffraction has been used to quantify the degree of hydration of cement clinker but has struggled with quantification of the glassy slag. The development of the PONKCS method [32, 33] enables accurate quantification of amorphous phases, so offers an alternative to measuring slag hydration. The method also allows simultaneous evaluation of hydrates and non-hydrated phases, ideal for

following hydration of cementitious materials. The reported applications have not confirmed the capability of the technique for complex mixes as non-hydration stopped ternary systems. The stability of the calibrated phases with different dehydration techniques has not also been examined previously.

Finally, limestone levels exceeding 15% in binary composite cements negatively affect the freeze-thaw resistance [6]. In ternary slag blends, the reactivity of limestone and slag are likely improved and in addition, new hydrates formed. The effect of these on the freeze-thaw resistance of limestone cements is not known. Moreover, there is no consensus on the mechanism for freeze-thaw damage [36, 37, 39, 40, 338]. Despite the crystallisation pressure and glue spall theories receiving much attention recently, none fully explains the carbonation related mechanism in composite slag cements. It appears that the entire freeze-thaw process needs to be approached more fundamentally by interrogating the problem in the presence of deionized water.

Chapter 3
Materials and methods

3.1 Materials

The cements investigated were formulated from CEM I, GGBS, limestone powder, and anhydrite, herein designated as C, S, L, and s respectively. The CEM I and GGBS were further classified as 1 or 2 according to their fineness, with those designated 2 being relatively finer. Two limestone powders, differing in fineness, were also examined. A list of the materials along with their Blaine fineness and specific gravity are given in Table 3-1. The chemical compositions of the materials, determined by XRF, are shown in

Table **3-2**.

The mineralogical composition of the cements and the supplementary materials are shown in Table 3-3 and Table 3-4 respectively. Particle size distributions of all materials, as measured by laser granulometry, also are shown in Figure 3-1 to Figure 3-3.

Table 3-1 List of materials and Blaine and their fineness for composite cements

Material	Designation	Blaine fineness (m^2/kg)	Specific gravity, g/cm^3
CEM I	C1	400	3.14
	C2	600	3.12
Slag	S1	400	2.94
	S2	600	3.0
Limestone	L1	400	2.72
	L2	700	3.01
Anhydrite	s	450	2.94
Quartz	Q1	300	2.98
	Q2	600	3.01

Table 3-2 Oxide composition of raw materials (%wt.)

Composition	SiO_2	Al_2O_3	MgO	CaO	K_2O	Na_2O	SO_3
CEM I [C]	20.37	5.56	1.65	62.10	0.65	0.49	3.54
Slag [S]	34.87	11.62	5.82	41.82	0.47	0.01	3.13
Limestone [L]	2.00	0.08	0.64	53.13	0.10	-	0.07
Anhydrite [L]	2.94	0.60	1.45	38.32	0.16	-	52.24

Table 3-3 Mineralogical compositions of the CEM I 42.5 R [C1] and CEM I 52.5 R [C2] (%wt.)

Phase	C_3S	C_2S	C_3A	C_4AF	Calcite	Anhydrite	Bassanite	Others
[C1]	54.0	17.1	9.3	7.5	3.9	2.1	2.2	3.9
[C2]	58.1	14.3	9.2	6.7	1.9	1.7	3.0	5.1

Table 3-4 Mineralogical compositions of supplementary materials (%wt.)

Phase	Calcite	Quartz	Anhydrite	Amorphous
Slag (%)	2.4	0.1	-	97.5
Limestone (%)	99.6	0.4	-	
Anhydrite	-	1.2	98.8	-
Quartz (%)	0.5	99.5	-	-

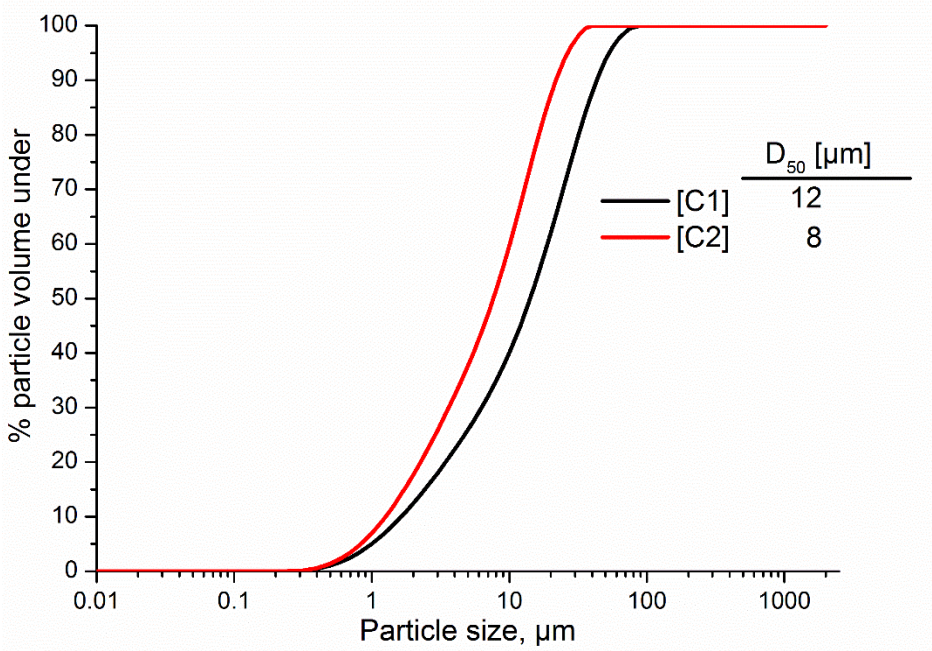

Figure 3-1 Particle size distribution of the investigated clinkers as determined by laser granulometry

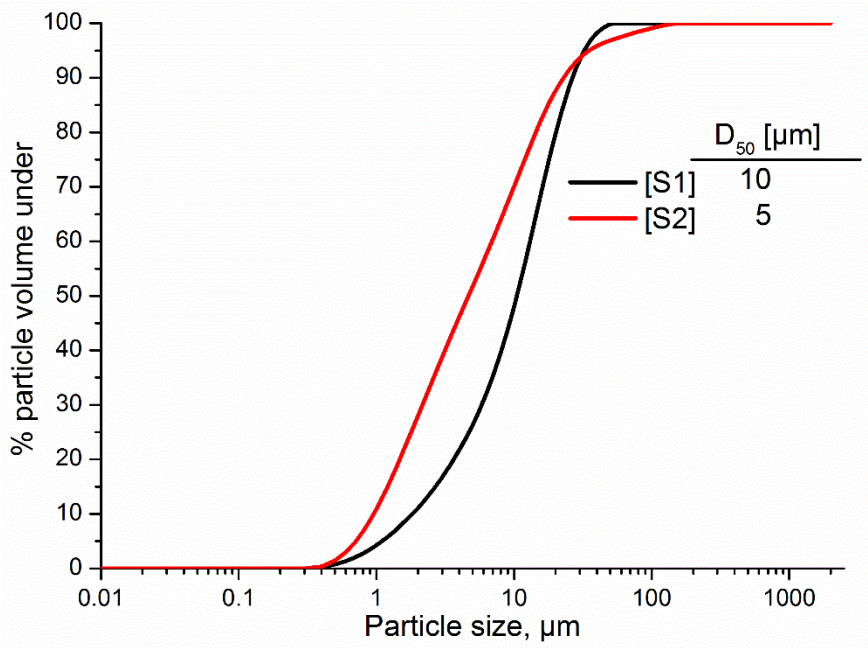

Figure 3-2 Particle size distribution of the investigated slags as determined by laser granulometry

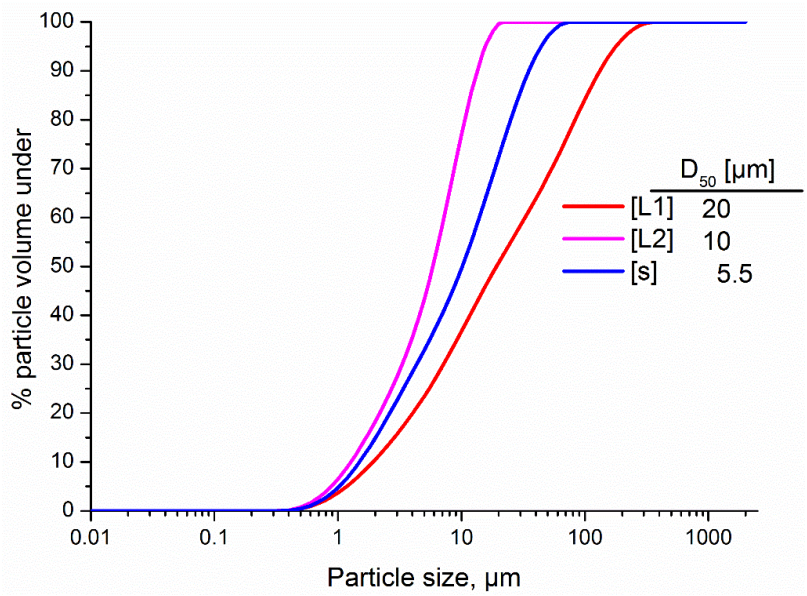

Figure 3-3 Particle size distribution of constituent materials

Limestone [L], anhydrite [s] and filter dust [F] used in this studied, as determined by laser granulometry

Particle size distribution and compositional analysis of the aggregates used for producing mortars and concretes are shown in Figure 3-4 and Table 3-5. The coarse aggregates were uncrushed quartzite.

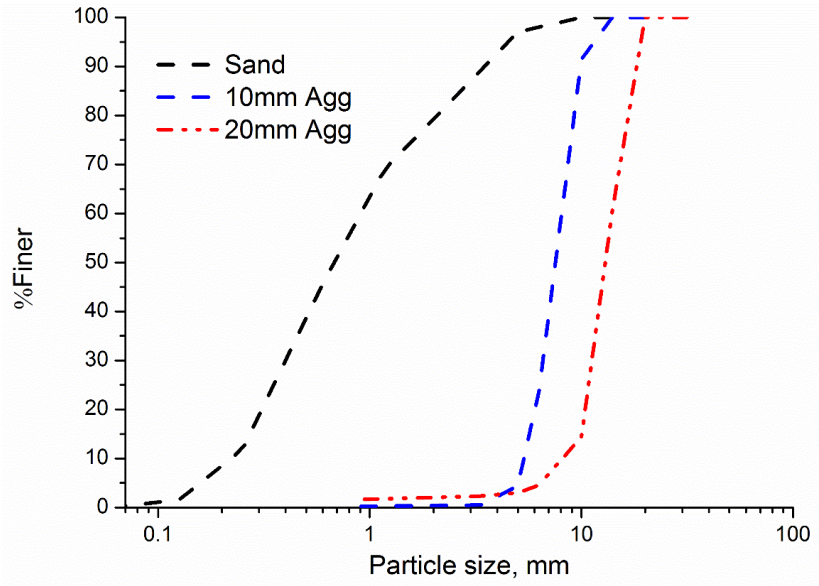

Figure 3-4 Particle size distribution of aggregates

Table 3-5 Properties of aggregates

Composition	Fine aggregates(%)	Coarse aggregates(%)
Fe_2O_3	0.045	0.65
CaO	28.3	24.5
SiO_2	23.6	44.3
MgO	4.78	4.1
Al_2O_3	15.15	2.1
TiO_2	0.05	0.12
K_2O	0.4	0.21
Na_2O	0.25	0.18
Water absorption (%)	0.9	2.0
Saturated surface dry density (g/cm^3)	2.61	2.57

3.2 Formulation of mixes

Twenty-two (22) mixes were prepared from the materials described in section 3.1 for the preliminary investigation into compressive strength development, chemical shrinkage and heat of reaction. In preparing the composite cements, slag with or without limestone was added to the CEM I according to the ratios described in Table 3-6. The formulation criteria were to maintain a clinker: SCM ratio of 1:1 and total sulphate content of 3 %. Limestone was considered as part of the SCM. Consequently, the limestone content already present in the CEM I as a minor additional component (4.1 % in CEM I 42.5 R and 1.9 % in CEM I 52.5 R) was taken into account while calculating the SCM content of the individual mixes. Additionally, the sulphate present in the CEM I as basanite or anhydrite was also taken into account while maintaining the 3 % sulphate content in all composite cements. Ground natural anhydrite was added to achieve the sulphate balance.

The objective of the scoping study was to identify key cement compositions which would provide a basis for examining the factors which influence the strength and freeze-thaw resistance of limestone ternary blends while also permitting the effect of composition on hydration and microstructure to be established as detailed in section 1.4.

Table 3-6 Proportioning and nomenclature of cements for preliminary study (% wt.)

Nomenclature	CEMI		Slag		Limestone		Anhydrite
	C1	C2	S1 (Q1)	S2 (Q2)	L1	L2	s
	%						
C1	100		-	-	-	-	
C2		100	-	-	-	-	
C1Q1	52.2		47.8(Q)	-	-	-	-
C2Q1	-	51.8	48.2(Q)	-	-	-	-
C1Q2	52.2		-	47.8(Q)	-	-	-
C2Q2	-	51.8	-	48.2(Q)	-	-	-
C1S1	50.9	-	46.6	-	-	-	2.51
C2S1		50.7	47.1	-	-	-	2.24
C1S2	50.9	-	-	46.6	-	-	2.51
C2S2		50.7	-	47.1	-	-	2.24
C1S1-10L1	51.9	-	38.1	-	7.5	-	2.51
C2S1-10L1		51.2	38.0	-	8.6	-	2.24
C1S2-10L1	51.9	-	-	38.1	7.5	-	2.51
C2S2-10L1		51.2	-	38.0	8.6	-	2.24
C1S1-10L2	51.9	-	38.1	-	-	7.5	2.51
C1S2-15L1	51.9			33.3	12.3	-	2.51
C2S1-15L1	-	51.2	33.3	-	13.3	-	2.24
C2S2-15L1		51.2	-	33.3	13.3	-	2.24
C1S2-20L1	51.9	-	-	28.5	17.0	-	2.51
C2S1-20L1	-	51.2	28.5	-	18.1	-	2.24
C2S2-20L1	-	51.2	-	28.5	18.1	-	2.24
C2S2-10L1-10L2	-	51.2	-	28.5	9.0	9.0	2.24

The results from the scoping studies are presented in Appendix A.1.2. Based on the results, three (3) mixes were selected for developing the PONKCS method for quantifying slag hydration. Details of these mixes are given in Chapter 4. Six (6) mixes were further chosen for the full-scale hydration, strength development and freeze-thaw resistance studies. The mixes considered while pursuing the individual objectives outlined in Section 1.4 will be given in the Chapters where the respective results are presented.

3.3 Sample preparation

3.3.1 Hydration and microstructure characterisation

The hydration studies were performed on cement pastes. The plastic pastes were prepared according to the procedure described in EN 196-1 but without aggregates. In all cases, the w/b ratio was 0.5 as has been used elsewhere [31, 196]. For isothermal calorimetry and chemical shrinkage, mixing was performed on a vortex mixer due to the size of samples and the need to avoid contamination of the samples. Samples were weighed into the test ampoules or beakers in the case of chemical shrinkage and the appropriate amount of water added. The mixing procedure involved 30 seconds of mixing at low speed followed by a 90-second pause. Mixing resumed afterwards for 60 seconds at high speed before the ampoules were either transferred into the calorimeter or for further processing in the case of chemical shrinkage.

For XRD, TGA, SEM and MIP, specimens were cast into 15ml plastic vials and covered with para film before capping the vials [29, 54, 339]. The filled vials were then kept on a tube rotator and centrifuged at 20 rpm for 12 hours. The objective here was to prevent bleeding in the pastes. The vials were subsequently placed

in a water bath which was maintained at 20 °C until testing. For pore solution analysis, the pastes were put into 200ml (up to 1 day) or 500ml (≥7 days) PE bottles, capped and sealed and stored at 20ºC [17].

Compressive strength tests were performed on mortar samples also prepared according to EN 196-1 as described previously. The mix ratio of binder/sand/water was 1:3:0.5 respectively. Sand was introduced after the initial 30 seconds of mixing the paste at low speed. However, the mixing following the addition of sand was at high speed. During the 90 seconds pause, mortar adhering to the sides of the mixer is scraped from the sides before further mixing. The mortars were cast into 40 x 40 x 160mm moulds. Filling of the moulds was done in two layers on a vibrating table operated at 50 Hz frequency. After demoulding, samples were immediately transferred into curing tank containing saturated lime solution which was kept at 20ºC.

3.3.2 Samples for freeze-thaw testing

The freeze-thaw tests aimed at assessing scaling and internal structural damage were performed on concrete samples. Microstructural changes associated with freeze-thaw were however characterised on cement paste samples.

The preparation of concrete specimens was according to EN 12390-1 in 150 mm cubes. The moulds were lightly oiled to ease moulding. Two opposite sides of the mould were then fitted with Polytetrafluoroethylene (PTFE) plates to provide the freeze-thaw test surfaces. The specimens were kept in the mould for 24 hours before demolding. The cubes were then transferred into curing tanks containing tap-water. When the cubes were 7 days old, they were removed from the curing tanks and then divided into two halves as illustrated in Figure 3-5.

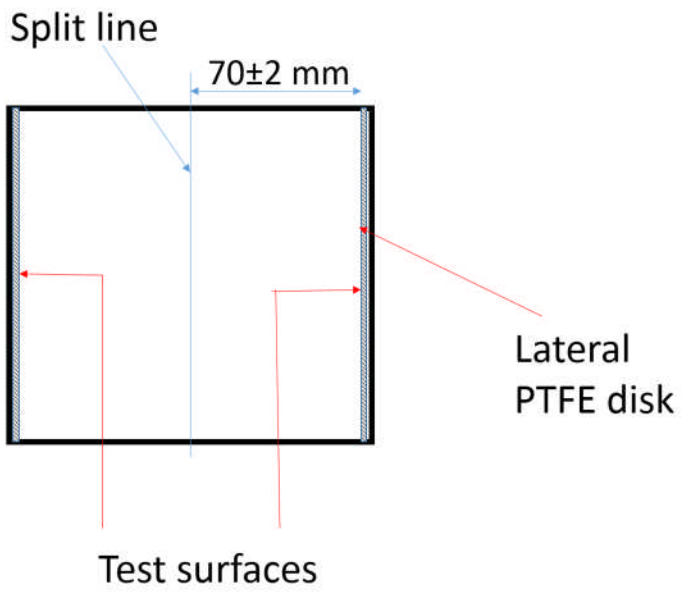

Figure 3-5 Arrangement of lateral PTFE and splitting of samples for freeze-thaw test

For monitoring the microstructural changes during freeze-thaw, four paste samples were prepared from cements C1[C], C2S1[CS], C2S1-10L [CS-L] and C2S1-20L [CS-2L]. The samples were prepared in accordance with the procedure outlined for the hydration studies in section 3.3.1. Two sets of each sample were prepared and each set was conditioned by one of two regimes as listed below:

1. Sealed for 7 days, then exposed for 21 days before saturation [340]. The rationale here was to simulate the surface of the samples when they have been exposed for 21 days following 7 days moist curing.
2. Sealed for 28 days before saturation. Here, objective was to simulate the state of the paste in the bulk of the sample

At the end of the 7 or 28 days curing under sealed conditions, each sample was crushed and then sieved into 1 – 2mm thick sized samples. For the 28 days sealed, crushing was done in the glove box to minimise carbonation. In addition to the

crushed samples, 2mm thick slices were obtained from each sample for microstructural investigations during freeze-thaw. The samples, sealed for 7 days and exposed for 21 days, were further saturated in deionized water for 7 days at a liquid/solid ratio of 1 in 100. Meanwhile, the 28 days sealed samples were saturated at the same liquid/solid ratio but with a saturated lime solution instead. As a result, the samples were labelled as [7d- 21d exp-7d sat] or [28d-0dexp-7d sat (lime)]. The timelines for testing of samples are shown in Figure 3-6. At each point, samples were analysed by XRD and TGA.

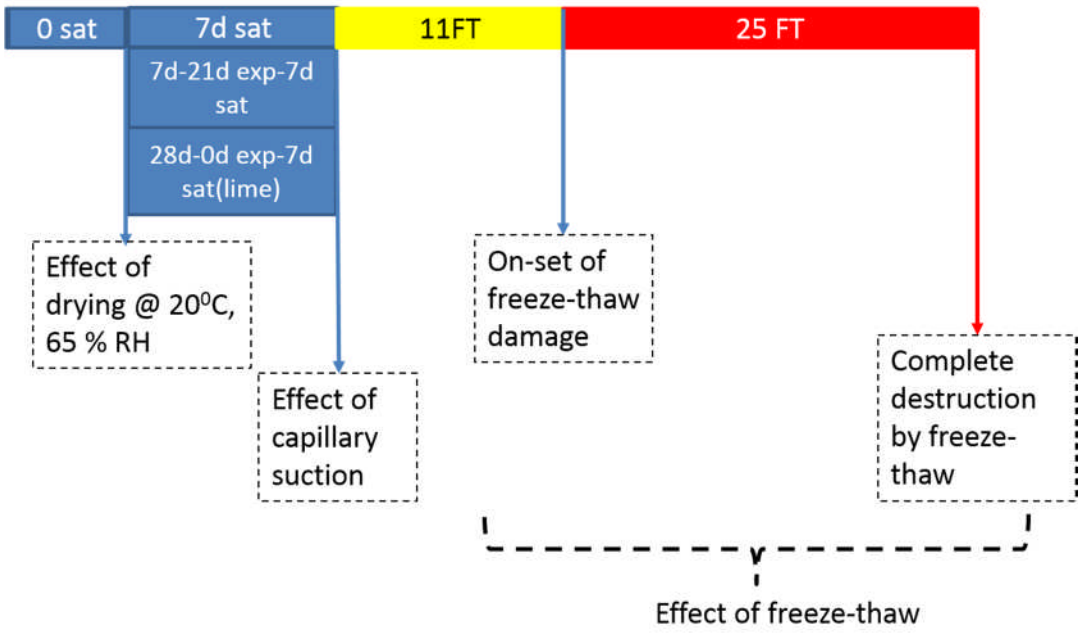

Figure 3-6 Programme for characterization of paste samples during freeze-thaw

Changes to the composition and mechanical properties of the C-S-H was also analysed for the paste samples which were conditioned according to CEN/TR 15177 [340] (i.e. 7d-21d exp-7d sat). The selected characterization points were after saturation (i.e. 0 FT) and then at the end of the experiment (i.e. 25 FT).

The indentation measurements were performed with a CSM-NHT cube corner indenter on 10 x10 grid. The grid matrices were spaced at 75 – 100 µm with the

applied load levels ranging between 250 mN to 400mN. An illustrative grid and indent is shown for the sample C-7d-21d exp-7d sat-25FT in Figure 3-7.

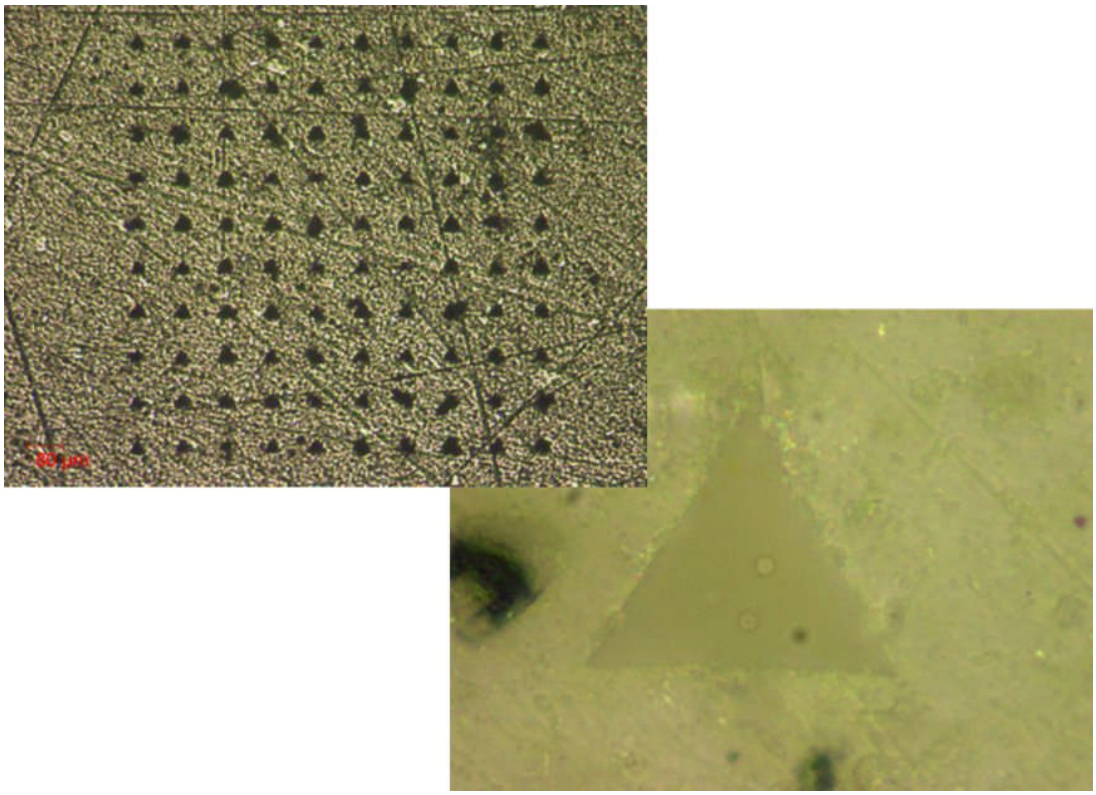

Figure 3-7 Illustrative grid and indent for evaluating changes in the mechanical properties of the C-S-H.

Complementary 15 mm diameter cylinders, were also prepared and conditioned according to [340]. The cylinders were saturated with deionized water and leachates analysed after the 7d saturation, then after 4, 11 and 25 FT cycles. Analysis of the leachate was performed on a Metrohm 940 Ion Chromatographer. Calcium and sulphates were the leachates of interest.

3.4 Hydration stopping

Technique constraints, for example, emptying of pores for MIP and SEM, as well as equipment availability issues, often impose a requirement to remove free water

from hydrating cement pastes. Water, however, may exist in different states within the hydrating cement matrix depending on its location – either in the hydrated assemblage as gel water or between hydrates as capillary water. During hydration stopping, the objective is to remove the capillary water. This can be challenging since the implementation of inappropriate dehydration techniques can impact significantly on the hydrated phase assemblages and the microstructure as a whole. Several methods have been implemented in the literature with notable studies on dehydration by Collier *et al.* [321] and Zhang and Scherer [322].

The question of which method is most appropriate remains an open one and very much depends on whether the dehydrated sample is to be characterised for phase assemblages or pore structure. Gallé [333] found freeze-drying to be least detrimental to the pore structure when compared to oven and vacuum drying. Not only were the intruded pore volumes different among the techniques, the pore size distributions were also different, with oven drying most detrimental. On the contrary, Collier *et al.* [321] found freeze-drying to induce the most cracks in the microstructure compared to oven drying at 60 ^{0}C and vacuum drying. Solvent exchange using acetone was suggested to preserve the pore structure but the structure of AFm was affected, as seen in the diminishing intensity of the XRD reflections for the phase. Knapen *et al.* [341] however noticed interactions between hydrated phase assemblages and ether, ethanol and methanol. Consequently, in the analysis of hydrated phase assemblages, they recommended vacuum drying over the solvent exchange, as the former does not present the environment for potential interactions with cement hydrates. A similar view was held by Zhang and Scherer [322] who recommended freeze-drying for chemical analysis of cementitious materials while solvent exchange by propan-2-ol was most efficient

for microstructural analysis. The studies by Whittaker and Black [342] however noticed decomposition of AFt and AFm phases after dehydration to constant weight through freeze-drying.

The literature cited above clearly shows reported weaknesses in existing dehydration methods. It is reasonable for phase assemblage characterization to be performed on freshly ground specimens or to use techniques which limit the modifications resulting dehydration. This is particularly important in limestone containing composite cements, where the AFm phase assemblages are of utmost importance. Furthermore, implementation of the PONKCS method to follow the residual slag content requires stricter control of the background function. This is, however, sensitive to the presence free water in the mix in addition to non-crystalline reaction products such as the C-S-H [33, 320].

The dehydration method was optimised through XRD and thermal analysis on three mixes after hydrating for 1, 2, 7 and 28 days. Four dehydration regimes were investigated and compared to freshly ground hydrated cement pastes as detailed in Chapter 4.

3.4.1 Freeze-drying

The freeze-drying technique removes water from the hydrated cement paste by sublimation [322, 333, 334]. The hydrated cement disks were cut 2 mm thick using a low-speed Isomet. The disks were weighed and immediately placed into liquid nitrogen where water in the pores was frozen at -196 ^{0}C. The disks were kept in the liquid until equilibrium; when no further boiling around the disk could be noticed. The disks were transferred from the liquid nitrogen into the Edwards Modulyo freeze dryer (operated at -45 ^{0}C). The pressure within the dryer was, however,

variable up to 4 bars and depended on the vapour pressure from the specimens. The freeze dryer was connected to an external pump to suck the sublimed water vapour from the chamber and hence maintain vacuum conditions. Specimens were weighed until the mass difference between successive measurements exceeded no more than 10% [144]. This was usually attained after 48 hours depending on the age of the specimens and consistent with the duration employed elsewhere [322]. Weaknesses of the freeze drying method including cracks induced by ice crystallisation [338], dehydration of AFt and AFm phases [343] and the C-S-H [339] are well documented.

3.4.2 Solvent exchange

The solvent exchange technique employs organic solvents to displace water from the pores. Propan-2-ol (IPA) is preferred to other solvents including acetone, ethanol and methanol due to its low vapour pressure, density and surface tension [322]. Due to its volatility, vacuum extraction [54] or direct drying methods [33] have used been for removal from porous materials. However the penetrable depth is limited by the specimen size, and also the evaporation rate is lower compared to other solvents. This implies longer times to ensure complete dehydration and IPA removal. This is overcome by reducing the sample sizes, increasing the IPA to sample ratio [322] and using alternative IPA removal techniques.

Propan-2-ol has a much higher boiling point than other common organic solvents. Consequently, a two-stage exchange with ether, with a boiling point of 35 ^{0}C, is common [52, 201]. Ether is less dense, almost inert with smaller polar surface area and surface tension at room temperature compared to IPA. It, therefore, reaches into finer pores causing minimal damage whilst displacing IPA by acting as receptors for hydrogen ions. Further reasons for the widespread use of IPA for

dehydration of cements include the high vaporisation pressure (0.602 KN/cm^2) and diffusion coefficient (2.02 x 10^5 cm^2/s). In the absence of standardised solvent exchange protocol, the chosen method must be optimised before adoption.

Two sample sizes were examined for solvent exchange method: 2 mm discs and then samples crushed into ~1 mm in IPA. For the samples crushed in IPA, the samples were left in the solvent for 20 minutes before filtering. The residue was subsequently flushed three times with diethyl-ether before drying at 40 °C for 20 minutes on a pre-heated glass plate. This procedure was performed entirely in a glove-box which was purged with nitrogen gas to minimise potential carbonation.

The 2 mm disks were stored in IPA for 48 hours with a 1:500 sample/IPA weight ratio as suggested elsewhere [344] and was not recycled. After 48 hours, the IPA was either removed by one of two methods. The first method involved rinsing the disks three times in diethyl-ether and then on a pre-heated glass plate for a further 20 mins. The second method involved 24 hours in a desiccator with vacuum maintained through Edwards vacuum pump operated at 22 mbar. The methods investigated were based on those employed in the literature [33, 54].

Irrespective of the method used, the hydration stopped specimens were stored plastic mini-grip bags and stored in a vacuum desiccator over silica gels.

3.5 Techniques for hydration studies

3.5.1 Isothermal conduction calorimetry

Calorimetry measurements were performed with an 8–twin channel TAM Air calorimeter shown in Figure 3-8. The 6.0 g sample taken from bulk batches of the neat or composite cements was mixed with 3.0g deionized water in 30ml

ampoules. The reference was quartz and proportioning was based on Equation 2.11 from section 2.8.1 taking into account the specific heat capacities of all materials [286, 287]. The reference mix was first prepared and introduced into the calorimeter (B of the relevant channel) before commencing the baseline acquisition. Test sample details were also pre-programmed into the data collection software. In this study, the moderate signal stability criterion was chosen [286]. The criterion was deemed satisfactory when the signal gradient was ≤ 2 μW/h and standard deviation of 4 μW. On attainment of the stability conditions, the test samples were mixed as described previously and introduced into designated channels using stainless steel hooks. Samples were run in blocks to avoid disturbances from adjacent channels. After introducing samples into the calorimeter, the signal was considered correct after 45 mins and data collection continued for 28 days. Samples were run in duplicates and reproducibility assessed through independent runs. On completing a run, the baseline was automatically acquired by and results resampled at 300 seconds equidistant intervals to facilitate comparison with the shrinkage data.

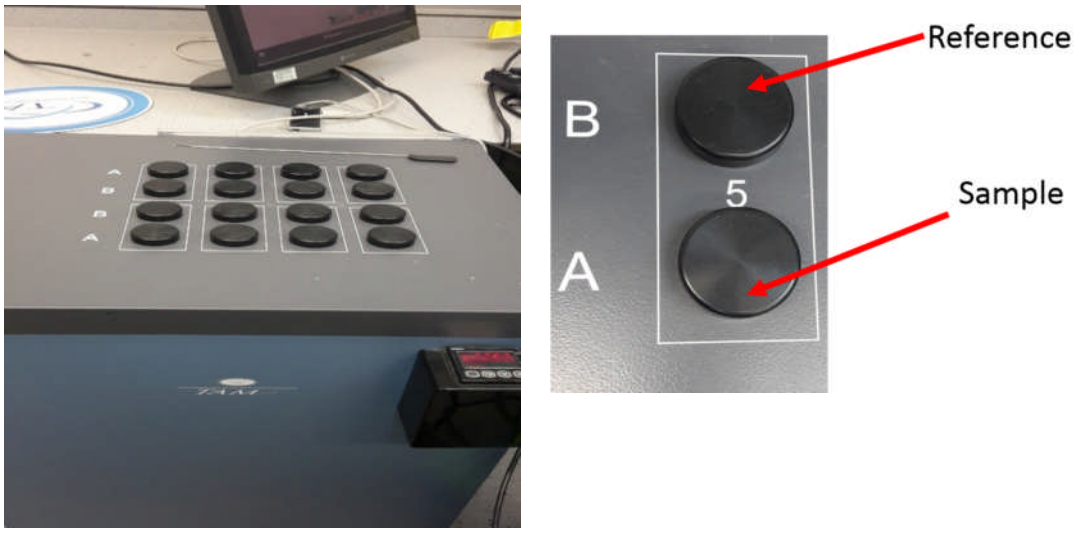

Figure 3-8 Setup for the acquisition of heat of reaction data

(Zoom into twin-channel showing reference and sample channels)

The extraction of the contribution of slag to the heat flow was based on a similar methodology as for chemical shrinkage discussed in the next section.

3.5.2 Chemical shrinkage

The chemical shrinkage tests were performed according to the methods described elsewhere [29, 31, 281]. The accessories and experimental setup are shown in Figure 3-9.

The 60ml plastic beakers were filled with 15g of paste, mixed as described previously, at 0.5 w/b ratio [31]. The beakers were gently tapped to expel entrapped air from the cement paste. The beakers, with the cement pastes evenly spread at the bottom with no visible entrapped air bubbles, were then carefully filled to the brim with deionized water. A rubber bung with pre-fitted 1mL pipette was carefully fixed to each filled beaker. The water displaced by the rubber bung rose through the pipette. The required water level was maintained by suction or pressing the bung.

Figure 3-9 Accessories and setup for recording the chemical shrinkage of cements

The water level in the pipette was then topped up with a film of orange-coloured oil which was the primary indicator of volumetric changes and hence used to follow the progress of hydration in the cements. The runs were performed over 28 days. Similar to calorimetry runs, specimens were run in duplicate and reproducibility assessed through independent runs.

The images were automatically recorded using a macro which was recorded with Work Space Macro software' at 3 minutes-40 seconds interval. There were 7000 images recorded from a complete 28-day run. The images were analysed using Carl-Zeiss Axiovision Analyzer and the steps involved are provided in Appendix A.1.1.

The scale was defined by the pixel equivalent of the 200mm line for any chosen image. This enabled the pixel/mm conversion factor (C) to be derived and subsequently applied to each set of data. The chemical shrinkage per cement paste was calculated according to Equation 3.1.

$$v = \frac{\pi y_{\nabla} d^2}{4m} C$$ ---------- Equation 3.1

Where, m= mass of paste, maintained at 15g, and d = pipette diameter

To extract the contribution of slag or limestone, the total shrinkage was normalised by the clinker content as illustrated in Figure 3-10. Subtraction of the shrinkage of the quartz blend from the composite slag cements yielded the shrinkage due to slag hydration.

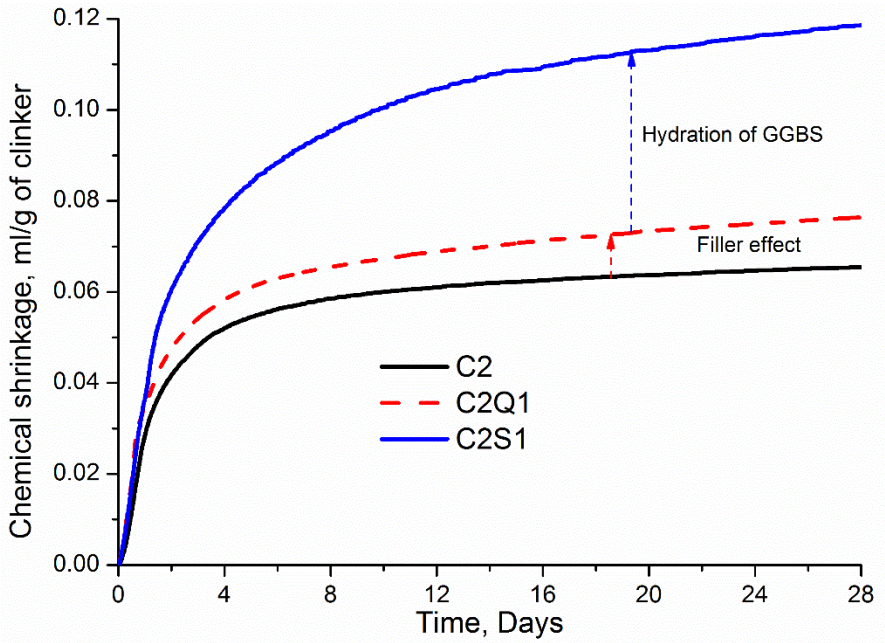

Figure 3-10 Illustration of filler effects and slag hydration on chemical shrinkage

3.5.2.1 XRD data acquisition

XRD data were acquired on a PANalytical MPD Pro using a CuKα anode operating at 40kV and 40mA, over a range of 5-80 °2θ. The equipment was equipped with scanning X'Celerator detector and the scanning step size was 0.334 °2θ. Automatic incident divergence and fixed anti-scatter slits were used together with

a 10mm incident beam mask. The continuous scan mode was adopted for all data acquisition.

Development of the PONKCS method

XRD data analysis was performed on TOPAS Academic software v4.2. A first order Chebyshev polynomial background function was adopted for the calibration and subsequent refinement. The fundamental parameter approach was used to model the slag phase because it enabled the instrument contribution to peaks to be modelled and separated from that of the sample [345]. The slag phase was modelled on a 100% slag sample and the model is shown in Figure 3-11.

Instrument parameters were defined as shown in Table 3-7 and fixed throughout the modelling and subsequent refinements. The fundamental parameter (*fp*) type peaks were introduced to describe the slag phase, taking care to avoid fitting the distinct peaks of quartz and calcite. The peaks were then indexed and refined by the Pawley method [32, 49]. This allowed the indexed details to be scaled together as a single *hkl* phase.

The *hkl* phase was calibrated on a 50:50 binary mix of slag and corundum. The ZM constant was determined by the internal standard method [32, 33, 307] based on equation 3.2, taking into account the traces of quartz and calcite in the slag. The accuracy of the modelling and calibration of the slag phase was tested on binary mixes with corundum and details will be given in Chapter 4.

$$(\mathrm{ZMV})_{\mathrm{a}} = \frac{\mathrm{W_a}}{\mathrm{W_{st}}}\frac{\mathrm{S_{st}}}{\mathrm{S_a}}(\mathrm{ZMV})_{\mathrm{st}}$$ ---------- Equation 3.2

Where Z is the number of formula units per unit cell, M and is mass of unit cell, V is volume per unit cell, S is scale factor, W is known weight in %, st denotes the reference standard, and a denotes the slag phase under calibration.

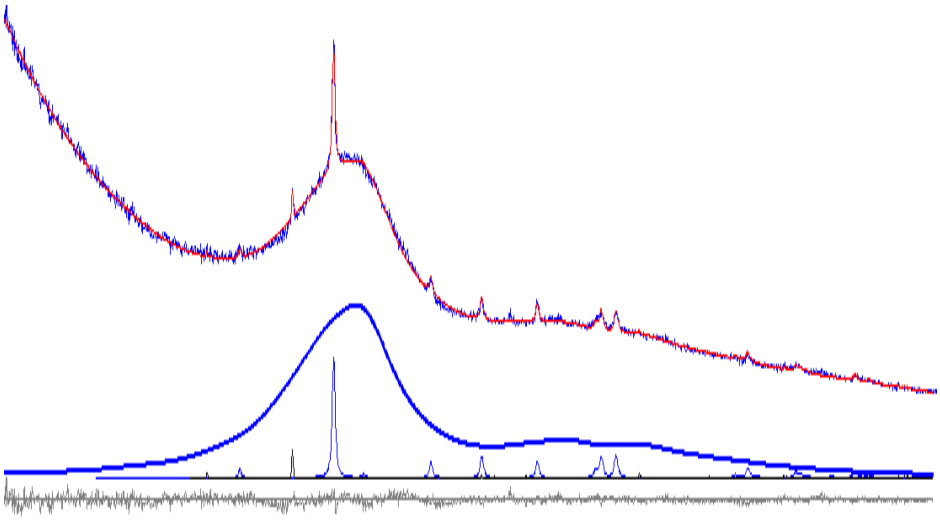

Figure 3-11 X-ray diffraction pattern of 100 % GGBS and the modelled PONKCS phase.

Also shown are deconvoluted calcite and quartz peaks.

Table 3-7 Instrument parameters which were fixed for calibration and refinement

Equatorial convolution (Linear PSD)	Axial convolution (Full Axial mode)
2 Theta range (°) = 2.122	Source/sample length = 10 mm
FDS angle = 1°	RS length = 12 mm
Beam spill/sample length = 10	Primary/secondary soller = 2.3°

The effect of water addition on the binary mixes was also assessed at 0.5 and 0.3 w/s ratios. The calibrated slag phase was subsequently implemented with the structures from other phase assemblages in the hydrated composite cements in the Rietveld refinement protocol.

Rietveld refinement and quantification

The refineable global parameter was the sample displacement due to the Bragg-Brentano geometry diffractometer. The lattice parameters and scale factors were refined for each structure and the scale factor only for the slag phase [33, 301]. Only structures with pre-defined temperature factors were used to account for atomic vibrations due to temperature in a manner similar to the occupancy factors used elsewhere [301]. The structures are listed in Table 3-8.

Table 3-8 Structures for Rietveld refinement from ICSDS

Phase name	ICSD number	Reference
Anhydrite	1956	Morikawa *et al.* [346]
Arcanite	79777	Ojima *et al.* [347]
Bassanite	262106	Schmidt *et al.* [348]
Belite	81096	Mumme *et al.* [349]
Brownmillerite	9197	Colville *et al.* [350]
Cubic C3A	1841	Mondal *et al.* [351]
Orthorhombic C3A	100220	Takeuchi *et al.* [352]
Calcite	80869	Maslen *et al.,* [353]
Dolomite	52149	Pilati *et al.* [354]
Ettringite		Renaudin *et al.* [355]
Haturite	94742	De la Torre *et al* [356]
Hemicarboaluminate	263124	Runcevski *et al.* [357]
Monocarboaluminate	263123	Runcevski *et al.* [357]
Hydrotalcite	81963	Bellotto *et al.* [358]
Periclase	104844	Taylor [359]
Portlandite	43433	Henderson *et al.* [360]
Quartz	174	Le Page *et al.* [361]

Typical refinement of composite slag cement and the incorporation of hkl models for water and the C-S-H are shown in Figure 3-12. All phases were quantified based on the external standard approach [318] with corundum as the reference material. The standard was measured regularly to account for the effect of tube ageing on the calibration factor, G according to equation 3.3 and the weight fraction of any given phase from equation 3.4 [313]. In calculating the phase contents, the mass attenuation coefficient (MAC) was calculated from the XRF composition, the used w/b ratio and attenuation coefficients from the International Tables of Crystallography [362]. The results obtained were subsequently normalised to the dry binder content.

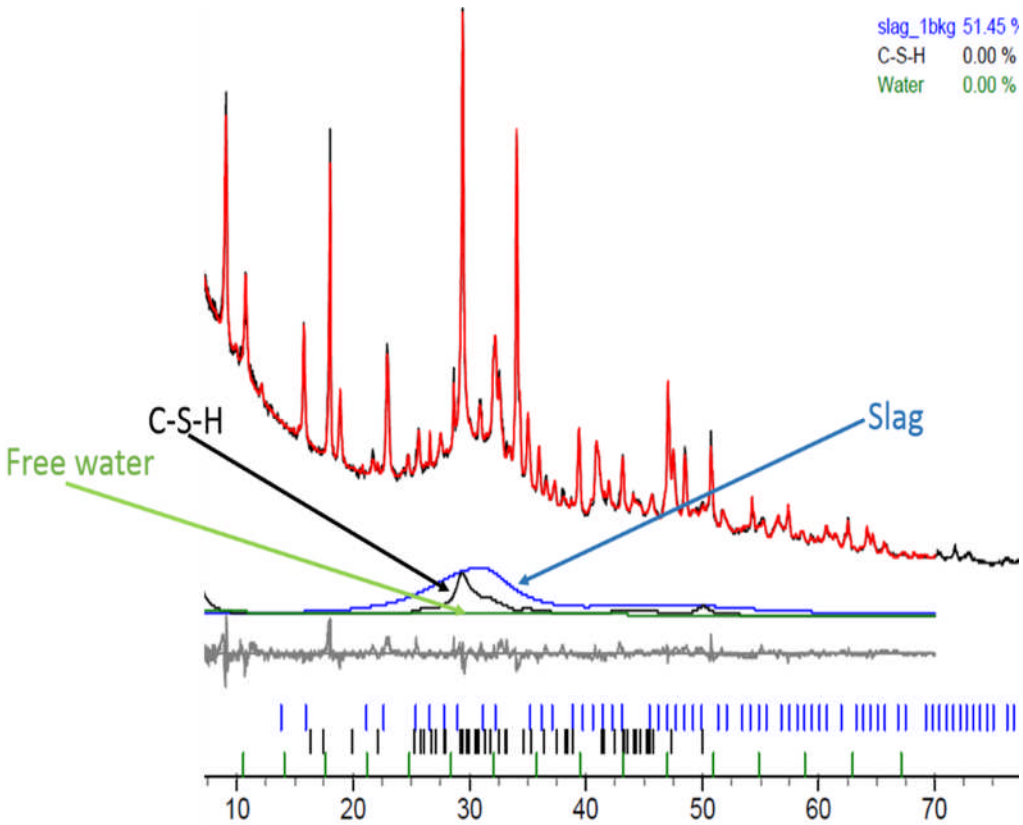

Figure 3-12 The calibrated slag phase in hydrated cement

Also incorporated are hkl models for C-S-H and water to account for background contributions in the Rietveld refinement. Other refined phases excluded for clarity

$$G = S_{st} \frac{\rho_{st} V_{st}^2 \mu_{st}}{C_{st}}$$ ---------- Equation 3.3

$$C_a = S_a \frac{\rho_a V_a^2 \mu_{sample}}{G}$$ ---------- Equation 3.4

3.5.2.2 Image Analysis

SEM was used to follow the degree of hydration of clinker and slag and perform the compositional analysis of the hydrates, specifically the C-S-H. The samples were hydration stopped by freeze drying. 2mm cement paste discs were impregnated in epoxy-resin under vacuum. The face containing the cement disk was ground with silicon carbide papers using #600, #1200 and #2500 grit sizes on a Rotopol polisher. The scratches were subsequently removed by polishing with diamond paste and cloths from 6 µm down to 0.25 µm. Polished specimens were subsequently coated with ~ 10nm thick layer of carbon prior to observing in the SEM.

SEM images were acquired in the backscattered electron mode using a Carl Zeiss EVO MA15 equipped with an 80mm detector. The instrument was operated at 15keV accelerating voltage since image quality and count rate for EDS analysis were optimised [31, 143]. For each sample, 50 images and their corresponding elemental maps were obtained at 800x magnification as suggested [46] and used elsewhere [29]. EDS point analysis was also performed to analyse the C-S-H composition at different hydration times.

The backscattered images were processed and analysed using the ImageJ software. The procedure included correcting for brightness and contrast and applying filters to remove noise and smoothening features [28]. For the porosity and residual clinker content, the images were thresholded after the initial

processing based on the grey-level histogram. This is illustrated in Figure 3-13 for extracting the area fraction of pores. For the analysis of the residual slag content, the slag and CH portions of the grey-level were thresholded, converted into a binary image which was subsequently inverted such that the thresholded regions appeared white and everything else black. This was then overlaid with the magnesium map [144] such that spots occupied by CH are excluded since they lack Mg. The area fraction of slag was thus calculated by thresholding the overlaid image (see Figure 3-13 d).

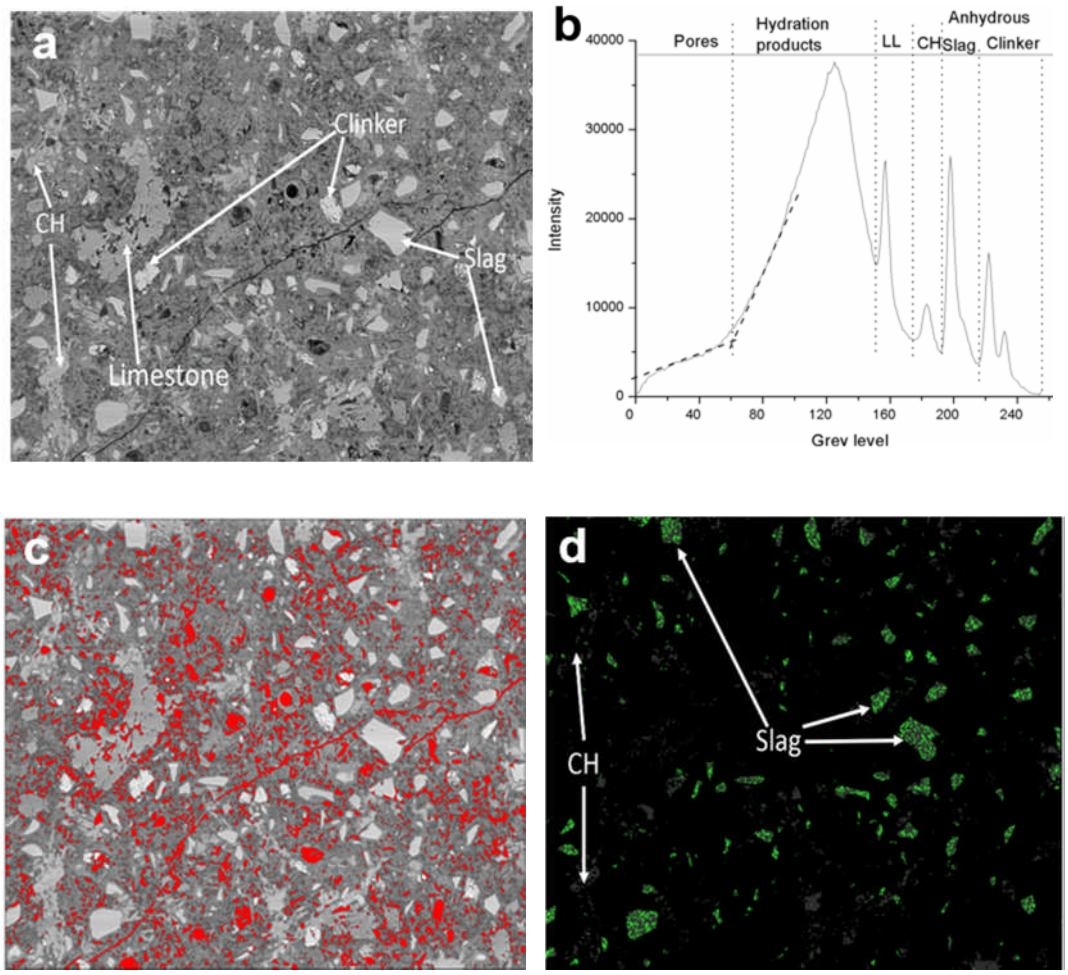

Figure 3-13 Illustration of porosity and area of residual slag extraction.

(a) BS image showing residual components; (b) grey-level histogram; (c) threshold for porosity; (d) flattened image to separate residual slag from CH.

Based on the densities of the materials ρ (Table 3-1) and weight fractions m of clinker, k, slag and limestone (LL) in the original mix (Table 5-1), the volume fractions at time, t = 0 can be calculated from equation 3.5.

$$V_{y,0} = \frac{m_{y,0}/\rho_{y,0}}{m_{CEMI,0}/\rho_{CEMI,0} + m_{slag,0}/\rho_{slag,0} + m_{LL,0}/\rho_{LL,0} + m_{H2O,0}/\rho_{H2O,0}}$$ --Equation 3.5

$V_{t\,(y)}$ is volume fraction of a component at time, t $V_{y,0}$ is volume fraction of a component at time, 0

Using the stereographic assumption of 2D conversion to 3D [28, 29, 31], the calculated area fractions are converted into volumes, V_t and subsequently used to calculate the degree of hydration of clinker (Equation 3.6) and degree of hydration of slag from (Equation 3.7).

$$\sigma^{CEMI} = 1 - \frac{V_{t\,(CEMI)}}{V_{y,0\,CEM\,I}(1-V_f)} 100\%$$ ---------- Equation 3.6

$$\sigma^{Slag} = 1 - \frac{V_{t\,(Slag)}}{V_{y,0\,(Slag)}} 100\%$$ ---------- Equation 3.7

σ^{Slag} Degree of hydration of slag σ^{CEMI} degree of hydration of CEMI

3.5.2.3 Thermal analysis

When subjected to higher temperatures exceeding 40 °C, paste components, including the C-S-H, ettringite, carboaluminates and portlandite decompose by losing the associated water and or carbon dioxide. These decompositions are accompanied with mass losses.

Temperature ranges at which different cement compounds decompose are well established [339, 363]. Mass loss arising from the decomposition of portlandite

and extraction from the TG curves is illustrated in Figure 3-14. The DTA curve was used to define the inflexion points [31].

A Stanton Redcroft Thermal Analyzer series 780 was used to acquire thermogravimetric data.

Dehydroxylation and decarbonation reactions of portlandite and calcite are shown in equations 3.8 and 3.9 respectively. The tangent method was used extract the mass losses associated with water loss from portlandite and carbon dioxide from calcium carbonate. The latter was chosen for its accuracy [339]. The corresponding portlandite and calcium calculated from equations 3.10 and 3.11 respectively.

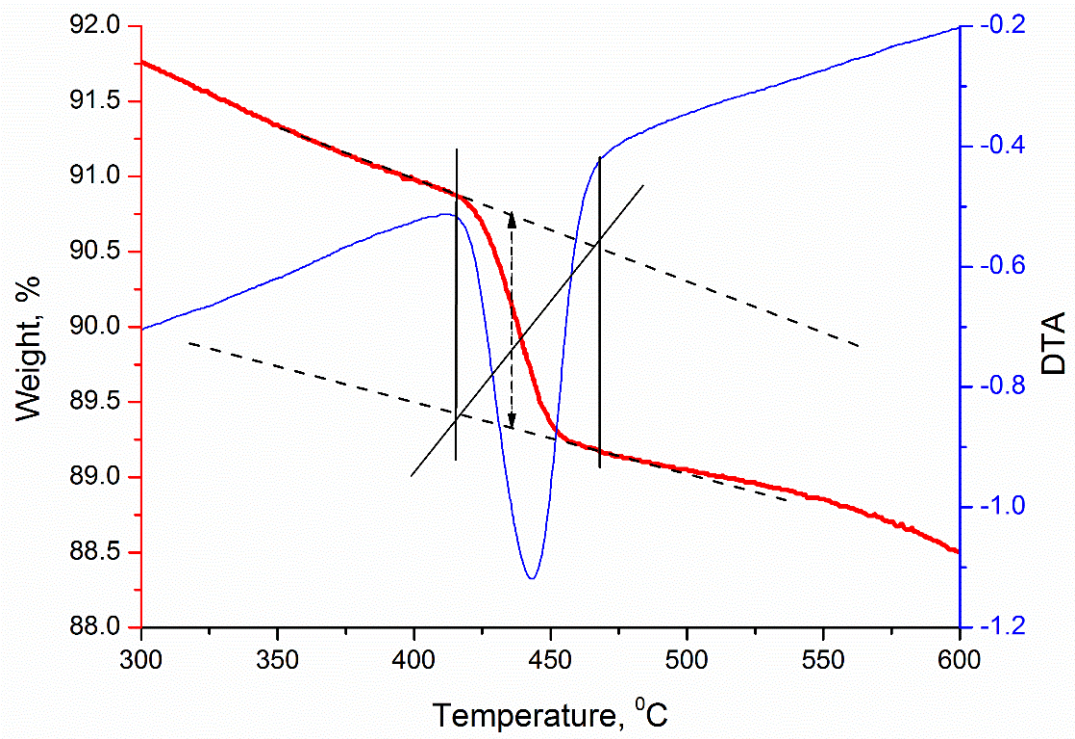

Figure 3-14 TG and DTA curves and extraction of CH

Carbonation of portlandite was ignored since hydration stopping was done in a glovebox purged with nitrogen gas and TG measurement was performed under

nitrogen gas as well. The weight fractions of portlandite and calcium carbonate were normalized to the ignited weights at 550 and 900 °C respectively.

$$Ca(OH)_2 \longrightarrow CaO + H_2O \quad \text{Equation 3.8}$$

74 56 18

$$CaCO_3 \longrightarrow CaO + CO_2 \quad \text{Equation 3.9}$$

100 56 44

$$[CH]\% = \Delta CH \frac{74}{18} \quad \text{Equation 3.10}$$

$$[CC]\% = \Delta CC \frac{100}{44} \quad \text{Equation 3.11}$$

3.5.2.4 Mercury intrusion porosimetry

MIP measurements were performed using a Quantachrome Instruments' PoreMaster-60. The hydrated specimens were crushed into 1- 2 mm and hydration stopped by the double solvent exchange method using IPA and diethyl ether as described previously.

3.5.2.5 Pore solution analysis

For pore solution analysis, the pastes were put into 200ml (up to 1 day) or 500ml (≥7 days) PE bottles, capped and sealed and stored at 20ºC. At given times, the pore solutions were extracted while the specimens remained in the bottle, using pressure filtration (up to 1 day) or at ≥7 days by the steel die method [364] using pressures up to 250MPa. The obtained solutions were filtered through a 0.45µm nylon filter in order to remove any remaining solids.

The elemental concentrations were determined by inductively coupled plasma optical emission spectroscopy (ICP-OES Varian Vista-Pro). Before any measurements, the solutions were acidified with HNO_3 to prevent any precipitation

of solids. The measurements were performed not later than 1 hour after pore solution extraction. For the later age samples (≥7 days), concentrations were determined using a Dionex DP ICS-3000 ion chromatograph. For determination of solution pH, undiluted solutions were used. The pH electrode was calibrated against KOH solutions of known concentrations and pH was measured directly after obtaining the solutions.

3.6 Freeze-thaw monitoring

The internal damage and scaling tests were performed on concrete samples prepared according to EN 12390:2. The fresh properties assessed were the slump, flowability (spread), density, and air content.

Specimens were kept in the mould for 24 hours and then stored in water for 7 days after de-moulding. When the specimens are 7 days, specimens were stored at ≈ 65 % RH and 20 °C temperature for 21 days as prescribed in PD CEN/TR 15177: 2006 [340]. The lateral sides of the specimen were sealed with epoxy sealant and then re-saturated for 7 days. This modification was necessitated by the volume of antifreeze and the type of freeze-thaw chamber used as shown in Figure 3-15 a. The complete freeze-thaw cycle took 24 hours (see Figure 3-15 b) as opposed to the 12-hour cycle in PD CEN/TR 15177: 2006 [340]. However, this is not expected to influence the results as reported elsewhere [43].

The freeze-thaw test solution was deionized water; both internal structural damage and scaling were measured. The setup for the internal structural measurement is shown in Figure 3-15 c. The internal damage was evaluated from the transit time measured by a PUNDIT ultrasonic pulse velocity measuring kit connected to an

acrylic container as shown in Figure 3-15 d. Before the transit time measurement, the stainless steel test containers were cleaned for 3 minutes in the ultrasonic cleaning bath. The scaled material was filtered on a 125 µm paper and dried at 110 °C for 24 hours and weighed when cooled.

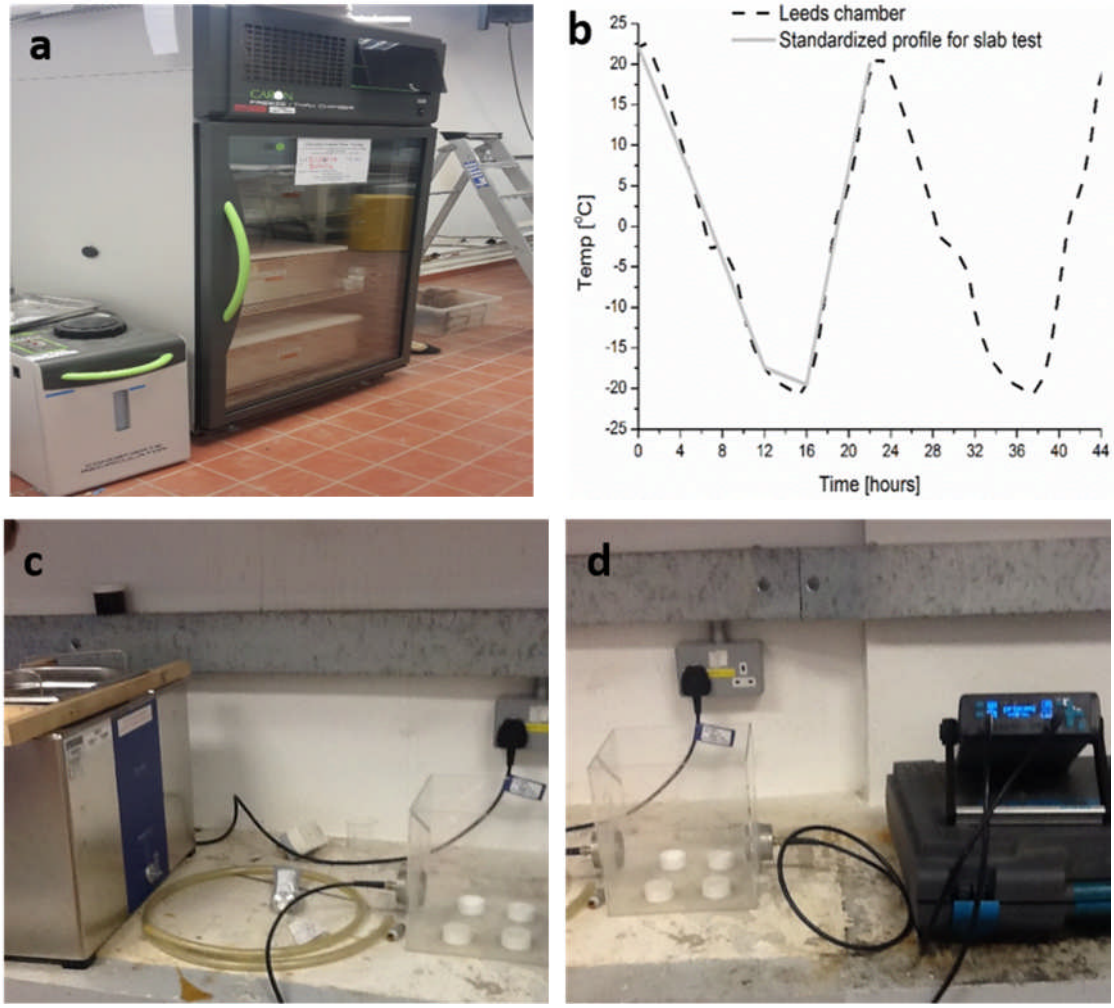

Figure 3-15 Setup for freeze-thaw testing

(a) chamber (b) temperature profile; (c) sonic bath for cleaning scaled material; (d) setup for pulse velocity measurement.

The microstructural changes during freeze-thaw were observed on 5mm thick slices of concrete. These were hydration stopped by double solvent exchange of IPA and ether. However, the samples were kept in the IPA for 14 days with the solvent recycled every 48 hours. The procedure for preparing the samples for SEM

was as described already. In parallel, cement paste samples were tested for phase assemblage variations. The samples were kept sealed for 7 days before being crushed to 1-2 mm thick sizes. They were then exposed to the laboratory conditions of ≈ 65 % RH and 20 °C to mimic the surface behaviour of the concrete test surface.

Chapter 4
Development and validation of the PONKCS Method

This chapter systematically presents results from the implementation of the calibrated PONKCS phase to quantify the slag contents from the Rietveld refinement of mixtures of increasing complexity. The calibrated phase was initially assessed on synthetic mixes of slag and corundum of varying proportions with and without water. Secondly, anhydrous composite cements were assessed. the modelled slag phase was implemented in composite slag and C-S-H system. Following on from this, the robustness of the method was assessed by implementing the calibrated slag phase in the refinement of hydrated slag cements. The impact of four different hydration stopping methods compared to freshly ground hydrated cements was examined. Sample preparation considerations which can influence the analysis are consequently reported.

4.1 Mixes considered

In the first instance, synthetic mixes of slag and corundum at ratios 100:0, 90:10, 60:40, 30:70, 10:90 and 0:100 respectively were considered.

Following on from this, the anhydrous composite cements as detailed in Table 4-1 were analysed. An additional objective here was to examine the effect of four dehydration methods on the quantitative analysis of phase assemblages and the unreacted slag and clinker content compared to freshly ground non-hydration stopped samples.

Table 4-1 Composite cements for assessing the robustness of the calibrated slag phase

Nomenclature	CEM I		GGBFS		Limestone	Anhydrite
	42.5 R	52.5 R	S1	S2	L	
	$\%_{mass}$					
C2		100	-	-	-	-
C2S1	-	50.68	47.08	-	-	2.24
C2S1-10L	-	51.18	38.03	-	8.55	2.24
C1S1-10L	51.93	-	38.06	-	7.50	2.51
C2S1-20L	-	51.18	28.53	-	18.06	2.24
C2S2-20L		51.18	-	28.53	18.06	2.24

Due to constraints of time and other resource, the hydrated systems reported here were limited to three (3) mixes C2, C2S1 and C2S1-10L. The hydration stopping regimes employed are detailed below:

i. Freshly ground

ii. Freeze-drying method [29, 31]

iii. Single solvent exchange and heated [33]

iv. single solvent exchange plus vacuum (24 hours) [54]

v. Double solvent exchange (ground) [178]

These were described in details under hydration stopping methods in section 3.4.

4.2 Implementation of the method in synthetic mixes

Slag is amorphous but may contain some crystalline phases which may form during quenching. The non-crystalline phase produces a halo between ~20 - 40 ° 2 theta range [31, 33, 67]. Figure 4-1 shows XRD plots of the synthetic mixes of slag and corundum in the various proportions as listed in section 4.1. For clarity, not all

analysed mixes are shown. It can be seen that the intensity of the halo is proportional to the slag content and decreases as the slag content reduces. Meanwhile, comparing the mix containing 10% slag + 90% corundum with the 100% corundum sample also shows that the amorphous slag content can be distinguished from the corundum. This clear distinction may be due to the high crystallinity of corundum [316, 365] but may not be necessarily true for other impure materials. Therefore, by using a model which describes the profile of slag, the residual slag content could be quantified.

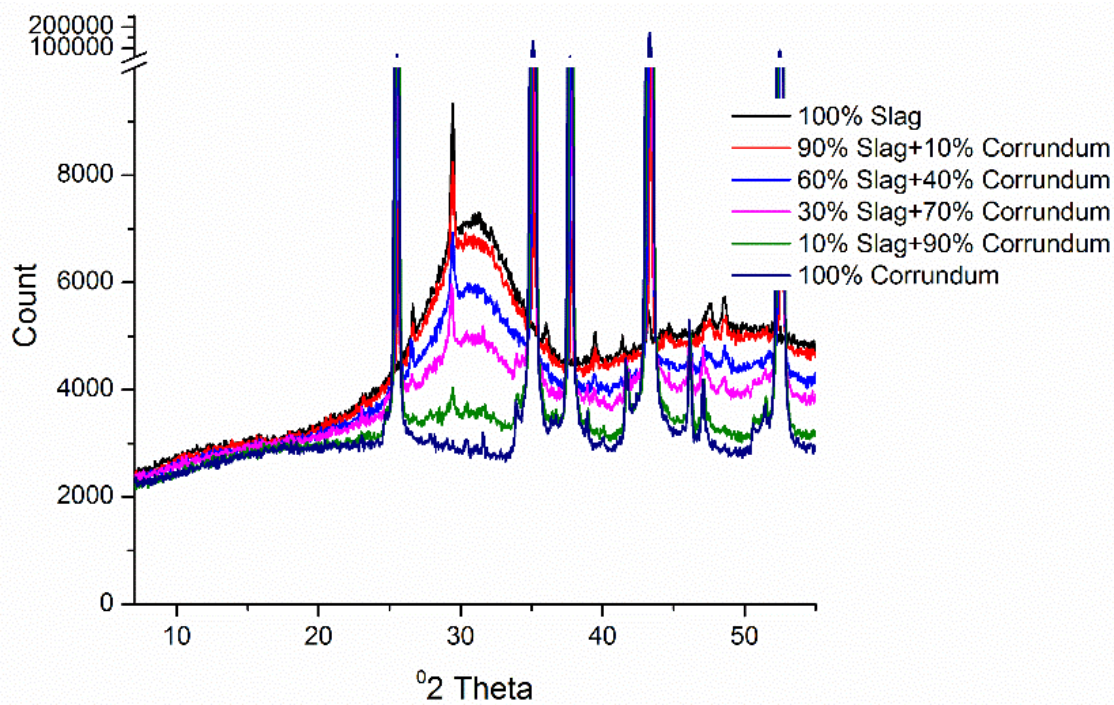

Figure 4-1 Plots of the diffraction patterns of binary slag-corundum mixes showing the variation of the halo intensity on the slag content.

Using the calibrated PONKCS phase for slag as described in Chapter 3, the slag contents of the scans shown in Figure 4-1 were analysed. A typical output from the refinement is shown in Figure 4-2. The plot illustrates the background, crystalline phases in the mix including corundum, the modelled slag phase and the

difference plot. The quantities shown in the figure are the relative contents of the refined phases. The true contents were recalculated from the scale factors and the known weight of corundum using the external standard method.

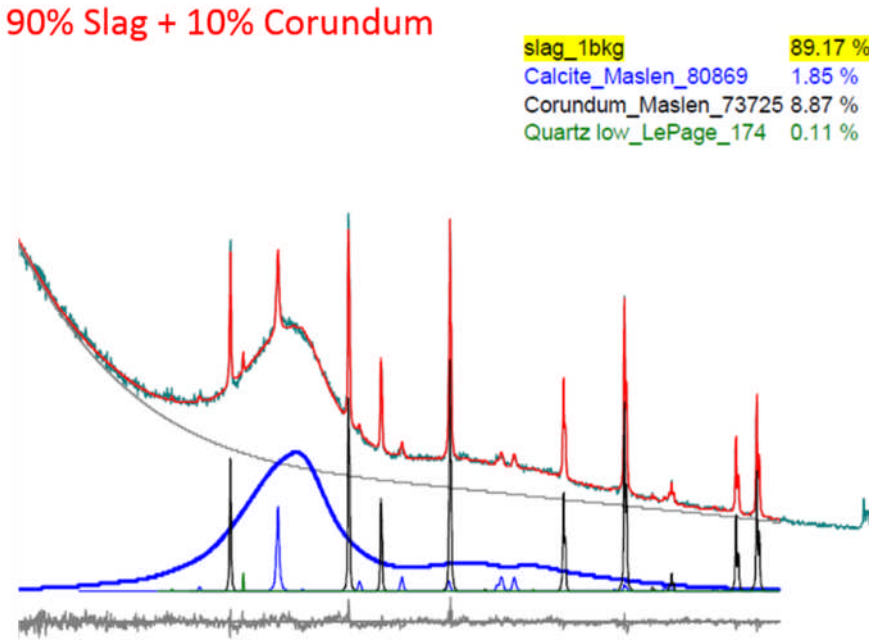

Figure 4-2 Refined phases in a binary slag and corundum mix.

The modelled slag halo is shown in deep blue, peaks for corundum in black, calcite in light blue and quartz in green. The difference plot and background are in grey colour.

Figure 4-3 shows a comparison between the originally weighed slag contents and those determined from the modelled phase through Rietveld refinement of the XRD scans. The effect of water addition was also assessed at 0.5 and 0.3 w/s ratios.

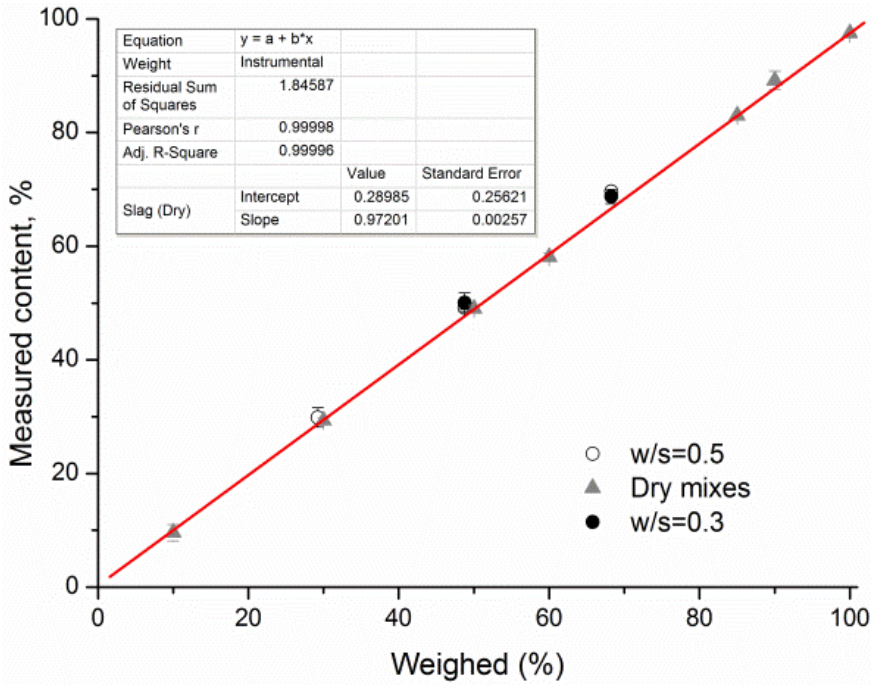

Figure 4-3 Relationship between actual and measured slag content

Note: Open circles are samples prepared at 0.5 w/s and solid circles for 0.3 w/s ratio.

A 1:1 relationship was found with a slope of 0.972 and an intercept of 0.290 and standard errors of 0.002 and 0.256 respectively. Consequently, a margin of error of ± 0.02 is thus calculated for the slope. This implies that up to 2% variation can be expected between the measured and determined slag contents. This is consistent with the margin reported by Snellings et al. [33]. The errors associated with the presence of water is ±0.3% and that due to changing w/s ratios was ±1.8%. These are both within the measurement error.

4.3 Implementation of the method in anhydrous cements

Five composite cements were analysed in this series. These varied with the slag content as well as the fineness of both slag and clinker. Figure 4-4 (a-c) show the

effect of clinker fineness, slag content and slag fineness respectively on the diffractogram. At a given slag content, the composite cement made with CEM I 52.5 R (C2) showed slightly lower background compared to that from CEM I 42.5 R.

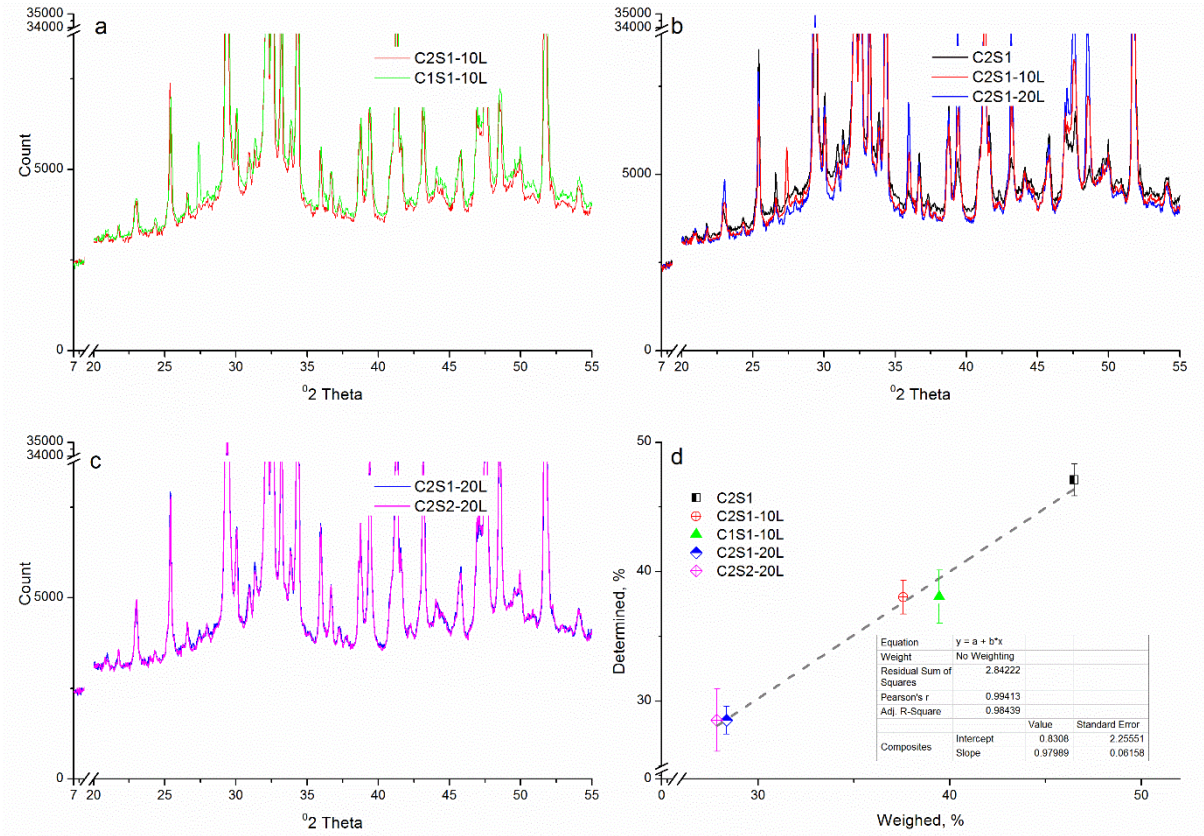

Figure 4-4 Effect of cement composition and fineness on the XRD background and impact on quantification.

(a) Clinker fineness; (b) effect of limestone content; (c) effect of slag fineness and (d) relationship between weighed and determined slag content

The homogeneity of the blend, differences in clinker fineness and instrument parameters could account for the slight differences. Some studies have confirmed non-existence of amorphous phases in anhydrous CEM I [303, 310]. However, Snellings *et al.* showed that variation in the clinker d_{50} from 10 µm to 25 µm

modified the amorphous content [303] and hence reflected in the XRD scan background. Increased crystallographic modifications arising from strain and size broadening effects [366] may also explain the peak shifts.

The influence of the slag content on the diffraction pattern is also shown in Figure 4-4 c. Similar to the synthetic mixes already presented, the intensity of the halo increased with the slag content. A reduction in the halo was noticed as the slag content reduced. The impact of slag fineness was followed using ternary systems containing 30% slag. Slag fineness had no impact on the halo. This implies that the calibrated PONKCS phase can be used to follow the slag contents in the composite slag cements presented above.

The relationships between the weighed and determined slag contents for the five composite cements are shown in Figure 4-4 d. The standard deviations from triplicate run from different batches are indicated as error bars. The margin of error from these was 6%. Therefore, at 95 % confidence level, the confidence interval is ± 0.07. This is considerably higher than that obtained from runs within the same batch as calculated for the synthetic mixes.

Potential reasons for the wider confidence interval from different batches include homogenization of constituent materials and potentially non-crystalline phases other than slag. Commercial OPC contains a negligible amorphous content [303, 310] and therefore does not influence the halo due to slag, even at increasing fineness, as noted from Figure 4-4 a. However, in multiple component systems such as ternary or quaternary or hydrated cements, potential overlap of the halos may be inevitable and care must be taken to model and implement these in the refinement.

4.4 Quantification of the slag content in composite cements

Hydrated cement systems present problems for the implementation of a PONKCS phase for slag. Firstly, water in porous materials modifies the sample mass thickness and hence the density of the absorbing surface. Consequently, the sample attenuation coefficient is affected since the latter is proportional to the fractional beam intensity. This normally reduces the peak intensities compared to dry samples. These effects are addressed by accounting for the water content when calculating the mass absorption coefficient and also normalising the determined weight fractions to the anhydrous cement content in the mix. Both steps require accurate determination of the water present in the mix from which the XRD scan was obtained. However, this value may vary with the dehydration technique employed [321, 322].

Secondly, the C-S-H formed from the hydration of clinker as well as slag is poorly crystalline and produces a ‘hump’ with a peak between 30 - 32° 2 theta and hence overlaps with slag [33, 320]. Therefore, simultaneous implementation of models for the C-S-H and slag are vital for the successful quantification of the residual slag content.

The possibility of the modelled PONKCS phase to differentiate between slag and other poorly crystalline materials with characteristic halos in the same region as slag was tested on a mixture between synthetic C-S-H and slag. The C-S-H had a Ca/Si ratio of 1.5 but contained some crystalline impurities. Details about the synthesised C-S-H are reported elsewhere [212]. An orthorhombic C-S-H model with F2dd space group was implemented [33]. The initial lattice parameters were

adopted from Bergold *et al.* [320] but the cell mass was chosen based on synthetic mixes of the C-S-H and corundum.

Figure 4-5 shows refinement plot on binary slag/C-S-H mix and the deconvoluted contributions from all refined phases. The identification of the crystalline impurities in the C-S-H is outside the present scope. Notwithstanding, the modelled slag phase can be differentiated from the C-S-H despite the co-location of the main peaks around the same °2 theta range. The relative slag and C-S-H contents following the refinement are reasonably accurate. Consequently, the two models can be implemented together in composite cements. The C-S-H crystallinity, however, varies with hydration time [320] but it was not possible to examine this effect.

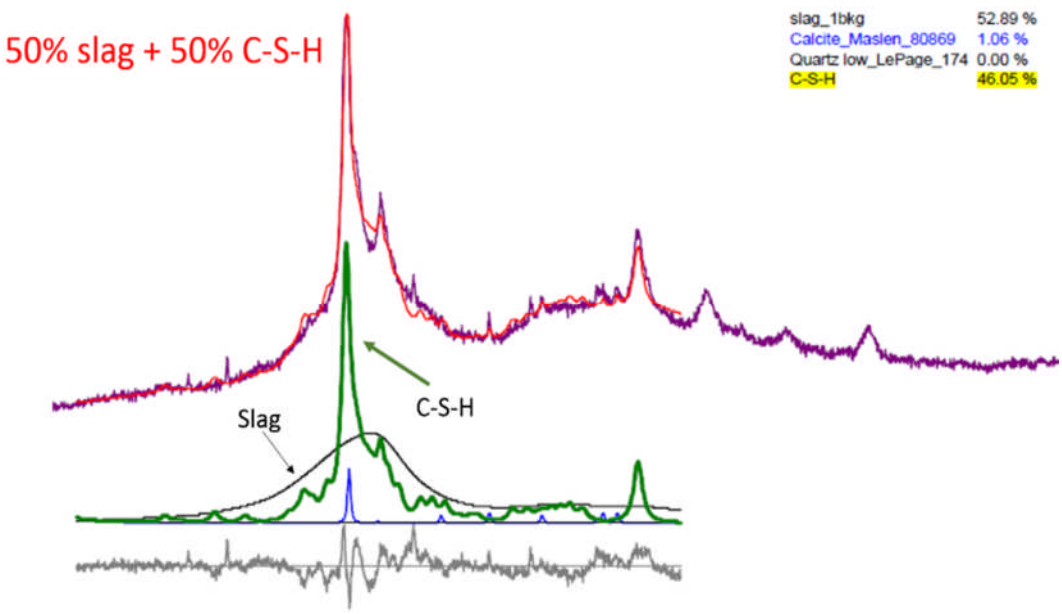

Figure 4-5 Refinement of 1:1 binary slag – C-S-H mix

Note: The halo due to slag (20 – 38 °2 theta) overlaps with that of the C-S-H. Traces of calcite in the slag and carbonation of the C-S-H also overlaps with the C-S-H hump.

4.4.1.1 Bound water content

Hydrated cements contain water which may be bound into hydrates or free [193, 292]. An accurate assessment of water content is, therefore, vital for making allowance in the attenuation coefficient of the mix from which the scan was performed [33]. For scans performed on freshly ground samples without dehydration, the proportion of water is the initial water content in the mix. If the samples are dehydrated, the bound water content is used instead [31, 301].

The bound water content, however, varies with the dehydration technique even for the same sample. The object of hydration stopping is to remove free water from the capillary pores with minimal influence on hydrates. However, the C-S-H, ettringite and carboaluminate phases incorporate a high proportion of water and thus, depending on the exposure time and aggressiveness of the dehydration technique may decompose. The effect of four commonly used hydration stopping methods on the decomposition of the C-S-H and ettringite as well as portlandite from the thermal analysis are compared to those of freshly ground samples from CEM I and limestone ternary blend in Figure 4-6 and Figure 4-7 respectively.

Within 20 – 1000 °C range, noticeable events would be mostly dehydroxylation of free water, C-S-H, ettringite and portlandite. Oxidation and phase transitions also occurred in the mixes reported and hence DTG was chosen over DTA and TG to reveal these details [339].

The decomposition peaks (i & ii) characterising free water, C-S-H and ettringite differed significantly between hydration stopped and freshly ground samples. At later hydration times, the difference was much smaller as most of the water was bound into hydrates. In the dehydrated systems, the impact of the hydration

stopping method on the C-S-H and AFt decomposition peaks was minimal apart from the freeze-drying technique which differed significantly irrespective of the mix composition. The efficiency of the different hydration stopping regimes is also apparent from the 28 days DTG plots for mix C2S1-10L where the free water and C-S-H and AFt can be distinguished. Some free water persisted in the samples dehydrated by solvent exchange.

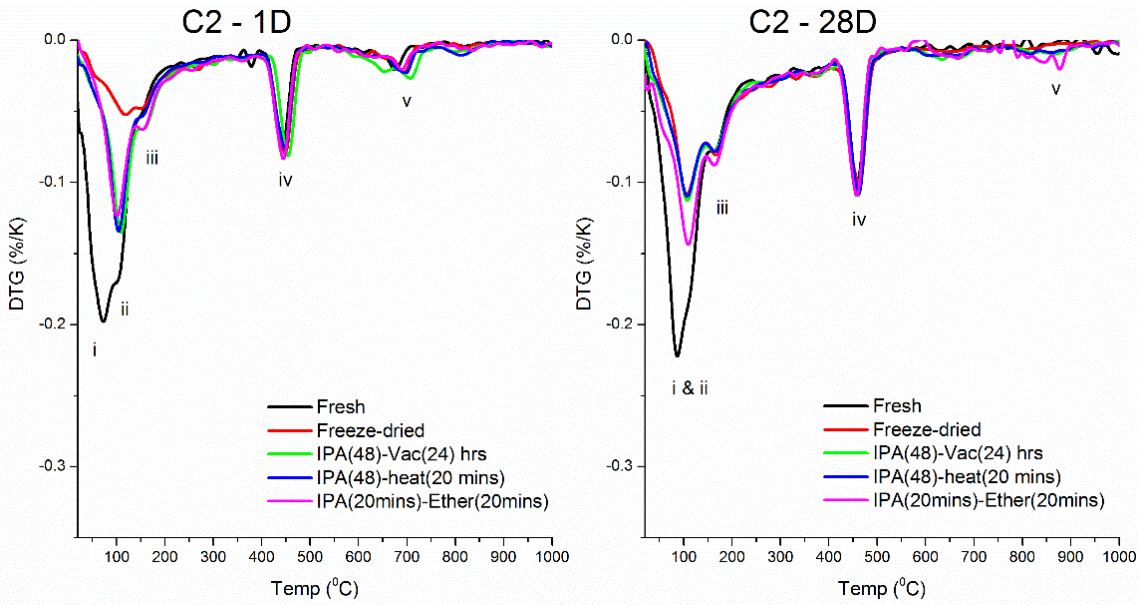

Figure 4-6 DTG of CEM I 52.5 R as a function of hydration stopping after 1 and 28 days

The DTG plots suggested that the drying method had minimal impact on the portlandite contents. However, the XRD diffractograms shown in Figure 4-8 and Figure 4-9 indicate significant modification of the AFt/AFm phases, plus slight modifications of the portlandite content depending on the dehydration technique. All investigated methods reduced or completely decompose ettringite and to a smaller extent, portlandite.

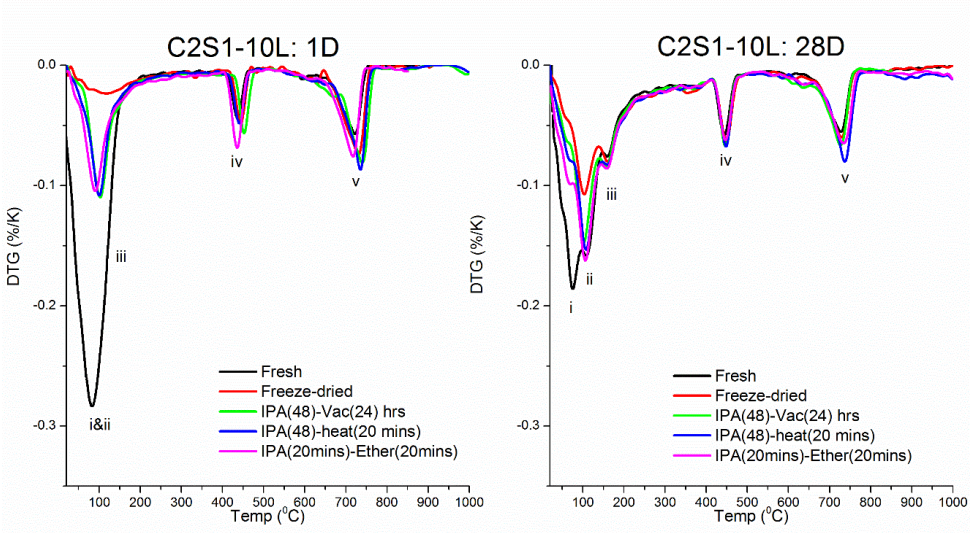

Figure 4-7 DTG of CEM I 52.5 R + slag + 10% limestone as a function of hydration stopping after 1 and 28 days

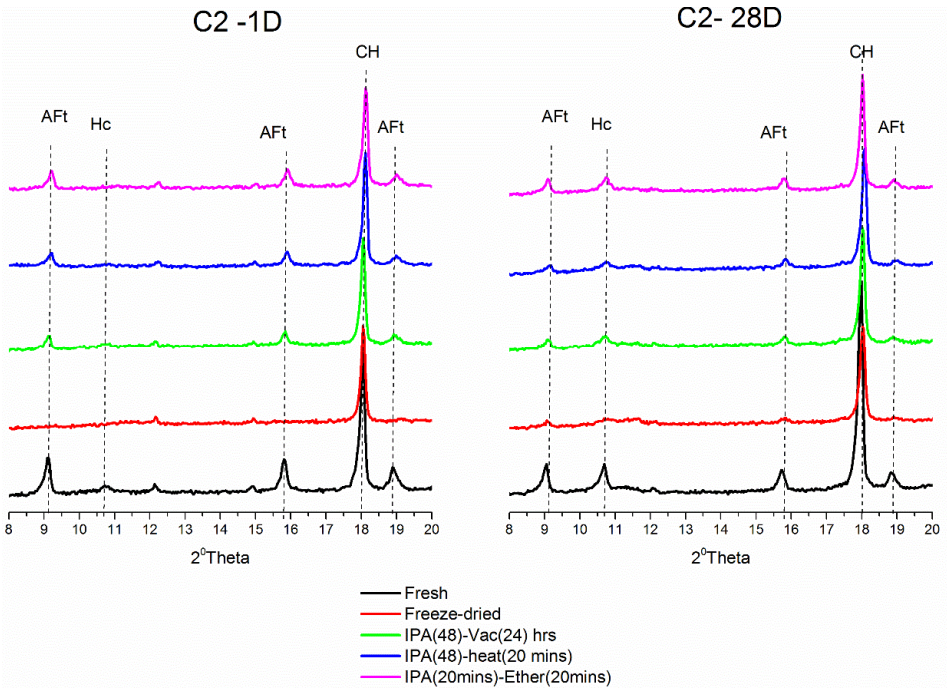

Figure 4-8 Effect of dehydration methods on the AFt/AFm and portlandite content in CEM I (C2)

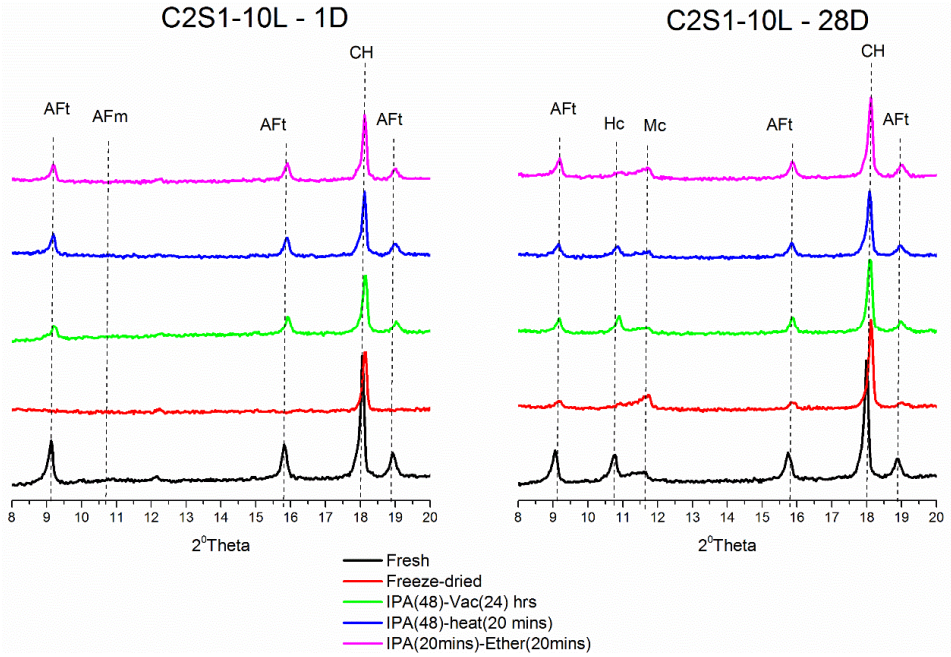

Figure 4-9 Effect of dehydration methods on the AFt/AFm and portlandite content in ternary slag/limestone cement (C2S1-10L)

The implication of the different techniques on the quantities of ettringite and portlandite from the Rietveld refinement of the XRD data are shown in Figure 4-10.

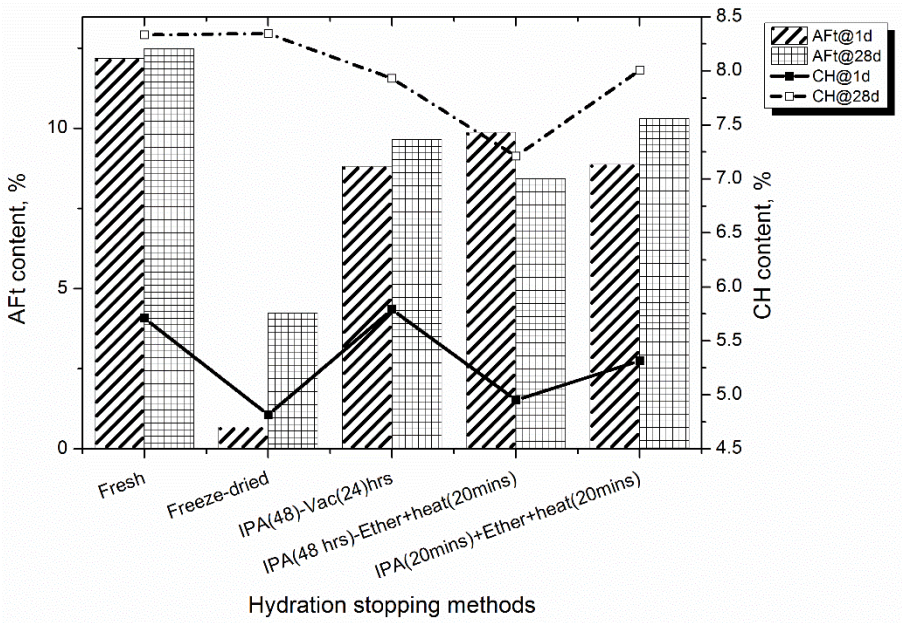

Figure 4-10 Effect of dehydration method on the contents of ettringite and portlandite from QXRD of C2S1-10L

The dehydration methods investigated did not only remove free water but also affected the ettringite and portlandite contents. With respect to the ettringite content, freeze-drying was most detrimental in agreement with elsewhere [321, 322, 343]. The effect of dehydration also dependent on the age of the specimen. For example, after 1 day, ettringite decomposed completely when hydration stopped by freeze-drying and also reduced significantly from the solvent exchange methods. After 28 days however, some ettringite was detected in all samples even after freeze-drying. These were also evident from the DTG plots in Figure 4-7. This suggests potential changes in crystallinity with hydration. Slight reductions in the portlandite content also accompanied hydration stopping, with the short double solvent exchange in IPA and ether (IPA(20mins)+ Ether+ heat (20mins)) least damaging compared to the freshly ground samples.

If the bound water is considered as that lost during stages ii, iii and iv of Figure 4-6 and Figure 4-7, then the weight change due to loss of water bound into hydrates should be between 50 – 550 °C for the dehydrated cements which is the conventional range [7, 339]. However, in the freshly ground samples, free and bound water cannot be distinguished at an early age. The DTG after 28 days indicates the persistence of free water up to 100 °C. Therefore, bound water was considered between 100 – 550 °C and same assumed for the 1-day old samples for comparison purposes. It must be remarked that decomposition of ettringite may have commenced well before 100 °C [367] and this assumption is only a proxy to compare with dehydrated samples. The freshly ground specimens had significantly higher bound water content when the temperature range was considered at 50 – 550 ^{0}C.

4.4.1.2 Impact of dehydration methods on the XRD pattern

Figure 4-11 shows the x-ray diffraction patterns of the two composite slag cements after 1 and 28 days as a function of dehydration methods. The data collection regime was constant and potential effects of tube ageing were captured in the scale factor of the reference material, which is discussed in the quantitative XRD section.

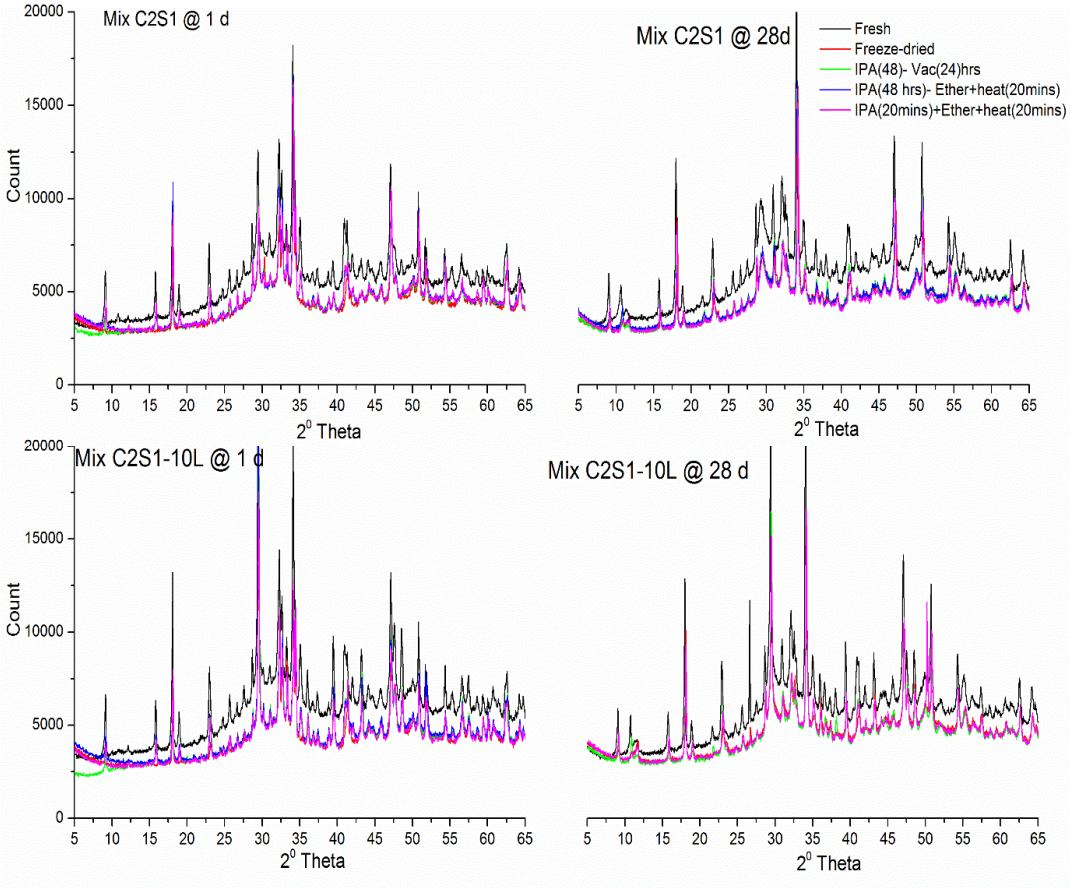

Figure 4-11 Effect of dehydration method on the XRD diffractogram of composite slag cements after 1 and 28 days.

The background was highest in the freshly ground samples, while the hydration stopped samples were similar, irrespective of the cement type and sample age. This observation is unlikely to be associated with x-ray tube ageing since the backgrounds were generally similar at low angles up to 9 °2 theta. Consequently, this may be attributable to the existence of free water. Slight deviations in the

backgrounds of the 1-day old samples subjected IPA (48)-Vac (24) hours can be noticed particularly at low angles. This cannot be explained on the basis of the bound water content but the results were repeatable.

4.4.1.3 Mass attenuation of hydrated samples

In the quantitative XRD analysis, water in the specimen is considered through the mass attenuation or absorption co-efficient (MAC). This varies as the inverse of specimen thickness and also determines the intensity of transmitted x-rays from the sample surface. For a given sample, the MAC, therefore, depends on the types of atoms present (i.e. total atomic cross section) and the atomic mass unit (i.e. relative abundance of elements) [368]. For most atoms, these constants are available from crystallographic tables. Therefore, knowing the proportion of constituent molecules (i.e. from XRF), the MAC of the mixture can be computed by superposition according to Equation 4.1. Among common oxides in cements, water has the lowest molecular attenuation co-efficient beside CO_2. However, the content of water, either as free or bound in normal cement pastes or concretes may be considerable and hence significantly influences the MAC, which is directly proportional to the phase content.

$$\mu_{sample} = \sum \frac{w_p \mu_p}{W} \text{ ---------- Equation 4.1}$$

Where μ_{sample} is MAC of sample, μ_p is MAC of a given molecule p; w is weight fraction of molecule p from XRF or TGA (for water); and W is total weight the of all molecules in the mix.

It has already been shown by TG that the significant differences existed in the quantities of ettringite and portlandite and the C-S-H (due to hydration stopping.

This led to differences in the bound water ($\%W_n$) contents as calculated by equation 4.2.

$$\%W_n = \frac{(M_{50^oC} - M_{550^oC})}{M_{550^oC}} x\ 100 \text{---------- Equation 4.2}$$

Where M_{50^oC} and M_{550^oC} are the ignited weights at 50 and 550 °C respectively.

The results from the individual methods were incorporated into the MAC calculations.

The MAC of the three cement pastes as a function of hydration stopping methods and age of sample are shown in Figure 4-12.

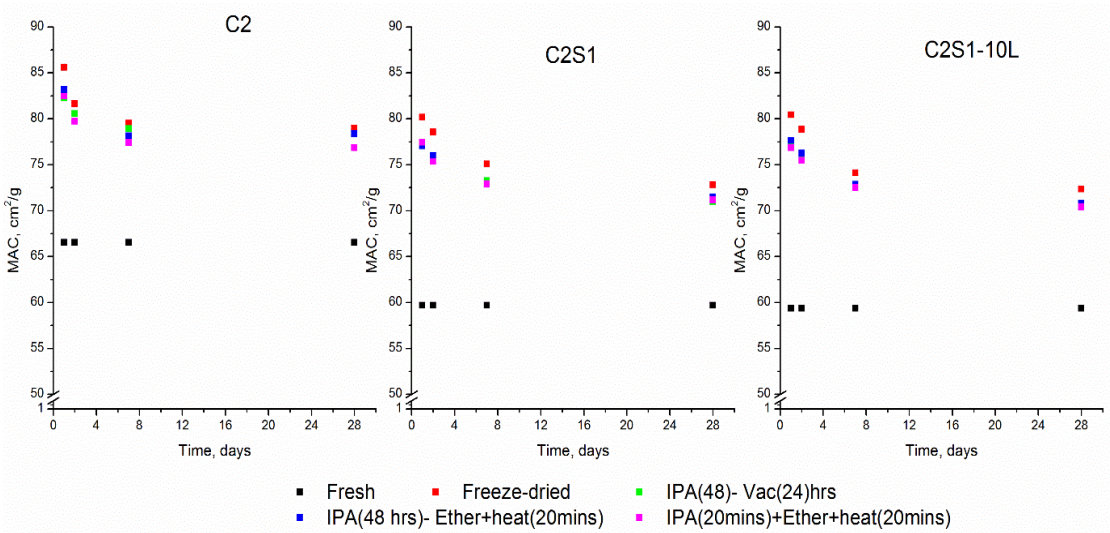

Figure 4-12 Mass absorption co-efficient for neat and composite cements pastes as a function of dehydration method and hydration time

For a given cement, the effect of cement composition was fixed, since the weight fractions implemented in the MAC calculation was based on the initial XRF composition. Thus, the variable in the computation was the water content, which remained unchanged in the freshly ground sample while it varied inversely with the

bound water content in the dehydrated samples. At a given age, the MAC of the paste was highest in the freeze-dried sample and lowest in the fresh sample. As a result, the diffracted x-ray intensities would be exponentially increased [368]. However, accounting for this effect is challenging with respect to distinguishing between free water and water bound into other hydrates as already discussed and hence usually approximated [29, 31].

4.4.1.4 Phase content calculations

Following determination of the MAC, the contents of residual and hydrated phases were extracted from the scale factors of the individual phases from the Rietveld refinement of the sample using the external standard method according to Equation4.3 [313, 318]. The starting structures for the crystalline clinker phases have been listed in Table 3-8.

$$C_j = S_j \frac{\rho_j \nu_j^2 \mu_{sample}}{G} \text{ ---------- Equation 4.3}$$

The scale factor from a given phase including slag depended strongly on the sample conditioning and tube performance. Figure 4-13 illustrates the refined scale factor for the slag phase in the two composite slag cements as a function of hydration stopping method after 1 day. A comparison with the scale factor of corundum measured with same instrument settings and dates as the samples is also presented. Irrespective of the phase of interest, the scale factors for the fresh samples were much higher than for the hydration stopped samples. However, the scale factors for corundum accompanying the freshly ground samples were also slightly higher than the hydration stopped samples.

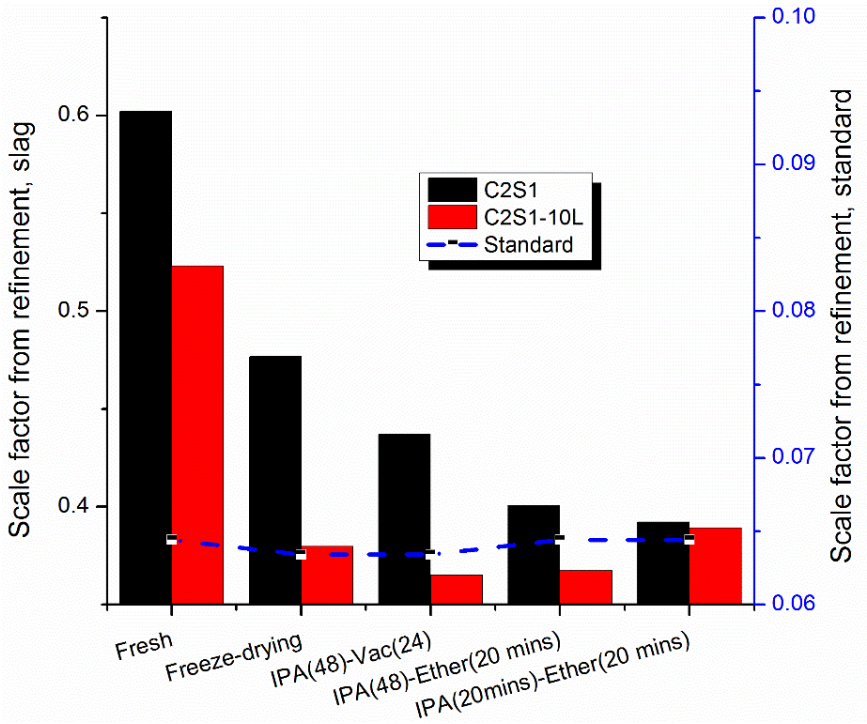

Figure 4-13 Scale factor of slag in mixes C2S1 and C2S1-10L after 1 day as a function of dehydration technique.

This is indicative of potential tube ageing effects [313] between recording the freshly ground and the hydration stopped measurements. Changes arising from the tube performance were addressed through the G-factor calculation. That from x-ray absorption due to water in the samples was also accounted through the sample MAC.

For calculating the degree of hydration, the phase contents were normalised to the anhydrous contents [369]. In the case of the non-hydration stopped samples, a factor of 1.5 was applied to the calculated phase contents from Rietveld. For the hydration stopped samples, the bound water content was applied.

Figure 4-14 shows the effect of dehydration methods on the degree of hydration of clinker after 1 and 28 days for the neat and composite slag cements. The degree

of clinker hydration was obtained from the superposition of the residuals of the major clinker phase assemblages [29, 309].

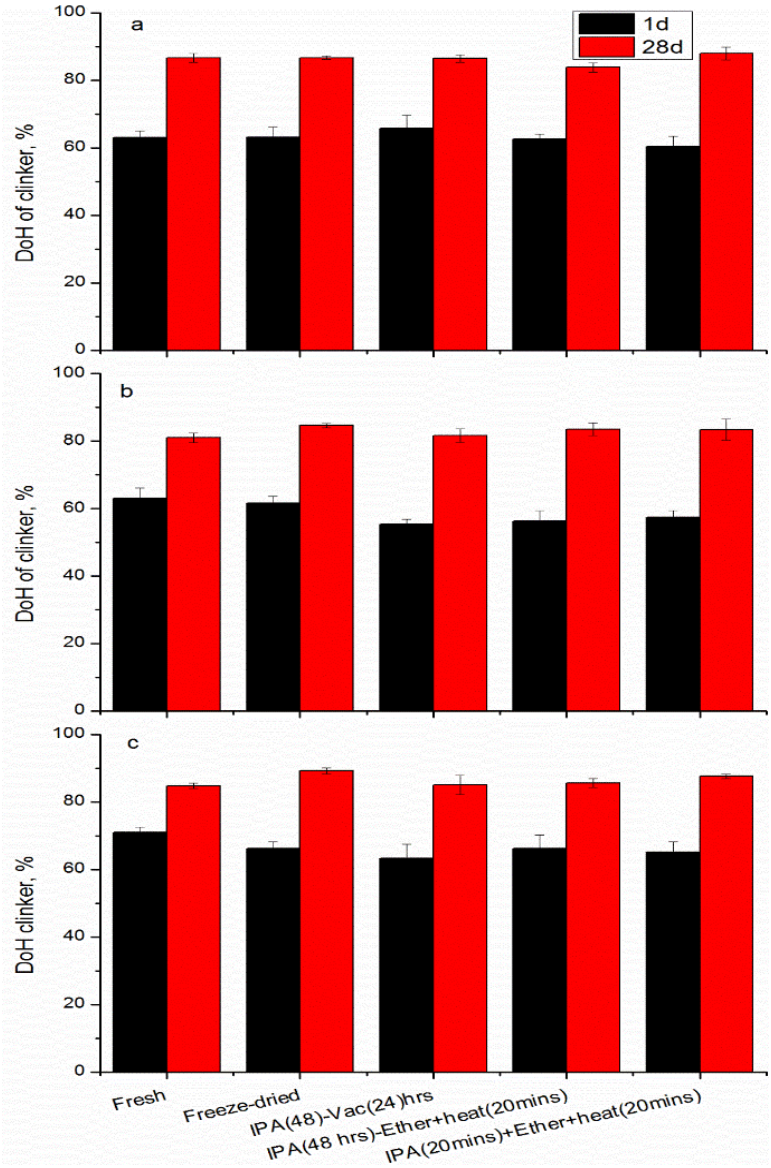

Figure 4-14 The degree of hydration of clinker as a function of hydration stopping technique.

(a) C2 (b) C2S1 and (c) C2S1-10L

For a given mix, the degree of clinker hydration was not significantly affected by the sample dehydration technique. The standard deviation was determined by increasing the order of polynomial [369] and recording the minimum and maximum

scale factors. The resulting implication on the residual slag or clinker content is indicated as error bars. The magnitude was random and generally lowest for the freshly ground and freeze-dried samples. Errors arising from the quantification of the degree of hydration due to sample dehydration was suggested by Scrivener *et al.* [309], but this has not been validated. Hydrated composite cements are more complex than synthetic mixes due to multiple amorphous phases. Consequently, implementation of the PONKCS phase is not straightforward.

As shown in Figure 4-13, the scale factor of the slag phase varied greatly with the dehydration technique and tube condition. However, using the G-factor and implementing the appropriate MAC, the degrees of slag hydration were comparable across the same sample, Figure 4-15.

Consistently, the calculated degree of slag hydration from freeze-drying was lower, irrespective of sample composition, and more distinct at an early age.

This may be ascribed to the excessive moisture removal as evident from Figure 4-10 which results in dehydrated calcium silicate gel being non-distinguishable from slag. This is only speculative as the variation of the slag phase versus C-S-H composition has not been verified with a different Ca/Si ratio or moisture content in the C-S-H.

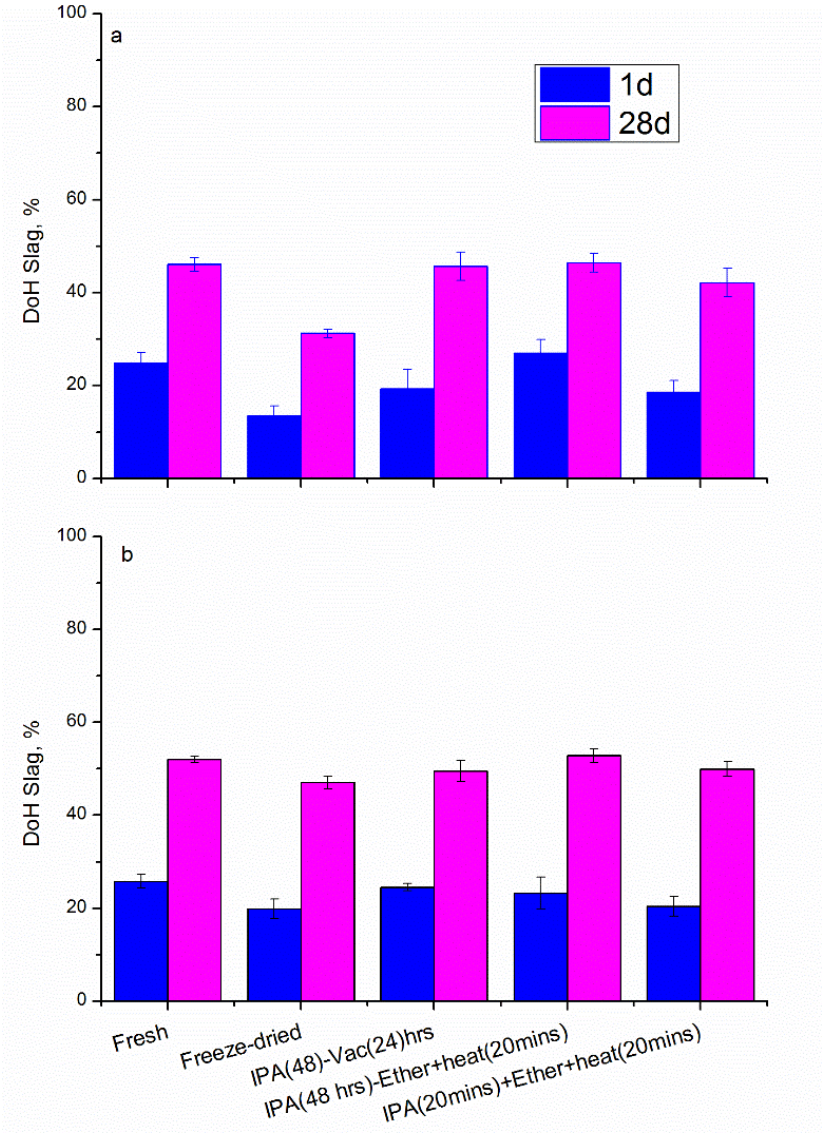

Figure 4-15 The degree of hydration of slag as a function of hydration stopping technique

(a) C2S1 and (b) C2S1-10L.

4.5 Accuracy of the PONKCS Method

The overall degree of hydration of clinker (Figure 4-14) shows that simultaneous implementation of the PONKCS phase has no bearing on the quantification of the crystalline phases hence clinker hydration. The hydration stopping technique had no significant influence on the degree of hydration. The average degree of

hydration of clinker from the mixes C2, C2S1, C2S1-10L was calculated to be 63, 58 and 66% after 1 day and 86.3, 82.8 and 87.6% respectively after 28 days. The standard deviation of the measurement ranged between 1.4 to 2.5 % and are consistent with those expected from the Rietveld refinement of cements [309]. The differences in the degree of hydration of clinker among the samples were as a result of the mix compositions (i.e. the presence of SCMs) rather than quantification errors.

The results from QXRD/ PONKCS must be validated by comparing with other independent methods [309, 369]. However, this is challenging for hydrated systems given that other independent methods have their inherent errors [29] as well as existence multiple semi-crystalline assemblages in hydrated cements which may interfere with the refinement. Based on the data presented above, it is clear that the degree of hydration of slag as measured by implementing the PONKCS phase was not significantly affected by the dehydration method [33, 369] except by freeze-drying. After excluding the freeze-dried data points, the precision of the measured residual slag content was ± 5% after 1 day as opposed to ± 2 - 3 % after 28 days. Consequently, the freshly ground sample which showed a minimal modification to the ettringite content (Figure 4-6 to Figure 4-10) was chosen to assess the accuracy of the technique. The composite slag cements reported in section 4.3 were hydrated for 1 and 28 days and then analysed by SEM/IA and QXRD/PONKCS and the results presented in Figure 4-16.

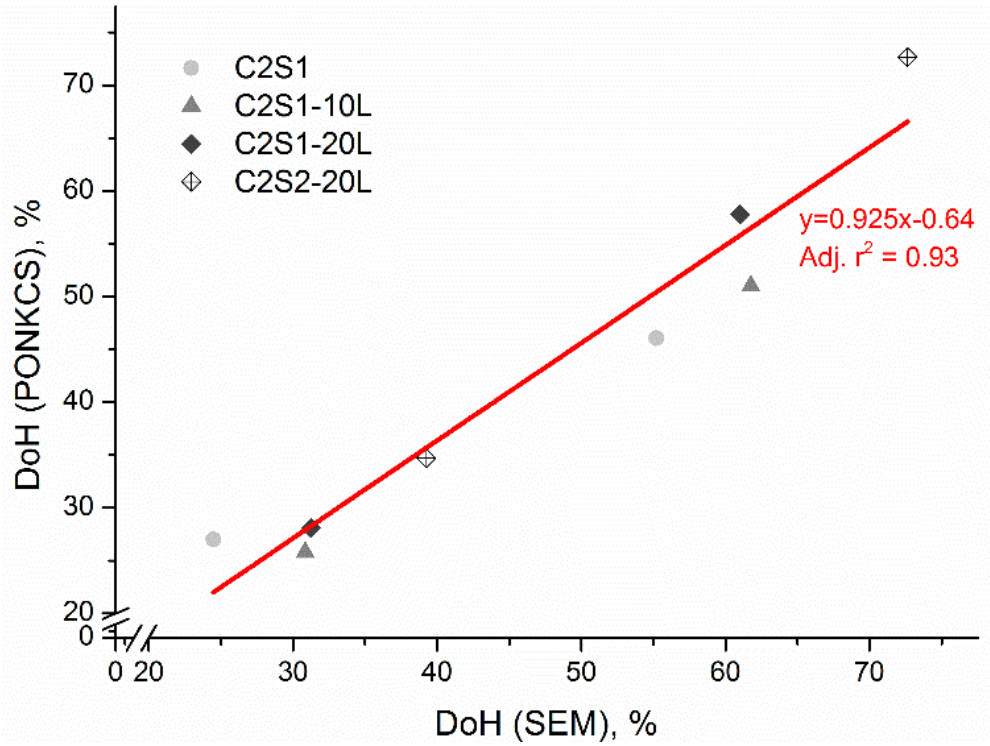

Figure 4-16 Comparison between the degree of hydration of slag by PONKCS method and SEM/IA

The standard deviation between the results from the two independent techniques ranged between 2 and 6 %. These were however distributed randomly among the data points.

A pitfall to SEM/IA is overestimation at early ages due to resolution problems and 2D representation of a 3 D problem [28, 29, 31]. Conversely, the PONKCS may also encounter problems at a higher degree of slag hydration as the amorphous phases increase in content at the expense of slag. Therefore, while the PONKCS method allows simultaneous evaluation of residual slag and clinker contents and hydrated phase assemblages, care must be taken to compare the data obtained with those from complementary techniques.

4.6 Recommendations for implementing the PONKCS method

The results presented in this section have demonstrated the sensitivity of the x-ray diffraction background to the water in the diffraction specimen. However, dehydration of samples can also modify the C-S-H, ettringite and to a lesser extent portlandite contents. These also have significant implications for the evaluation of the amorphous phase contents by PONKCS. However, the results have shown that, as long as the water content in the sample is adequately accounted for in the mass attenuation co-efficient, the solvent exchange has minimal impact on the residual slag content. Freeze-drying led to underestimation.

As a trade-off between the implementation of PONKCS and evaluation of hydrates, non-hydration stopped samples are recommended. By this, the MAC is held constant for hydrated samples as long as the sample w/b ratio is known. This preserves hydrates except for grinding effects and reduces errors in normalising the residual phase contents for the degree of hydration calculations. Subsequent data from PONKCS in this thesis are based on freshly ground non-hydration stopped samples. Double solvent exchange using iso-propanol and ether is adopted for TG due to less modification of the AFt/AFm contents compared to the other methods examined in this chapter.

Chapter 5
Hydration and microstructure of limestone ternary blends

In this Chapter, results and discussions on the hydration and microstructure of composite slag cements with and without limestone are presented. Hydration kinetics were followed by a combination of isothermal calorimetry, chemical shrinkage, XRD and thermogravimetric analysis. The hydration of slag was followed by SEM image analysis and implementation of the QXRD/PONKCS method developed in Chapter 4. The microstructure was followed by SEM and MIP. The pore volume and pore solution chemistry were further examined to clarify the synergistic effects between limestone and slag.

5.1 Mixes investigated

Six (6) primary mixes were selected from the preliminary mixes in Table 3-6 in Chapter 3. The rationale behind the selection of the mixes was as follows:

1. Identify the influence of limestone on the kinetics of clinker and slag hydration in ternary blends
2. Identify compositional effects of ternary blends on the microstructure and mechanical properties
3. Identify the drivers for the synergy in limestone ternary blends

Derivative mixes in which limestone or slag was replaced with quartz of similar fineness were also examined. The objective of the complementary quartz mixes was to isolate the filler effect from the active reaction of slag and limestone [29]. Details of the mixes investigated in the series are given in Table 5-1 and the techniques to characterise hydration and microstructure are given in Table 5-2.

Table 5-1 Mixes for investigating hydration and microstructure of limestone ternary blends

Nomenclature	CEM I		GGBFS		Limestone	Anhydrite
	42.5 R	52.5 R	S1	S2	L	s
	$\%_{mass}$					
C2		100	-	-	-	-
C2S1	-	50.68	47.08	-	-	2.34
C2Q1	-	51.84	48.16	-	-	-
C2S1-10L	-	51.18	38.03	-	8.55	2.24
C2Q1-10L	-	52.35	38.9[Q]	-	8.55	-
C1S1-10L	51.93	-	38.06	-	7.50	2.51
C1Q1-10L	53.27	-	39.0[Q]			
C2S1-20L	-	51.18	28.53	-	18.06	2.24
C2S1-20Q	-	51.18	29.2[Q]		18.47	-
C2S2-20L		51.18	-	28.53	18.06	2.24
C2Q2-20L		52.35	-	29.2[Q]	18.47	-

Table 5-2 Experimental matrix for the samples under investigation

Mix ID	Experimental Techniques						
	QXRD/ PONKCS	Calorimetry	Chemical shrinkage	SEM/IA	Pore solution	MIP	Thermal analysis
C2	√	√	√	√	-	√	√
C2S1	√	√	√	√	√	√	√
C2Q1	√	√	√	-	-	√	√
C2S1-10L	√	√	√	√	√	√	√
C2S1-10Q	√	√	√	-	√	-	√
C2Q1-10L	-	√	√	-	-	-	-
C1S1-10L	√	√	√	√	-	-	√
C1Q1-10L	-	√	√	-	-	-	-
C2S1-20L	√	√	√	√	√	√	√
C2S1-20Q		√	√	-	-	-	-
C2S2-20L	√	√	√	√	-	√	√
C2Q2-20L	-	√	√	-	-	-	-

5.2 Overview of hydration

The bound water, portlandite contents, and chemical shrinkage over the course of hydration gave a general indication of the progress of hydration in the investigated cements [12, 31, 285]. These parameters were all lower in the composite cements compared to the CEM I systems, when expressed per total binder mass.

Figure 5-1 shows the chemical shrinkage evolution in the key mixes for the first 28 days of reaction measured according to the methods described elsewhere [29, 31, 281]. The active role of slag from the very early stages of reaction can be seen from a comparison between mixes C2S1 and C2Q1.

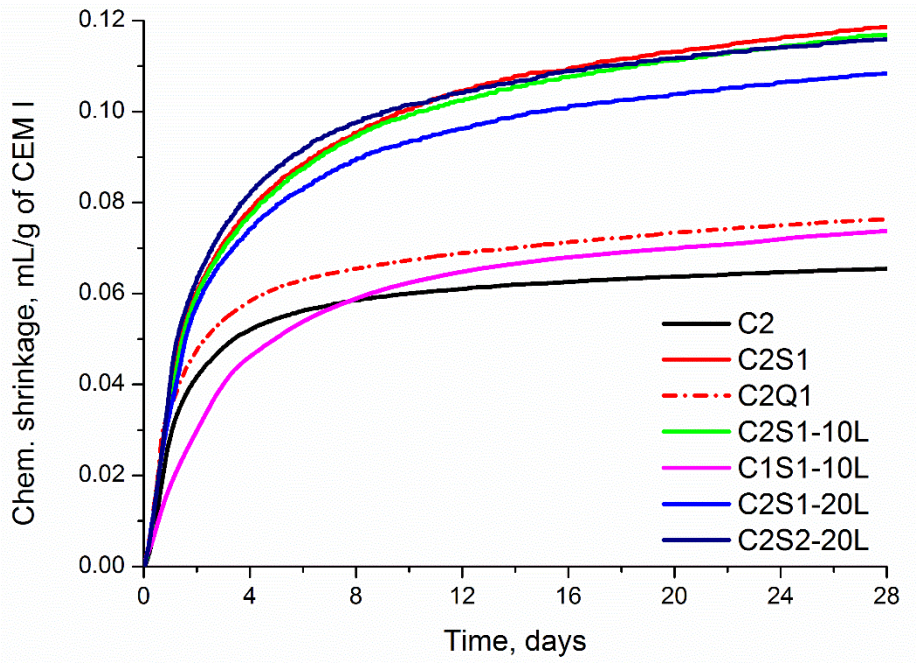

Figure 5-1 Evolution of chemical shrinkage in limestone ternary blends, normalised to the CEM I content.

The higher chemical shrinkage resulted from active hydration of slag and the filler effect on hydration of the major clinker phases. The filler effect, evidenced by mix C2Q1 compared to mix C2, increased the CEM I hydration. Similar observations

have been reported elsewhere [29, 31]. The indication of an active contribution from slag at an early age is not surprising considering that, slag is latently hydraulic and hence dissolution is initiated by the rise in pH following alite hydration [53, 86, 189, 193].

In the presence of 10 % limestone, shrinkage was similar to the binary slag blend except for slight increase at longer hydration times. However, increasing the limestone content further led, if anything, to a reduction in shrinkage, indicating an optimum limestone content or limestone to slag ratio.

The effects of the CEM I and slag fineness were also evident from Figure 5-1. Shrinkage increased at higher CEM I and slag fineness. However, the effect of CEM I fineness was more significant compared to slag such that a doubling of the CEM I fineness increased shrinkage proportionately. On the other hand, increasing the slag fineness by a similar factor only increased shrinkage by ~ 20%. Consequently, despite increasing fineness leading to the improved reactivity of slag in composite cements, it seems that raising the CEM I fineness affected shrinkage more positively than slag.

The effect of limestone in the ternary blend becomes clearer in a like-to-like comparison of ternary blends where quartz is utilised instead. This is illustrated in Figure 5-2 also as a function of the CEM I fineness.

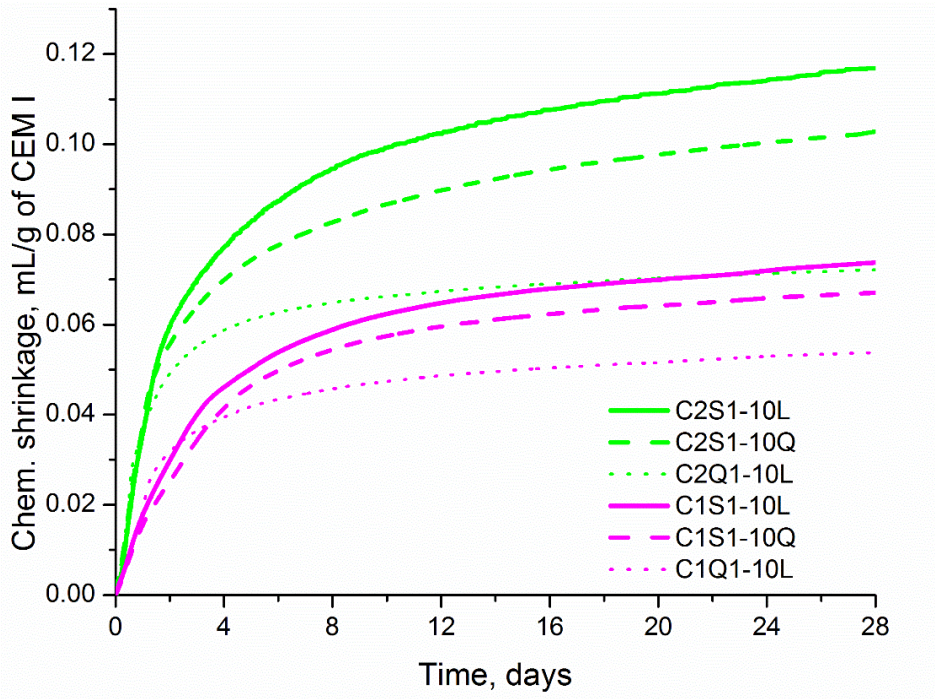

Figure 5-2 Effect of slag, limestone and CEM I fineness on the chemical shrinkage of ternary blends.

Shrinkage increased in the presence of limestone compared to the ternary blend with the inert filler. This is indicative of the positive impact of limestone as espoused previously [177]. The inertness of limestone in OPC-limestone cements is suggested elsewhere [224] but in the presence of alumina-rich systems, the reaction of these is encouraged [7, 177, 178].

An indication of the influence of limestone being dependent on reacted slag can also be deduced from the difference between the limestone and quartz ternary blends (Figure 5-2). The impact of limestone was greater in the CEM I 52.5R blend compared to the CEM I 42.5R blend. This also suggests that the synergy between alumina-rich SCMs and limestone [7, 177, 370] is also dependent on the fineness of components.

Portlandite evolved as a product of CEM I hydration but in composite cements, these would be consumed by the reaction of slag and limestone as well as ettringite formation [7, 17, 174]. Consequently, the portlandite content is a function of the degree of hydration of CEM I and SCMs [12, 18]. Figure 5-3 indicated that the portlandite content as measured from the TG data may be higher or lower than the neat cement depending on the mix composition.

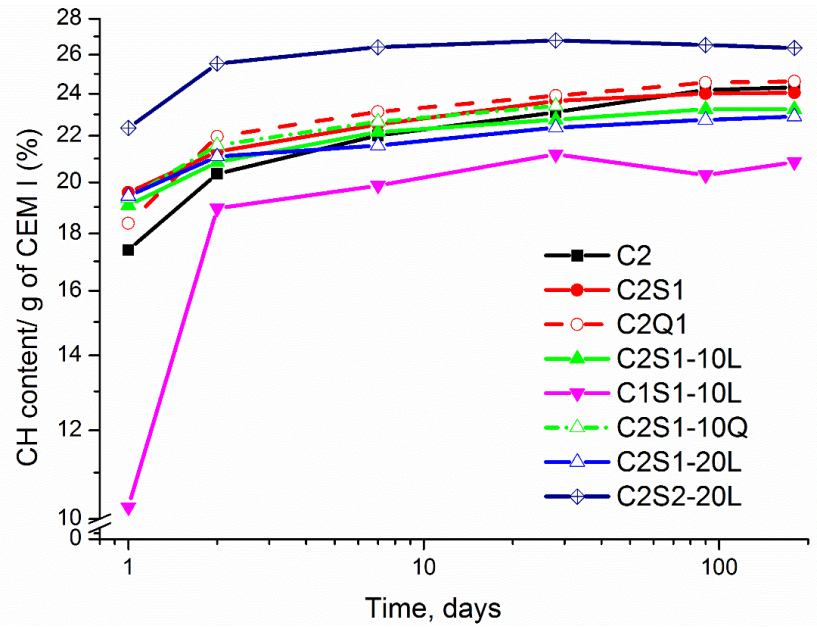

Figure 5-3 The influence of slag, limestone and fineness on the evolution of portlandite, by TGA

The samples reported here were hydration stopped by the double solvent exchange technique as recommended in Section 4.6.

In the CEM I 52.5R (C2) blends, a higher portlandite content was measured compared to the reference mix C2 (after normalising to the clinker content), for the first 7 days. This is suggestive of enhanced clinker hydration in the presence of the SCMs and quartz. Slightly higher portlandite contents in the composite slag cements after 1 day suggests an enhanced filler effect in these mixes compared to

the quartz-bearing mix. This is consistent with results reported elsewhere [51]. The higher portlandite in the composite slag cements may also arise from the alkalis present in the slag, yet absent in the quartz. The K_2O content in the slag (0.47%) and the Na_2O were the same as in clinker. These alkalis will accelerate clinker reaction [371-373]. After 2 days, however, the portlandite content in mix C2Q1 was consistently higher than the composite slag cements and the neat system. The lack of portlandite-consuming reactions in mix C2Q1 compared to the slag blends may explain this. Similar trends have been reported elsewhere [52].

Gradual consumption of portlandite in the slag blends explains the lower portlandite content over the course of hydration. The contents in mixes C2S1 and C2S1-Q were similar but lower in the limestone containing cements. Increasing the limestone content from 10 to 20% further reduced the portlandite content. This is indicative of the formation of calcium bearing hydrates including additional C-S-H from slag and carboaluminates from limestone [7, 14, 177, 370].

The slag and clinker fineness significantly influenced the portlandite content as evident from Figure 5-3. At a given replacement level, the CH content increased with both the CEM I and slag fineness. The effect of CEM I fineness was more critical at early hydration times (≤ 1 day) such that after 1 day, the CH content in the CEM I 42.5 R ternary blend was ~ 50 % lower than a similar mix but with CEM I 52.5 R. The shortfall in the CH content, however, became smaller from 2 days onwards. This observation is consistent with the findings of Vuk *et al.* [374]. Enhanced alite hydration with increasing clinker fineness as well as the acceleration of alite in the presence of limestone accounted for these. From the mineralogical composition in Chapter 3, the CEM I 52.5 R contained ~5 % more

C_3S than the CEM I 42.5 R. Consequently, more CH would be expected to evolve. In the ternary blend containing 20 % limestone, the finer slag also had ~ 2 – 3 % more portlandite than the normal slag. This is due to the effect of slag fineness on the dissolution of alite and belite as reported elsewhere [191].

Interpretation of the implications of the portlandite content must take into account the cement composition, progress of hydration and hydrates. For example, the finer slag combined with 20 % limestone means higher nucleation centres and substrates for hydrate growth and increased effective w/b ratio. The combined effect may accelerate hydration of the major clinker phases and slag and at the same time promote limestone dissolution [51]. On the other hand, for mix C1S1-10L, the clinker hydration is much slower. This can promote [141] or hinder slag dissolution in terms of maintaining the pH as calcium is bound into the C-S-H upon slag dissolution. In either case, the impact on the microstructure may be greater. Hindered slag hydration may be advantageous for CEM I hydration due to the available space. Conversely, promoted slag dissolution may also yield a better microstructure.

The nature and volume of hydrates formed determines the amount of water bound into hydrates for a given mix [12, 55, 375]. The bound water contents of the various systems also normalised to the CEM I content are shown in Figure 5-4. The bound water content in mix C2Q1 was slightly higher than in mix C2 which is indicative of the filler effect [10, 53, 67]. The bound water contents in the composite slag cements were considerably higher than the filler and the neat reference cement. This is attributable to the additional C-[A]S-H evolved from slag hydration [31, 211], the tendency for the C-[A]-S-H in composite cements to incorporate higher

proportions of alkalis [194] and oxidation of sulphides in slag into sulphate bearing hydrates [376].

Mixes C2S1 and C2S1-Q showed similar bound water contents but that in mix C2S1-10L was higher from 7 days onwards. Increasing the limestone content from 10% to 20% slightly reduced the bound water content. Nucleation effects of limestone on CEM I hydration [51, 67] plus stabilised ettringite and carboaluminate formation [177] explains the higher bound water content in the presence of limestone. However, due to the limited amount of limestone which may actively react [17, 173, 178], a higher limestone content led to reductions in the actively hydrating constituents and hence lower bound water content. This is consistent with the experimental and thermodynamic data presented elsewhere [201].

The hydraulic activity in composite cements is also influenced by the physical attributes of constituents [377] as evident from Figure 5-4. The bound water contents were significantly lower in the CEM I 42.5 R ternary blend up to 28 days but the difference became narrower with hydration time. The slower reaction rate in the CEM I 42.5R explains the early age deviation in the bound water content and this is also reflected in the CH content. The effect of slag fineness was comparatively small with the margin becoming less distinct over the course of hydration. This indicates that the slag fineness may not have significant implications on the nature of hydrates but the CEM I fineness seems definite. A similar conclusion was reached by Oner *et al.* [197] who recommended finer grinding of clinker as opposed to slag in maximising strength development.

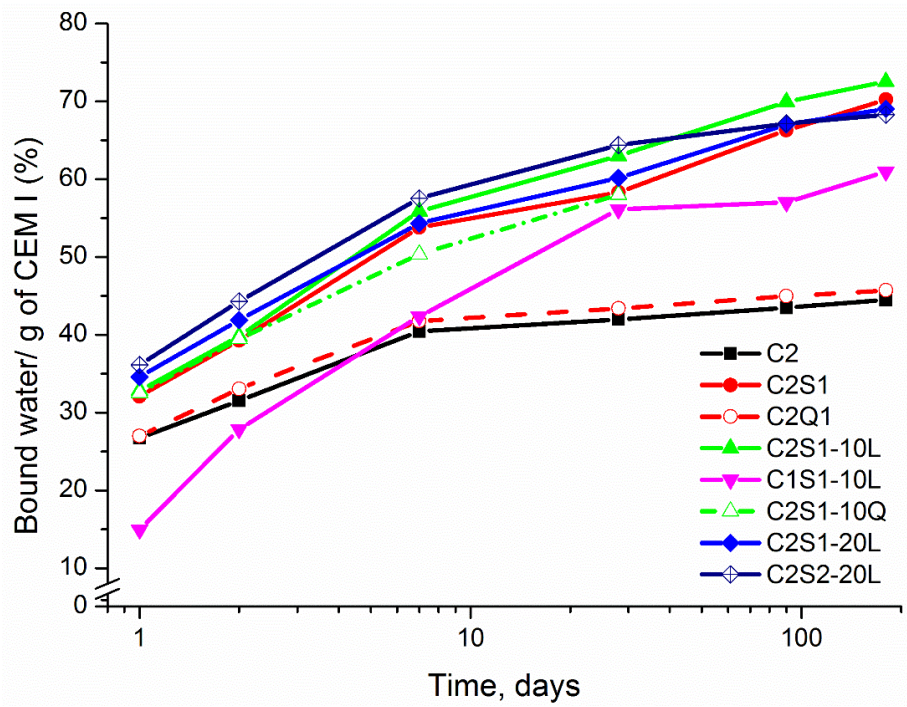

Figure 5-4 The influence of slag, limestone and fineness on the bound water contents of ternary blends, by TGA

The discrepancy between the bound water and portlandite contents can be explained by considering how the two properties vary with the progress of hydration. Bound water increases due to slag hydration [160, 243], while portlandite content decreases upon slag hydration [10, 31, 193]. Therefore, an increased portlandite content can only be ascribed to increased hydration of the clinker phases, while increased bound water and shrinkage cannot be unambiguously assigned. Notwithstanding, all three indicators (i.e. bound water, portlandite contents and chemical shrinkage) suggest that the effect of limestone in the composite cements is clearly distinct from a filler effect.

5.2.1 Influence of slag and limestone on the kinetics

The filler and reactive roles of slag and limestone on the early stage hydration were further examined through calorimetry and quantitative XRD.

The effect of slag on the rate of reaction is shown in Figure 5-5. The filler effect on clinker hydration and the reaction of slag can be distinguished. In the presence of slag or quartz, the induction period was slightly shortened; with the acceleration of the reaction peak attributable to alite hydration. The acceleration possibly arose from the CH consumption which then displaced equilibrium and consequently further alite dissolution [196] rather than surface area effects since the clinker (CEM I 52.5 R) had higher Blaine than slag.

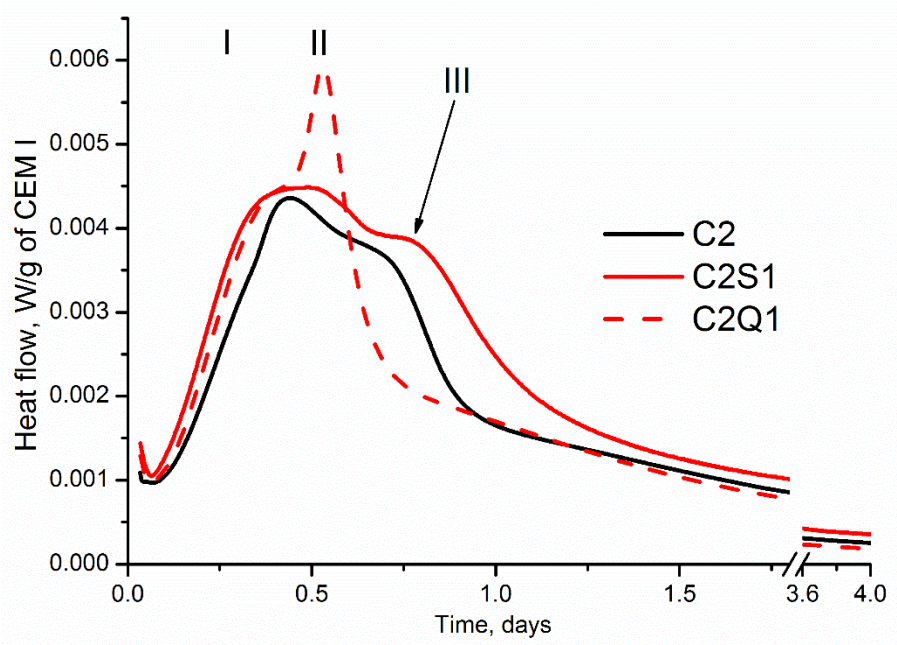

Figure 5-5 The influence of slag and inert filler on the rate of reaction

The alite hydration peak was of similar intensity in mixes C2S1 and C2Q1 but was higher than for the mix C2. This has often underpinned the assertion about the inertness of slag at the early stages of hydration [51]. However, slag is latently hydraulic [378, 379], and therefore dissolution should commence upon portlandite availability. However, the chemical shrinkage and cumulative heat flow (Appendix A.1.2) yield uncertain results about slag hydration in the first 12 hours but this may change with increasing slag hydration [191].

A shoulder (denoted II) was noticed in all mixes. This peak was previously assigned to the effect of slag on the aluminate reaction [31, 55, 370], slag hydration [190] and sulphate depletion [107]. The position of the peak (II) was similarly affected by slag and quartz and occurred earlier in the composite cements compared to the control mix C. The intensity was however much higher in the mix C2Q1 than C2S1 because there was no additional sulphate, apart from that interground with the CEM I 52.5 R. The effect of the inert filler was similar to those of rutile and corundum but differed from the quartz mix reported elsewhere [315]. The fineness of the filler and replacement level may explain the difference such that, nucleation centres increase with the replacement and hence extended reaction [51].

The anhydrite added to the composite cements resulted in a third reaction peak which is labelled III (Figure 5-5). This is consistent with the results from other studies [178, 283]. Despite being more soluble compared to gypsum and hemihydrate, dissolved sulphates from anhydrite can also persist longer in the pore solution [380]. The ensuing calcium reduces the pH which then affects the release of aluminates from slag to withdraw these from solution. The global effect of this, however, depends on the dosage and distribution in the hydrating matrice.

Comparison between the binary and ternary slag blends with limestone and quartz are shown in Figure 5-6. The effect of quartz on the alite hydration was similar in the binary and ternary blend.

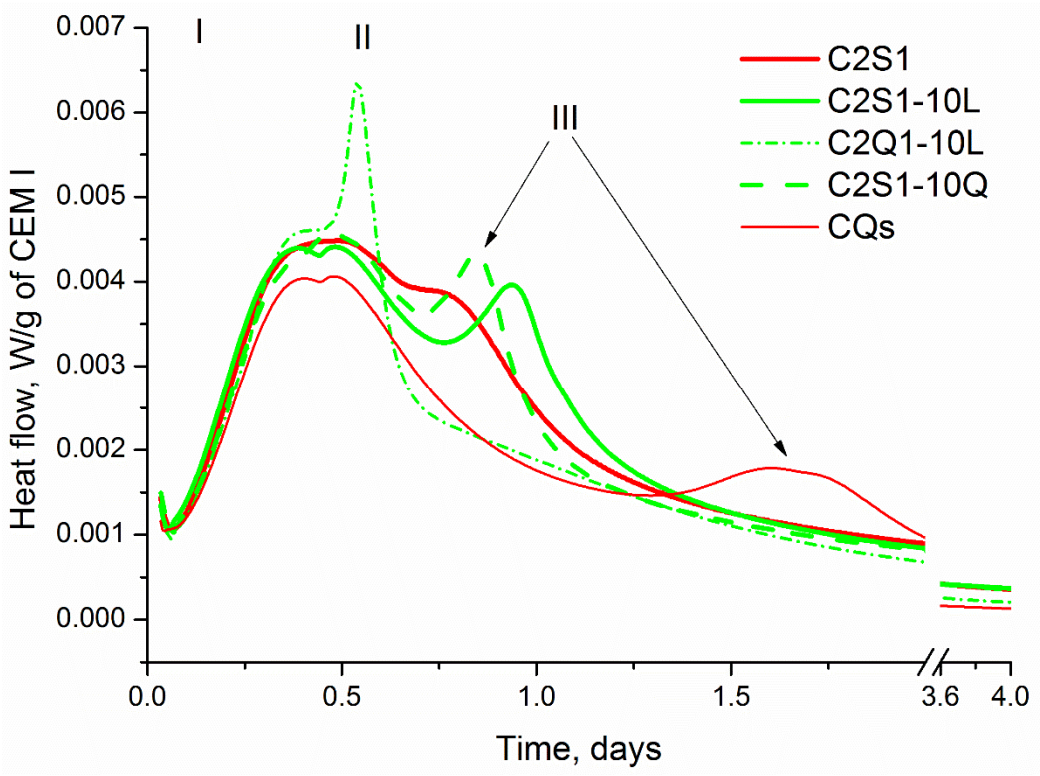

Figure 5-6 The influence of limestone and added sulphate on the rate of reaction of ternary blended cements.

The alite hydration peak was accelerated but the presence of limestone further accelerated this. This is consistent with the observations of Berodier and Scrivener [51] that limestone exhibits a stronger filler effect than quartz. The acceleration effect of sulphates on alite hydration suggested elsewhere [283] was not observed when anhydrite was combined with the quartz blend and the aluminate reaction was further delayed. A slight shoulder which seems to be merged with the alite peak was also noticed in the ternary blends and the peak intensity was similar to that in the binary blends of quartz and slag. This peak, denoted as II has been termed the aluminate reaction peak [107]. This is possibly attributable to the depletion of sulphates interground with the CEM I as discussed already for the binary blend.

The anhydrite depletion peak, III was further delayed in the ternary blends than in the binary mix C2S1. The is attributed an increase in the SO_3/Al_2O_3 ratio [381] upon partially replacing slag with limestone. At equivalent SO_3/Al_2O_3 ratio, the inert filler had an accelerating effect on the consumption of the added anhydrite in the ternary blend while the reverse was true for the binary mix C2Q$. In the ternary blends, the maximum of this secondary peak was observed after 20.4 and 22.7 hours in mixes C2S1-10Q and C2S1-10L respectively. The observation in the binary mixes confirms the persistence of sulphates in the pore solution [380] due to short supply of aluminates. In the ternary blends, however, the common ion effect of calcium in anhydrite and calcite [382] may have explained the effect of quartz and limestone on the peak III. Here, despite higher solubility of anhydrite compared to calcite, simultaneous dissolution of limestone is usually the case [17] and hence further delays the precipitation of ettringite.

Beyond the major reaction peaks, heat evolution from the slag mix was consistently higher than from the quartz blend and the neat CEM I 52.5 R mixes. This is indicative of active contribution of slag hydration.

5.2.2 Influence of limestone content and constituent fineness on the kinetics of hydration

Figure 5-7 shows the implications of limestone content plus the fineness of clinker and slag on the early age reaction kinetics.

5.2.2.1 Limestone content

Increasing the limestone content from 10 to 20 % would be expected to increase the number of nucleation centres [51]. This explains the shortened induction period with increasing limestone content as indicated in Figure 5-7. However, the intensity

of the alite reaction peak (I) and the sulphate depletion/aluminate peak II were not affected by the limestone content. The effect of the limestone content agrees with the findings on ternary blends reported elsewhere [225] but deviates from OPC-limestone systems [220].

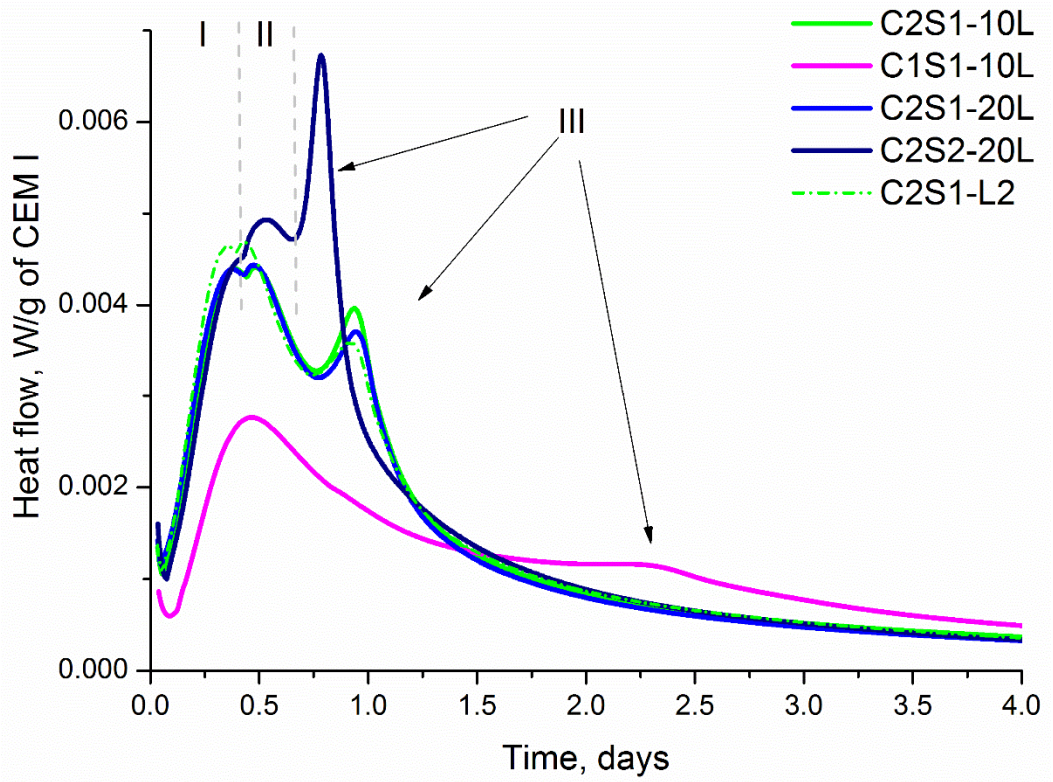

Figure 5-7 The influence of limestone content, slag and CEM I fineness on the rate of reaction of ternary blended cements.

The factors leading to the enhanced alite reaction may not be limited to nucleation effects only. Additionally, the reaction of calcite with portlandite [9, 159, 383] can destabilise the portlandite – C_3S equilibrium and consequently promote silicate dissolution. The accelerating effect of SO_3 on alite hydration has been espoused elsewhere [384] but this effect was not noticed by Zajac *et al.* [178]. If influential at all, the sulphate content would be similar across the cements and hence can be discounted. Consequently, limestone accounted for the accelerated alite reaction.

A reduction in the intensity of the peak III was noticed upon increasing the limestone content from 10 to 20 %. This may be attributed to suppressed aluminate reaction [159] but inconsistent with the results reported elsewhere [178]. It, therefore, appears that the occurrence of the peak (i.e. position) to a greater extent depended on the threshold SO_3/Al_2O_3 ratio in the mix but the intensity reduced when the ratio increased.

5.2.2.2 Clinker fineness

The higher clinker fineness accelerated dissolution and intensified alite hydration (Figure 5-7). This arose from the increased surface area of hydrating grains in direct contact with water in the finer cement. In agreement with the chemical shrinkage, bound water and portlandite contents, the heat associated with the alite reaction was ~50 % lower in the CEM I 42.5 R blends compared to the companion mixes made with CEM I 52.5 R. A decreasing trend of the rate of reaction of the silicate peak with coarser clinker is reported elsewhere [220, 385] and the Figure 5-7 shows consistence. The first aluminate reaction peak II was not distinct but the peak III was also delayed until ~ 54 hours as opposed to 24 hours in the CEM I 52.5 R blends.

5.2.2.3 Slag fineness

For a given CEM I fineness, there was no further acceleration or intensified alite reaction peak after increasing the fineness of slag. This may seem inconsistent with the findings reported elsewhere [191]. However, the fineness range reported in [191] was much wider between 10 – 50 µm whereas the D_{50} for the two GGBS investigated here were 10 and 5 µm for S1 and S2 respectively (see Figure 3-2). Notwithstanding, slag S2 had finer particles under 5 µm than S1 and hence would be expected to provide additional nucleation sites for alite hydration unless a

threshold probably existed for this. The likelihood of there being a threshold for slag fineness beyond which the nucleation effects yield no marginal returns cannot be dismissed on the basis of the findings reported elsewhere [191, 197].

The slag fineness significantly affected the aluminate peaks (II and III). The position of the II did not change with the slag fineness. This indicates that, for a given cement and sulphate level, the slag fineness had no accelerating effect on the C_3A hydration [178] which accounted for the peak II. Contrary suggestions have been made elsewhere [14]. The intensified peaks, II may be ascribed to an enhanced conversion of the intermediate hydrate, C_3AH_6 [386]. The accelerated peak III with increasing slag fineness may have arisen from the uptake of dissolved sulphates in solution [381] by additionally dissolved aluminates from the finer GGBS.

5.2.2.4 Limestone fineness

At a given CEM I and slag fineness, the alite hydration peak (I) was accelerated and intensified by using a finer limestone. This is consistent with the data reported elsewhere [370] and can be explained by the increased surface area and nucleation centres [51] provided by the finely ground limestone. The possibility to form an amorphous carbo-silicate product has also been suggested elsewhere [387] for the enhanced alite hydration. However, the solubility of calcite is significantly lower than silicates and hence, co-precipitation is least probable. A condusive substrate seems likely. The finer limestone enhanced peak II at the expense of III (Figure 5-7) but the positions were marginally accelerated.

Having examined the influence of the composition and fineness, the reaction kinetics can be separated into physically (peaks I) and chemically (II and III) driven

steps. The observations from clinker, slag and limestone fineness reinforce the view that the early age reactions (I) is filler-induced [51, 375] and limestone is favourable. Peak II depends on the sulphate type, dosage and dissolved aluminates probably from C_3A. The anhydrite depletion peak, III heavily depends on aluminates coming into solution which is in turn enhanced by the slag and clinker fineness. Beyond the major reaction peaks, the rate of reaction was highest in the limestone containing cements particular the CEM I 42.5 R mix compared to the CEM I 52.5 R mixes. This may be attributable to the simultaneous hydration of CEM I and slag.

5.2.3 Impact on the hydration of the major clinker phases

With calorimetry suggesting differences in the alite and aluminate hydration, quantitative XRD was used to evaluate the reaction of the major clinker phase assemblages. The focus here was on the implications of slag, limestone content plus the fineness of CEM I and slag. Complementary mixes where slag and limestone were alternately replaced with quartz enabled the filler effect to be separated from SCMs reaction. The degree of reaction of the four major clinker phase assemblages is shown in Figure 5-8.

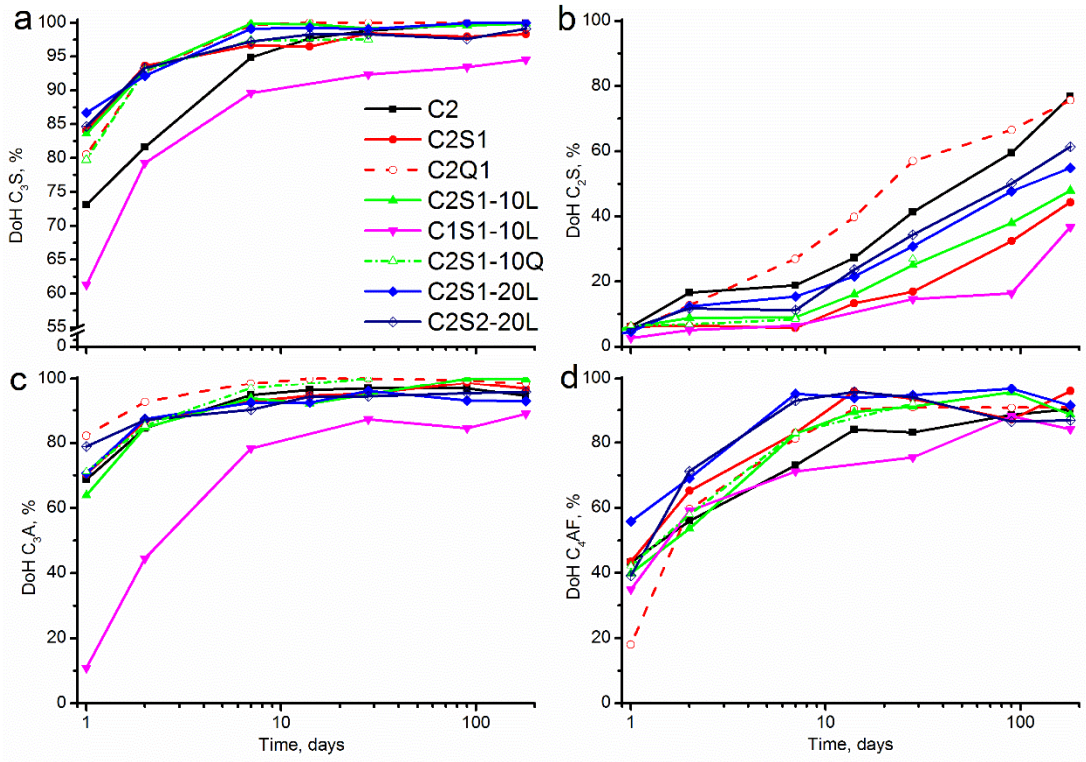

Figure 5-8 Influence of slag, limestone and inert filler on the hydration of the major clinker phase, as determined by QXRD

Note: Measured by QXRD, error margin ±2%; (a) Alite, C_3S; (b) Belite, C_2S; (c) C_3A and (d) Brownmillerite, C_4AF

Alite hydration was accelerated in all composite cements in the first 7 days as can be noticed from Figure 5-8a. The accelerating effect of slag on alite hydration was greater than that of the inert filler. This means that filler effect from slag and quartz on alite hydration are different as opposed the results presented in [51]. The difference in CEM I fineness and mineralogical composition compared to the previous investigations may explain the acceleration. Notwithstanding, limestone providing a better substrate for nucleation [51], the alite reaction was not distinctly accelerated after 1 day. Increasing the limestone content did not enhance alite hydration further. Enhanced dissolution at the very early age stages of reaction due to the high clinker fineness may have overshadowed the acceleration [178,

374]. Increasing the fineness of clinker enhanced hydration alite hydration such that, the degree of hydration of alite in the mix C1S1-10L was ~ 20 % lower than that of C2S1-10L. The slag fineness resulted in a slightly higher alite hydration after 1 day but was not different from the other cements beyond this; consistent with [191]. The early age alite hydration is consistent with the calorimetry (Figure 5-5) portlandite evolution (Figure 5-3). It is evident that for the particle size ranges considered, the finely ground clinker (CEM I 52.5 R) influenced alite hydration more than slag despite the latter being more finer.

Figure 5-8 b indicates lower degree of belite hydration in the binary slag mix (C2S1) compared to the neat cement, C2. Indeed, retarded belite hydration in composite slag cements has been suggested elsewhere [29, 31]. Comparison between mixes C2S1 and C2Q1 indicates that the effect of slag on belite hydration is not associated with the filler effect. The highest reaction of belite was noticed in the binary quartz blend. This may also explain the slightly higher portlandite content measured in the mix C2Q1.

In the ternary blends, however, the presence of limestone compensated for the retarded belite hydration, such that the residual belite content was similar to that seen in mix C2 beyond 7 days. The accelerated belite hydration was however not observed in the first 7 days when slag was blended with quartz instead of limestone, i.e. it is the presence of limestone in the ternary blend which accelerated belite hydration. Limestone providing favourable nucleation sites for C-S-H compared to quartz [388] may explain the accelerated belite hydration at an early age. However, the extent of belite hydration in samples C2S1-10Q and C2S1-10L was similar after 7 days. This seems to suggest that the available space for hydrate

growth [193] alone may not be responsible for the enhanced belite hydration. The extent of belite hydration at 20% limestone was much higher than at 10%. Belite reaction was enhanced with the CEM I fineness but the slag fineness was disadvantageous especially at an early age but became insignificant at longer hydration times. These may be associated with pore fluid compositional effects of dissolved carbonates and silicate dissolution [389].

Slag and quartz both accelerated the hydration of ferrite but the effect of limestone was relatively small. The C_3A content was influenced by the presence of the inert filler, slag and/or limestone. The C_3A content in the binary quartz blend was slightly higher than in the composite slag cements. The effect, however, seem to be an early age one as the difference was consistent throughout the investigated hydration times. However, by 1 day the C_3A remaining in mix C2Q1 was about half that in the slag blends. The higher slag fineness also had an accelerating effect on the C_3A hydration but no difference was noticed beyond 2 days. The clinker fineness affected the C_3A similar to all other phase assemblages; being retarded in the CEM I 42.5 R blend. These effects were also evident in the calorimetry plots in Figure 5-5 to Figure 5-7. Consequently, the presence of slag, limestone and the inert filler improved the overall clinker hydration as shown in Figure 5-9.

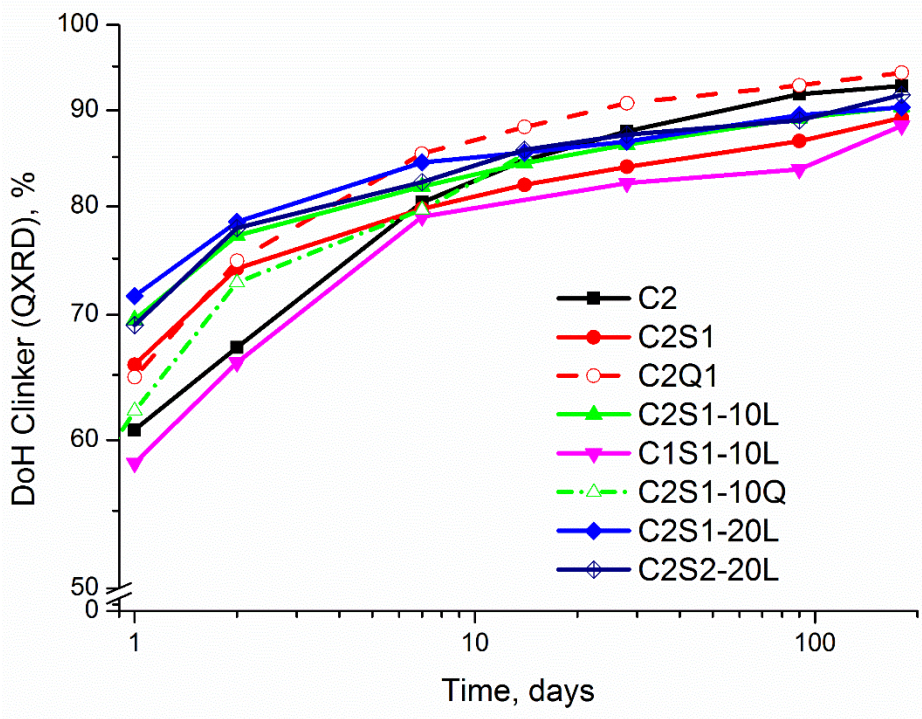

Figure 5-9 Influence of slag, limestone and constituent fineness on the degree of hydration of clinker.

Note: DoH of clinker is the sum of the degree of hydration of the major clinker phases in the CEM I as measured by QXRD. The error margin of the measurement is ±2%.

It is, however, noteworthy that from 2 days onwards, the degree of clinker hydration was slightly lower in the composite slag cements compared to the binary CEM I - quartz mix.

5.2.4 Impact on slag reaction

The data presented so far have shown differences in the kinetics of hydration of the major clinker phases due to the presence of slag, limestone and quartz. Consequently, the effect on the kinetics of slag hydration is worth examining. Using the procedure described elsewhere [29, 31], the net chemical shrinkage due to slag hydration in the different blends were extracted from the data presented in Figure 5-1 and Figure 5-2. The shrinkage as associated with slag hydration is shown in Figure 5-10.

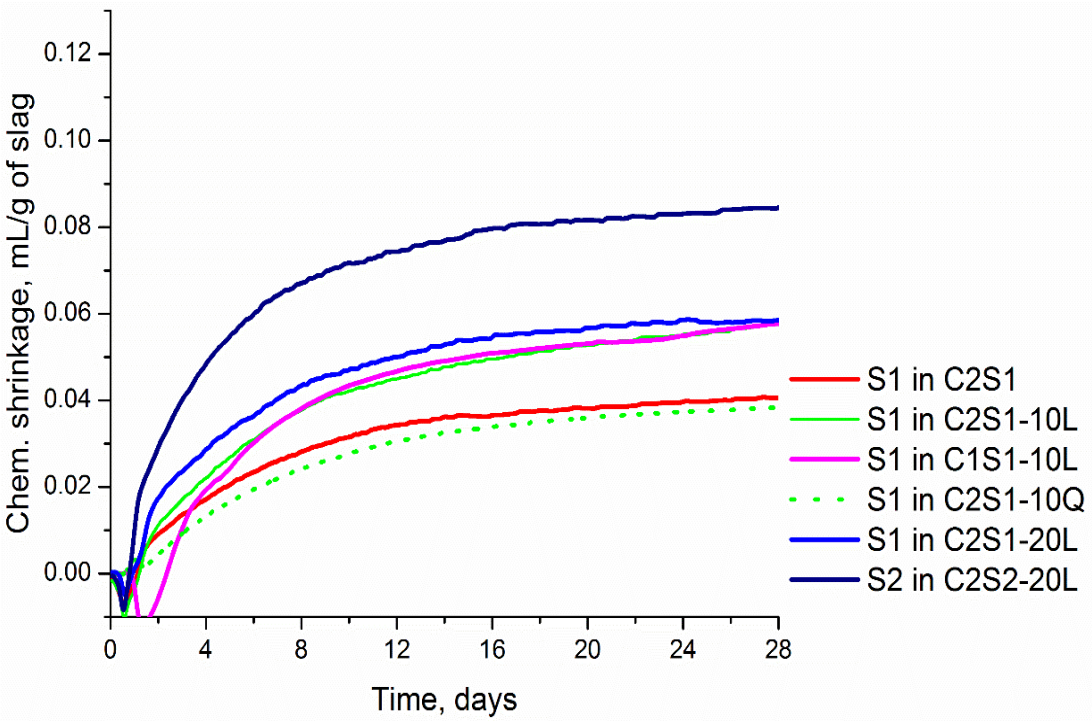

Figure 5-10 Chemical shrinkage due to slag reaction in composite slag cements.

It can be noticed that in all composite cements investigated, slag underwent hydration from the very early ages. The noise in the data at an early age is associated with the differences between the filler effects arising from slag and the inert quartz [51, 144]. The presence of limestone enhanced slag hydration, while the replacement of limestone with quartz had a slightly deleterious impact on slag hydration. This indicates that limestone plays an active role on the hydration of slag.

The shrinkage due to slag hydration increased with increasing limestone content but the effect of slag fineness was more dominant. Despite a significantly lower shrinkage per mass of paste in the mix C1S1-10L (Figure 5-1), the shrinkage due to slag hydration was comparable to the CEM I 52.5 R blend. The exception was at an early age where the degree of hydration was lower in the former. The independence of the degree of slag hydration on the clinker fineness has been

reported elsewhere [143]. Consequently, the higher clinker fineness was only advantageous for the early age reactions but the effects in the long term were insignificant. This is consistent with the degree of hydration of clinker (Figure 5-9). Accelerated clinker hydration with increasing fineness led to rapid precipitation of portlandite which in turn raised the pH for slag dissolution.

The chemical shrinkage method is however only semi-quantitative and requires calibration in order to estimate the actual degree of reaction of slag [29]. Two independent methods, implementation of a PONKCS phase for GGBS in the Rietveld refinement of XRD and BSEM/IA, were subsequently used to quantitatively measure the degree of slag hydration. Representative BSE images and their corresponding Magnesium maps are given in appendix A.1.4. Plots of the Rietveld refinement of the mixes including the implementation of the PONKCS phase for GGBS are also given in appendix A.1.3. Figure 5-11 shows the degree of slag hydration up to 180 days, as measured by QXRD/PONKCS.

Measured by the QXRD/PONKCS method, error in the measurement is ± 2%.
Slag hydration was greater in the limestone-containing cements at all ages. The clinker fineness was only influential at an early age as also indicated by chemical shrinkage. The slag fineness had a clear influence right from the early age. However, the method has an inherent error of ±2 %, thus the effects at early ages cannot be definitely stated. By 1 day, the degree of slag hydration was about 25 % in the CEM I 52.5 R blends with or without limestone and 20 % in the CEM I 42.5 R blend whilst the finer slag blend was ~ 35 %.

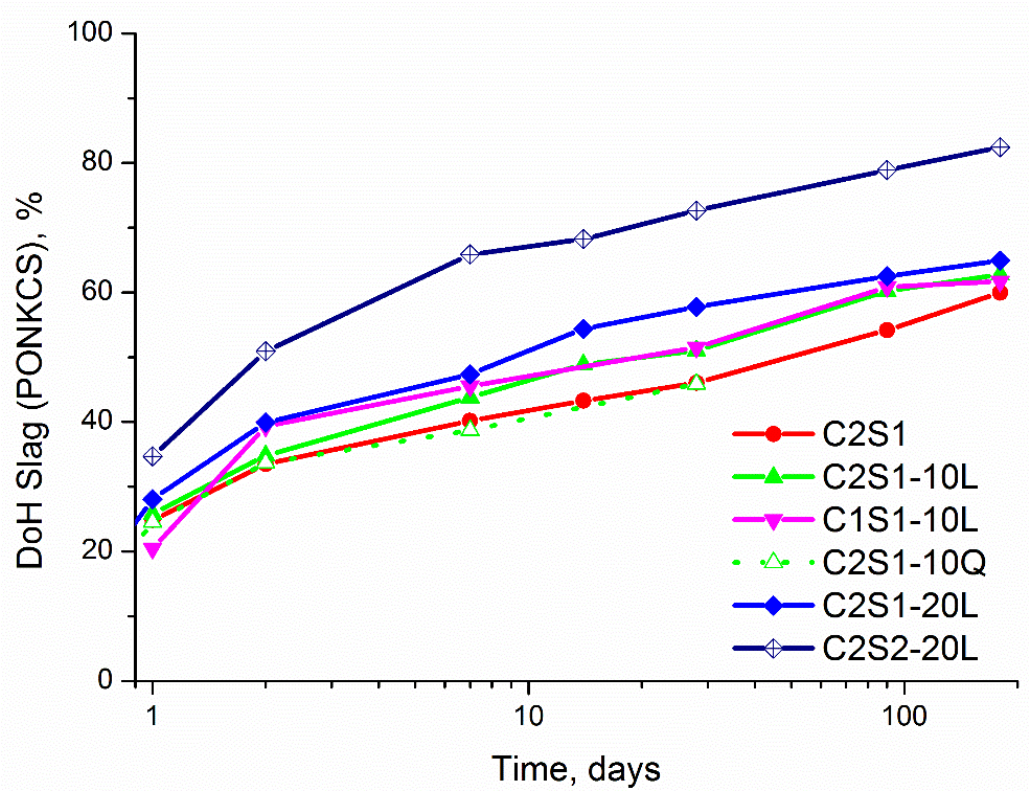

Figure 5-11 Effect of limestone and inert filler on slag hydration of composite cements.

The degree of hydration values are similar to the values reported elsewhere for slags of similar composition [29, 31], but greater than those reported by Snellings *et al.* [33]. By 2 days, the enhanced reaction of slag in the presence of limestone became clearer, with the effect slightly increasing with increasing limestone content. Substitution of limestone with quartz clearly demonstrated that the interaction which led to improved slag hydration is not observed with the inert filler.

Comparison between the degree of hydration as obtained from QXRD/PONKCS and BSEM/IA is shown in Figure 5-12. The two independent methods gave similar trends of slag hydration. The residual plot of the data points was randomly distributed. Consequently, the coefficient of determination was computed as 0.96. It is noticed that the BSEM/IA overestimates the degree hydration of slag by approximately 13% especially at the early ages.

Chemical shrinkage is a method commonly used as an alternative to evaluate slag hydration in composite cements [29, 31]. The comparison between the shrinkage and the degree of slag hydration from the PONKCS method up to 28 days is shown in **Figure 5-12** (inset). The chemical shrinkage due to slag at the very early stages of reaction does not fit into the linear relationship which is seen from 1 day onwards.

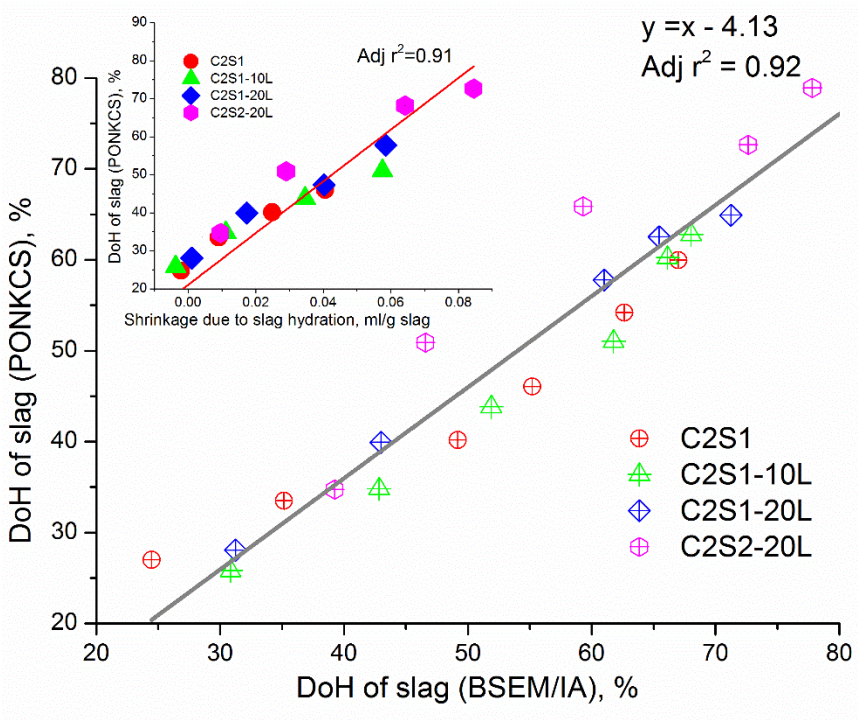

Figure 5-12 Comparison between DoH as quantified by QXRD/PONKCS BSEM/IA and chemical shrinkage.

Inset is the degree of slag hydration by QXRD/PONKCS versus chemical shrinkage due to slag. Note ±2 % margin of error associated with the data from QXRD/PONKCS

In fact, negative shrinkage is calculated for some of the mixes after 12 hours. This may seem to suggest that the hydrates in the quartz blends (assumed to be inert) are more voluminous than in the slag blends. But this is inconsistent with the results from the other techniques. Rather, the differences in the precipitated C-S-

H density at higher water contents may account for the larger chemical shrinkage in the quartz blends [390].

5.2.5 Impact on limestone reaction

The kinetics of clinker and slag hydration suggest that limestone powder played the dual role of a filler and reactant. The reactive role was followed by thermogravimetry. Consequently, the consumption of limestone was investigated by thermal analysis.

The DTG plots in Figure 5-13 show reductions in the calcite endotherms across all four ternary blends.

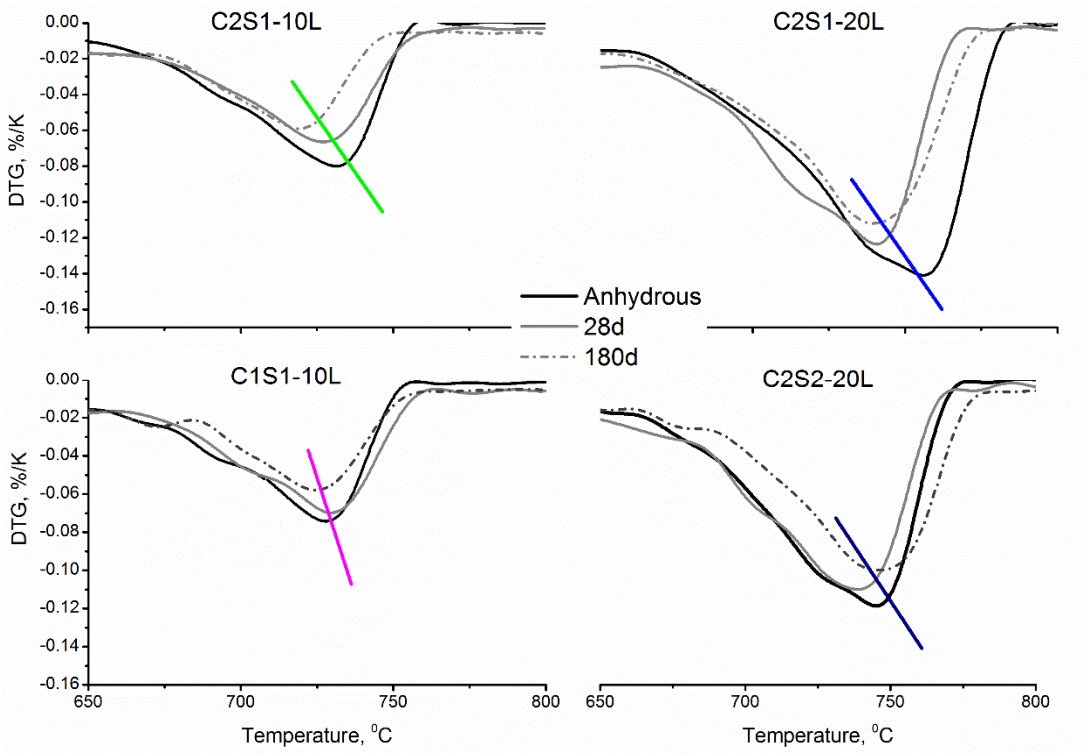

Figure 5-13 Consumption of limestone in the ternary blends

Shifts in the lowest point of the endotherm were noticed. However, there was no consistent pattern to the endotherm shifts. Notwithstanding the shifts, consumption

of calcite is evident as has been reported by several authors [7, 177, 370, 375]. The consumption rates, however, seems different in the composite cements.

To clarify the kinetics, the degree of reaction was quantified from the TG data and the results shown in Figure 5-14. The degree of reaction after 1 day was 20 % in the mix C2 but mostly under 10 % in the composite cements except for the mix C2S2-20L which had ~ 15 % of calcite reacted. This means that more calcite was consumed in the composite cements than the neat cement. The higher dissolution of calcite at the early age is associated with the moderate pH of the pore solution in the composite cements compared to the neat cement [178, 391].

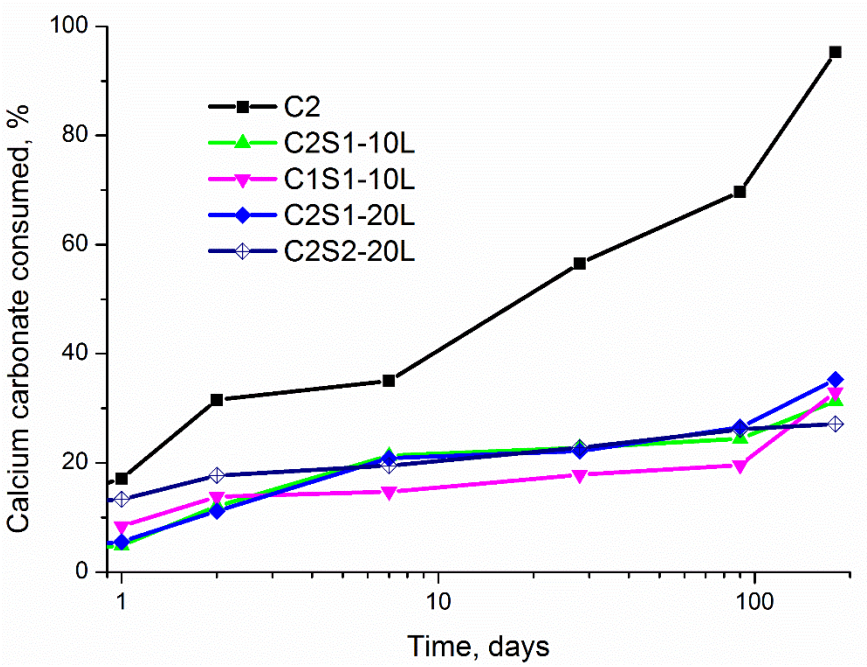

Figure 5-14 Degree of reaction of limestone in composite cements compared to the neat cement

The dissolution of calcite also contributes calcium to the pore while clinker hydration is also accelerated by limestone; both could potentially increase the pH to levels where calcite dissolution may be inhibited (pH> 13). However such effects would be counteracted by the reaction of slag [194] thus promoting further

dissolution of calcite. Moreover, the additionally dissolved alumina from slag also may also act as precursor [178] and hence promote calcite dissolution.

The 1.9% of calcite present in the anhydrous CEM I 52.5 R reacted completely after 180 days. However, the ternary slag-limestone blends still contained significant residual calcite after this time. Calcite consumed in the fine slag blend was higher than the other ternary blends within the first 2 days. That in the CEM I 42.5 R blend was comparable to the normal slag (S1) blends but then was consistently lower until 180 days where the degree of calcite reacted was similar among the various cements.

The degree of reaction of calcite ranged between 27 and 35 % in the investigated cements. This translates to ~ 3.5 and 7 % in the mixes containing 10 % and 20 % limestone respectively. The lower bound is consistent with the limited reaction of calcite as reported elsewhere [17, 178]. The higher degree of calcite consumption in the mixes containing 20 % limestone may be related to the dissolved SO_3/Al_2O_3 ratios [173, 174]. The previous section indicated enhanced slag dissolution (which due to the increased alumina content of the slag equates to more dissolved Al_2O_3) in the 20 % limestone blend compared to 10 %. This means that, at the 3 % SO_3 content in all composite cements, the SO_3/Al_2O_3 ratio decreased with the slag dissolution and consequently promoted calcite dissolution [173]. This could also be due to the preferential formation of monocarboaluminate over hemicarboaluminate at 20 % limestone content (to be discussed in section 5.1.7) which then shifts the carbonate-aluminate-sulphate balance [173, 174].

The fineness of slag and clinker impacted on the reaction rates but not the overall calcite reacted. The higher slag fineness promoted the early dissolution of calcite.

The seemingly higher early age calcite consumption in the C1S1-10L can be attributed to the ~ 3.9 % $CaCO_3$ interground with the CEM I 42.5R. This is consistent with the results reported elsewhere [220].

5.2.6 Effect of slag and limestone on the hydrates formed

The fineness of CEM I and slag have been shown to influence kinetics. However, these would not be expected to impact on the nature of hydrates [10, 31, 178, 392]. Consequently, this section mostly focused on the effect of slag and limestone additions and less so on the fineness of constituents.

The hydration products were identified by TG, XRD and SEM-EDX. It should be noted that all composite cements except mix C2Q1 contained 3 % total sulphate content. Aluminates from the dissolution of slag affected the SO_3/Al_2O_3 ratio in the pore solution and hence the sulphate and carbonate-bearing phase assemblages [173, 174]. Figure 5-15 shows DTG plots from the various mixes. The C-S-H & AFt endotherm was lowest in the mix C2Q1 at all hydration times due to the reduction in the overall aluminate and sulphate content.

Precipitation of ettringite was observed in all mixes from 1 day, with mixes C2 and C2S2-20L also showing evidence for AFm. This is consistent with the results from calcite dissolution (Figure 5-14). There was also more ettringite and C-S-H in the mix C2 compared to the slag blends after 1 day due to more C_3S per binder [14] and higher aluminates in solution from C_3A than slag. The sulphate interground with the CEM I [381] may also partially account for more ettringite in mix C2 than the composite cements at an early age.

At longer hydration times, the ettringite and C-S-H content were higher in the composite cements. The presence of limestone increased the ettringite/C-S-H

content compared to the binary slag blend and the trend was consistent throughout the study. Additional C-S-H from slag [10, 31, 194, 196] and the stabilised ettringite in the presence of limestone [7, 155, 159, 177] may explain the deeper endotherm.

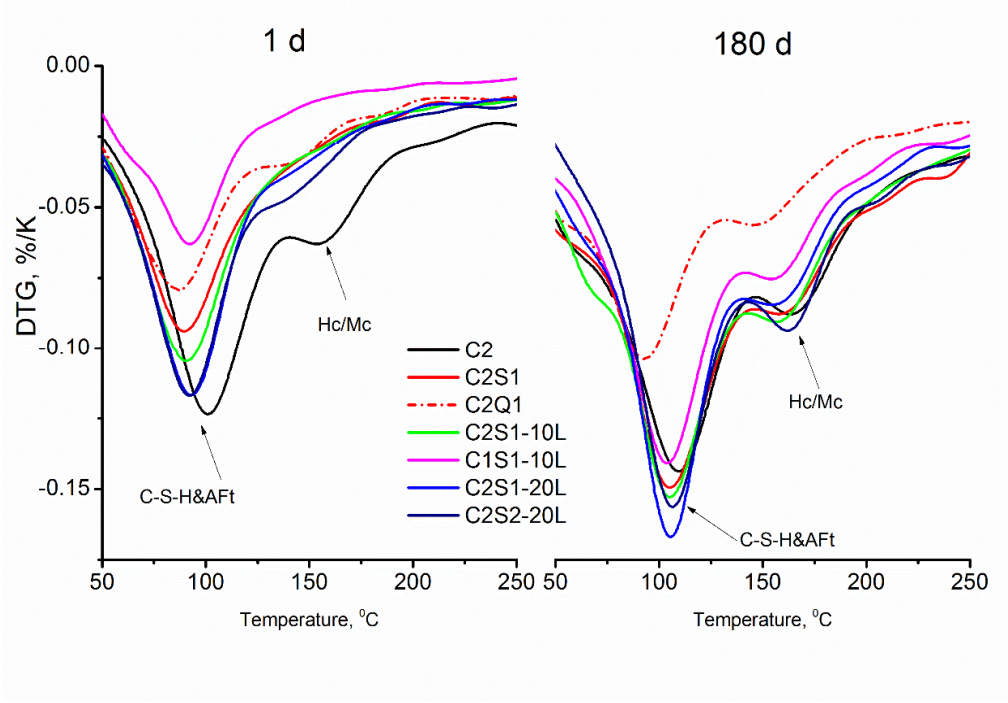

Figure 5-15 DTG of paste samples hydrated for 1 and 180 days.
AFt= ettringite; Hc/Mc= calcium hemi carboaluminate and calcium mono carboaluminate.

The CEM I 42.5 R ternary blend, however, showed lower C-S-H/AFt endotherm compared to the CEM I 52.5 R blends except after 180 days due to the additionally formed C-S-H. The effect of slag fineness was less distinct from DTG trace apart from the Hc/Mc contents. The observations after 1 day are consistent with the calorimetry data with respect to alite and aluminate reactions (Figure 5-7) and the calcite consumption (Figure 5-14).

The TGA data (Figure 5-15) showed co-existence of sulphate- and carbonate-bearing phases over the course of hydration. However, mass losses due to these

phases overlapped other hydrates such as C-S-H. XRD gives a better resolution of the different hydrates.

Precipitation of ettringite was evident in all the cements after 1 day (Figure 5-16). In the mix C2, all the ettringite was formed within 1 day, beyond this the content decreased slightly, but no monosulphate was formed. Instead, hemicarboaluminates were formed, ultimately transforming to monocarboaluminates [7, 17, 155].

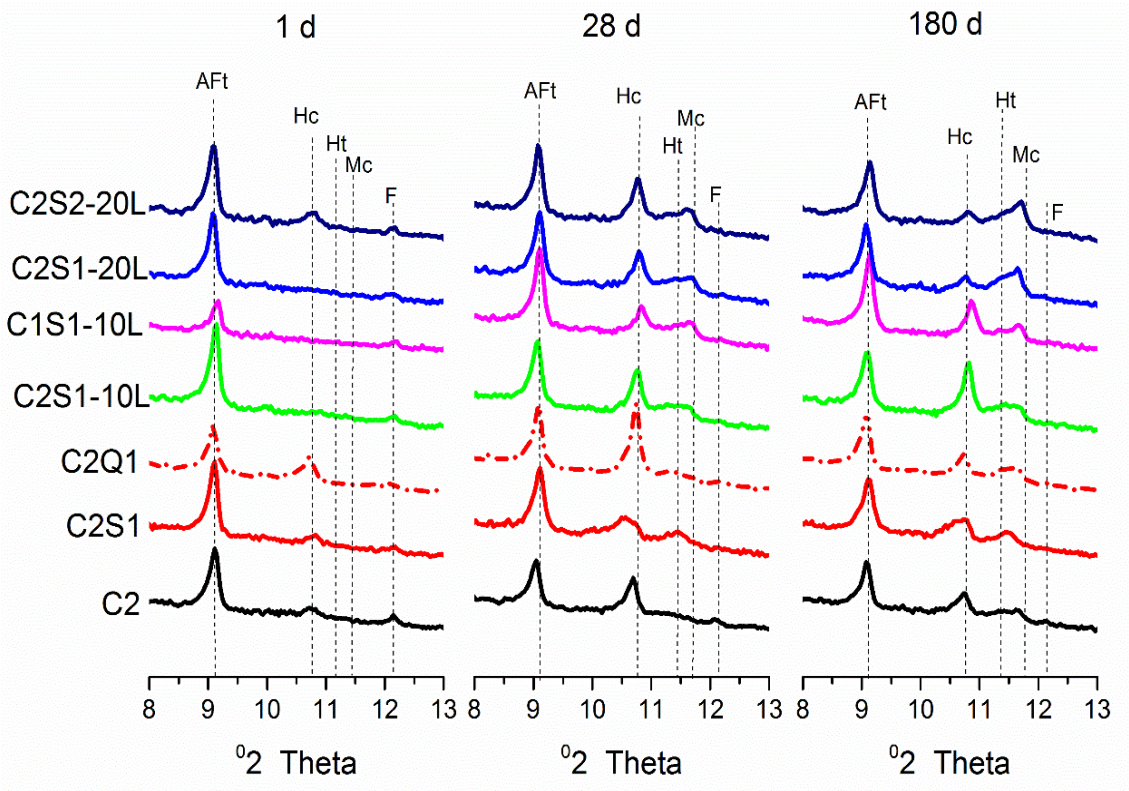

Figure 5-16 Effect of slag and limestone interaction on the sulphate and carbonate-bearing phase assemblages after 1, 28 and 180 days hydration.

The evolution in the binary quartz blend was similar to that in mix C2. In the slag blends however, the ettringite peaks were slightly higher than in the mix C2, but with elevated carboaluminate levels. Hemi and mono-carboaluminates were

formed after similar durations in the binary blends and the mix C2, but sooner in the limestone blends. The balance between hemi and mono-carboaluminates shifted to mono with increasing limestone content [173, 174]. This is a further indication of progressive calcite dissolution and agrees with the degree of calcite consumption shown in Figure 5-14.

A hydrotalcite peak (Ht) can be seen in all slag blends; becoming more prominent after longer hydration times [31, 143, 393]. The ettringite content was significantly lower in the mix C1S1-10L compared to the CEM I 52.5 R blends. The higher slag fineness only promoted hemicarboaluminate formation as was also evident from the DTG but no effects in the long term. The observations are consistent with the data on kinetics reported in the preceding sections and specifically with the C_3A hydration shown in Figure 5-8c.

Quantitative analysis of the ettringite and carboaluminates (Figure 5-17) confirm differences in the aluminate bearing phase assemblages. The highest ettringite content was noted in the reference mix, CEM I 52.5 R but the content reduced with time. Mix C2S1 was showed similar evolution to the reference but those in the ternary blends were stabilised [7, 17, 155, 159, 177]. The conversion from hemi- to mono-carboaluminates commenced after 7 days but the two coexisted even after 180 days. Monocarboaluminates precipitated earlier in the ternary blends and the contents were considerably higher than the neat cement and the binary slag blend.

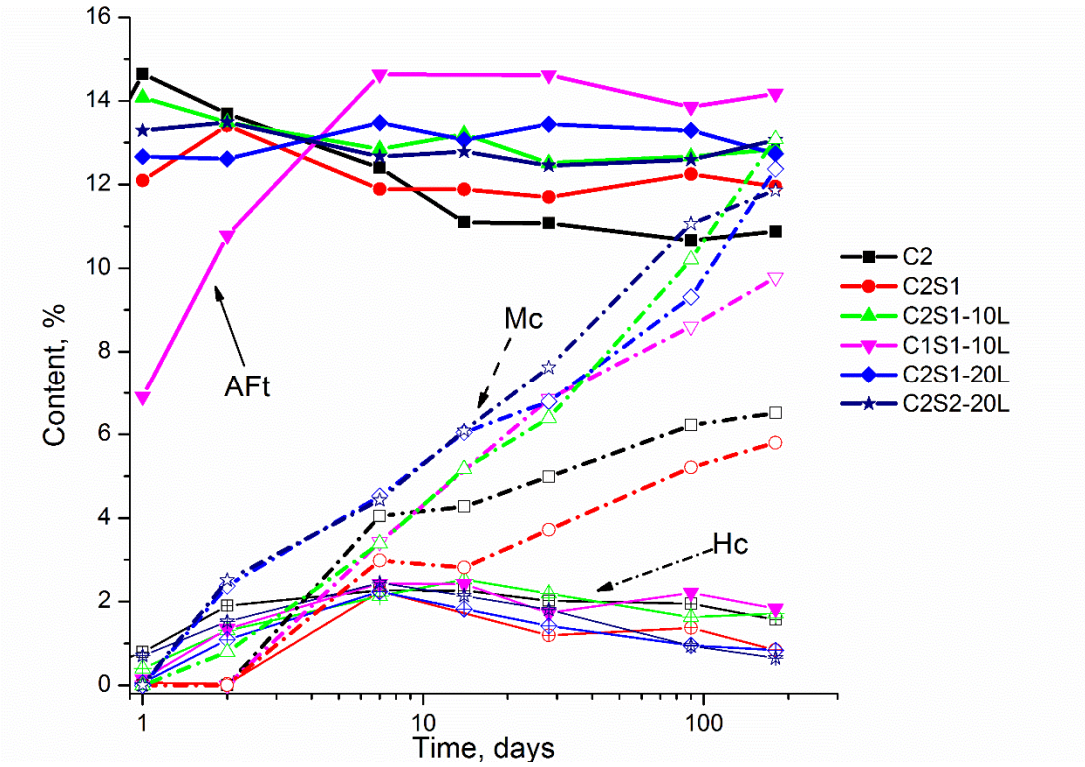

Figure 5-17 Effect of limestone content, slag and clinker fineness on the evolution of ettringite and carboaluminate assemblages.

The reactivity of limestone is evident from the carboaluminate evolution and the controlling mechanism for calcite dissolution can be deduced. More calcite reacted in the ternary blends compared with the control but this was independent of the initial limestone content [178]. However, that monocarbolauminates precepitated earlier at 20 % limestone replacement indicate accelerated dissolution with increasing limestone content. This is underpinned by accelerated slag reaction at this replacement level and hence the aluminates to form AFm. Secondly, the C-S-H or carboaluminates themselves may reduce the alkalinity of the medium [103, 194] and consequently promote dissolution.

More ettringite and carboaluminates in the limestone blends (Figure 5-16 and Figure 5-17) would influence the alumina concentration in the pore solution [17] and consequently the incorporation into the C-S-H. The Al/Ca versus Si/Ca ratios

of the C-S-H was investigated by SEM/EDX and the results shown in Figure 5-18. The atomic Ca/Si, Al/Si ratios of the C-S-H and Mg/Al ratio of the slag rim are summarised in Table 5-3.

The composite cements had different C-S-H composition compared to the pure cement system [31, 143, 194]. The Ca/Si ratio decreased from 1.92 in mix C2 to 1.52 in mix C2S1. Similar Ca/Si values have been reported elsewhere [143]. However, the ternary limestone mixes showed slightly higher Ca/Si ratios (1.61 and 1.72). The effect of limestone on the C-S-H composition is not well documented for ternary systems. Chowaniec [394] reported the C-S-H composition as a function of the C_3A and sulphate content in a composite cement containing 10 % limestone. It was reported that the Ca/Si increased with gypsum dosage. Montanaro *et al.* [395] also reported lower Ca/Si ratios in the presence of either anhydrite or limestone. Consequently, the increase in the Ca/Si ratio observed may be ascribed to additional calcium from the enhanced belite hydration in the presence of limestone Figure 5-8b or dissolution of calcite.

The use of slag in the blends led to an increase in the C-S-H Al/Si ratio, consistent with the data reported elsewhere [31, 207, 211]. However, the ternary blends showed slightly lower C-S-H Al/Si ratios than mix C2S1. However, the C-S-H Al/Si ratio did not a change upon increasing the limestone content. The alumina bound into other hydrates may explain the fixation of the content in the C-S-H.

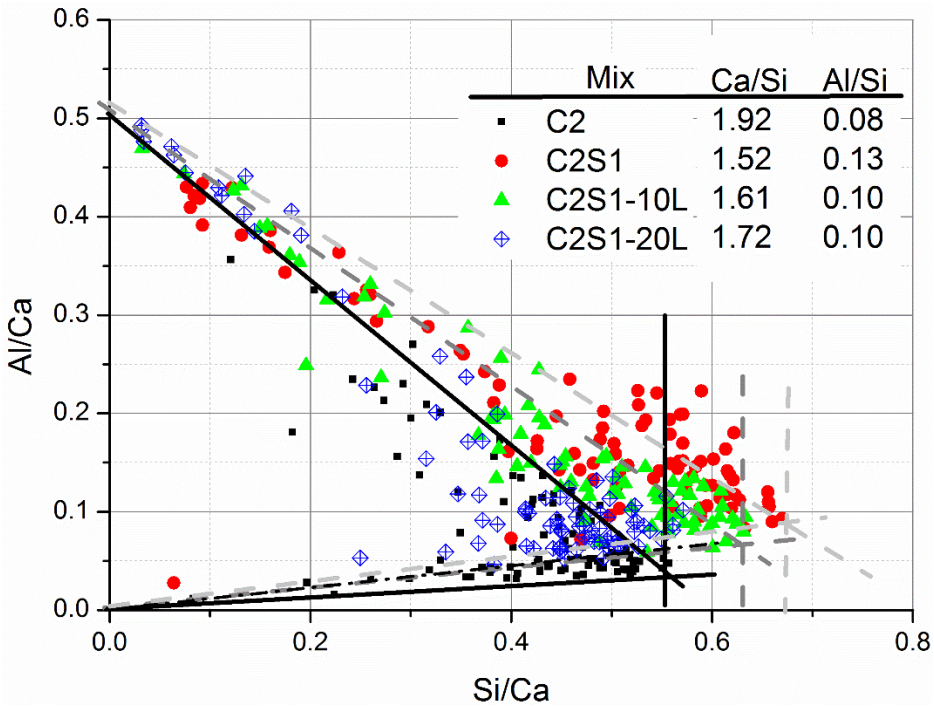

Figure 5-18 Effect of slag and limestone interaction on the C-S-H composition as analysed by SEM/EDS.

SEM/EDS data may also be used to determine the composition of the hydrated slag rim. Representative image for analysing the composition of the slag rim is shown in Figure 5-19. The composition was determined from 50 EDS points taken across several hydrated slag particles. The Ca/Si and Al/Si ratios were determined as for the C-S-H (Figure 5-18) but the Mg/Al ratio of the hydrotalcite-like phase was taken as the slope of the Mg/Si and Al/Si plot upon slag hydration [31].

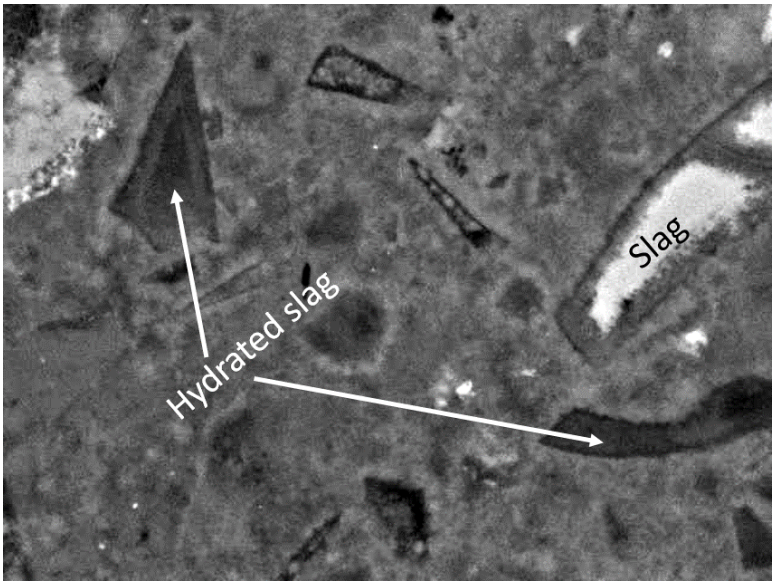

Figure 5-19 Representative SEM image for compositional analysis of hydrates

Table 5-3 shows the atomic Ca/Si, Al/Si and Mg/Al ratios of the C-S-H and the slag rim at the three limestone replacement levels (0, 10 and 20 %). These are consistent with the ratios reported elsewhere at similar replacement levels [194, 396].

Table 5-3 Effect of slag and limestone interaction on the composition of the C-S-H and the slag rim (± 0.02)

Phase	Atomic ratio	C2S1	C2S1-10L	C2S1-20L
C-S-H	Ca/Si	1.521	1.612	1.722
	Al/Si	0.130	0.105	0.103
Slag rim	Ca/Si	1.354	1.393	1.475
	Al/Si	0.203	0.325	0.314
	Mg/Al	2.18	2.69	2.56

The Ca/Si and Al/Si ratios increased in the presence of limestone and further at higher limestone content. The hydrotalcite in the binary mix had an Mg/Al ratio of 2.18, while the limestone bearing mixes showed a higher ratio up to 2.69.

5.2.7 Effect of slag and limestone on the pore structure

An overview of the distribution of hydrates in the four mixes is illustrated in the backscattered SEM image recorded after 180 days, Figure 5-20.

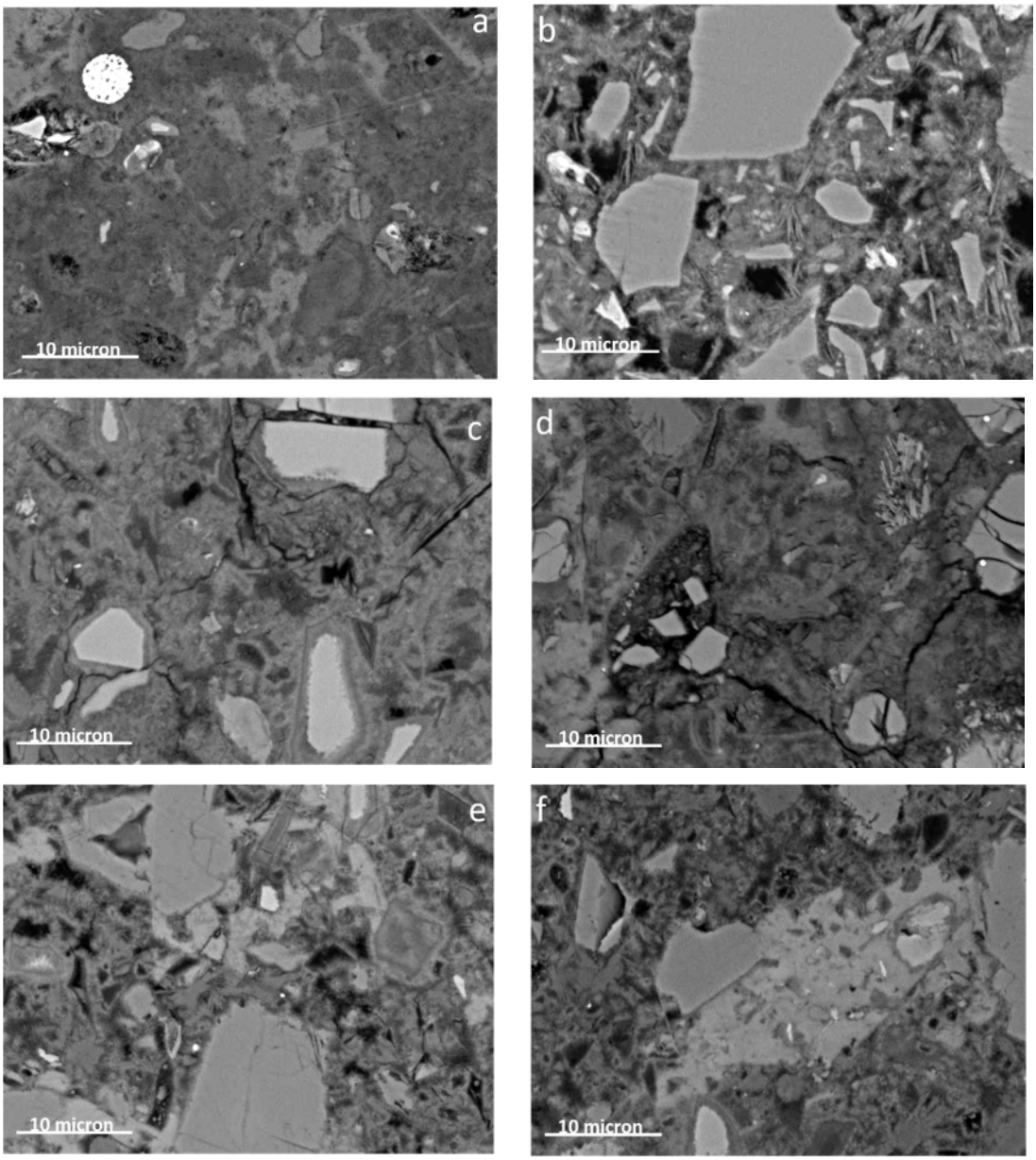

Figure 5-20 Microstructures of composite slag-limestone cements after 180d

(a) C2 (b) C2Q1; (c) C2S1; (d) C2S1-10L; (e) C2S1-20L; and (f) C2S1-20L: Images recorded at 2000x magnification and 15KeV accelerating voltage

A compact mixture of the C-S-H, portlandite, unreacted grains and pores can be noticed in all mixes. In the mix C2, the microstructure appears to a uniformed C-S-H with an intersperse of portlandite, pores and unreacted grains. The visually identifiable pores are also finer compared to the composite cements. The mix C2Q1 is visibly more porous due to the inert quartz.

The hydrotalcite-like product of slag hydration is recognisable from the composite cements. The finer grains can be identified as having reacted completely alongside partially reacted larger grains. A similarly compact but less porous microstructure was observed for the mix containing 10 % added limestone. Thus efficient utilisation of slag in the presence of limestone [10, 67].

A more porous microstructure, however, ensued upon increasing the limestone content to 20 % but increasing the slag fineness counteracted this.

This indicates a more refined microstructure upon increasing the slag fineness [54, 103]. The pore structures were characterised by the pore entry diameter, as determined by MIP, and the results after hydration for 1, 7, 28 and 180 days are shown in Figure 5-21. The mixes considered were C2, C2Q1, C2S1-10L and C2S1-20L.

The critical pore sizes were refined as hydration progressed in the various cements. The smaller changes in the critical diameters in mix C2 (55nm to 40nm by 180 days) was due to the more rapid early age hydration in this mix. The composite slag cements showed slightly coarser critical pore diameters than mix C2 after 7 days. However, by 28 days the situation was reversed, and their pore structures were much finer, particularly than for mix C2Q1, i.e. the mix containing the inert filler. There was not a significant change in critical pore sizes upon the

addition of limestone, with values for mixes C2S1, C2S1-10L and C2S1-20L of 90nm, 80nm and 90nm respectively after 7 days. However, there was an increase in the total intruded volume with increasing limestone content. These are consistent with the pore distribution data reported elsewhere [54].

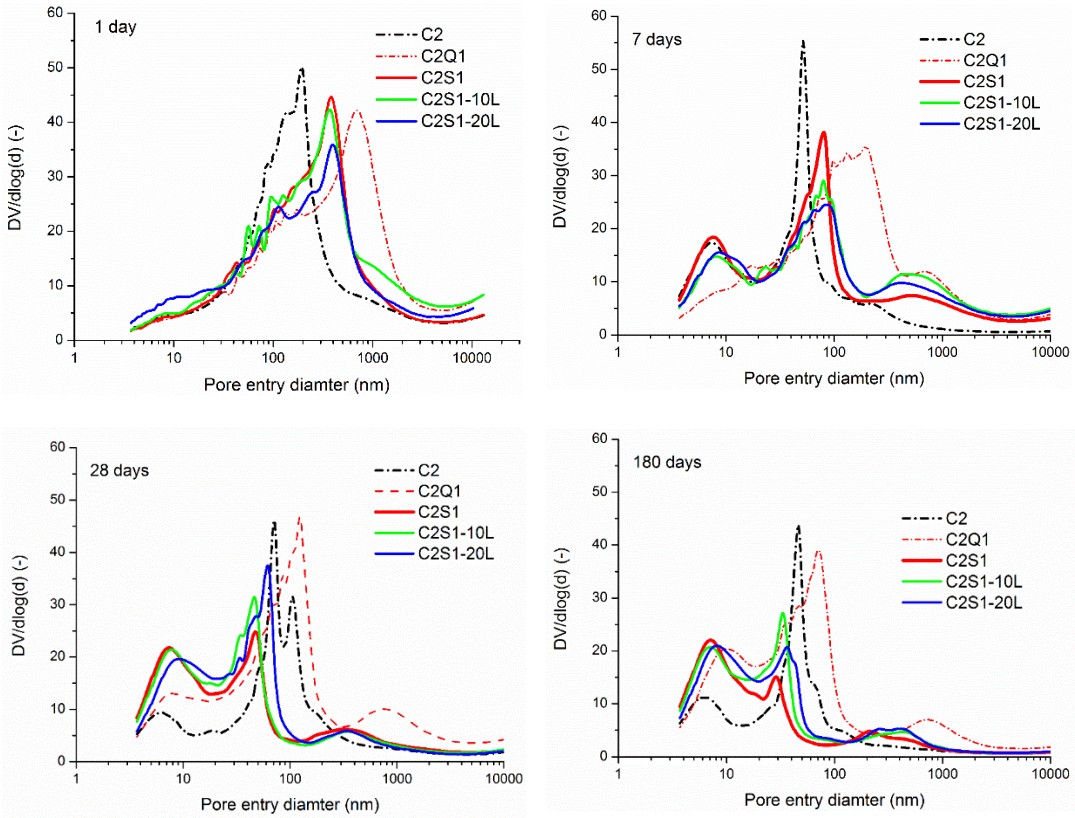

Figure 5-21 Effect of slag and limestone interaction on the pore structure of composite cement as determined by MIP after 1, 7, 28 and 180 days.

The critical pore sizes were further refined to 20nm in mixes C2S1 and C2S1-10L and 25nm in mix C2S1-20L after 180 days. There was also a higher fraction of finer pores (below 10nm) in the composite cements compared to the pure system; indicative of more efficient space-filling in the composite slag cements than in mix C2. The presence of 10% and 20% limestone in the composite slag cements had no detrimental effect on the pore structure. Differences between the pore

connectivity in slag cements and the neat mix C2 have been reported previously [54].

Porosity was also measured from the analysis of BSEM images using the image J software. The grey-level histograms for extracting the area fraction of pores for the various mixes are given in appendix A.1.4. The images were collected at 15 keV accelerating voltage, the magnification of 800x and resolution of 2048 x 1536. Consequently, the minimum measurable pore size is 0.34 µm (i.e. 340 nm) hence denoted as coarse porosity.

The results in Figure 5-22 indicate progressive reductions in porosity with hydration time in all investigated mixes. The lowest porosity was measured in the reference CEM I 52.5 R mix, C2 and the highest in the binary quartz mix, C2Q1. Among the composite cements however, the differences in porosity were small with or without limestone and were between those of the CEM I 52.5 R and mix C2Q1. Both MIP and BSEM image analysis, therefore, indicate similar pore structures in the composite slag cements with or without limestone.

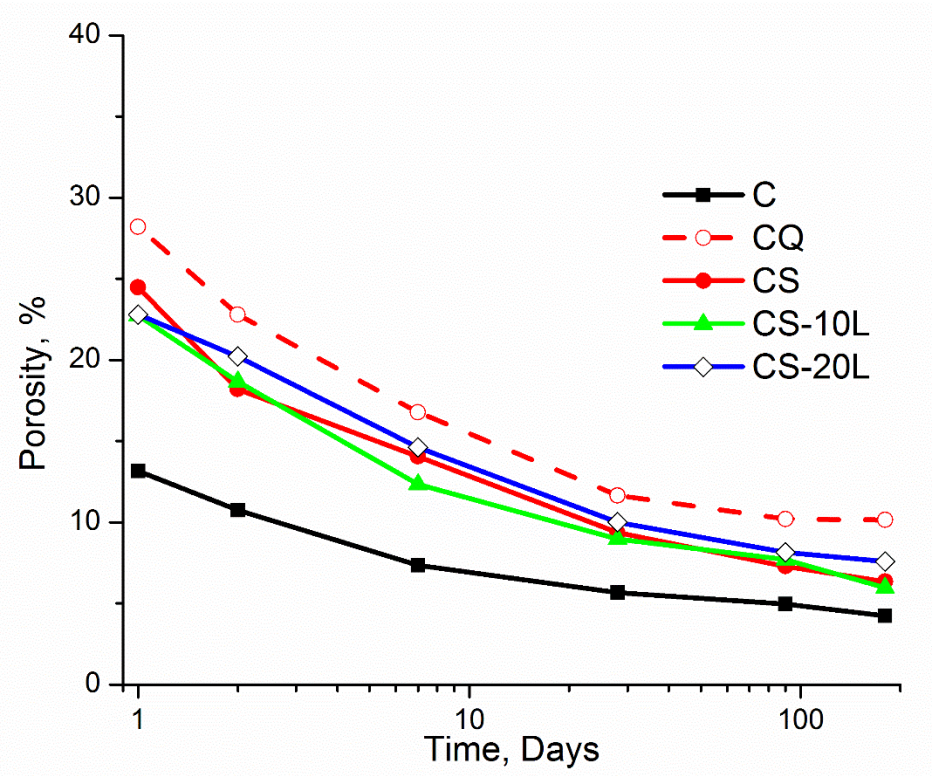

Figure 5-22 Effect of the slag-limestone interaction on porosity (BSEM/IA)

5.2.8 Effect of limestone on the pore solution chemistry

The underlying mechanisms governing the interaction between limestone and slag in the various cements were investigated by examining the pore solution chemistry as a function of hydration time. The measured total concentrations of Ca, OH, Al and SO_4^- are shown in Figure 5-23 (refer to Appendix A.1.5 for Na, K and Si). As hydration progressed, the Ca and SO_4^- concentrations decreased while Al and OH- increased. These trends are consistent with those reviewed by Vollpracht *et al.* [397]. The additional K and Na ions seem to arise from the dissolution of slag and clinkers and the decrease in the amount of pore solution and were unaffected by the presence of limestone. Significant changes in the Ca, K and Na ion concentrations occurred between 6 hours and 7 days.

At the early stages of hydration, the Ca concentration in the pore solution primarily depends on the dissolution of the clinker phases and the precipitation of portlandite. A slightly higher Ca ion concentration was observed in the limestone containing cements compared to mixes C2S1 and C2S1-10Q. This was however limited to the acceleration stage of hydration (up to 12 hours). Limestone providing a better substrate for clinker hydration [51] may explain the higher Ca concentration in the limestone ternary blends. The reduction in Ca ion concentration arises from the increase of pH once sulphate is consumed [17].

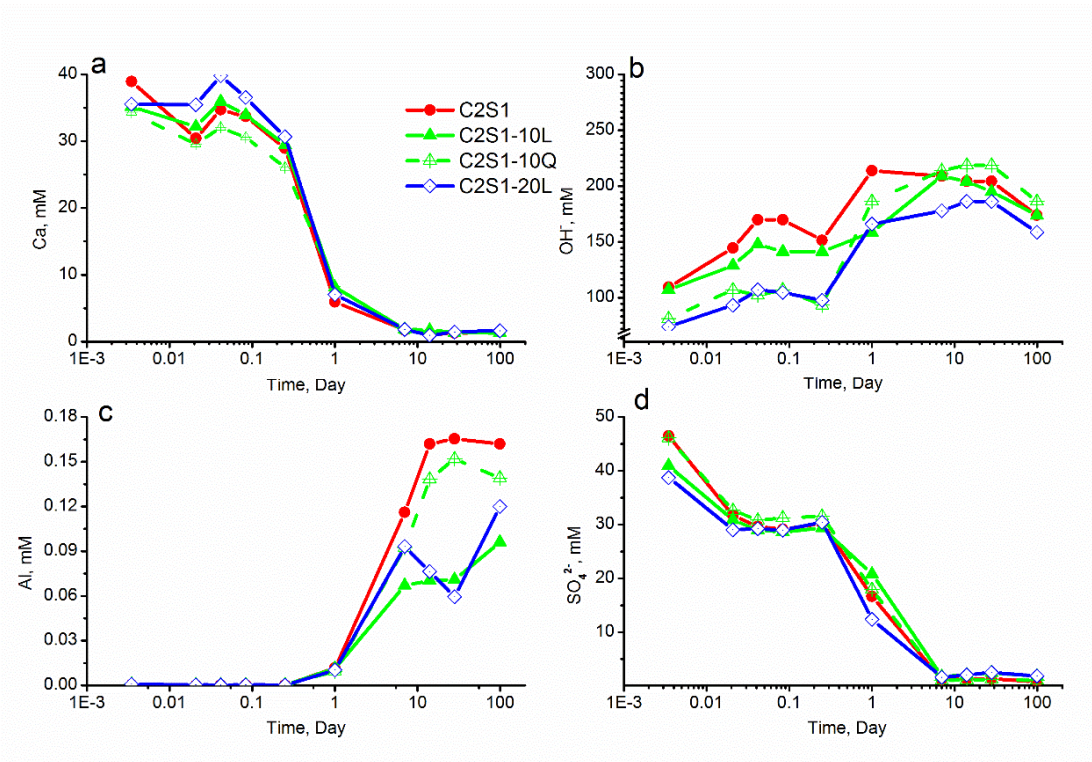

Figure 5-23 Effect of limestone on the pore solution chemistry during hydration. Measured by ICP-OES (≤1 day) and ion chromatography (≥7 days)
(a) Calcium; (b) hydroxyl; (c) aluminium; and (d) sulphates

Continuous dissolution of anhydrite and basanite maintained the sulphur concentration in the pore solution. The sulphur ion concentrations were similar in

all the blends due to fixing the total sulphate content at 3 % in all composite cements. The concentration, however, fell steadily over time and reached negligible levels after 7 days and beyond due to precipitation of ettringite and potential adsorption onto the C-S-H. The SO_3 in GGBS is known to influence the sulphur species measured [55, 397], however, the sulphate concentration falling below the detection limit upon depletion of anhydrite is indicative of the former exerting negligible influence. Also, the silicon concentrations were generally low.

The change in aluminium ion concentration over time is shown in Figure 5-23c. The Al concentrations at longer hydration times are about twice the levels of slag blended cements reported in [397] and [55] despite the GGBS in the latter having similar alumina content. Significant differences were observed over the course of hydration. Levels were low in all systems over the first 24 hours, rising beyond that. The aluminium concentration in the limestone containing cements was clearly lower than the binary slag blend, mix C2S1. Meanwhile, the aluminium concentration in the pore solution of mix C2S1-10Q was slightly lower than in the binary blend, but still considerably higher than in the limestone bearing blend. This suggests a contribution to the aluminium concentration from the slag [141, 203]. The reaction between limestone and dissolved aluminates from the slag led to the observed lower concentration. This is consistent with the C-S-H composition (Figure 5-18) and the evolution of AFt/AFm phase assemblages (Figure 5-17).

5.2.9 Implications of the synergy on compressive strength evolution

Compressive strength development in each of the 7 key mixes from 1 to 180 day of curing is shown in Figure 5-24. The samples were cured in saturated lime solution after removing from the moulds as described in Chapter 3.

As expected, early age strength development was slower in the composite cements compared to the reference cement (C2). However, at later ages, strengths were comparable between C2, C2S1 and C2S1-10L. By 28 days, the mixes C2S1, C2S1-10L and C2S2-20L had attained comparable strengths to the CEM I 52.5R and outperformed this after 180 days. Comparison between the composite cements and mix C2Q1 confirms the active contribution of slag hydration to compressive strength development. For example, the compressive strength in mix C2S1 was ~ 51 % higher than C2Q1 after 1 day and increased progressively with hydration time. This does not arise from the filler effect [10, 51, 218], but instead from slag hydration as already indicated from the kinetic studies reported previously. The effect of limestone on the compressive strength development is also evident from mix C2S1-10L versus C2S1-10Q. It can be noticed that, at equivalent replacement and fineness, limestone had a positive influence on strength development compared to quartz. The margin was much higher at an early age for example after 1 day where limestone instead of quartz led to ~45 % higher strength. However, the difference margin reduced with hydration time.

The CEM I 42.5 R blend had consistently lower compressive strength while increasing the slag fineness improved compressive strength development at all ages [4, 191, 219]. The combined effects of slag and limestone on clinker and slag hydration plus phase assemblages may explain the difference in strength resulting from the slag fineness (i.e. enhanced hydration with increasing fineness). These results agree with the measured bound water content, kinetics as well as the porosity data.

The strength evolution at 20 % limestone content may appear inconsistent with the enhanced slag hydration. However, interpretation must take into account the reduction in slag content, sulphate in the C-S-H [283] and the hydrates formed [398] as well as the overall degree of hydration plus the porosity of the various mixes.

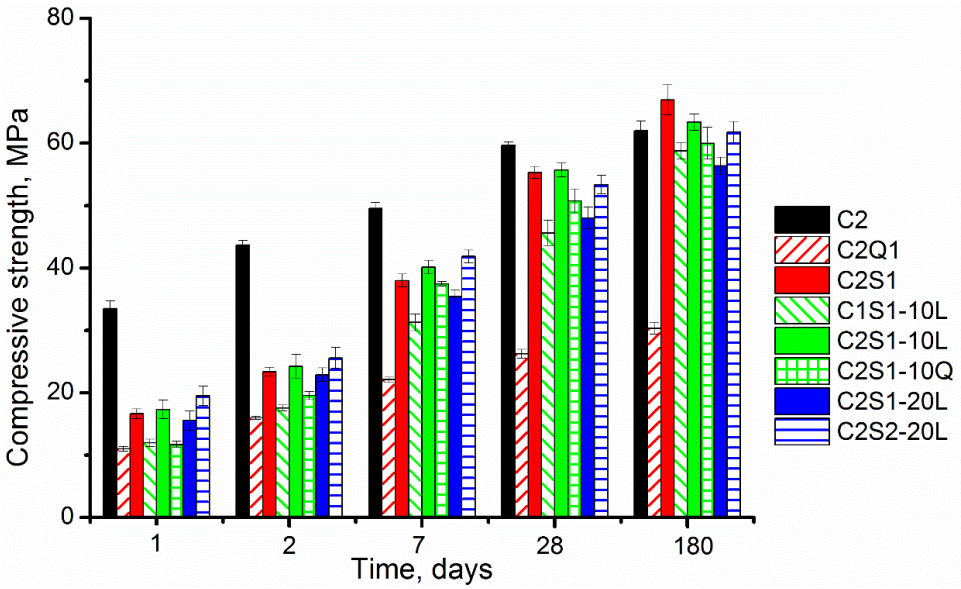

Figure 5-24 Effect of limestone on the compressive strength evolution between 1 and 180d days.

To this end, the overall degree of hydration was calculated by superposition of the extent of reaction of the individual mix components and assuming that all constituent materials including water may fully react. The results plus the coarse porosity of the primary mixes as determined from image analysis (see Figure 5-22) are shown in Figure 5-25.

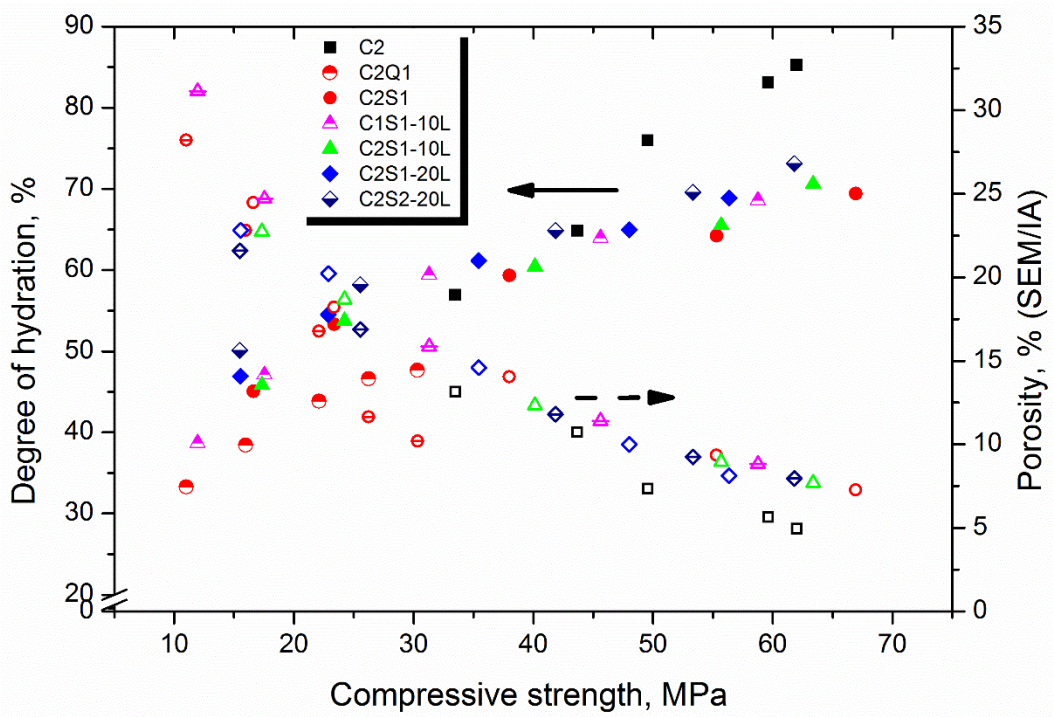

Figure 5-25 Relationship between compressive strength, porosity and degree of hydration

Note: Solid shapes for degree of hydration and open shapes for porosity

Strength showed a negative correlation with porosity [177]. The degree of hydration also correlated positively but the slopes were different. From the MIP results in section 5.1.9, it is evident that progressive slag hydration efficiently refines the gel pores [51] but not necessarily the coarse capillary pores as predominantly measured through backscattered SEM/IA [7]. This may partly explain the lower compressive strength in the mix CS-2L despite slag being more reactive in this mix.

5.2.10 Summary of hydration and microstructure studies

Further insight has been gained from a detailed investigation into hydration kinetics and microstructure of ternary blended slag-limestone cements. Limestone affected the hydration of the major clinker phases as well as slag. Alite hydration was

affected by slag and quartz in a similar way but the presence of limestone led to further acceleration. Belite hydration was retarded in the binary slag cements but it was enhanced in the limestone ternary blends. However, hydration of the interstitial phases was not significantly influenced by the presence of limestone or slag apart from the fineness of the constituent materials. Generally, the reaction kinetics were accelerated by increasing the fineness of the CEM I and slag. However, the CEM I fineness exerted more pronounced effect on the overall reaction kinetics of the composite cement compared to the fineness of slag.

Despite the limited reaction of calcite from limestone, the accelerated reaction kinetics in the limestone containing mixes led to similar pore structures and consequently compressive strength in the ternary blends compared to the binary slag blend.

Calcite reacted with dissolved alumina to form carboaluminates in the limestone-containing cements. This stabilised ettringite over monosulfoaluminate with the latter observed in the mixes without the additional limestone. The carboaluminates in addition to ettringite lowered the alumina concentration in the pore solution. Since the latter is at equilibrium with other hydrates, lower alumina was also incorporated into the C-S-H. The alumina in the hydrotalcite was also lowered in the presence of limestone. This lowering of the alumina concentration explains accelerated slag and belite reaction.

Chapter 6
Freeze-thaw resistance of limestone ternary blends

In this chapter, studies performed on concretes made with the composite cements investigated in the previous chapter are reported. Results on the impact of cement composition on fresh properties of concretes are initially presented and then the freeze-thaw resistance. Finally, the microstructure of concretes and parallel cement paste samples characterised by TG, XRD and SEM are presented. The objectives here were two fold. First, to measure the internal structural damage and scaling resistance of the concrete samples subjected to cyclic freezing and thawing. The second objective was to identify microstructural changes arising from freeze-thaw of paste samples [47] and hence verify the controlling mechanisms for the freeze-thaw performance of the investigated systems.

6.1 Samples investigated

The concrete samples investigated for freeze-thaw resistance were made from the composite cements listed in Chapter 3. CEM I 42.5 R was chosen as the baseline for comparing the freeze-thaw resistance of the composite cements as it is the norm in the industry.

The concrete mix design was based on the yield method taking into account the specific gravities of the constituent materials including CEM I, slag, limestone, anhydrite and the aggregates. An allowance for 2.5% entrapped air content was also factored into the design while prefixing the ratio between fine and coarse aggregates. This, in addition to 20% of the coarse aggregates of sizes 10mm or lower, was established from preliminary trials of concrete mix design. The cement content was fixed at 320kg/m^3 of concrete according to the specifications for high

water saturation, without de-icing agent (i.e. exposure class XF3) according to EN 206-1 [399]. Concrete mix details of the selected cements are shown in Table 6-2.

Table 6-1 Composite cements investigated for freeze-thaw resistance

Nomenclature	CEM I		GGBFS		Limestone	Anhydrite
	42.5 R	52.5 R	S1	S2	L	s
	$\%_{mass}$					
C1		100	-	-	-	-
C2S1	-	50.68	47.08	-	-	2.24
C2S1-10L	-	51.18	38.03	-	8.55	2.24
C1S1-10L	51.93	-	38.06	-	7.50	2.51
C2S1-20L	-	51.18	28.53	-	18.06	2.24
C2S2-20L		51.18	-	28.53	18.06	2.24

Table 6-2 Mix design to yield a cubic metre of concrete

Nomenc.	Binder*	Water	Aggregates		
			Fine	10mm	20mm
C1	320.3	189.8	651.8	237.7	950.8
C2S1	320.3	189.8	648.8	236.6	946.4
C2S1-10L	320.3	189.6	648.1	236.4	945.5
C1S1-10L	320.3	189.6	648.3	236.4	945.7
C2S1-20L	320.3	189.5	647.4	236.1	944.5
C2S2-20L	320.3	189.5	647.4	236.1	944.5

*Note: Binder in the table refers to either CEM I 42.5 R or the composite cements where applicable. The formulation of the cements is given in Table 6-1. The designed entrapped air content was 2.5%. Also, the water content has been adjusted to include the absorption by aggregates.

6.2 Fresh properties of concrete

The fresh properties assessed were the flow diameter, slump, air content and fresh density. Table 6-3 summarises the results from the five composite slag cements and the CEM I 42.5 R concrete mixes.

Table 6-3 Fresh properties of composite cements compared to CEM I

Mix	Slump (mm)	Spread (cm)	Density(kg/m^3)	Air content (%)
C1	170	43	2370	1.1
C2	65	30	2380	1.1
C2S1	80	36	2350	1.4
C1S1-10L	120	42	2340	1.3
C2S1-10L	110	40	2360	1.3
C2S1-20L	140	42	2340	1.2
C2S220L	105	35	2365	1.1

The clinker and slag fineness, as well as the presence of limestone, influenced the fresh properties. The slump and the flow table test yielded similar trends in workability, both decreasing with increasing clinker fineness. The presence of slag improved workability compared to the neat CEM I 52.5 R but mixes were still stiffer than CEM I 42.5 R mixes, despite replacing 50 % of the clinker. This aligns closely with the similarity in the particle grading of the slag and CEM I 52.5 R as evident from the particle size distribution of the materials in Chapter 3. The presence of limestone improved concrete workability compared to the binary slag blends, and workability was further enhanced with increasing limestone content. The composite cement with the finer slag however reduced workability, which can be attributed to the increased surface area of the cement grains.

The designed fresh air content was 2.5 % in all mixes (see section 3.3.2). However, the measured contents shown in Table 6-3 varied between 1.1 to 1.4 % depending on the cement type. With an error of ± 0.3 % points between repeated measurements, the differences in the air contents were not significant. Additionally, the fresh densities varied between 2340 and 2380 kg/m^3; being highest in the CEM I. The differences were small among the composite cements.

Therefore with the exception of slight variations in workability, the concretes for the durability investigations had similar fresh properties. This provided a basis for discounting the potential influence of fresh properties on the hardened concretes.

6.3 Compressive strength evolution

The compressive strengths of concretes made from the five composite cements and the control mix CEM I 42.5 R are shown in Figure 6-1. The samples were moist cured for 7 days and then exposed conditioned at 20 °C and 65 % RH for 21 days. After 7 days, the composite slag cements were much weaker compared to the neat cement mix, C2 [219]. The compressive strengths differed slightly among the composite cements with an average of 25.5 (±3) MPa, i.e. approximately 67 % of the strength of the CEM I 42.5 R mix. The highest strength was observed in mix C2S2-20L and the lowest in C1S1-10L. Thus, increasing the CEM I fineness impacted more positively on compressive strength compared to the slag fineness [191, 220]. For example, after the 7-day moist curing, the cube strength of mix C2S1-10L was 26 % higher than C1S1-10L while that between C2S1-20L and C2S2-20L was 15 %. The presence of limestone also increases strength by 11 % compared to the binary CEM I/ slag mix. However, at a given CEM I and slag fineness, an increase in the limestone content from 10 to 20 % reduced compressive strength by 14 % [6]. This is in agreement with the measurements on mortar samples reported in Figure 5-24, in that an optimum limestone/slag ratio exists to maximise the synergistic effects.

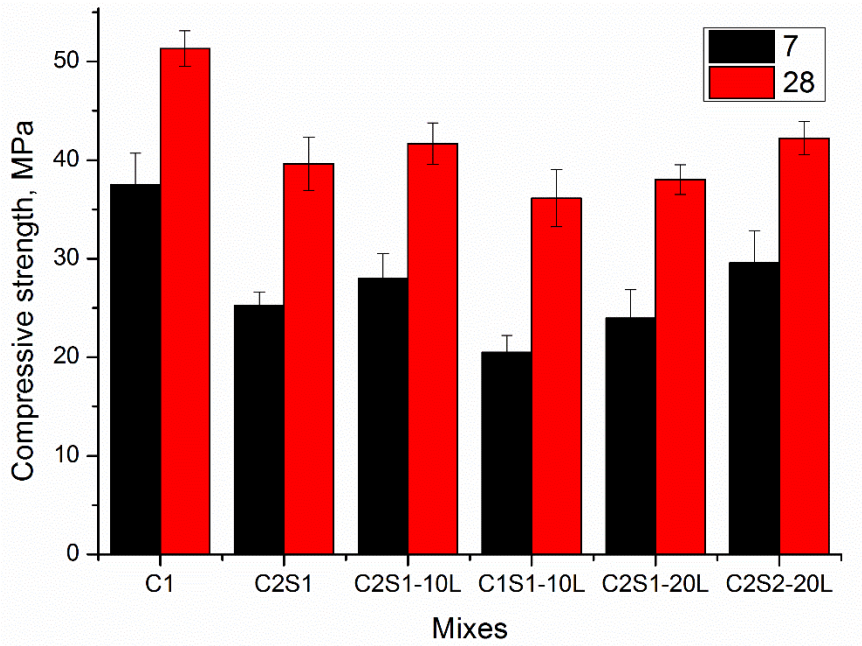

Figure 6-1 Compressive strength of concrete before and after exposure at 20 °C and 65 % RH for 21 days

The strength gain between 7 and 28 days was highest in mix C1S1-10L but lowest in the CEM I mix. This was not surprising considering that approximately 80% of the compressive strength of CEM I mortar samples was attained within the first 7 days, as discussed in Chapter 5. The strength gain between 7 and 28 days in the composite cements ranged between 40 and 70%. The lowest was observed in mix C2S1 and the highest in mix C1S1-10L. The relative differences in clinker fineness and hence the proportion of clinker which may hydrate during this period may account for the higher later strength gain in the CEM I 42.5 R compared to the composite cements. The differences in strength gain in mixes C2S1 and C2S1-10L, as well as C2S1-20L, further highlights the positive contribution of limestone [177, 370, 375]. Notwithstanding these effects, the average compressive strength of the composite cements was 22 % lower than the neat cement concretes at the time of commencement of the freeze-thaw test. This could impact on the freeze-

thaw performance [268] but the microstructure of individual samples could also exert a greater influence depending on the nature of hydrates and distribution [47].

6.4 Effect of conditioning on the capillary suction

6.4.1 Early stage capillary suction

Water suction into the capillaries gives an approximate indication of the porosity of the accessible zone. In the present work, concrete samples conditioned according to the CIF test method (65 % RH and 20 ^{0}C) were measured just before the 7-day capillary suction. The test method differed from that used for the initial surface absorption test (ISAT) according to BS 1881-208:1996. The variations included capillary suction under gravity (i.e. without applied pressure) as well as testing specimens without oven drying. The modifications were necessary in order to obtain comparable information about the capillary suction potential of the freeze-thaw samples.

Figure 6-2 presents results from the initial water absorption test. The errors associated with the measurement ranged between 2 and 16% and have been shown as error bars. The initial suction capacity rates of the CEM I, C2S1 and the 10 % limestone blends were similar. But changing the cement has an impact, as does raising the limestone content.

Water absorption under gravity or applied pressure follows Darcy's theory of capillary flow and hence the flow constant (i.e. sorptivity) is a unique material property [228, 400]. Linear regression analysis of the absorption data for the individual concrete mixes yielded a linear relationship against the square root of time, with a correlation co-efficient exceeding 0.9. Consequently, the slope of the linear fit was extracted as 'apparent' sorptivity and the results shown in Table 6-4.

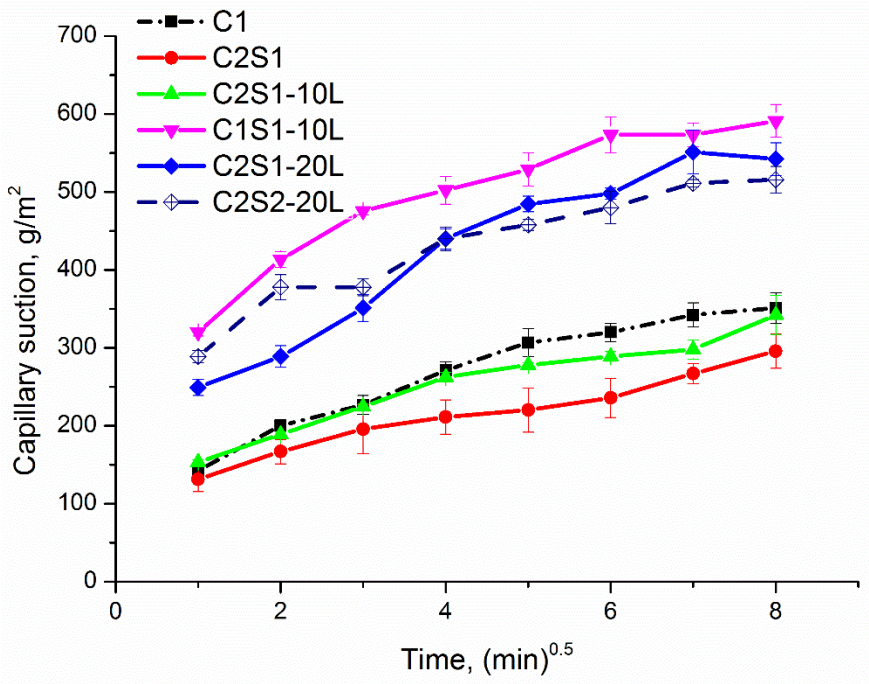

Figure 6-2 Initial water absorption before saturation for freeze-thaw testing

Table 6-4 'Apparent' sorptivity of concretes samples

Mixes	C1	C2S1	C2S1-10L	C1S1-10L	C2S1-20L	C2S2-20L
Sorptivity $g.mm^{-2}.min^{-0.5}$	29.63	21.19	24.71	5.93	35.92	30.69

The presence of slag modified the pore structure of the concretes such that, despite replacing 50 % of the CEM I 52.5 R with GGBS (i.e. mix C2S1), the apparent sorptivity was lower than the value measured for the CEM I 42.5 R. However, the CEM I was comparable to the mix containing 10 % limestone (i.e. C2S1-10L). Increasing the limestone content to 20 % further increased sorptivity. This is indicative of a more porous microstructure in the mixes containing 20% limestone content. The effect of slag can be attributed to the additional C-S-H formed and agrees with the data published elsewhere [401]. Sorptivity further improved with increasing clinker and slag fineness [191, 197, 374]. Both are

advantageous for slag reactivity which leads to densification of the C-S-H and hence reduced porosity. As indicated in Chapter 5, limestone reactivity is limited [17, 173, 402]. Consequently, porosity increased with increasing limestone content and hence the higher sorptivity.

Ordinarily, specimens are pre-dried to constant weight for the absorption test, and therefore capillary pores are assumed unsaturated. Consequently, the rate of water ingress over time can reflect the accessible pore volume to some precision. The use of unconditioned samples, however, meant that the pores were saturated to variable extents and hence the apparent sorptivity shown in Table 6-4 reflects the available pore structure rather than the absolute pore structure.

6.4.2 Long term capillary suction in concretes

The objective for measuring the initial water absorption and hence the apparent sorptivity was to identify correlations (if any) with the long term suction capacity of the mixes. The capillary suction of deionized water through the test surface for the six mixes, expressed as a percentage of the initial weight of specimens, are shown tabulated alongside initial sorptivity and porosity as measured by SEM in Table 6-5.

The overall water absorbed per original mass of concrete was similar in mixes C1, C2S1 and C2S1-10L, but the suction capacity increased with increasing limestone content. However, the effect of slag fineness on the absorbed water content was not significant, despite a slightly higher initial suction rate in mix C2S1-20L. The clinker fineness had a more pronounced effect on the suction capacity of the composite cement; with a higher absorbed mass for lower clinker fineness.

Table 6-5 Water absorbed by the concrete samples compared to initial sorptivity and porosity of the paste

Mixes	Capillary suction, after 7days (g/m^2)	Stdev	SEM porosity, %
C1	0.623	0.02	7.351
C2S1	0.616	0.029	10.05
C2S1-10L	0.599	0.008	12.32
C1S1-10L	0.802	0.020	15.85
C2S1-20L	0.685	0.128	14.65
C2S2-20L	0.693	0.021	11.80

This is a further indication of the differences in the nature of the pores filled by the hydrates in composite cements. Mix C1S1-10L, prepared with CEM I 42.5 R was ~ 4% more porous than mix C2S1-10L, as measured by SEM/IA. This is, however, the coarse porosity [46, 177], aligning more closely with the capillary pore fraction. The total pore volumes in the mixes C2S1-10L and C1S1-10L before conditioning at 65 %RH and 20 °C as measured by MIP were however 34.5 and 34.8% respectively. Consequently, the blend with the CEM I 42.5 R resulted in a microstructure dominated by capillary pores as opposed to the CEM I 52.5 R blend. The impact of using slag with higher fineness was not evident from the suction capacity after 7 days, being similar in both the 20 % limestone ternary blends. It is possible that the slag hydrates refined pores in the range which were not affected by the capillary suction. This is despite capillary porosity by SEM being much lower in the fine slag mix.

6.5 Freeze-thaw performance of composite cements

6.5.1 Methodological remarks

The freeze-thaw resistance of concrete is a function of the freezing rate [43, 252]. Deviations in the implemented temperature profile compare to the CIF method

[340] and conformity to that of the slab test [403] have already been discussed in Chapter 3. Figure 6-3 and Figure 6-4 show a comparison between the results from samples tested by the CIF method based on CEN TR/15177 [340] (herein referred to 'ref') and the test profile (herein as 'test'). A comparison of the results from the different profiles is first discussed.

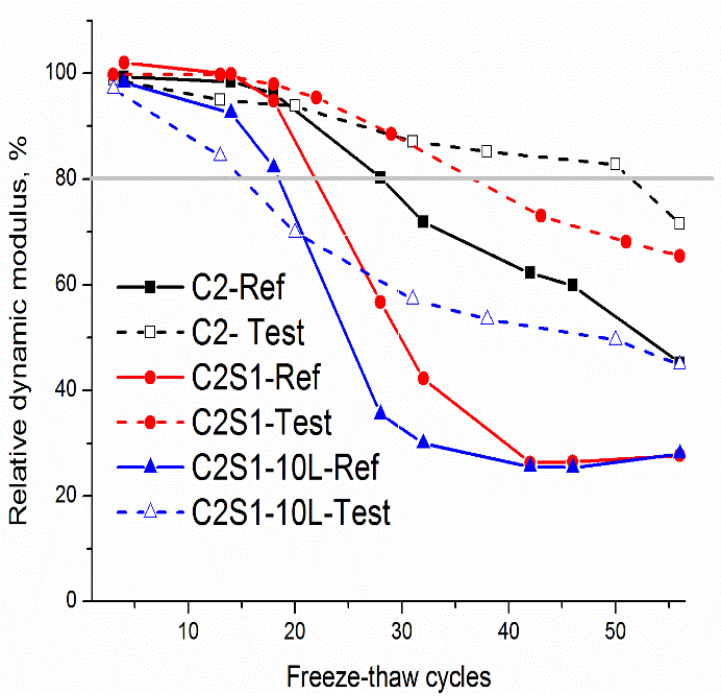

Figure 6-3 Comparison between the internal structural damage measured on CEN TR/15177 (Ref) and an extended freezing rate (Test) freeze-thaw profiles

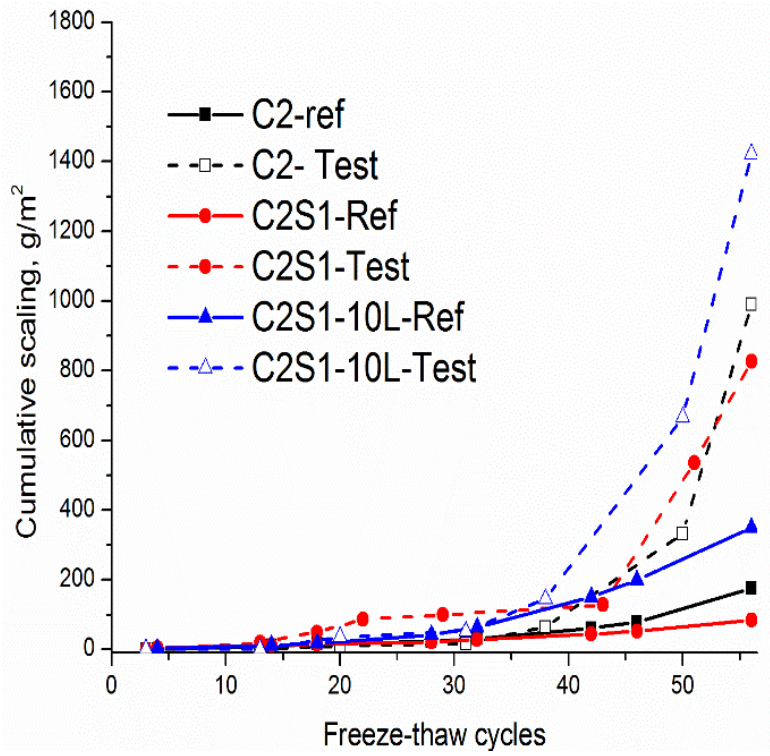

Figure 6-4 Comparison between the scaled matter measured on CEN TR/15177 (Ref) and extended freezing rate (Test) freeze-thaw profiles

The trends in the internal structural damage were similar, the magnitudes, however, differed between the two methods. No consistent pattern in the variations in magnitude was found. In the ternary blends, attainment of the 80 % failure limit was comparable in the different methods. However, the neat and binary cements failed after much longer freeze-thaw cycles compared to those tested according to the reference method. The cumulative scaled matter also differed in both trend and magnitude for the two methods. For a given dataset, the trends in internal damage were proportional to the associated scaling. However, the cumulative mass of scaled materials was significantly higher as measured in the 'test' chamber irrespective of the mix composition.

The freezing/heating rates in the ‘ref’ and ‘test’ chambers were 5 °C/hr and ~1.7 °C/hr respectively. This meant slower cooling but higher dwell time at any given temperature in the ‘test’ chamber. On the basis of the hydraulic pressure theory [37, 38, 404], the higher freezing rate would lead to greater internal damage which is consistent with the observations in the ‘ref’ specimens. However, the variation is well within the ~1.8 to 6 °C/hr freezing rate over which the critical degree of saturation of the test samples would not be affected by suction during freeze-thaw [252]. Consequently, the extended dwell time at 1.7 °C/hr freezing rate may account for the higher scaled mass. This stems from the fact that pore water freezes more quickly between 0 and -10 °C than at lower temperatures [405]. Therefore, the longer the specimens were exposed between 0 and -10 °C, the greater would be the damage. That the magnitude of the internal damage did not follow a similar pattern is indicative of controlling mechanisms other than the critical degree of saturation. Further analysis of the data would, therefore, be based on the results from samples tested in the extended profile.

6.5.2 Effect of composition on the freeze-thaw performance

6.5.2.1 Overview of freeze-thaw resistance of cements

The relative dynamic modulus (E_{dyn}) is indicative of the extent of the internal structural damage. This was calculated from the transit time [340] and shown in Figure 6-5 as a function of freeze-thaw cycles. The failure criterion adopted was from the recommendations of RILEM TC 176 [406]. The relative dynamic modulus decreased as the freeze-thaw cycles increased. This occurred sooner in the CEM I 52.5 R ternary blends such that, 80 % of the initial dynamic modulus was lost after 16 to 22 freeze-thaw cycles. The binary slag blend was more resistance than the ternary blends while the CEM I 42.5 R blend was comparable to the control mix

(C1). The slag fineness had minimal impact on the internal damage at the investigated level of replacement.

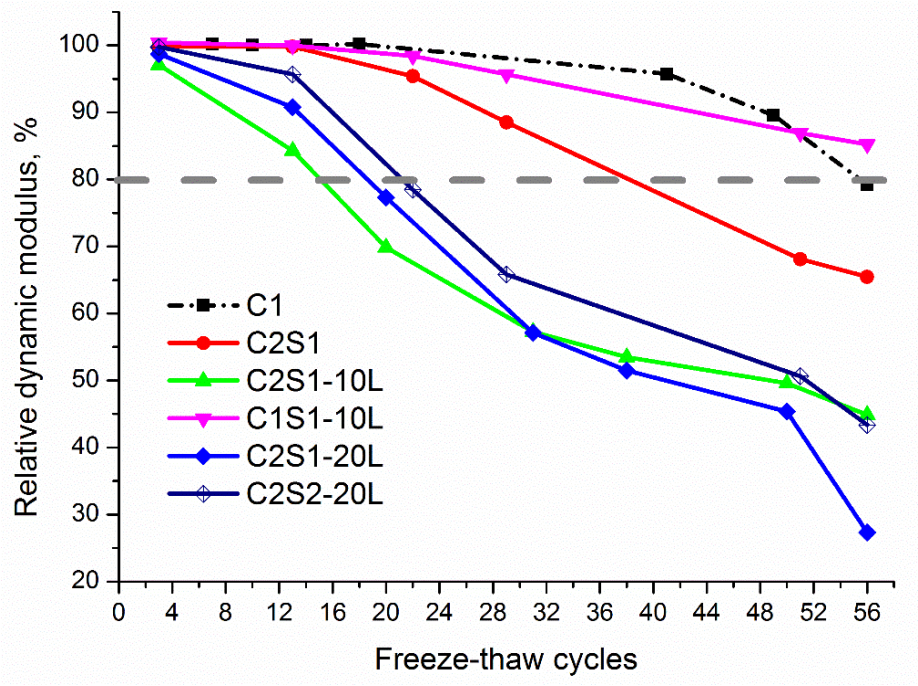

Figure 6-5 Effect of cement composition on the internal structural damage in concretes.

Scaling of the surface matter (Figure 6-6) progressed gradually in all cements except mix C1S1-10L. In the latter, scaling observed after 12 cycles and increased significantly with increasing freeze-thaw cycles. In the CEM I 52.5 R blends, scaling was higher in the composite cements compared to the control. The 10 % limestone addition had minimal influence on the scaling resistance. However, increasing the content to 20 % was reduced the scaling resistance with the slag fineness having no recognisable effect.

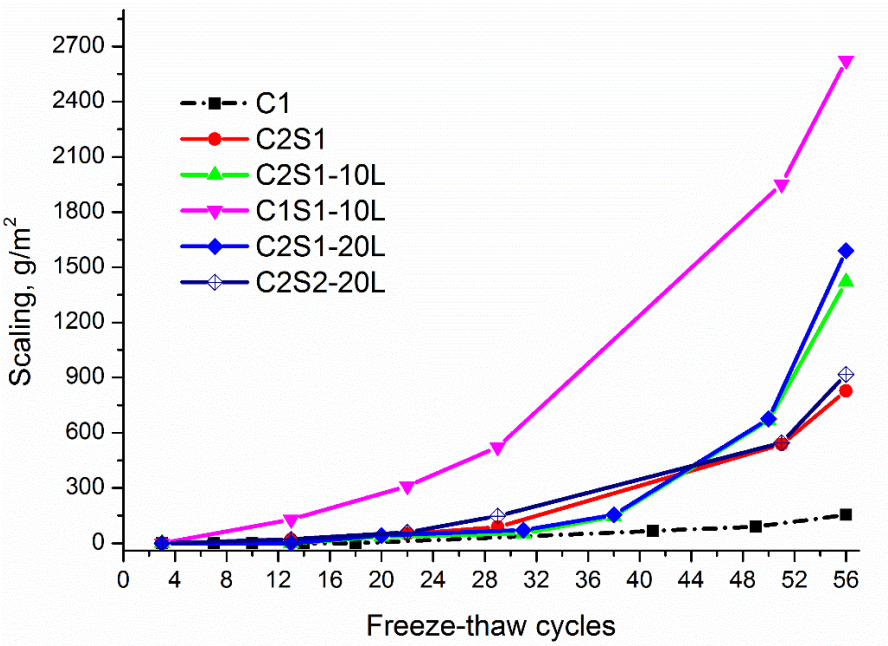

Figure 6-6 Effect of cement composition on the scaling resistance of concretes.

The rate of water ingress (i.e. sorptivity) is an approximate indicator of permeability of concrete structures [228, 407]. Water uptake [406] during the 7d capillary suction and freeze-thaw are shown for the different mixes in Figure 6-7. Suction was lower in the control mix as compared to the composite cements, being highest in mix C1S1-10L. Freeze-thaw however significantly increased water uptake in all mixes; reaching a maximum of ~ 2.8 % as opposed to 0.6 % after the 7-day capillary suction. The suction rate was similar among the CEM I 52.5 R blends but differed from the CEM I 42.5 R mixes including the neat cements.

The plateau in the water uptake curve is indicative of saturation while further sorption beyond the nick-point implies filling of air pores [252, 408]. There was no definite nick-point before the freeze-thaw cycles (Figure 6-7) commenced. A plateau was however noticed in the course of freeze-thaw with this occurring at a lower moisture content in mix C1S1-10L as compared to the other composite cements.

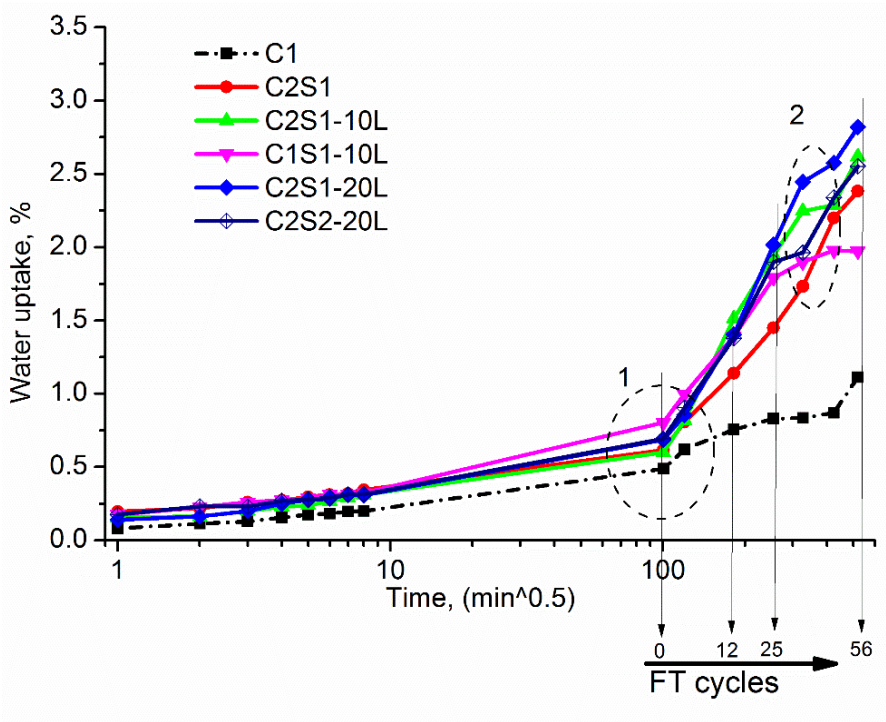

Figure 6-7 Water uptake during freeze-thaw as a function of cement composition.

The influence of cement composition on the measured parameters is subsequently discussed.

6.5.2.2 Effect of slag in composite cements

Figure 6-8 shows the control CEM I 42.5R mix and the binary slag blend after freeze-thaw testing. The neat cement concrete was visibly more resistant. The extent of damage was characterised by the cumulative scaling and changes in the dynamic modulus. As shown in Figure 6-5, there was no measurable internal damage in the first 40 freeze-thaw cycles. After this, the reductions were sharper, reaching the 80% critical point by 56 cycles. Meanwhile, capillary suction data (Figure 6-7) showed that approximately 60 % of capillary suction occurred within the initial 20 freeze-thaw cycles, after which the increments were gradual.

Consequently, the prevalence of unsaturated capillary pores offered a safety net against freeze-thaw damage.

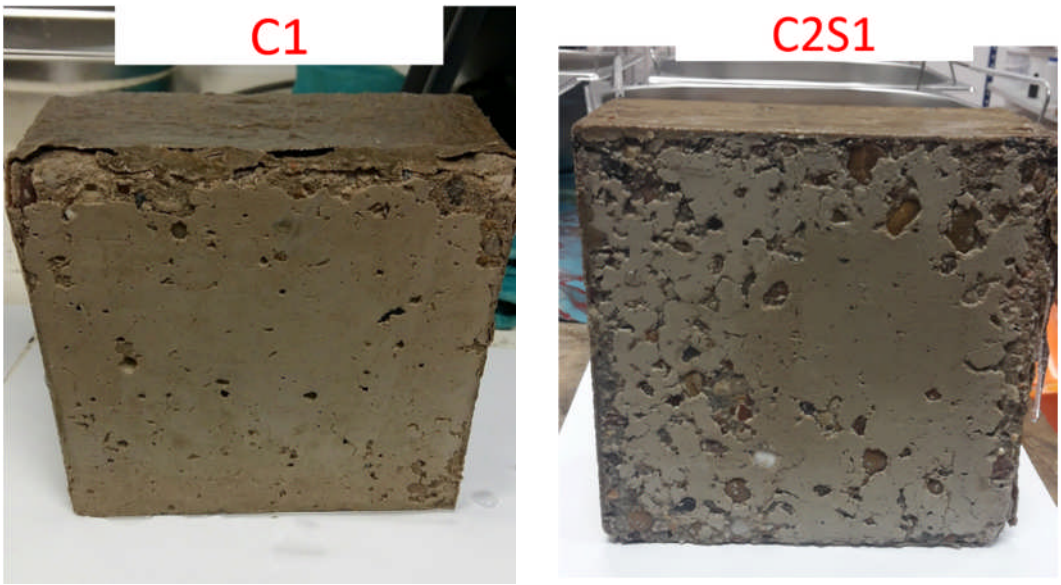

Figure 6-8 Comparison of the test surfaces after 56 freeze-thaw cycles showing the effect of slag.

On the left: CEM I 42.5R and; right: binary slag concrete mix

Meanwhile, the mass of scaled matter in the control mix was relatively small within this period. The water uptake increased gently between 20 and 56 freeze-thaw cycles. This was, however, commensurate with the sharp decrease in the dynamic modulus and high scaling.

Water uptake gradient was 0.0042 in the binary slag mix as opposed to 0.0035 $g/m^2/\sqrt{min}$ in the neat cement (Figure 6-7). The higher uptake rate may be explained by a larger volume of pores (Figure 6-13) plus additionally formed cracks acting as reservoirs for water, or cryogenic suction of water during freezing or melting [409, 410]. The suction of the test solution itself would not induce cracks since the pressure associated with liquid water is far below the tensile strength of

the pore wall [39, 338]. Consequently, even if the test surface was fully saturated at the start of freeze-thaw, it should not necessarily cause internal damage straight away as evident from the plateau of water uptake in mix C1. Besides, there is no evidence of full saturation of pores after the 12th freeze-thaw cycle and hence sudden amplification of cryogenic suction is less likely.

6.5.2.3 Effect of limestone in composite slag cements on freeze-thaw

Limestone as cement supplement is noted to impair freeze-thaw resistance [411]. Figure 6-9 indicates significant removal of the surface material in the ternary blends. Figure 6-7 had already indicated similar water uptake rate in both mixes. The ultimate water uptake after 56 cycles was also comparable. This is also consistent with the internal damage and scaling resistance.

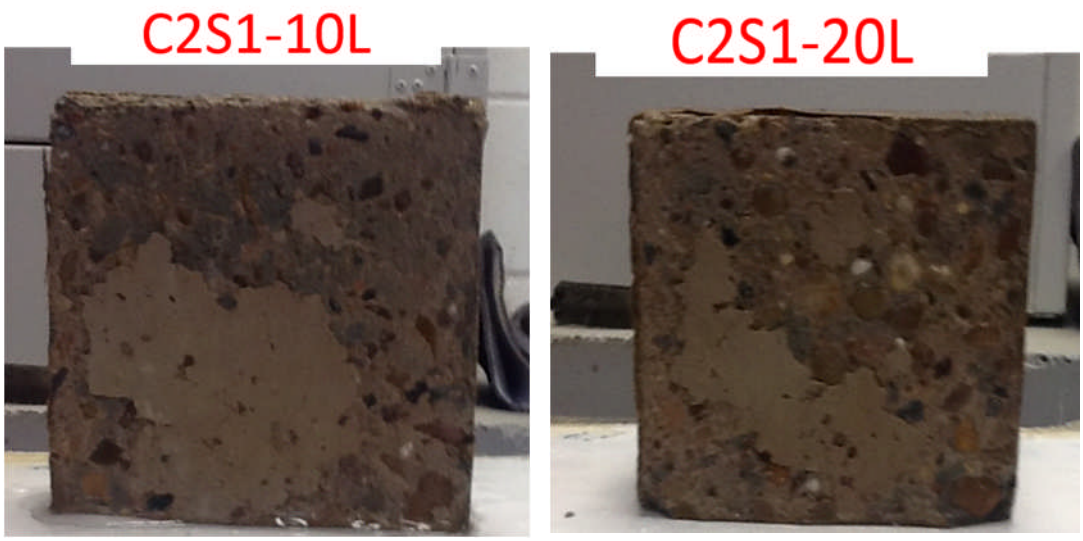

Figure 6-9 Effect of limestone content on the scaling resistance of concrete after 56 freeze-thaw cycles.

On the left: 10% limestone and; right: 20 % limestone ternary concrete mixes.

The attainment of constant weight is indicative of full saturation of the accessible capillaries [408] and labelled as nick point 2 in the test specimens. Comparison with the scaling plot indicates that once the maximum suction marked the onset of a sharp increase in the scaled matter. Marginal suction, coupled with the simultaneous loss of material led to further reductions in the weight of the test specimens. However, increasing the limestone content from 10 to 20 % was only found to marginally increase the water uptake capacity.

The microstructure of the paste samples gives further insight into the effect of limestone on the freeze-thaw performance of the paste phase. It must be emphasised however that these may be altered in the bulk concrete. The pore size distribution data presented in Chapter 5 indicated a higher volume of pores ranging from 100 – 1000 nm in the presence of limestone. However, these were refined further when the limestone content was increased from 10 - 20 %, although both were higher than in the binary mix. This is consistent with the higher sorptivity in the limestone containing mixes, as shown in Table 6-4. However, the sorptivity only partially explains the above observations, especially when the freeze-thaw data is compared to the suction after 7 days (Table 6-5). Here, the suction capacity was comparable between the binary blend and that containing 10 % limestone but was higher in the blend containing 20 % limestone. This validates the observations in the 20 % limestone concrete. Notwithstanding, the scaling and internal damage were comparable to the 10 % limestone mix, thus suggesting microstructural phenomenon other than porosity as the controlling mechanism.

6.5.2.4 Effect of CEM I and slag fineness on the freeze-thaw performance

The effect of CEM I and slag fineness in the ternary blends are shown in Figure 6-10 at 10 % and 20 % limestone replacement respectively.

From the internal measurement (Figure 6-5) and the scaling (Figure 6-6) results, it is noted that the limestone ternary blend formulated with the CEM I 42.5 R showed significantly lower internal damage compared to the CEM I 52.5 R blend. However, the reverse was true with respect to scaling. The scaling resistance was so poor that, after the 12th cycle, the cumulative scaled material was 150g/m^2 in mix C1S1-10L. Meanwhile, mass losses of similar magnitudes were seen in the corresponding CEM I 52.5R mix (i.e. C2S1-10L) after 36 cycles. Despite significant scaling by the 12th freeze-thaw cycle, measurable changes in the internal damage were not found until the 20th cycle. The reductions were, however, small compared to that in mix C2S1-10L which exceeded the 80 % limit before the 16th freeze-thaw cycle.

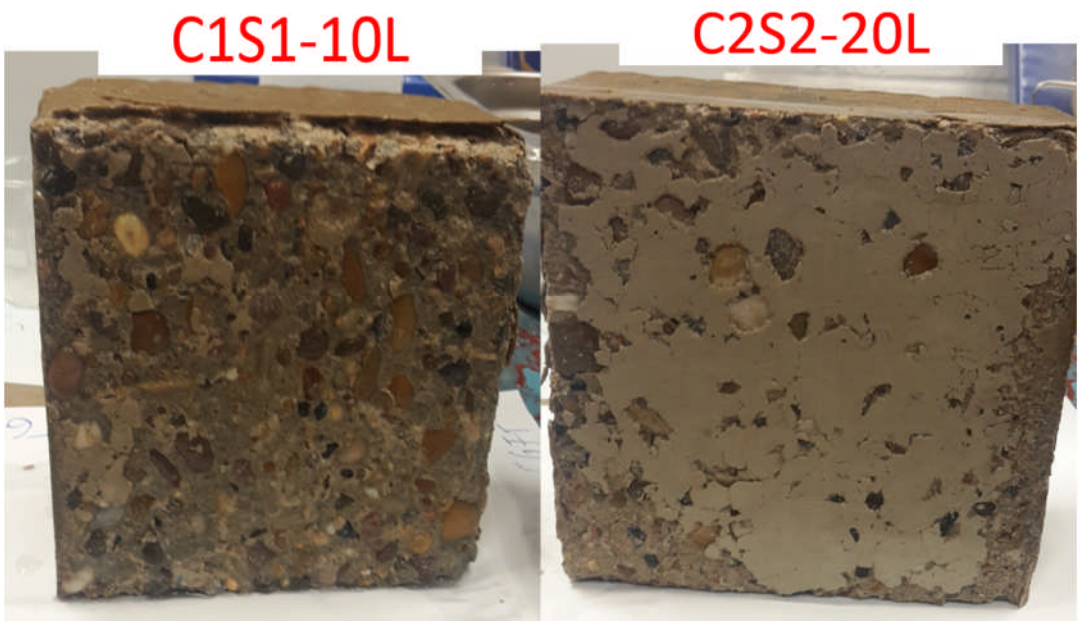

Figure 6-10 Effect of CEM I and slag fineness on the scaling resistance of concrete after 56 freeze-thaw cycles.

On the left: CEM I 42.5 R plus 10% limestone ternary blend and; right: Slag 2 plus 20 % limestone ternary blend concrete mixes

Water uptake during freeze-thaw cycle (Figure 6-7) offered some insight into the above observations. The capillary suction during pre-saturation was highest in the mix C1S1-10L (i.e. ~ 0.8 % before freeze-thaw testing). The water uptake gradient for the latter was 0.0032 g/m^2/√min while that for mix C2S2-20L was similar to the other CEM I 52.5 R blends. Consequently, despite being more porous (as discussed in Chapter 5), permeability was low.

Moreover, the degree of slag hydration was not influenced by the clinker fineness (Chapter 5) and [143]. Therefore, at lower permeability, carbonation of portlandite is also low. Consequently, the buffer against C-S-H is prolonged. However, such a hypothesis does not also explain the internal structural damage observations and hence require elucidation of additional microstructural information in order to clarify the controlling mechanism.

The effect of higher limestone content was marginal with respect to scaling and internal damage as discussed in the previous section. Comparison at 20 % replacement level indicated improved resistance to scaling with increasing slag fineness (see Figure 6-10 and Figure 6-6). The improvement in the resistance to internal structural damage was however not proportionate to the scaling resistance. It, therefore, seems that finer clinker and slag (which are more reactive) played different roles with respect to internal damage and surface scaling during freeze-thaw testing in de-ionized water. These effects are discussed in the next section.

6.6 Microstructure before freeze-thaw

6.6.1 Effect of carbonation

Hydrating cements exposed to atmospheric conditions may not only be influenced by densification of the C-S-H but also carbonation of portlandite and other hydrated

phase assemblages [240, 241, 412, 413]. Comparison between the samples which were kept sealed for 28 days and those sealed for 7 days followed by 21 days exposure at 65% RH at 20 °C gives some indication about phase assemblage modifications during sample conditioning for freeze-thaw.

Compared to the neat cement, early exposure of composite cements at 65 % RH is detrimental, as evident from the DTG plots in Figure 6-11.

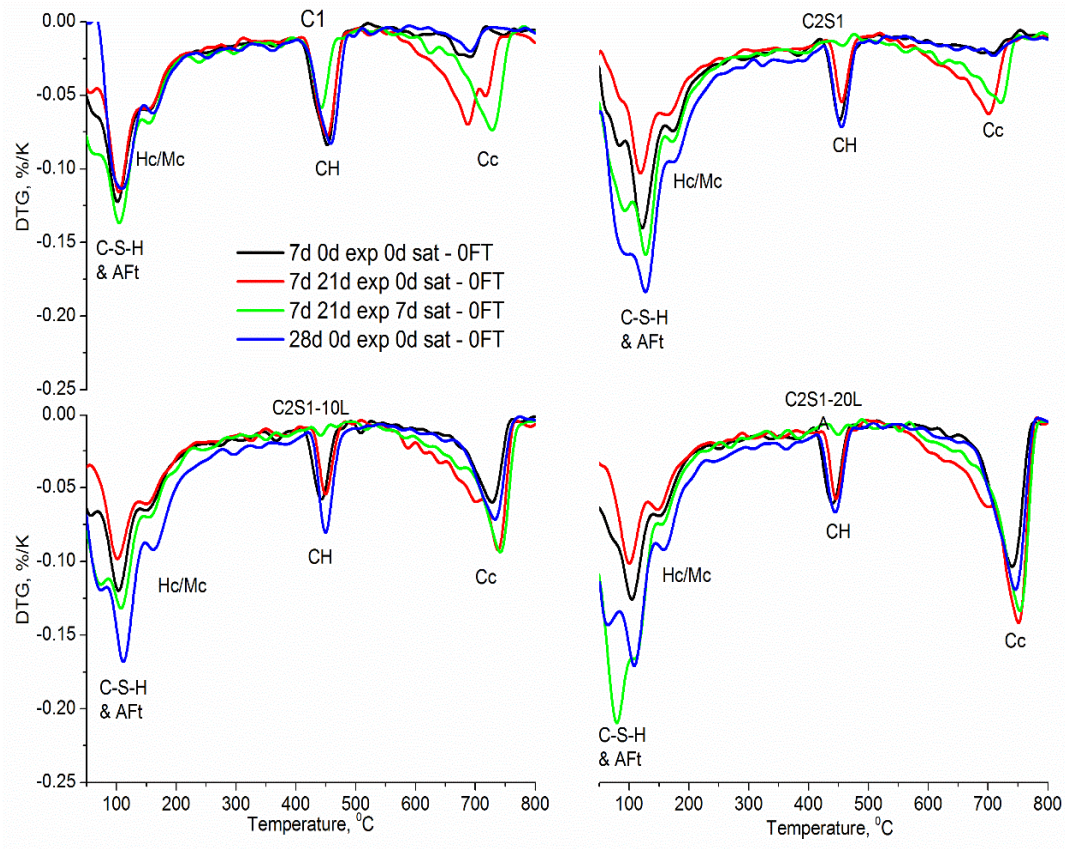

Figure 6-11 Effect of conditioning on C-S-H/AFt, portlandite and calcite contents compared to samples cured under sealed conditions for 7 and 28 days

Comparison of the data before and after drying depicts reduced portlandite and C-S-H/ettringite contents in the composite cements but less so in the CEM I. Notwithstanding, the calcium carbonate content increased in all four cements as a result of drying at 65% RH as reported elsewhere [246]. At 65 % RH, a humidity

gradient exists between the capillary pores and ambient. Consequently, dissolution of CO_2 is promoted. It must be emphasised that the connectivity of the pores has an equally important influence on the progress of carbonation.

The portlandite contents of the four mixes after the three conditioning or saturation are presented in Figure 6-12. Continuous hydration of clinker between 7 and 28 days increased the portlandite content in all cements as would be expected [4, 17, 51]. In the samples exposed for 21 days, however, the portlandite content was much lower compared to those cured continuously under sealed conditions and much lower than in the samples exposed for 21 days. This is consistent with carbonation of the samples as indicated by TG.

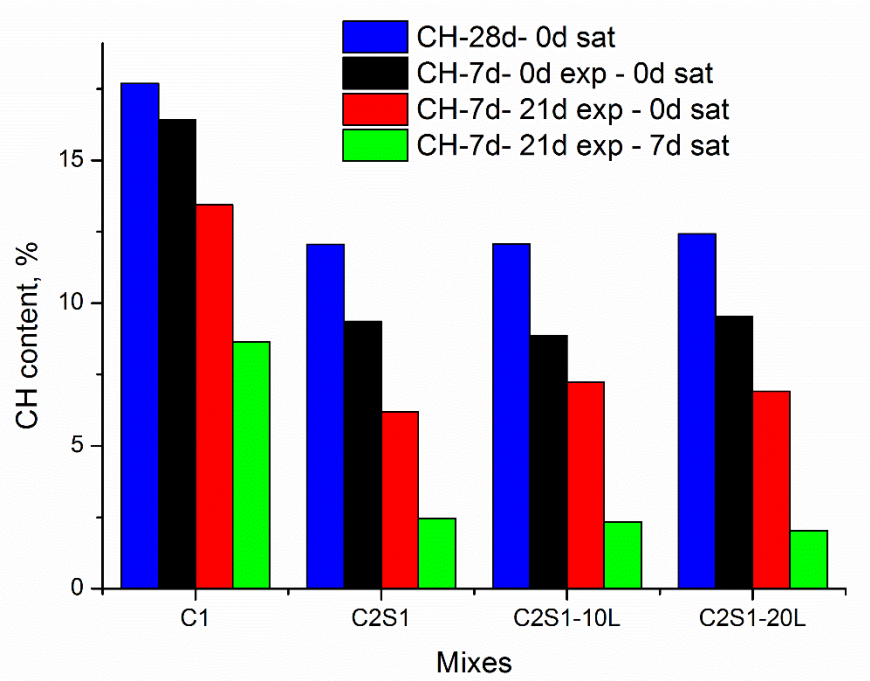

Figure 6-12 Effect of the 21 d conditioning and saturation on the portlandite content compared to the CH content in non-exposed samples cured for 7 and 28 days.

To further verify the extent of carbonation of the C-S-H/ettringite and portlandite, the equivalent lime content in the four mixes reported in Figure 6-11 were computed. The calculation considered the residual portlandite plus the calcium

carbonate due to carbonation. The results are shown in Table 6-6 in comparison with those from sealed samples cured for 7 and 28 days.

The equivalent lime content of the samples conditioned at 20 °C and 65% RH for 21 days exceeded that only from portlandite in all mixes, whether cured for 7 or 28 days. Therefore, the calcium carbonates in all mixes as noticed from Figure 6-11, do not solely originate from portlandite, but from other sources including the C-S-H/AFt [412, 413].

Table 6-6 Equivalent lime from portlandite and calcite due to carbonation compared to complementary non-exposed samples

Mix/exposure	Sealed 7d, 0d exposed	Sealed 28d, 0d exposed	Sealed 7d, 21d exposed		
	[CaO][1]	[CaO][1]	[CaO][1]	[CaO][2]	[CaO][3]
C1	12.4	13.4	10.2	6.1	16.3
C2S1	7.1	9.2	4.7	6.4	11.1
C2S1-10L	6.7	9.1	5.4	5.8	11.2
C2S1-20L	7.2	9.4	5.2	6.7	11.9

[CaO][1] is equivalent lime from portlandite
[CaO][2] is equivalent lime from calcite due to carbonation
[CaO][3] is equivalent lime from portlandite and carbonation

Both ettringite and C-S-H could carbonate. However, residual portlandite in the various mixes during exposure buffers against carbonation of ettringite. Consequently, the other sources of calcium as indicated in Table 6-6 is likely to be the C-S-H. This hypothesis is consistent with the simultaneous C-S-H and portlandite carbonation reported elsewhere [229].

6.6.2 Effect of capillary suction on the microstructure

Saturation of the samples caused further decalcification in all cements as evident from Figure 6-11 and Figure 6-12. Comparison between the calcium carbonate

content before and after saturation also indicated no further carbonation during saturation. Consequently, saturation had a more drastic implication on the portlandite content than did carbonation. The residual portlandite in the composite cements after saturation was just above the quantifiable limit. This may have arisen from the fact that, the portlandite content in the composite cements is already lower compared to the neat cement (see chapter 5). Additionally, the microstructure in the composite cements at the start of the conditioning may be more susceptible to carbonation of the CH [27, 229, 241].

Leaching during saturation is a flow around scenario [414] and hence the limiting step is mass transport through the given media. Connectivity of the pores has an equally important influence on leaching. The capillary pore volume, as measured through MIP, at the start of drying is illustrated in Figure 6-13.

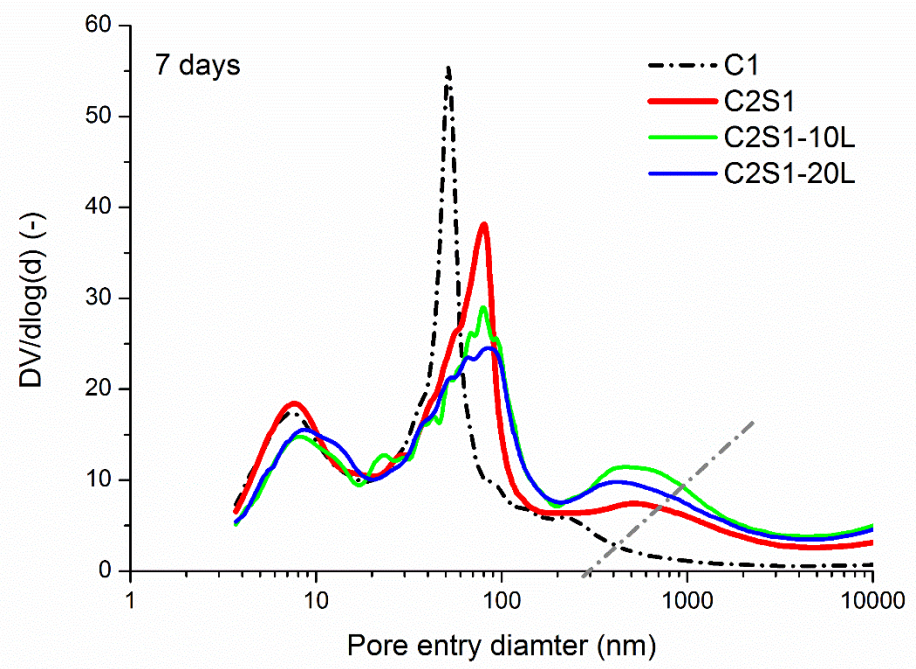

Figure 6-13 Pore distribution of hydrated cements before drying at 65 %RH and 20 ◦C.

The pores ranging between 200nm - 0.01mm were more prevalent in the composite cements. The neat cement, on the other hand, contained more gel pores which ranged up to 100nm in comparison to the composite cements. Since the capillary pores are the accessible centres during capillary suction, their connectivity will dictate the egress of ionic species.

Leaching of matter from the hydrated samples would depend on the pore structure as well as the state of constituents [415, 416]. It seems reasonable to believe that the mechanism which led to carbonation due to the RH gradient may also partly explain the leaching behaviour. For carbonation, CO_2 is drawn into hydrated cements by the gradient between ambient and the specimen. Conversely, the crushed particles equilibrate at 20 °C and 65 % RH during the conditioning. On capillary suction, however, the RH of the pores is lower (~65 %RH) than the ambient (now at 100 %RH) and consequently lead to migration of ions rather from the sample into solution. However, the 1 – 2 mm size of particles considered would imply that such a gradient may be lost within a short period of saturation.

The 7 days capillary suction did not only affect portlandite, but also the C-S-H and ettringite. The dehydroxylation reaction from DTG for AFt/C-S-H increased for all samples (see Figure 6-11). The bound water contents determined as the ignited mass change from 50 – 550°C were measured when the samples were 7 days, then following the 21d conditioning at 20°C and 65% RH and after the 7 days saturation (i.e. capillary suction) of the paste samples are summarised in Table 6-7. Irrespective of the cement, the bound water content decreased during the conditioning but then increased significantly following the 7 days capillary suction.

Despite the lack of evidence regarding the existence of dehydrated calcium sulphate after the 21 days conditioning, saturation led to an increase in the ettringite content particularly for the composite cements (see Figure 6-14).

Table 6-7 Effect of conditioning and pre-freeze thaw capillary suction on the bound water contents.

Mix	7d-0d exp-0d sat	7d-21d exp-0d sat	7d-21d exp-7d sat
C1	17.72	16.03	18.69
C2S1	17.79	13.48	19.55
C2S1-10L	17.03	14.40	18.05
C2S1-20L	17.74	14.07	20.98

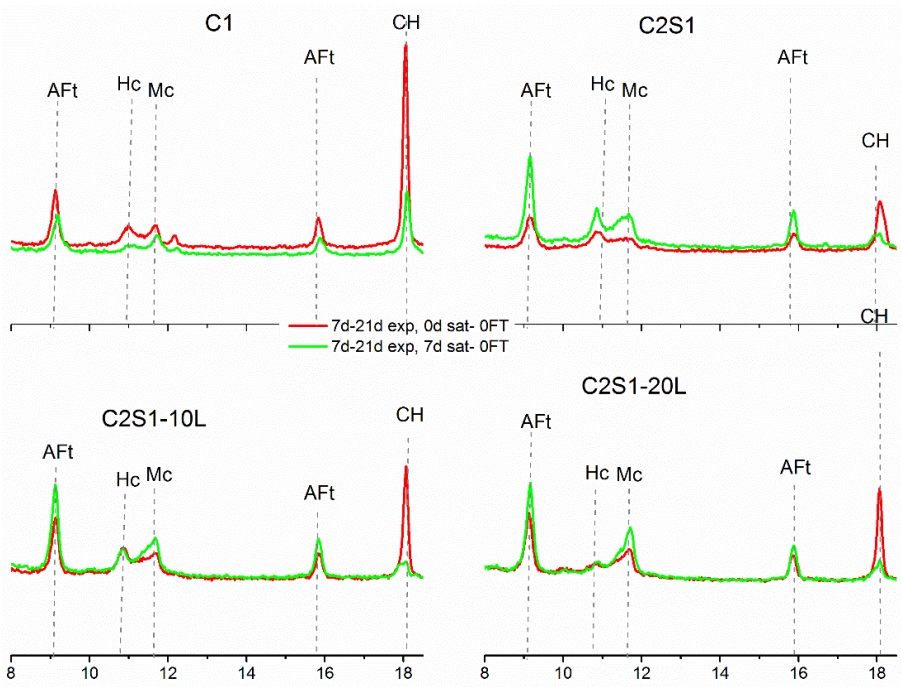

Figure 6-14 Effect of saturation on the AFt/AFm contents relative to portlandite loss

The increased bound water content (Table 6-7) indicate that the higher ettringite content as noticed from the XRD reflection peaks (Figure 6-14) and DTG (Figure 6-11) was due to the reverse dilution effect, where loss of CH meant a greater proportion of the binder was ettringite and C-S-H. On the contrary, renewed

hydration plus the increase in ettringite content during the 7 days capillary suction explain the increased bound water content. It is possible that ettringite was rather dehydrated during conditioning and possibly formed an amorphous phase rather than carbonating [417]. This interpretation is based on the continuous prevalence with portlandite in the carbonated samples. It is well documented that the presence of portlandite can offset the carbonation of ettringite [418].

6.7 Microstructural response to freeze-thaw of composite slag cements

The data presented in the preceding sections indicated that scaling and internal damage resistance were lower in the composite cements despite different trends. The microstructure of the cements after the 7 days capillary suction also indicated significant reductions in the portlandite content. This section presents results from four mixes – C1, C2S1, C2S1-10L and C2S1-20L (hereafter C, CS, CS-L and CS-2L respectively), as a function of freeze-thaw cycles. The objective here was to clarify the microstructural changes during freeze-thaw testing. Thermal analysis, XRD and SEM were combined for this purpose. Paste samples were used for compositional characterization while concrete samples at the end of experiments were used to obtain an overview of the microstructure of by SEM. The pastes for thermal analysis and XRD were crushed into 1 – 2mm thick samples after the 7 days curing under sealed conditions while slices were obtained for SEM/EDX analysis. In addition, 20mm by 50mm long cylinders were prepared and cured as the concrete and crushed samples for leaching test.

6.7.1 Freeze-thaw of cement paste samples

Photographs of the cylinder samples after 0, 11 and 25 freeze-thaw cycles are shown in Figure 6-15.

0 FT	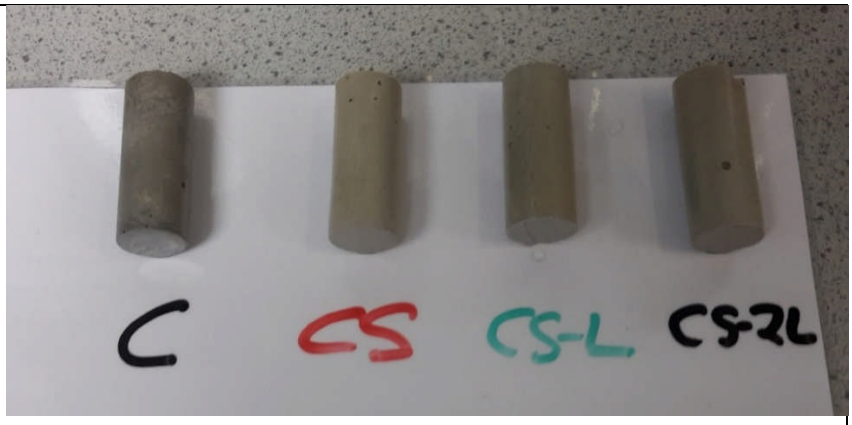
11FT	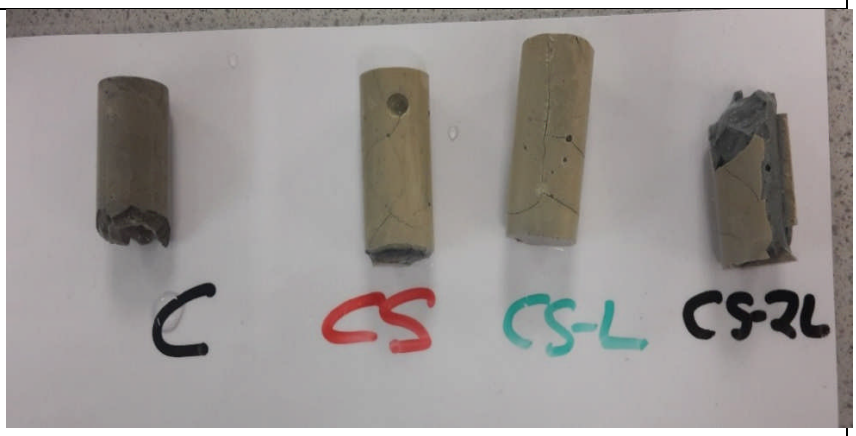
25 FT	

Figure 6-15 Effect of cement composition on freeze-thaw: Cement pastes observations.

After 0 (top), 11(middle) and 25 (bottom) freeze-thaw cycles: C = Mix C1; CS= Mix C2S1; CS-L= Mix C2S1-10L and CS-2L= Mix C2S1-20L

All samples were intact at the start of freeze-thaw testing despite significant leaching during saturation. However, the weaknesses of the composite cements were already evident by the 11th freeze-thaw cycle such that the mix C2S1-20L had already lost material from the surface through spalling. Noticeable cracks could also be seen on the surfaces of mixes CS and CS-L. The broken edge on mix C appeared to be an artefact arising from a trapped bubble during sample preparation.

A failure mode can be deduced from the comparison between mix CS-L and the other composite cements after 11 cycles and then the degraded particles after 25 freeze-thaw cycles. Clearly, the failure mode differed between the neat cement, C and the composite cements. After the 11th freeze-thaw cycle, mix CS-2L, the test specimen comprised of an outer component (i.e. blanket) which enclosed an inner core. Cracks, therefore, appeared originally in the outer envelope and only propagated as deep as this layer extended. Similar cracks can be noticed on mixes CS and CS-L after 11 freeze-thaw cycles with a regular pattern in all samples. These cracks, therefore, provide channels for the ingress of the test solution which would then expand upon freezing to cause spalling. This mode is consistent with the glue-spall mechanism which has been espoused elsewhere [35, 40, 260, 261]. However, this differed between the neat cement paste and the composite cements. There was no outer envelope neither was there visually noticeable crack patterns in the mix C.

6.7.2 Effect of freeze-thaw on hydrated phase assemblages

To verify whether the outer envelope and the core responded differently to freeze-thaw and also if different mechanisms influenced the degradation of the different cements, two sets of the four cements were further investigated. The objective of

the first set (surface) was to mimic the outer envelope and was accomplished through an investigation of crushed paste samples. The crushed samples were conditioned following the procedure to the CIF method for concrete [340] and then freeze-thawed in deionized water. The second set was again paste samples but rather cured continuously for 28 days (to simulate the core) and freeze-thawed in saturated lime solution with the objective of simulating the hydrating environment of cements. These were crushed before the freeze-thaw test but in a glove box to minimise carbonation due to sample preparation.

The simulated ‘surface’ and ‘core’ samples from all four cements were characterised after 0, 11 and 25 freeze-thaw cycles. The 0 FT cycle was taken as the end of the 7-day saturation in either deionized water or saturated lime solution. Figure 6-16 to Figure 6-18 show the DTG traces and the corresponding reflection peaks from XRD for the ‘surface’ and the ‘core’ samples for mixes C, CS and CS-2L. The mix CS-L was similar to CS-2L and hence not duplicated here. Further details are can be found in Appendix A.1.6.

From DTG, differences can be noticed in the endotherms at ~ 110, 160, 450 and 700 °C. These correspond to dehydration of the C-S-H and ettringite, carboaluminates, portlandite and decarbonation of calcite respectively [339, 363, 419]. The C-S-H and ettringite endotherm (~ 110 °C) increased with the freeze-thaw cycles irrespective of the cement composition and the location [234, 420]. In the mix C however, a slight reduction in the ettringite reflection peak was noticed by the 25th cycle for both ‘surface’ and ‘core’ samples.

The composite cements on the other hand exhibited steady changes except for mix CS-2L which did not change significantly between the 11th and 25th cycles for

both surface and core samples. The increase in the C-S-H endotherm corresponds to progressive hydration [161, 363]. Meanwhile, the endotherm at ~160°C, attributed to carboaluminates, was not affected by the freeze-thaw cycles, whether from the surface or the core.

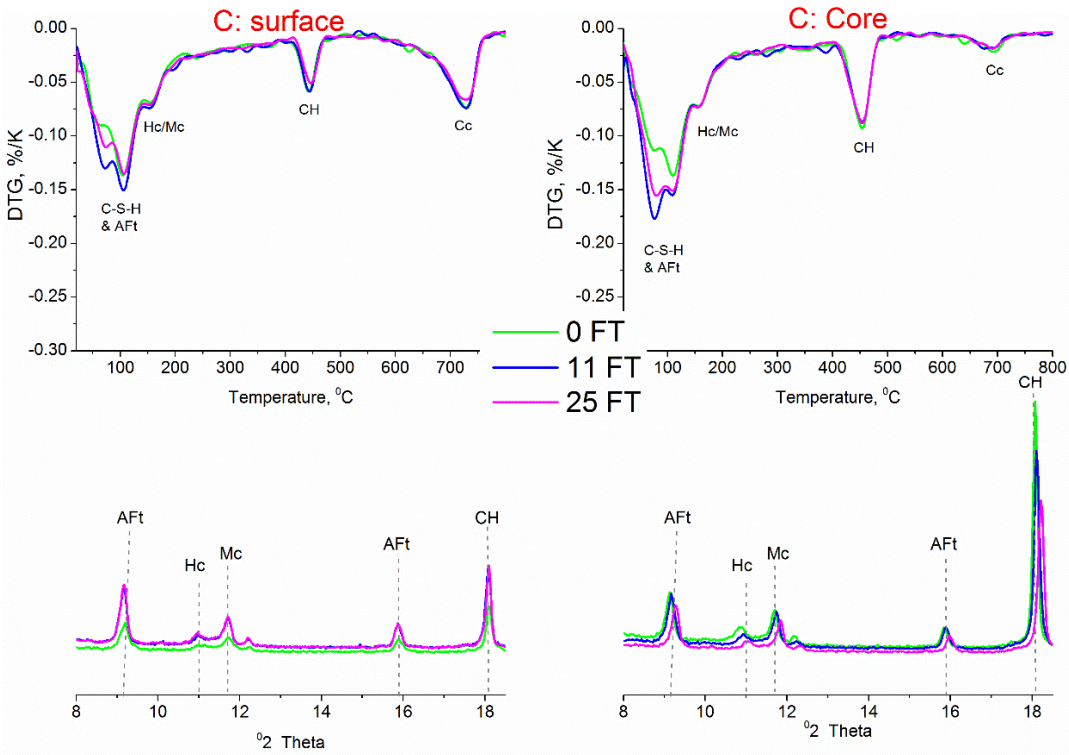

Figure 6-16 Effect of freeze-thaw on the microstructure of surface and core of cements in the neat cement, C

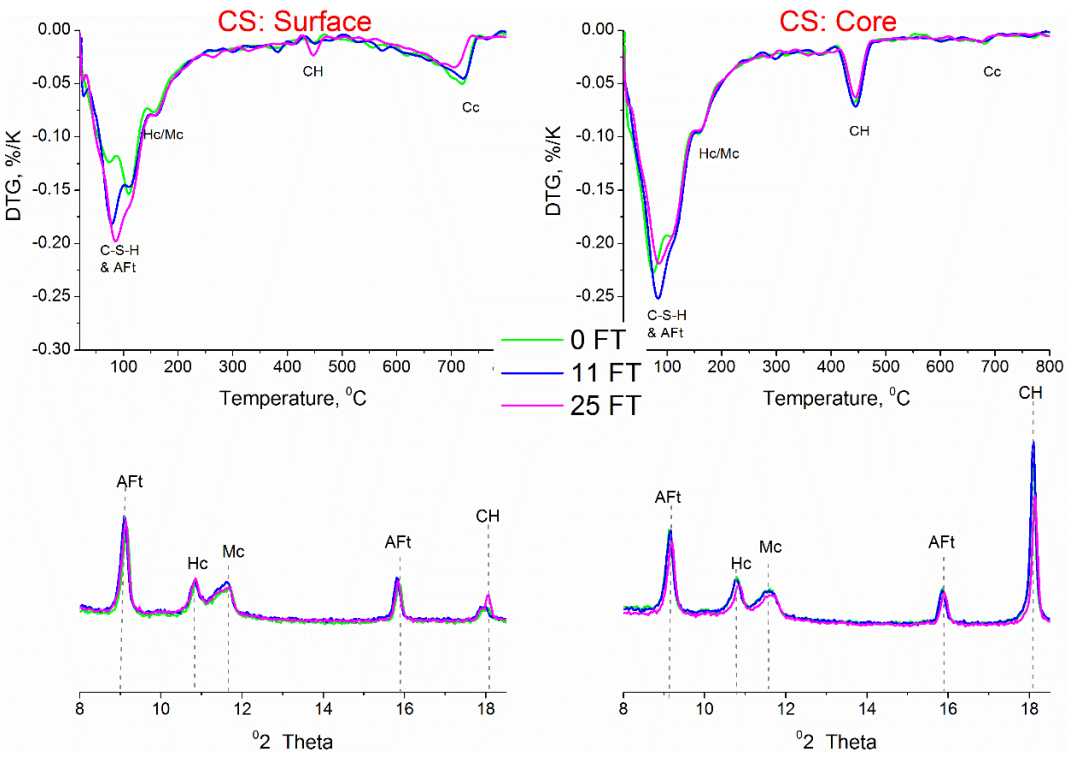

Figure 6-17 Effect of freeze-thaw on the microstructure of surface and core of cements in the binary mix, CS

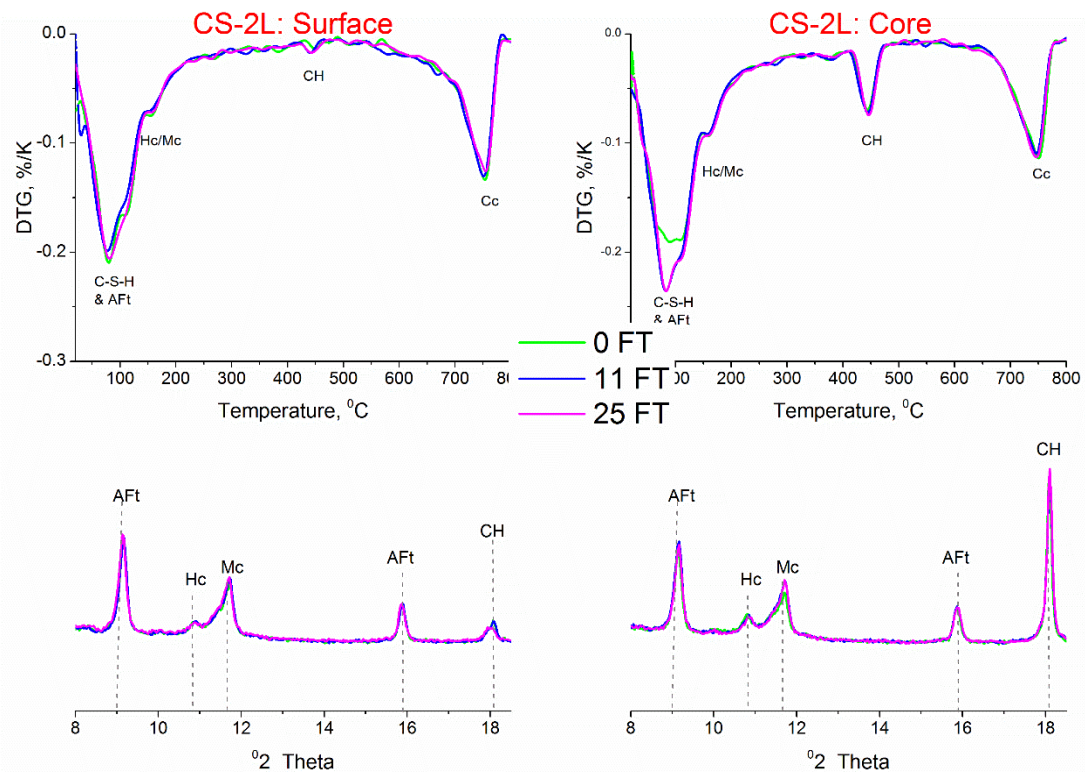

Figure 6-18 Effect of freeze-thaw on the microstructure of surface and core of cements in the binary mix, CS-2L.

The trends from DTG are also consistent with the XRD plots. Therefore, the carboaluminate content was also not affected by freeze-thaw.

The portlandite content (~ 450 °C) was strongly affected by freeze-thaw [265, 270]. In the composite cements, insignificant amount of portlandite was present in the surface samples at the start of the freeze-thaw test. In mix C however, the portlandite content on the 'surface' increased with the freeze-thaw cycles while the reverse was noticed on the 'core' samples (see Figure 6-16). It was established in section 6.3.3 that, hydration ceased at least at the 'surface' during the conditioning at 65 % RH [246] but then resumed upon capillary suction (see Figure 6-14). This was true for the surface but not the core samples, which then explains the additionally formed portlandite in the surface samples for mix C. This is consistent with the increasing C-S-H content of the 'surface' sample (see DTG trace in Figure 6-16), thus indicating progressive hydration. This obscures the impact of freeze-thaw on the portlandite content in the neat cement. However, decreasing portlandite in the core samples clarifies this effect particularly in mixes C and CS. With progressive freeze-thaw cycles, the portlandite content decreased even in the presence of saturated lime. This suggests that decalcification may be an important mechanism as has been speculated elsewhere [273].

In the slag blends, however, there was an insignificant amount of portlandite in the surface samples but not the core samples. There was no variation in the portlandite content in the cores samples of mix CS-2L with increasing freeze-thaw cycles. This may be attributed a pore blocking barrier following carbonation of these samples [412]. Consequently, a high pH 'core' samples in these cements may have lowered the solubility of portlandite and hence avert leaching.

Comparison between the ‘surface’ and the ‘core’ samples of the cements after the 11th cycle further confirm changes to no other phase assemblages beside portlandite. Indeed, the ettringite and carboaluminate contents were even similar between the ‘core’ and the ‘surface’ of the cements. This also suggests that there was no carbonation of ettringite. The fact that, sulphates were detected in the test solution during saturation also indicates that, if these had evolved from carbonated sulphate bearing phases, then it was restored from another source possibly the C-S-H.

6.8 Mechanism of freeze-thaw damage of composite cements in deionized water

By relating the portlandite content in the ‘core’ to the depleted portlandite on the surface ‘samples’, two possible explanations can be deduced for the performance of the cements subjected to freeze-thaw. Namely, susceptibility to carbonation and leaching on one hand and the mechanical properties of the C-S-H on the other hand.

The additional calcium carbonate arising from carbonation during the 21-day exposure at 65 % RH and leaching during capillary suction were calculated from thermogravimetry. The rationale was to address the question of susceptibility to decalcification. The baseline values were taken as the calcite and portlandite contents before drying, based on the assumption that negligible hydration occurred at the 65 %RH [246]. In addition, negligible limestone consumption was assumed during the exposure period. The results are presented in Figure 6-19. The composite cements were more susceptible to carbonation and portlandite leaching compared to the neat cement. It is also evident that in all the cements investigated,

portlandite was more susceptible to leach out of the samples than it would carbonate.

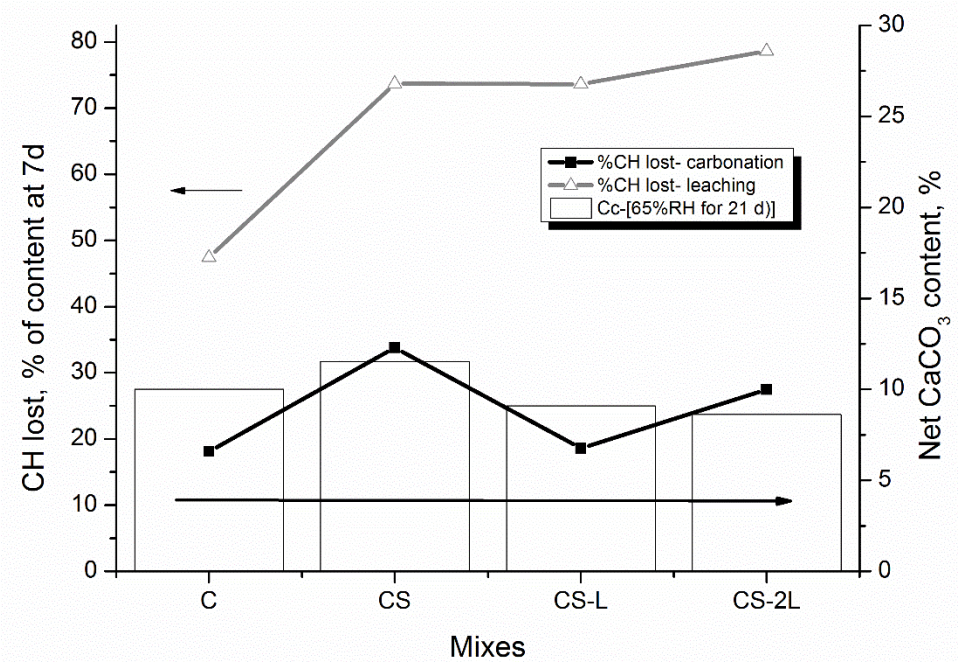

Figure 6-19 Susceptibility of the investigated cements to decalcification of portlandite

Expressed as % of the CH content at the start of conditioning. Note: column plot for the $CaCO_3$ due to carbonation; solid squares = CH lost due to carbonation during conditioning; and open triangles = CH lost due to leaching). C = Mix C1; CS= Mix C2S1; CS-L= Mix C2S1-10L and CS-2L= Mix C2S1-20L

Analysis of the leachates from the cylindrical specimen presented in Figure 6-15 is shown in Figure 6-20. The solid to liquid ratio was 1:100 by weight and the leachates were analysed on a Metrohm Ion Chromatograph without further dilution.

Calcium was present in the test solutions throughout the freeze-thaw cycles. In all mixes, the calcium concentration generally decreased with the number of freeze-thaw cycles. This is consistent with the literature and can be explained by the relative humidity gradient imposed by the temperature cycles during freeze-thaw [416]. In the composite cements, almost all portlandite was lost from the surface

of the samples before the commencement of freeze-thaw. The leachate analysis also showed continuous decalcification despite depletion of portlandite. Coupling the leaching results with TG and XRD which indicated fixation of ettringite during freeze-thaw, the source of the additional calcium can be narrowed to the C-S-H.

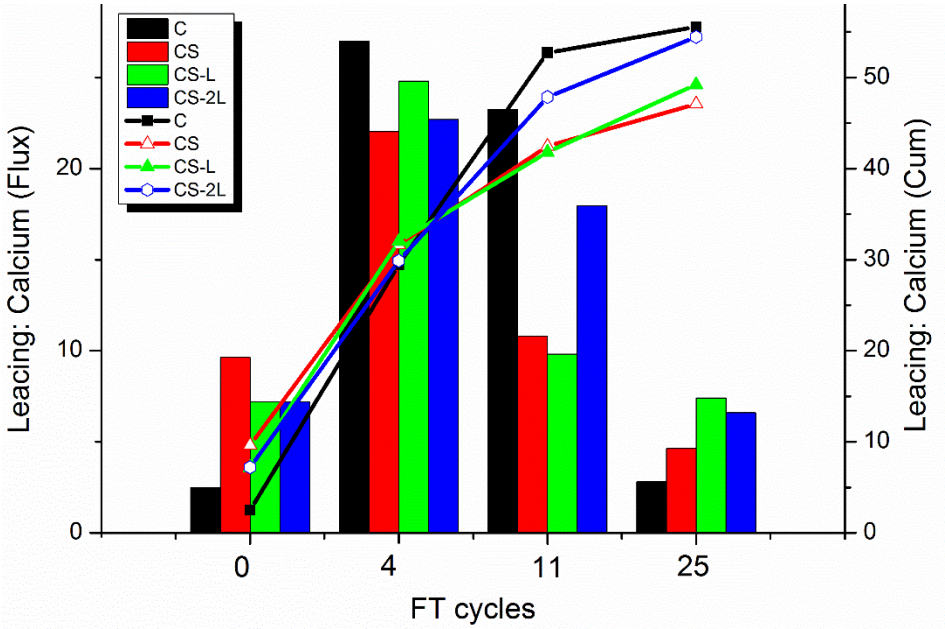

Figure 6-20 Leaching of calcium ions during freeze-thaw

Note: Columns plot = flux; line and symbol= cumulative concentration. **C =** Mix C1; CS= Mix C2S1; CS-L= Mix C2S1-10L and CS-2L= Mix C2S1-20L

An overview of the microstructure after the capillary suction (i.e. 0FT) and 25 freeze-thaw cycles is shown in Figure 6-21 for mixes C and CS-2L. The matrix is heterogeneous, comprising hydrates and pores, plus unreacted clinker, slag and limestone.

Changes during freeze-thaw were more evident in the neat cement. While portlandite persisted, the C-S-H was modified and visibly became more porous. The C-S-H in the ternary blend appeared different from the neat cement at the start of the freeze-thaw test and did not seem to change significantly after 25 freeze-thaw cycles.

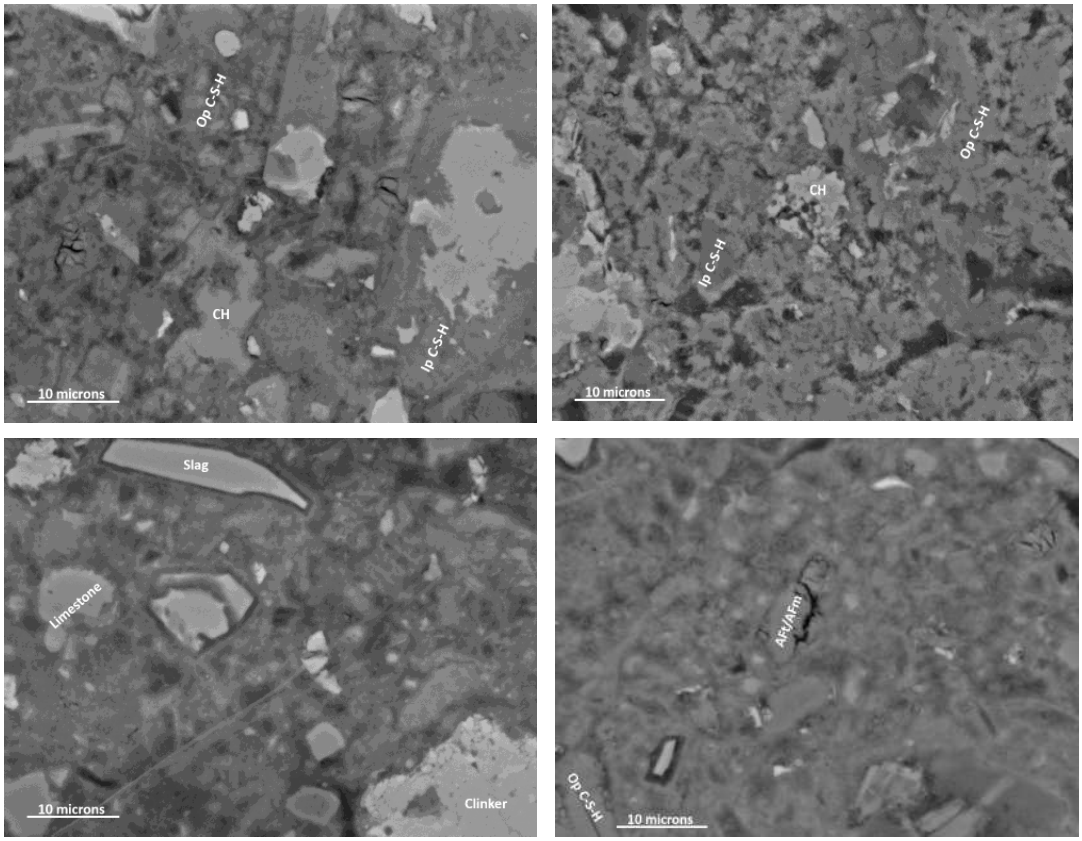

Figure 6-21 Effect of freeze-thaw on the microstructure of composite cements

Note: C1(top) and CS-2L (bottom) rows, after 0 FT (left) and 25 FT (right) cycles; 5000x magnification.

Modifications in the C-S-H of the neat cement due to leaching and carbonation are consistent with the literature [412, 415]. The decalcified C-S-H is often considered as a silica-rich gel [413]. This reduces ductility and consequently impairs mechanical performance. The composition of the C-S-H for the mixes C and CS-2L after 0 and 25 FT were analysed and the results are shown in Figure 6-22. The C-S-H in the cement had a Ca/Si of 1.82 at the commencement of exposure. Upon carbonation and capillary suction during freeze-thaw, a higher Ca/Si ratio was found in mix C as opposed to a slight reduction in the mix CS-2L. The Ca/Si ratios are typical for blended cements. It is, however, surprising that, the C-S-H Ca/Si

ratio rather increased in the neat cement [143] despite the latter showing modifications in the appearance of the C-S-H (see Figure 6-21). As already indicated (Figure 6-20), the C-S-H carbonated alongside portlandite while Ca also leached. Consequently, lower C-S-H Ca/Si ratio was expected [421]. Consequently, higher Ca/Si may be ascribed to renewed hydration [143].

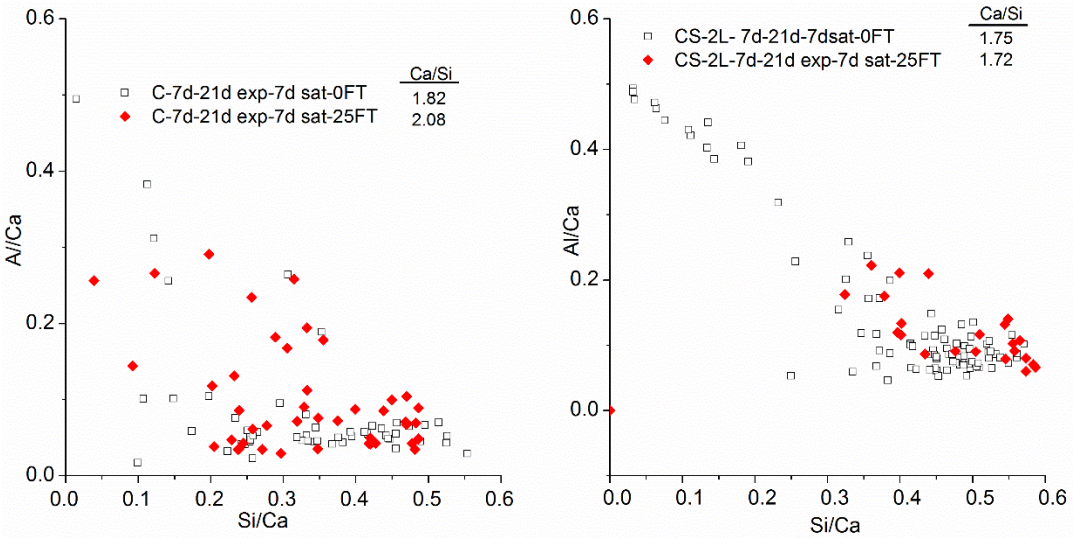

Figure 6-22 C-S-H composition of mixes C (left) and CS-2L (right) after 0 and 25 FT.

An increased surface area of the C-S-H following decalcification has also been suggested elsewhere [421]. The authors attributed the transformation to the denser inner product C-S-H. However, the observations from this study indicate among other effects that, coupled decalcification and freeze-thaw tend to initially attack the outer product C-S-H upon the depletion of portlandite in the ice front as illustrated in Figure 6-23.

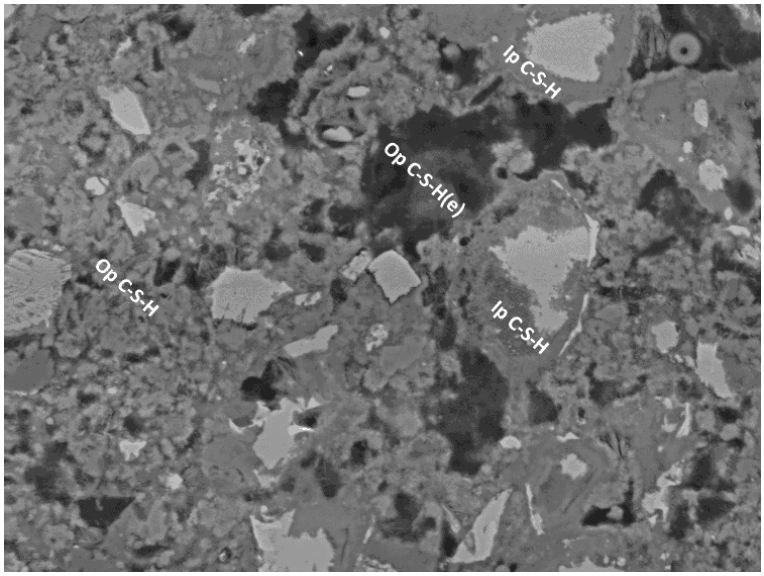

Figure 6-23 Effect of freeze-thaw on the C-S-H

For mix C after 25 freeze-thaw cycles.

Decalcification has implications on the mechanical properties of the microstructure due to the dominance of calcium in cement hydrates [213, 214]. Micro-indentation measurements were performed on the four mixes after 0 and 25 FT cycles in order to verify the mechanical implications of the decalcified portlandite and the C-S-H plus structural modifications of the latter. The measurements were performed at 50-micron scale and hence heterogeneity could not be avoided. Illustrative frequency density plots for mixes C and CS-2L are given in Figure 6-24 and the Young's modulus (Eit) of all mixes after the 7-day capillary suction (0FT) and the 25th freeze-thaw cycle are presented in Table 6-8.

A shift towards a higher elastic modulus can be noticed in the neat cement. Meanwhile, no significant changes were observed in the composite cements. These findings are consistent with the Ca/Si ratio changes during freeze-thaw. The mixes C and CS attained similar and higher elastic modulus by the 25th cycle. However, while the modulus in mix CS did not change, that in the neat cement

increased from 23 GPa to 29GPa. Those in the ternary blends were 22 and 24 GPa at 10 and 20% limestone contents respectively.

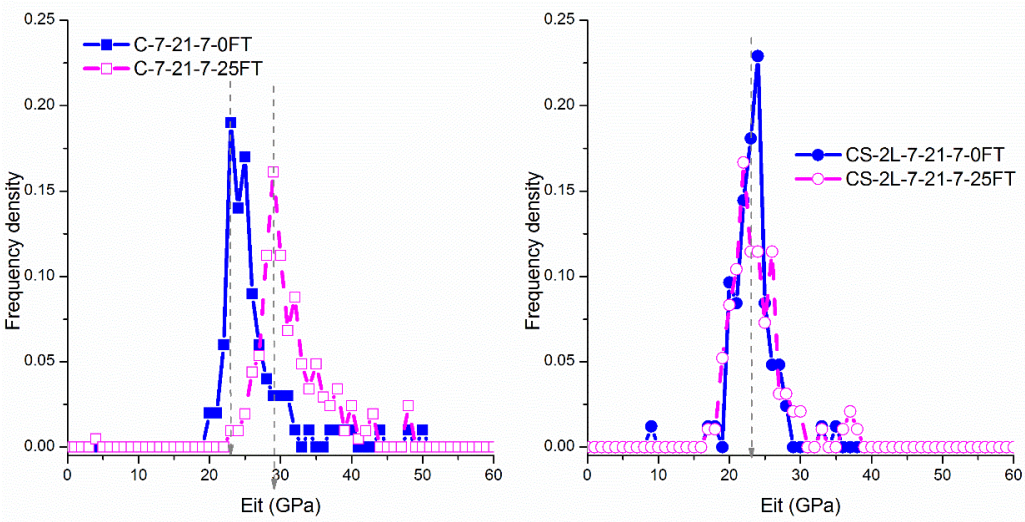

Figure 6-24 Illustrative frequency density plots of the effect of freeze-thaw on the Young's modulus of the C-S-H for mixes C and CS-2L

Table 6-8 Effect of freeze-thaw on the Young's modulus (GPa) of the C-S-H in CEM I and composite cements

Mixes	0 FT	25 FT
C	23	29
CS	29	29
CS-L	22	22
CS-2L	24	22

The unchanged Young's modulus in the composite cements with increasing freeze-thaw cycles raises the question about the relative influence of decalcification of portlandite and C-S-H on the mechanical properties of clinker based cements. This question has been addressed elsewhere [398, 415]. It was established that partial decalcification of the C-S-H could account for ~ 6 % reduction in strength and porosity as opposed to the global depletion of portlandite. Consequently, the gain in portlandite due to progressive hydration in the neat cement could only improve

the mechanical performance as rightly observed (see Table 6-8). On the other hand, the depletion of portlandite, even before subjection to freeze-thaw meant that changes in porosity and strength due to the C-S-H would be marginal as may be localised.

6.9 Correlation between microstructure and freeze-thaw resistance of composite cements

The freeze-thaw resistance of the investigated cements in deionized water is a function of the mechanical properties of the microstructure. This however, depended largely on the portlandite content to a larger extent compared to decalcification of the C-S-H. The composite cements were more susceptible to carbonation during the sample conditioning at 65 % RH and leaching of calcium from portlandite during the capillary suction and also during freeze-thaw. The severity was such that, after conditioning the specimens according to the CIF method, insignificant amounts of portlandite remained in the composite cements even from the start of the freeze-thaw test. This deficiency rendered the C-S-H vulnerable against stresses induced by ice growth in the capillary pores and hence significantly lower freeze-thaw resistance in the composite cements.

Whilst limestone enhances slag reactivity (Chapter 5), portlandite is consumed in the process to form additional C-S-H and carboaluminates. Despite the evolution of more C-S-H, the restraining effect of portlandite is somewhat reduced as depicted in Table 6-8. Regarding, the content of limestone, the mechanical properties of C-S-H increased slightly due to densification by the additional C-S-H; this however consumed further portlandite. The effect of fineness of clinker and slag lies in the nature of pores filled by their hydrates.

Chapter 7
Discussions, Conclusions and recommendations for further studies

The investigations carried out and reported in this thesis were in three main parts. The first part involved the development of the PONKCS method to analyse ternary blends. The PONKCS phase was subsequently employed in addition to complementary techniques to investigate the impact of limestone on the kinetics of hydration of ternary blends. The focus was to establish the impact of limestone on the hydration of slag in ternary blends and then to identify the factors which influence the synergy between limestone and aluminosilicate SCMs. Finally, the relationship between hydration and microstructure on one hand and the mechanical and freeze-thaw performance of composite cements on the other hand were established.

7.1 The PONKCS Phase in the Rietveld refinement

The PONKCS method [32, 33] was implemented successfully as part of the Rietveld refinement of composite slag cements. The contents of slag, clinker and hydrated phase assemblages were quantified simultaneously. Careful calibration of the slag phase meant that the method could be used without the need for hydration stopping. Consequently, the AFt/AFm phase assemblages were quantified without interference from organic solvents often employed for dehydration. The effect of dehydration techniques was also assessed.

The often used hydration stopping methods modified the scale factor from the quantification. However, after accounting for the differences in the bound water contents, the measurement precision of the different dehydration methods was ±5 %.

When comparing PONKCS with BSEM/IA, the latter appeared to overestimate the degree of slag hydration at an early age. This may partially be attributed to the size of the smallest features which may be observed by image analysis [28, 31]. At 800x magnification and 1024*68 pixel resolution, the pixel size is 0.17x0.17μm. This is equivalent to approximately 3% of the slag fraction according to the particle size distribution. This does not fully account for the overestimation of the degree of slag hydration [29], and additional overestimation may arise from using a 2-dimensional cross-section to represent a 3-dimensional microstructure. The PONKCS method considers the bulk sample, and with the associated 2% deviation, can be considered more accurate than BSEM/IA.

Comparison between the two independent methods, however, indicated up to 6 % deviation. This is higher than anticipated and future work should aim to compare the two techniques over the larger data set. The XRD halo for slag overlaps with the C-S-H. Consequently, the calibrated PONKCS phase for slag should also be tested against different C-S-H compositions – particularly the different Ca/Si ratio and the water content.

7.2 Effect of limestone on hydration in ternary blends

Limestone influenced the hydration kinetics as a filler and a reactant. Consequently, the hydration of clinker and slag in the ternary cements were affected. With respect to clinker, alite and belite hydration were accelerated through a combination of the nucleation and dilution effects. Limestone also accelerated the hydration of slag. The results led to the identification of a multitude of factors which influenced the synergy. These are discussed in greater detail in

section 7.4. Kinetics were also influenced by fineness but the clinker fineness had a greater consequence than slags.

The reaction of calcite was limited. About 35 % degree of hydration was found after 180 days irrespective of original content in the ternary blend. However, dissolution kinetics were influenced by clinker and slag fineness but had no bearing on the ultimate consumption.

7.3 Effect of limestone on the microstructure of in ternary blends

7.3.1 Hydrated phase assemblages

The composition of the C-S-H in composite slag cements is well documented [31, 103, 143, 207] but less so for ternary blends with limestone. The results indicated higher C-S-H Ca/Si ratio in the ternary blends compared to the binary slag cement but the reverse was true for the C-S-H Al/Si ratio. Both deviated strongly from the neat cement. The accelerated belite hydration and simultaneous dissolution of limestone may explain the higher Ca/Si ratio.

Limestone does not only influence the AFt/AFm stability and contents. It also affects the distribution of the alumina in all of the other hydrates [17]. Slightly greater ettringite contents were observed in the limestone-containing blends compared to the binary blend. The increased carbonate to aluminate ratio in the ternary blends led to increased carboaluminate phase assemblages, which in turn raised the sulphate to available aluminate ratio, thus stabilising ettringite. In addition, this reduced the alumina concentration in the pore solution [17]. Consequently, less aluminium was available for incorporation into the C-S-H as seen by the decrease of the Al/Si ratio in C-S-H.

The increased formation of carboaluminate phases and the consequent reduction in alumina concentrations in solution also had an effect on other alumina-bearing phases. The Mg/Al ratio of the hydrotalcite-like phase was higher in the limestone containing cements than the binary slag mix. The latter values are consistent with those reported elsewhere for a similar slag [31]. This change in the Mg/Al ratio by replacing 10% of slag with limestone reflects the lower alumina content in solution while increasing the limestone content from 10 to 20% did not affect the Mg/Al ratio of the hydrotalcite.

7.3.2 Pore structure

The porosity was assessed by SEM/IA and MIP. The latter also provided information about the pore distribution as a function hydration time and cement composition. Both techniques indicated consistently porosity in the slag blends compared to the neat cement, however with decreasing margin. MIP further indicated that, at early ages, the pore volume increased with the limestone content but the trend was reversed at later hydration times due to the limited reaction of calcite. The effect of replacing up to 20 % slag with limestone had no significant influence on porosity. Consequently, refinement of the porosity was more efficient in the ternary blends compared to the binary slag blend. The fineness of clinker and slag was significant at an early age but not at longer hydration times.

7.4 Mechanisms behind the synergy in limestone ternary blends

7.4.1 Nucleation effect

The presence of slag, limestone, or even quartz, in the composite cements affects the clinker hydration kinetics differently. The chemical shrinkage and calorimetry

data indicated enhanced hydration in the blends compared to the neat cement system. At the very early stages of hydration (up to 1 day), the data show similar trends among the composite cements. A comparison between the neat cement , quartz mixes and the composite cements show the nucleation effects of slag and quartz [51, 52]; being slightly higher in the presence of slag. The alite hydration peak was accelerated by the addition of slag or quartz, and further still by the addition of limestone. The acceleration of the reaction of aluminates is very significant and agrees with the trends reported elsewhere [10], with the effect particularly evident in the quartz mix.

The quantitative XRD data enables detailed evaluation of the changes in kinetics with respect to the major clinker phase assemblages. In the binary slag blends, hydration of alite was accelerated whilst belite was retarded, as has been reported elsewhere [29, 31]. In the limestone containing cements however, the hydration of alite was further accelerated, whilst belite hydration was not retarded, suggesting that limestone compensates for the retarded belite reaction in the presence of slag. The addition of either slag or quartz accelerated the aluminate and ferrite reactions similarly, in agreement with the findings of Hoshino *et al.* [14]. However, the impact of limestone on the interstitial clinker phases was slight. The accelerated alite hydration which also led to the shortened induction period in the calorimetry test confirms limestone as a better substrate for heterogeneous C-S-H nucleation [51]. The trends in the degree of hydration of clinker suggest that the nucleation effects on clinker hydration are dominant only at the early ages.

The implications of the filler effect on slag hydration are the improved availability of portlandite from the very early age due to accelerated clinker reactions.

Accelerated aluminate dissolution can retard silicate dissolution [384] unless aluminium is readily incorporated into secondary hydrates.

7.4.2 Dilution effect

The magnitude of the dilution effect of SCMs on kinetics is a function of time, replacement level and composition of supplementary material [51, 52, 422]. Slag in composite cements reacts slowly compared to clinker. Consequently, at early ages and at a given replacement level, this increases the effective w/c ratio and space for the growth of hydrates. The influence of the available water and space for hydrate growth (dilution effects) are separately considered below.

In this study, each of the composite cements contained 50% clinker and were prepared at 0.5 w/b ratios. Therefore at the very early stages of the reaction, the water available for hydration (i.e. dilution effect) would be similar. Consequently, the kinetics were controlled by the rate of dissolution [86].

At longer hydration times, C-S-H will form around most hydrating surfaces including slag and clinker and the availability of water has an important role on slag reaction. Table 7-1 shows the free water/binder ratios in the different mixes after 180 days.

Table 7-1 The unbound water contents (%) after 180d

Mix ID	Effective w/b	Bound water (%/paste)	Free w/b
C	0.50	28.2	0.36
CQ	1.00	15.2	0.85
CS	0.50	22.7	0.38
CS-L	0.56	23.9	0.43
CS-2L	0.63	23.6	0.48

Considering the high availability of water, an internal dessication-driven mechanism is unlikely to account for differences in the slag hydration in the presence of limestone.

The availability of water and space is essential for slag hydration [54]. The pore volumes calculated from the MIP data are shown in Figure 7-1. Some scatter in the slag blends were apparent at early ages but became similar at longer hydration times (>7 days). This indicates that, if influential at all, the effects of space for hydration products to form would be very small. Other factors must also account for some of the differences in hydration behaviour, for example, the pore solution chemistry.

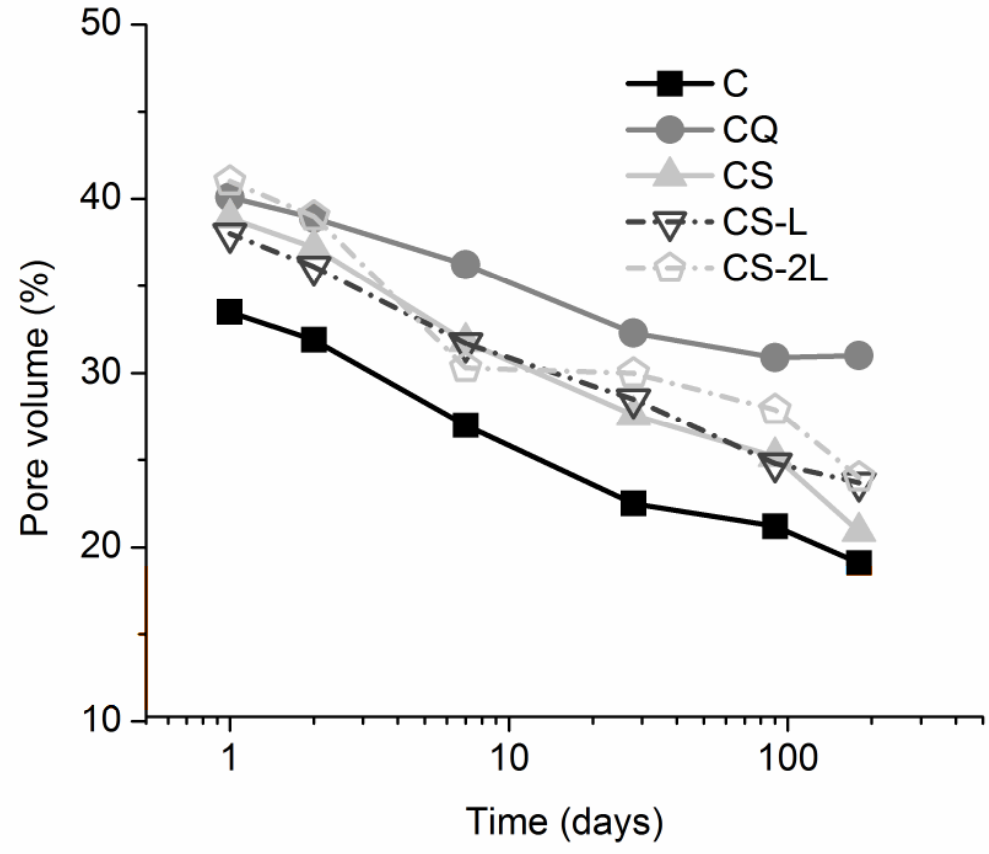

Figure 7-1 Effect of slag and limestone on the pore volume as determined by MIP

7.4.3 Pore fluid composition-based mechanisms

Higher aluminium concentrations in the pore solution retard silicate dissolution [203, 423], as the sorption of aluminium on the surface sites of silicates slows down dissolution. Consequently, lower aluminium levels in the pore solution can promote the dissolution of glasses [203] and also of slag [141]. The results from the pore solution analysis show lower aluminium concentrations in the limestone containing blends as has been previously observed for binary Portland cement-limestone binders [17, 174]. The lower aluminium concentrations are related to the stabilisation of ettringite and monocarboaluminate in the presence of limestone compared to ettringite and hemicarboaluminate or monosulfoaluminate in the presence of small amounts of limestone, as discussed in detail in [17, 174, 201]. The XRD plots in (Figure 5-16) indicate the absence of monosulphoaluminate in the investigated systems without limestone. Instead, ettringite and hemicarboaluminate were present in C, CQ and CS, while in the limestone-containing blends, ettringite was stabilised and mainly calcium monocarboaluminate were observed, consistent with the thermodynamic predictions [174, 201].

Although the measured aluminium concentrations show some variations, the limestone containing mixes show consistently lower aluminium concentrations than those without additional limestone. A plot of the measured Al concentrations against the measured slag dissolution and the chemical shrinkage after 28 days (shown in Figure 7-2) confirms, in fact, the negative influence of higher aluminium concentrations on slag dissolution. This observation of the influence of aluminium on the slag reaction confirms that in cements the same effects are important as in

diluted alkaline solutions [141, 203]. In addition, it shows that the positive effect of adding limestone to blended cements is not only due to its ability to stabilise ettringite but that limestone via the lowering of aluminium concentrations in the solution is able to promote the slag reaction.

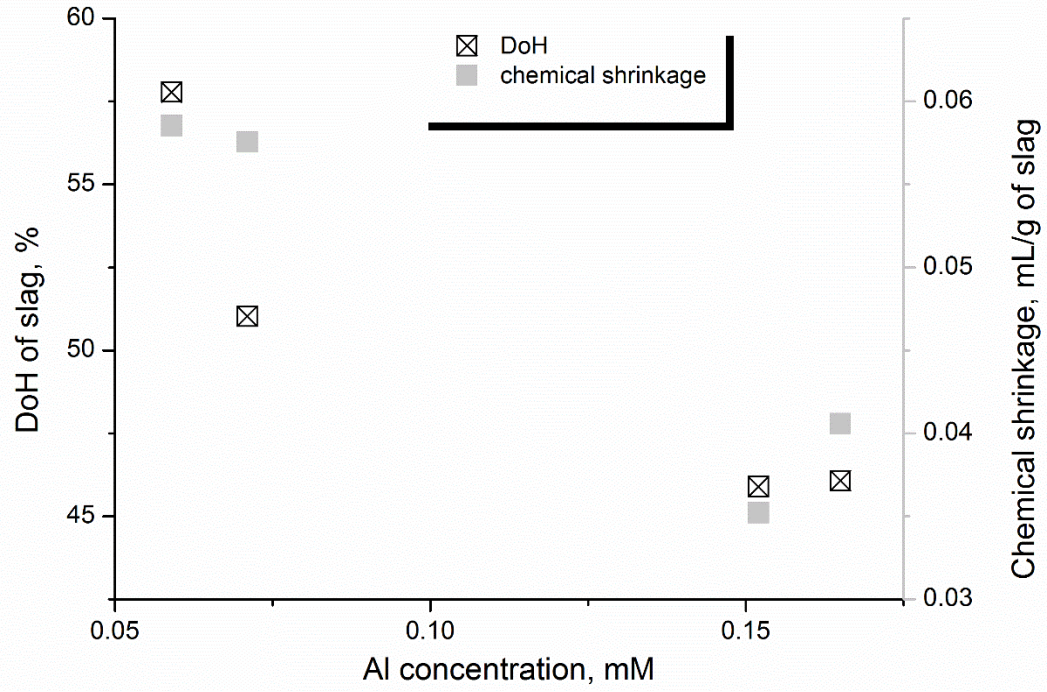

Figure 7-2 The relationship between Al concentration in the pore solution and chemical shrinkage and degree of hydration of slag.

Note, there is 2% error associated with the method for measuring the DoH of slag.

7.5 Relationship between hydration, microstructure and compressive strength

The composite cements were weaker at early age but the compressive strengths were similar at longer hydration times. The finer clinker and slag blends offset the

early strength deficit. The strength increased with hydration time and hence depended on the microstructure of the cements.

The preceding sections have discussed differences in the hydration kinetics and the ensuing microstructures for the cements investigated. The C-S-H, ettringite and portlandite contents were higher in the neat cement and consequently the bound water content and lower porosity. These explain the higher compressive strength in the neat cement compared to the composite cements at an early age.

There was more ettringite in the limestone ternary blends after 2 days while the contents decreased in the neat cement and binary slag blend. At the same time, lower portlandite content but more carboaluminates were seen in the limestone ternary blends. Notwithstanding, compressive strengths were still lower than the neat cements until after 28 days. Consequently, the distribution of hydrates is as important as their nature for compressive strength development [424]. The discussion on pore structure in the investigated cements (section 7.3.2) already highlighted differences in the contribution of the slag and limestone to the pore structure. The ternary plot of strength versus overall degree of hydration and porosity (Figure 5-25) indicated an asymptote for strength at longer hydration times. Porosity versus strength was consistently linear. Meanwhile continuous refinement of pores < 100nm was more prevalent in the slag blends as revealed by MIP. It can, therefore, be concluded that the rate of strength gain following densification of the C-S-H was much lower compared to capillary pore filling (SEM).

7.6 Relationship between hydration, microstructure and freeze-thaw resistance in deionized water

7.6.1 Microstructure on freeze-thaw

Freeze-thaw testing was performed on concrete samples but the detailed microstructural characterization was conducted on cement pastes conditioned similarly to the concrete samples. Interestingly, the changes noted in the pastes were also similar for the corresponding concrete samples too except being less destructive in the cements. The investigation focused on freeze-thaw in the presence of deionized water only. This was imposed by the objective of identifying microstructural-related factors which affected freeze-thaw resistance. No air entrainers were used in the concretes. However, the concrete mix design allowed for 2.5 % entrapped air volume.

At the 0.5 w/c ratio investigated, the freeze-thaw resistance of the ternary blends was much lower. The 80 % relative dynamic modulus failure criterion was attained sooner in the limestone ternary blends compared to the binary and control CEM I 42.5 R mix. The onset of internal structural damage was shorted at higher limestone content. The slag fineness, however, had minimal influence on both scaling and internal structural damage resistance. However, the clinker fineness was more influential. The resistance to internal structural damage was significantly improved but the scaling resistance was worst. In all cases, internal structural damage preceded scaling but the CEM I 42.5 R blend deviated.

The microstructures of the paste phase in the composite cements were similar but differed from the neat cement at the start of the 21 days conditioning at 65 % RH

and 20 °C[340]. Some degree of carbonation occurred during this period but the calcium carbonate formed were similar among all investigated cements including the control mix. However, at the end of the 7 days capillary suction which followed the conditioning, almost all portlandite was lost from the composite cements. Leaching experiments confirmed leaching of calcium and sulphates during the saturation. Loss of portlandite was also confirmed by TGA and XRD.

Analysis of the leachates indicated continuous leaching of calcium during freeze-thaw despite depletion of portlandite after the conditioning. SEM also indicated changes in the C-S-H morphology but minimal modifications to the C-S-H Ca/Si ratio. In fact comparison between the Ca/Si ratios after conditioning and 25 freeze-thaw cycles show a slight increase in the reference mix. Conversely, a slight reduction was noted in the ternary blends. The mechanical properties of the C-S-H, assessed through micro-indentation found a slight increase in the Young's modulus of the contol mix during freeze-thaw which is consistent with the increased C-S-H Ca/Si ratio. There was no change in the elastic modulus of the composite cements during freeze-thaw except ~ 8 % loss in the 20 % limestone blend. Additionally, the C-S-H modulus at 20 % limestone content was lower than the neat cement and the binary slag mix.

Comparison between degraded and non-degraded portions of the same cements found the loss of portlandite as the must dominant microstructural change plus as well changes in the C-S-H morphology. Therefore, the lower freeze-thaw resistance in the ternary blends can be ascribed to decalcification. Decalcification of the C-S-H by leaching has been reported elsewhere [230, 421]. The micro-indentation results indicate that decalcification of portlandite had a far reaching

implication on mechanical properties of the C-S-H than decalcification of the C-S-H due to the large volume of the latter [415].

7.6.2 The mechanism of freeze-thaw

Many authors have hypothesised the freeze-thaw mechanism as discussed in section 2.6. The results from this study support a chemo-mechanical mechanism (see Figure 6-15) similar to the glue-spall theory [35, 280]. The compositionally related mechanism arises from carbonation and leaching of calcium during conditioning and pre or during freeze-thaw capillary suction. The affected zone is weakened and possess cracks which facilitate further leaching and water ingress. Consequently, least resistance is offered against the induced pressure from ice growth which then exposes the next layer.

7.7 Conclusions

The key findings from this study are summarised below:

1. The PONKCS method was successfully implemented as part of the Rietveld refinement protocol to monitor the progress of slag hydration in limestone ternary blended cements. The precision of measurement on synthetic mixes was 2 % but decreased in hydrated composite cements. Across different hydration stopping methods, 5 % precision was found. The accuracy, when compared to BSEM/IA, was 6%.
2. Limestone influenced the hydration of all major clinker phase assemblages. Of much significance is the impact on the hydration of belite. While significantly retarded in the presence of slag, belite hydration in the limestone ternary blends was comparable to the neat cement. The

nucleation effect accounted for the acceleration of alite hydration whereas dilution and pore solution effects led to the enhanced belite hydration.

3. Limestone in the ternary blends also accelerated slag hydration. The improvement in slag reactivity was smaller upon increasing the limestone content from 10 to 20 %. Therefore, an optimum calcite/slag ratio exists for maximising the synergy.
4. The reactivity of calcite was limited in all ternary blends. However, more calcite reacted at higher replacement levels but the overall degree of hydration was independent of the original content. The mix composition and the physical properties of constituents modified the kinetics of calcite dissolution but not the ultimate calcite consumed.
5. Alumina in the pore solution was preferentially incorporated into other hydrates in the order of ettringite, carboaluminates, C-S-H and hydrotalcite. This, however, depended on the other hydrates and the dissolved species in the pore solution.
6. Ettringite formed while there were sulphates in solution. On sulphate depletion, carboaluminates precipitated and thus curtailed the conversion of ettringite to monosulphate. Carboaluminates precipitated in the ternary blends but increasing the limestone content led to a shift in the hemi/monocarbonaluminate balance, towards more mono.
7. The additionally formed carboaluminates lowered the Al concentration in the pore solution and consequently the Al/Si ratio in C-S-H. The Mg/Al ratio in the hydrotalcite-like phase in the hydrated slag rim was also higher in the ternary blends than the binary slag mix. However, Mg in slag does not incorporate into the C-S-H [195, 207, 211]. Therefore, Higher Mg/Al ratio

can be ascribed to lower Al concentration in hydrotalcite due to uptake into carboaluminates.

8. The presence of limestone led to lower pore volume at an early age. The hydration of slag also refined the pore distribution but the volume of pores finer than ~ 4 nm was higher in the composite cements.
9. Pore solution effects and space availability were identified as the controlling mechanisms behind the synergy in limestone ternary blends. These effects complemented each other. Dilution/water availability, however, seems to play a lesser role.
10. Concrete samples prepared from ternary slag-limestone composite cements at 0.5 w/c ratios without any entraining agents were less resistant to cyclic freeze-thaw in the presence of deionized water. Decalcification during sample conditioning, saturation and freeze-thaw were identified to be an important microstructural effect. The composite cements, with already lower portlandite contents, were again found to be more susceptible to carbonation and, more importantly, also susceptible to leaching. After the prescribed 7 days suction during standard freeze-thaw tests, the samples showed no significant residual portlandite. Therefore, the C-S-H present within the test surface was already weakened before the test commenced.
11. A chemo-mechanical mode of failure was identified from the freeze-thaw test. This was similar to the recently advanced glue-spall mechanism. Successive layers were removed upon decalcification.

7.8 Recommendations for further studies

1. The accuracy of the PONKCS method in the analysis of hydrated composite cements can be improved further. This is only possible by extensive calibration of the model against other amorphous materials particularly the C-S-H. Since the structure of the C-S-H changes with hydration time, it is imperative to check the model against a range of C-S-H compositions. The composite cements studied were also observed to incorporate alumina into the C-S-H. A model of the C-A-S-H phase is therefore required other than assuming a 14 Å tobermorite C-S-H structure.
2. The synergy between limestone and slag was considered at a fixed sulphate content. The pore solution effects depended on alumina uptake. However, calcite dissolution is slow compared to sulphates. It is imperative to ascertain the impact of sulphate on the synergy.
3. Decalcification was identified as a microstructural response to freeze-thaw. Extensive curing would improve the microstructure through refined pore system and more additional C-S-H. Leaching of calcium from the C-S-H does not have the same effect as from portlandite. Consequently, prolonged curing of composite cements may improve the freeze-thaw resistance in the deionized water. It was not possible from the current scope of works to validate the effect of restrained leaching of calcium in full-scale concrete tests. Validation through freeze-thaw testing of non-carbonated and unleached specimens would be useful for clarifying the underlying mechanisms.

4. Development of cements which depend less on portlandite assemblages for mechanical properties may also present an alternative to improving the freeze-thaw resistance of limestone ternary blends.

List of References

[1] J.S. Damtoft, J. Lukasik, D. Herfort, D. Sorrentino, E.M. Gartner, Sustainable development and climate change initiatives, Cement and Concrete Research, 38 (2008) 115-127.
[2] ECOBA, European Coal Ash Unitlisation, in, 2016.
[3] J.A. Ober, Mineral commodity summaries 2016, in, US Geological Survey, 2016.
[4] V. Bonavetti, H. Donza, V. Rahhal, E. Irassar, Influence of initial curing on the properties of concrete containing limestone blended cement, Cement and Concrete Research, 30 (2000) 703-708.
[5] R. Hooton, M. Nokken, M. Thomas, Portland-limestone cement: state-of-the-art report and gap analysis for CSA A 3000, Cement Association of Canada University of Toronto, (2007).
[6] P.D. Tennis, M.D.A. Thomas, W.J. Weiss, State-of-the-Art Report on Use of Limestone in Cements at Levels of up to 15%, in, Portland Cement Association, Skokie, Illinois, 2011, pp. 78.
[7] K. De Weerdt, M. Ben Haha, G. Le Saout, K.O. Kjellsen, H. Justnes, B. Lothenbach, Hydration mechanisms of ternary Portland cements containing limestone powder and fly ash, Cement and Concrete Research, 41 (2011) 279-291.
[8] G. Menéndez, V. Bonavetti, E.F. Irassar, Strength development of ternary blended cement with limestone filler and blast-furnace slag, Cement and Concrete Composites, 25 (2003) 61-67.
[9] M. Moesgaard, S.L. Poulsen, D. Herfort, M. Steenberg, L.K. Kirkegaard, J. Skibsted, Y. Yue, Hydration of Blended Portland Cements Containing Calcium-Aluminosilicate Glass Powder and Limestone, Journal of the American Ceramic Society, 95 (2012) 403–409.
[10] B. Lothenbach, K. Scrivener, R.D. Hooton, Supplementary cementitious materials, Cement and Concrete Research, 41 (2011) 1244-1256.
[11] X. Wu, W. Jiang, D.M. Roy, Early activation and properties of slag cement, Cement and Concrete Research, 20 (1990) 961-974.
[12] J.I. Escalante, L.Y. Gómez, K.K. Johal, G. Mendoza, H. Mancha, J. Méndez, Reactivity of blast-furnace slag in Portland cement blends hydrated under different conditions, Cement and Concrete Research, 31 (2001) 1403-1409.
[13] J. Cailetti, A.M. Soliman, M.L. Nehdi, Effects of nano- and micro-limestone addition on early-age properties of ultra-high-performance concrete, Materials and Structures, 46 (2013) 881-898.
[14] S. Hoshino, K. Yamada, H. Hirao, XRD/Rietveld analysis of the hydration and strength development of slag and limestone blened cement, Advanced Concrete Technology, 4 (2006) 357-367.
[15] S. Ogawa, T. Nozaki, K. Yamada, H. Hirao, R.D. Hooton, Improvement on sulfate resistance of blended cement with high alumina slag, Cement and Concrete Research, 42 (2012) 244-251.
[16] S. Tsivilis, E. Chaniotakis, E. Badogiannis, G. Pahoulas, A. Ilias, A study on the parameters affecting the properties of Portland limestone cements, Cement and Concrete Composites, 21 (1999) 107-116.

[17] B. Lothenbach, G. Le Saout, E. Gallucci, K. Scrivener, Influence of limestone on the hydration of Portland cements, Cement and Concrete Research, 38 (2008) 848-860.
[18] M. Moesgaard, D. Herfort, M. Steenberg, L.F. Kirkegaard, Y. Yue, Physical performances of blended cements containing calcium aluminosilicate glass powder and limestone, Cement and Concrete Research, 41 (2011) 359-364.
[19] A.M. Ramezanianpour, R.D. Hooton, Sulfate resistance of Portland-limestone cements in combination with supplementary cementitious materials, Materials and Structures, 46 (2012) 1061-1073
[20] T. Schmidt, B. Lothenbach, M. Romer, J. Neuenschwander, K. Scrivener, Physical and microstructural aspects of sulfate attack on ordinary and limestone blended Portland cements, Cement and Concrete Research, 39 (2009) 1111-1121.
[21] K.u. Githachuri, M.G. Alexander, Durability performance potential and strength of blended Portland limestone cement concrete, Cement and Concrete Composites, 39 (2013) 115-121.
[22] B. Persson, Internal frost resistance and salt frost scaling of self-compacting concrete, Cement and Concrete Research, 33 (2003) 373-379.
[23] S. Grzeszczyk, P. Podkowa, The Effect of Limestone Filler on the Properties of Self Compacting Concrete, ANNUAL TRANSACTIONS OF THE NORDIC RHEOLOGY SOCIETY, , VOL. 17 (2009).
[24] R.K. Dhir, M.C. Limbachiya, M.J. Macarthy, A. Chaipanich, Evaluation of Portland limestone cements for use in concrete construction, Materials and Structures, 40 (2007) 459 - 473.
[25] J. Stark, H.M. Ludwig, Freeze-deicing salt resistance of concretes containing cement rich in slag, in: M.J. Setzer, R. Auberg (Eds.) Frost Resistance of Concrete Proceedings of the International RILEM Workshop, E & FN SPON, University of Essen, 1997, pp. 123-138.
[26] B. Espion, B. Lebon, O. Germain, A. Hellebois, Characterisation of new ternary cements with reduced clinker content in: K. Sakai (Ed.) Proceedings of the First International Conference on Concrete Sustainability, Tokyo, Japan, 2013, pp. 145 - 152.
[27] M. Collepardi, S. Collepardi, J.J. Ogoumah Olagot, E. Simonelli, The Influence of Slag and Fly Ash on the Carbonation, in: V.M. Malhotra (Ed.) Eighth CANMET/ACI International Conference on Fly Ash, Silica Fume, Slag, and Natural Pozzolans in Concrete 2004.
[28] M. Ben Haha, K. De Weerdt, B. Lothenbach, Quantification of the degree of reaction of fly ash, Cement and Concrete Research, 40 (2010) 1620-1629.
[29] V. Kocaba, E. Gallucci, K.L. Scrivener, Methods for determination of degree of reaction of slag in blended cement pastes, Cement and Concrete Research, 42 (2012) 511-525.
[30] K. Luke, F.P. Glasser, Selective dissolution of hydrated blast furnace slag cements, Cement and Concrete Research, 17 (1987) 273-282.
[31] M. Whittaker, M. Zajac, M. Ben Haha, F. Bullergahn, L. Black, The role of the alumina content of slag, plus the presence of additional sulfate on the hydration and microstructure of Portland cement-slag blends, Cement and Concrete Research, 66 (2014) 91-101.
[32] N.V.Y. Scarlett, I.C. Madsen, Quantification of phases with partial or no known crystal structures, Powder Diffraction, 21 (2006) 278-284.

[33] R. Snellings, A. Salze, K.L. Scrivener, Use of X-ray diffraction to quantify amorphous supplementary cementitious materials in anhydrous and hydrated blended cements, Cement and Concrete Research, 64 (2014) 89-98.
[34] J. Marchand, Y. Maltais, Y. Machabee, C. TAlbot, M. Pigeon, Effects of fly ash on microstructure and deicer salt scaling resistance of concrete, in: M.J. Setzer, R. Auberg (Eds.) Frost Resistance of Concrete Proceedings of the International RILEM Workshop, University of Essen, 1997, pp. 11 - 20.
[35] J.J. Valenza Ii, G.W. Scherer, A review of salt scaling: II. Mechanisms, Cement and Concrete Research, 37 (2007) 1022-1034.
[36] J.J. Valenza, G.W. Scherer, A review of salt scaling: I. Phenomenology, Cement and Concrete Research, 37 (2007) 1007-1021.
[37] T.C. Powers, A Working Hypothesis for Further Studies of Frost Resistance of Concrete, ACI Journal Proceedings, 41 (1945) 245-272.
[38] T.C. Powers, R.A. Helmuth, Theory of volume changes in hardened Portland cement paste during freezing, Highway Research Board, 32 (1953).
[39] G.W. Scherer, Crystallization in pores, Cement and Concrete Research, 29 (1999) 1347-1358.
[40] G.W. Scherer, J. Valenza, Mechanisms of frost damage, Materials science of concrete, 7 (2005) 209-246.
[41] P.-w. Gao, S.-x. Wu, P.-h. Lin, Z.-r. Wu, M.-s. Tang, The characteristics of air void and frost resistance of RCC with fly ash and expansive agent, Construction and Building Materials, 20 (2006) 586-590.
[42] G.-F. Peng, Q. Ma, H.-M. Hu, R. Gao, Q.-F. Yao, Y.-F. Liu, The effects of air entrainment and pozzolans on frost resistance of 50–60 MPa grade concrete, Construction and Building Materials, 21 (2007) 1034-1039.
[43] K. Fridh, Internal frost damage in concrete - experimental studies of destruction mechanisms, in: Division of Building Materials, University of Lund, 2005.
[44] J. Deja, Freezing and de-icing salt resistance of blast furnace slag concretes, Cement and Concrete Composites, 25 (2003) 357-361.
[45] D.J. Janssen, M.B. Snyder, Resistance of concrete to freezing and thawing, 1994.
[46] K.L. Scrivener, Backscattered electron imaging of cementitious microstructures: understanding and quantification, Cement and Concrete Composites, 26 (2004) 935-945.
[47] R.J. Detwiler, B.J. Dalgleish, R.B. Williamson, Assessing the durability of concrete in freezing and thawing, ACI Materials Journal, 86 (1989) 29-35.
[48] M. Tang, Y. Tian, X.B. Mu, M. Jiang, The Pore Fractal Characteristics of Concrete Materials under Salt Freezing Conditions in Cold Area, Advanced Materials Research, 233 - 235 (2011) 2522 - 2527.
[49] N.V. Scarlett, I.C. Madsen, Current state of quantitative phase analysis, in: Accuracy in Powder Diffraction, APD-IV, 2013.
[50] E. Gartner, Industrially interesting approaches to “low-CO2” cements, Cement and Concrete Research, 34 (2004) 1489-1498.
[51] E. Berodier, K. Scrivener, Understanding the filler effect on the nucleation and growth of C-S-H, Journal of the American Ceramic Society, 97 (2014) 3764-3773.
[52] F. Deschner, F. Winnefeld, B. Lothenbach, S. Seufert, P. Schwesig, S. Dittrich, F. Goetz-Neunhoeffer, J. Neubauer, Hydration of Portland cement with

high replacement by siliceous fly ash, Cement and Concrete Research, 42 (2012) 1389-1400.
[53] K.L. Scrivener, P. Juilland, P.J.M. Monteiro, Advances in understanding hydration of Portland cement, Cement and Concrete Research, 78, Part A (2015) 38-56.
[54] E. Berodier, K. Scrivener, Evolution of pore structure in blended systems, Cement and Concrete Research, 73 (2015) 25-35.
[55] B. Lothenbach, G. Le Saout, M. Ben Haha, R. Figi, E. Wieland, Hydration of a low-alkali CEM III/B–SiO2 cement (LAC), Cement and Concrete Research, 42 (2012) 410-423.
[56] CEMBUREAU, Environmental benefits of using alternative fuels in cement production: A life-cycle approach, in, The European Cement Association, 2010.
[57] G. Habert, C. Billard, P. Rossi, C. Chen, N. Roussel, Cement production technology improvement compared to factor 4 objectives, Cement and Concrete Research, 40 (2010) 820-826.
[58] G.P. Hammond, C.I. Jones, Embodied energy and carbon in construction materials, Proc Institution of Civil Engineers: Energy, (2008).
[59] Ernst Worrell, Lynn Price, Nathan Martin, Chris Hendriks, L.O. Meida, Carbon dioxide emissions from the global cement industry, Annual Review of Energy and the Environment, 26 (2001) 303-329.
[60] P. Mehta, H. Meryman, Tools for Reducing Carbon Emissions Due to Cement Consumption, Structure Magazine, (2009) 11-15.
[61] P. Purnell, L. Black, Embodied carbon dioxide in concrete: Variation with common mix design parameters, Cement and Concrete Research, 42 (2012) 874-877.
[62] J.H. Sharp, E.M. Gartner, D.E. Macphee, Novel cement systems (sustainability). Session 2 of the Fred Glasser Cement Science Symposium, Advances in Cement Research, 22 (2010) 195-202.
[63] A. Palomo, M.W. Grutzeck, M.T. Blanco, Alkali-activated fly ashes: A cement for the future, Cement and Concrete Research, 29 (1999) 1323-1329.
[64] F. Winnefeld, B. Lothenbach, Hydration of calcium sulfoaluminate cements — Experimental findings and thermodynamic modelling, Cement and Concrete Research, 40 (2010) 1239-1247.
[65] Y. Li, B. Chen, Factors that affect the properties of magnesium phosphate cement, Construction and Building Materials, 47 (2013) 977-983.
[66] J.W. Phair, Green chemistry for sustainable cement production and use, Green Chemistry, 8 (2006) 763-780.
[67] K. Scrivener, B. Lothenbach, N. De Belie, E. Gruyaert, J. Skibsted, R. Snellings, A. Vollpracht, TC 238-SCM: hydration and microstructure of concrete with SCMs, Materials and Structures, 48 (2015) 835-862.
[68] E. Badogiannis, S. Tsivilis, Exploitation of poor Greek kaolins: Durability of metakaolin concrete, Cement and Concrete Composites, 31 (2009) 128-133.
[69] T.W. Cheng, J.P. Chiu, Fire-resistant geopolymer produced by granulated blast furnace slag, Minerals Engineering, 16 (2003) 205-210.
[70] K.L. Scrivener, J.-L. Cabiron, R. Letourneux, High-performance concretes from calcium aluminate cements, Cement and Concrete Research, 29 (1999) 1215-1223.
[71] J. Bensted, Calcium aluminate cements, in: J.Bensted, P.Barnes (Eds.) Structure and Performance of Cements, SPON Press, 2002, pp. 114-138.

[72] K. Scrivener, Calcium aluminate cements, in: J. Newman, B.S. Choo (Eds.) Advanced Concrete Technology 1: Constituent Materials, Butterworth-Heinemann, 2003, pp. 2/1-2/29.
[73] F.P. Glasser, L. Zhang, High-performance cement matrices based on calcium sulfoaluminate–belite compositions, Cement and Concrete Research, 31 (2001) 1881-1886.
[74] K. Quillin, Performance of belite–sulfoaluminate cements, Cement and Concrete Research, 31 (2001) 1341-1349.
[75] J.L. Provis, Geopolymers and other alkali activated materials: why, how, and what?, Materials and Structures, 47 (2014) 11-25.
[76] S.A. Bernal, J.L. Provis, R.J. Myers, R. San Nicolas, J.S. van Deventer, Role of carbonates in the chemical evolution of sodium carbonate-activated slag binders, Materials and Structures, 48 (2015) 517-529.
[77] P. Duxson, A. Fernández-Jiménez, J.L. Provis, G.C. Lukey, A. Palomo, J.S.J. van Deventer, Geopolymer technology: the current state of the art, Journal of Materials Science, 42 (2007) 2917-2933.
[78] A. Fernández-Jiménez, A. Palomo, Composition and microstructure of alkali activated fly ash binder: Effect of the activator, Cement and Concrete Research, 35 (2005) 1984-1992.
[79] A. Fernández-Jiménez, A. Palomo, M. Criado, Microstructure development of alkali-activated fly ash cement: a descriptive model, Cement and Concrete Research, 35 (2005) 1204-1209.
[80] B.C. McLellan, R.P. Williams, J. Lay, A. Van Riessen, G.D. Corder, Costs and carbon emissions for geopolymer pastes in comparison to ordinary Portland cement, Journal of Cleaner Production, 19 (2011) 1080-1090.
[81] D.N. Huntzinger, T.D. Eatmon, A life-cycle assessment of Portland cement manufacturing: comparing the traditional process with alternative technologies, Journal of Cleaner Production, 17 (2009) 668-675.
[82] H.F.W. Taylor, Nanostructure of C□S□H: Current status, Advanced Cement Based Materials, 1 (1993) 38-46.
[83] H.F.W. Taylor, Cement Chemistry, 2nd ed., Thomas Telford, 1997.
[84] N.L. Thomas, D.D. Double, The hydration of Portland cement, C3S and C2S in the presence of a calcium complexing admixture (EDTA), Cement and Concrete Research, 13 (1983) 391-400.
[85] P. Barret, D. Ménétrier, Filter dissolution of C3S as a function of the lime concentration in a limited amount of lime water, Cement and Concrete Research, 10 (1980) 521-534.
[86] J.W. Bullard, H.M. Jennings, R.A. Livingston, A. Nonat, G.W. Scherer, J.S. Schweitzer, K.L. Scrivener, J.J. Thomas, Mechanisms of cement hydration, Cement and Concrete Research, 41 (2011) 1208-1223.
[87] H.F.W. Taylor, P. Barret, P.W. Brown, D.D. Double, G. Frohnsdorff, V. Johansen, D. Ménétrier-Sorrentino, I. Odler, L.J. Parrott, J.M. Pommersheim, M. Regourd, J.F. Young, The hydration of tricalcium silicate, Matériaux et Construction 17 (1984) 457-468
[88] S. Mindess, J.F. Young, D. Darwin, Concrete, Prentice Hall PTR, 2003.
[89] D. Stephan, S. Wistuba, Crystal structure refinement and hydration behaviour of 3CaO·SiO2 solid solutions with MgO, Al2O3 and Fe2O3, Journal of the European Ceramic Society, 26 (2006) 141-148.

[90] M. Bigare, A. Guinier, C. Mazieres, M. Regourd, N. YannaquisS, W. Eysbl, T. HahnA, E. Woermann, Polymorphism of Tricalcium Silicate and Its Solid Solutions, Journal of the American Ceramic Society, 50 (1967) 609-619.
[91] S. Ma, W. Zhou, S. Wang, W. Li, X. Shen, Polymorph transformation kinetics of Ca3SiO5 with MgO, Phase Transitions, 88 (2015) 888-896.
[92] M.-N. de Noirfontaine, M. Courtial, F. Dunstetter, G. Gasecki, M. Signes-Frehel, Tricalcium silicate Ca3SiO5 superstructure analysis: a route towards the structure of the M1 polymorph, in: Zeitschrift für Kristallographie Crystalline Materials, 2012, pp. 102.
[93] F. Dunstetter, M.N. de Noirfontaine, M. Courtial, Polymorphism of tricalcium silicate, the major compound of Portland cement clinker: 1. Structural data: review and unified analysis, Cement and Concrete Research, 36 (2006) 39-53.
[94] I. Odler, Hydration, Setting and Hardening of Portland Cement in: Lea's Chemistry of Cement&Concrete, Butterworth Heinemann, Oxford, 2001, pp. 241.
[95] S. Abdul-Maula, I. Odler, Structure and properties of tricalcium silicate doped with MgO, Al 2 O 3 and Fe 2 O 3, in: Proc Br Ceram Soc, 1984, pp. 83.
[96] D. Stephan, S.N. Dikoundou, G. Raudaschl-Sieber, Hydration characteristics and hydration products of tricalcium silicate doped with a combination of MgO, Al2O3 and Fe2O3, Thermochimica Acta, 472 (2008) 64-73.
[97] G.L. Valenti, V. Sabatelli, B. Marchese, Hydration kinetics of tricalcium silicate solid solutions at early ages, Cement and Concrete Research, 8 (1978) 61-72.
[98] I.a. Odler, S. Abdul-Maula, Polymorphism and Hydration of Tricalcium Silicate Doped With ZnO, Journal of the American Ceramic Society, 66 (1983) 1-4.
[99] H.R. Stewart, J.E. Bailey, Microstructural studies of the hydration products of three tricalcium silicate polymorphs, Journal of Materials Science, 18 (1983) 3686-3694.
[100] A. Bazzoni, S. Ma, Q. Wang, X. Shen, M. Cantoni, K.L. Scrivener, The Effect of Magnesium and Zinc Ions on the Hydration Kinetics of C3S, Journal of the American Ceramic Society, 97 (2014) 3684-3693.
[101] T. Staněk, P. Sulovský, The influence of the alite polymorphism on the strength of the Portland cement, Cement and Concrete Research, 32 (2002) 1169-1175.
[102] L. Fernandez, C. Alonso, A. Hidalgo, C. Andrade, The role of magnesium during the hydration of C3S and CSH formation. Scanning electron microscopy and mid-infrared studies, Advances in cement research, 17 (2005) 9-21.
[103] I.G. Richardson, G.W. Groves, Microstructure and microanalysis of hardened ordinary Portland cement pastes, Journal of Materials Science, 28 (1993) 265-277.
[104] I.G. Richardson, A.R. Brough, R. Brydson, G.W. Groves, C.M. Dobson, Location of Aluminum in Substituted Calcium Silicate Hydrate (C-S-H) Gels as Determined by 29Si and 27Al NMR and EELS, Journal of the American Ceramic Society, 76 (1993) 2285 - 2286.
[105] C. Tashiro, S. Tatibana, Bond strength between C3S paste and iron, copper or zinc wire and microstructure of interface, Cement and Concrete Research, 13 (1983) 377-382.

[106] D. Jansen, S.T. Bergold, F. Goetz-Neunhoeffer, J. Neubauer, The hydration of alite: a time-resolved quantitative X-ray diffraction approach using the G-factor method compared with heat release, J Appl Cryst, 44 (2011) 895-901.
[107] D. Jansen, F. Goetz-Neunhoeffer, B. Lothenbach, J. Neubauer, The early hydration of Ordinary Portland Cement (OPC): An approach comparing measured heat flow with calculated heat flow from QXRD, Cement and Concrete Research, 42 (2012) 134-138.
[108] J.B. Ings, P.W. Brown, G. Frohnsdorff, Early hydration of large single crystals of tricalcium silicate, Cement and Concrete Research, 13 (1983) 843-848.
[109] J.J. Thomas, H.M. Jennings, J.J. Chen, Influence of Nucleation Seeding on the Hydration Mechanisms of Tricalcium Silicate and Cement, The Journal of Physical Chemistry, 113 (2009) 4327-4334.
[110] A. Comotti, G. Castaldi, C. Gilioli, G. Torri, P. Sozzani, Step-by-step observation of the hydration of C3S by magic-angle spinning 29Si nuclear magnetic resonance: the masking effect of D2O, Journal of Materials Science, 29 (1994) 6427-6433.
[111] J.J. Thomas, S.A. FitzGerald, D.A. Neumann, R.A. Livingston, State of Water in Hydrating Tricalcium Silicate and Portland Cement Pastes as Measured by Quasi-Elastic Neutron Scattering, Journal of the American Ceramic Society, 84 (2001) 1811-1816.
[112] E. Pustovgar, R.P. Sangodkar, A.S. Andreev, M. Palacios, B.F. Chmelka, R.J. Flatt, J.-B. d/'Espinose de Lacaillerie, Understanding silicate hydration from quantitative analyses of hydrating tricalcium silicates, Nat Commun, 7 (2016).
[113] E.M. Gartner, Hydration mechanisms I, American Ceramic Society, 1 (1989) 95-125.
[114] P. Juilland, E. Gallucci, R. Flatt, K. Scrivener, Dissolution theory applied to the induction period in alite hydration, Cement and Concrete Research, 40 (2010) 831-844.
[115] A. Nonat, The structure and stoichiometry of C-S-H, Cement and Concrete Research, 34 (2004) 1521-1528.
[116] E.M. Gartner, H.M. Jennings, Thermodynamics of calcium silicate hydrates and their solutions, J Am Ceram Soc 80 (1987) 743–749.
[117] H.N. Stein, J.M. Stevels, Influence of silica on the hydration of 3 CaO,SiO2, Journal of Applied Chemistry, 14 (1964) 338-346.
[118] H.M. Jennings, P.L. Pratt, An experimental argument for the existence of a protective membrane surrounding portland cement during the induction period, Cement and Concrete Research, 9 (1979) 501-506.
[119] S. Garrault, T. Behr, A. Nonat, Formation of the C−S−H Layer during Early Hydration of Tricalcium Silicate Grains with Different Sizes, The Journal of Physical Chemistry B, 110 (2006) 270-275.
[120] S. Garrault, E. Finot, E. Lesniewska, A. Nonat, Study of C-S-H growth on C3S surface during its early hydration, Materials and Structures, 38 (2005) 435-442.
[121] F. Tzschichholz, H. Zanni, Global hydration kinetics of tricalcium silicate cement, Physical Review E, 64 (2001) 016115.
[122] A. Kumar, S. Bishnoi, K.L. Scrivener, Modelling early age hydration kinetics of alite, Cement and Concrete Research, 42 (2012) 903-918.

[123] A.K. Chatterjee, High belite cements—Present status and future technological options: Part I, Cement and Concrete Research, 26 (1996) 1213-1225.
[124] J.G. Jang, H.K. Lee, Microstructural densification and CO2 uptake promoted by the carbonation curing of belite-rich Portland cement, Cement and Concrete Research, 82 (2016) 50-57.
[125] T. Link, F. Bellmann, H.M. Ludwig, M. Ben Haha, Reactivity and phase composition of Ca2SiO4 binders made by annealing of alpha-dicalcium silicate hydrate, Cement and Concrete Research, 67 (2015) 131-137.
[126] S.N. Ghosh, P.B. Rao, A.K. Paul, K. Raina, The chemistry of dicalcium silicate mineral, Journal of Materials Science, 14 (1979) 1554-1566.
[127] Y.J. Kim, I. Nettleship, W.M. Kriven, Phase Transformations in Dicalcium Silicate: II, TEM Studies of Crystallography, Microstructure, and Mechanisms, Journal of the American Ceramic Society, 75 (1992) 2407-2419.
[128] H.-M. Ludwig, W. Zhang, Research review of cement clinker chemistry, Cement and Concrete Research, 78, Part A (2015) 24-37.
[129] H. Ishida, S. Yamazaki, K. Sasaki, Y. Okada, T. Mitsuda, α-Dicalcium Silicate Hydrate: Preparation, Decomposed Phase, and Its Hydration, Journal of the American Ceramic Society, 76 (1993) 1707-1712.
[130] K. Fukuda, N. Wakamatsu, S. Ito, Improvement in Hydration Reactivity of α-Phase Belite by Remelting Reaction, Journal of the American Ceramic Society, 84 (2001) 639-641.
[131] K. Morsli, Á.G. De La Torre, S. Stöber, A.J.M. Cuberos, M. Zahir, M.A.G. Aranda, Quantitative Phase Analysis of Laboratory-Active Belite Clinkers by Synchrotron Powder Diffraction, Journal of the American Ceramic Society, 90 (2007) 3205-3212.
[132] X. Li, W. Xu, S. Wang, M. Tang, X. Shen, Effect of SO3 and MgO on Portland cement clinker: Formation of clinker phases and alite polymorphism, Construction and Building Materials, 58 (2014) 182-192.
[133] K. Fukuda, I. Maki, K. Toyoda, S. Ito, Kinetics of the α-to-α′H Polymorphic Phase Transition of Ca2SiO4 Solid Solutions, Journal of the American Ceramic Society, 76 (1993) 1821-1824.
[134] I. Jelenić, A. Bezjak, M. Bujan, Hydration of B2O3-stabilized α′-and β-modifications of dicalcium silicate, Cement and Concrete Research, 8 (1978) 173-180.
[135] Y.-M. Kim, S.-H. Hong, Influence of Minor Ions on the Stability and Hydration Rates of β-Dicalcium Silicate, Journal of the American Ceramic Society, 87 (2004) 900-905.
[136] R. Trettin, G. Oliew, C. Stadelmann, W. Wieker, Very early hydration of dicalcium silicate-polymorphs, Cement and Concrete Research, 21 (1991) 757-764.
[137] K. Fukuda, H. Taguchi, Hydration of α′L- and β-dicalcium silicates with identical concentration of phosphorus oxide, Cement and Concrete Research, 29 (1999) 503-506.
[138] A.J.M. Cuberos, Á.G. De la Torre, M.C. Martín-Sedeño, L. Moreno-Real, M. Merlini, L.M. Ordónez, M.A.G. Aranda, Phase development in conventional and active belite cement pastes by Rietveld analysis and chemical constraints, Cement and Concrete Research, 39 (2009) 833-842.

[139] L. Nicoleau, A. Nonat, D. Perrey, The di- and tricalcium silicate dissolutions, Cement and Concrete Research, 47 (2013) 14-30.
[140] D. Damidot, F. Bellmann, B. Möser, T. Sovoidnich, Calculation of the dissolution rate of tricalcium silicate in several electrolyte compositions, Cement Wapno Beton, 12/74 (2007) 57-67.
[141] P. Suraneni, M. Palacios, R.J. Flatt, New insights into the hydration of slag in alkaline media using a micro-reactor approach, Cement and Concrete Research, 79 (2016) 209-216.
[142] F. Bellmann, D. Damidot, B. Möser, J. Skibsted, Improved evidence for the existence of an intermediate phase during hydration of tricalcium silicate, Cement and Concrete Research, 40 (2010) 875-884.
[143] V. Kocaba, Development and evaluation of methods to follow microstructural development of cementitious systems including slags, in: Laboratoire des matériaux de construction, EPFL, 2009, pp. 145.
[144] M.J. Whittaker, The Impact of Slag Composition on the Microstructure of Composite Slag Cements Exposed to Sulfate Attack, in: School of Civil Engineering University of Leeds, 2015, pp. 116.
[145] A.C.A. Muller, K.L. Scrivener, A.M. Gajewicz, P.J. McDonald, Densification of C–S–H Measured by 1H NMR Relaxometry, The Journal of Physical Chemistry C, 117 (2013) 403-412.
[146] W.A. Gutteridge, J.A. Dalziel, Filler cement: The effect of the secondary component on the hydration of Portland cement: Part I. A fine non-hydraulic filler, Cement and Concrete Research, 20 (1990) 778-782.
[147] R.J. Flatt, G.W. Scherer, J.W. Bullard, Why alite stops hydrating below 80% relative humidity, Cement and Concrete Research, 41 (2011) 987-992.
[148] F.A. Steele, W.P. Davey, THE CRYSTAL STRUCTURE OF TRICALCIUM ALUMINATE, Journal of the American Chemical Society, 51 (1929) 2283-2293.
[149] P. Mondal, J.W. Jeffery, The crystal structure of tricalcium aluminate, Ca3Al2O6, Acta Cryst, B31 (1975) 689-697.
[150] L. Gobbo, L.l. Sant'Agostino, L. Garcez, C3A polymorphs related to industrial clinker alkalies content, Cement and Concrete Research, 34 (2004) 657-664.
[151] S.P. Varma, C.D. Wall, A monoclinic tricalcium aluminate (C3A) phase in a commercial Portland cement clinker, Cement and Concrete Research, 11 (1981) 567-574.
[152] R.M. Herath Banda, F.P. Glasser, Crystallization of the molten phase in portland cement clinker, Cement and Concrete Research, 8 (1978) 665-670.
[153] E. Breval, C3A hydration, Cement and Concrete Research, 6 (1976) 129-137.
[154] L. Black, C. Breen, J. Yarwood, C.-S. Deng, J. Phipps, G. Maitland, Hydration of tricalcium aluminate (C3A) in the presence and absence of gypsum—studied by Raman spectroscopy and X-ray diffraction, Journal of Material Chemistry, 16 (2006) 1263 - 1272.
[155] H.J. Kuzel, H. Pöllmann, Hydration of C3A in the presence of Ca(OH)2, CaSO4·2H2O and CaCO3, Cement and Concrete Research, 21 (1991) 885-895.
[156] P. Meredith, A. Donald, N. Meller, C. Hall, Tricalcium aluminate hydration: Microstructural observations by in-situ electron microscopy, Journal of materials science, 39 (2004) 997-1005.

[157] T.D. Ciach, E.G. Swenson, Morphology and microstructure of hydrating portland cement and its constituents I. Changes in hydration of tricalcium aluminate alone and in the presence of triethanolamine or calcium lignosulphonate, Cement and Concrete Research, 1 (1971) 143-158.
[158] D. Stephan, S. Wistuba, Crystal structure refinement and hydration behaviour of doped tricalcium aluminate, Cement and Concrete Research, 36 (2006) 2011-2020.
[159] M. Collepardi, G. Baldini, M. Pauri, M. Corradi, Tricalcium aluminate hydration in the presence of lime, gypsum or sodium sulfate, Cement and Concrete Research, 8 (1978) 571-580.
[160] P. Hewlett, Lea's chemistry of cement and concrete, Butterworth-Heinemann, 2003.
[161] H. Taylor, Cement chemistry, (1997).
[162] J. Pourchez, P. Grosseau, B. Ruot, Current understanding of cellulose ethers impact on the hydration of C3A and C3A-sulphate systems, Cement and Concrete Research, 39 (2009) 664-669.
[163] H. Minard, S. Garrault, L. Regnaud, A. Nonat, Mechanisms and parameters controlling the tricalcium aluminate reactivity in the presence of gypsum, Cement and Concrete Research, 37 (2007) 1418-1426.
[164] L. Amathieu, T.A. Bier, K. Scrivener, Mechanisms of set acceleration of Portland cement through CAC addition, in: International conference on calcium aluminate cements, 2001, pp. 303-317.
[165] P.K. Mehta, Effect of lime on hydration of pastes containing gypsum and calcium aluminates or calcium sulfoaluminate, Journal of the American Ceramic Society, 56 (1973) 315-319.
[166] A.P. Kirchheim, V. Fernandez-Altable, P.J.M. Monteiro, D.C.C. Dal Molin, Analysis of cubic and orthorhombic C3A hydration in presence of gypsum and lime, Journal of Materials Science, 44 (2009) 2038 - 2045.
[167] D.A. Silva, P.J. Monteiro, Early formation of ettringite in tricalcium aluminate–calcium hydroxide–gypsum dispersions, Journal of the American Ceramic Society, 90 (2007) 614-617.
[168] J. Skalny, M. Tadros, Retardation of tricalcium aluminate hydration by sulfates, Journal of the American Ceramic Society, 60 (1977) 174-175.
[169] M. Merlini, G. Artioli, T. Cerulli, F. Cella, A. Bravo, Tricalcium aluminate hydration in additivated systems. A crystallographic study by SR-XRPD, Cement and Concrete Research, 38 (2008) 477-486.
[170] R.F. Feldman, V.S. Ramachandran, The influence of CaSO4.2H2O upon the hydration character of 3CaO.Al2O3, Magazine of Concrete Research, 18 (1966) 185 –196.
[171] P. Gupta, S. Chatterji, J. Jeffery, Cement Technology 4, in, I-4, 1973.
[172] H.J. Kuzel, Initial hydration reactions and mechanisms of delayed ettringite formation in Portland cements, Cement and Concrete Composites, 18 (1996) 195-203.
[173] T. Matschei, B. Lothenbach, F.P. Glasser, The role of calcium carbonate in cement hydration, Cement and Concrete Research, 37 (2007) 551-558.
[174] T. Matschei, B. Lothenbach, F.P. Glasser, The AFm phase in Portland cement, Cement and Concrete Research, 37 (2007) 118-130.

[175] J.J. Beaudoin, V.S. Ramachandran, A new perspective on the hydration characteristics of cement phases, Cement and Concrete Research, 22 (1992) 689-694.
[176] A. Quennoz, K.L. Scrivener, Hydration of C3A–gypsum systems, Cement and Concrete Research, 42 (2012) 1032-1041.
[177] K. De Weerdt, K.O. Kjellsen, E. Sellevold, H. Justnes, Synergy between fly ash and limestone powder in ternary cements, Cement and Concrete Composites, 33 (2011) 30-38.
[178] M. Zajac, A. Rossberg, G. Le Saout, B. Lothenbach, Influence of limestone and anhydrite on the hydration of Portland cements, Cement and Concrete Composites, 46 (2014) 99-108.
[179] J.J. Beaudoin, V. Ramachandran, A new perspective on the hydration characteristics of cement phases, Cement and Concrete research, 22 (1992) 689-694.
[180] C. Plowman, J. Cabrera, Mechanism and kinetics of hydration of C3A and C4AF. Extracted from cement, Cement and Concrete Research, 14 (1984) 238-248.
[181] D.E. Rogers, L.P. Aldridge, Hydrates of calcium ferrites and calcium aluminoferrites, Cement and Concrete Research, 7 (1977) 399-409.
[182] B.Z. Dilnesa, B. Lothenbach, G. Renaudin, A. Wichser, D. Kulik, Synthesis and characterization of hydrogarnet Ca3(AlxFe1 − x)2(SiO4)y(OH)4(3 − y), Cement and Concrete Research, 59 (2014) 96-111.
[183] B.Z. Dilnesa, E. Wieland, B. Lothenbach, R. Dähn, K.L. Scrivener, Fe-containing phases in hydrated cements, Cement and Concrete Research, 58 (2014) 45-55.
[184] B.Z. Dilnesa, B. Lothenbach, G. Renaudin, A. Wichser, E. Wieland, Stability of monosulfate in the presence of iron, Journal of the American Ceramic Society, 95 (2012) 3305-3316.
[185] B.Z. Dilnesa, B. Lothenbach, G. Le Saout, G. Renaudin, A. Mesbah, Y. Filinchuk, A. Wichser, E. Wieland, Iron in carbonate containing AFm phases, Cement and Concrete Research, 41 (2011) 311-323.
[186] G. Renaudin, A. Mesbah, B. Zeleke Dilnesa, M. Francois, B. Lothenbach, Crystal chemistry of iron containing cementitious AFm layered hydrates, Current Inorganic Chemistry, 5 (2015) 184-193.
[187] B. EN197-1, Cement: composition, specifications and conformity criteria for common cements, British Standards Institution, London, (2011).
[188] M. Öner, A study of intergrinding and separate grinding of blast furnace slag cement, Cement and Concrete Research, 30 (2000) 473-480.
[189] H.M. Jennings, Colloid model of C−S−H and implications to the problem of creep and shrinkage Materials and Structures, 37 (2004) 59-70.
[190] X. Wu, D.M. Roy, C.A. Langton, Early stage hydration of slag-cement, Cement and Concrete Research, 13 (1983) 277-286.
[191] C. Çetin, S.T. Erdoğan, M. Tokyay, Effect of particle size and slag content on the early hydration of interground blended cements, Cement and Concrete Composites, 67 (2016) 39-49.
[192] G. Puerta-Falla, A. Kumar, L. Gomez-Zamorano, M. Bauchy, N. Neithalath, G. Sant, The influence of filler type and surface area on the hydration rates of calcium aluminate cement, Construction and Building Materials, 96 (2015) 657-665.

[193] K.L. Scrivener, A. Nonat, Hydration of cementitious materials, present and future, Cement and Concrete Research, 41 (2011) 651-665.
[194] J. Duchesne, M.A. Be´rube´, Effect of supplementary cementing materials on the composition of cement hydration products, Advanced Cement Based Materials, 2 (1995) 43-52.
[195] I.G. Richardson, A.R. Brough, G.W. Groves, C.M. Dobson, The characterization of hardened alkali-activated blast-furnace slag pastes and the nature of the calcium silicate hydrate (C-S-H) phase, Cement and Concrete Research, 24 (1994) 813-829.
[196] J.I. Escalante-Garcia, J.H. Sharp, The chemical composition and microstructure of hydration products in blended cements, Cement and Concrete Composites, 26 (2004) 967-976.
[197] M. Öner, K. Erdoğdu, A. Günlü, Effect of components fineness on strength of blast furnace slag cement, Cement and Concrete Research, 33 (2003) 463-469.
[198] S. Kumar, R. Kumar, A. Bandopadhyay, T.C. Alex, B. Ravi Kumar, S.K. Das, S.P. Mehrotra, Mechanical activation of granulated blast furnace slag and its effect on the properties and structure of portland slag cement, Cement and Concrete Composites, 30 (2008) 679-685.
[199] M.B. Haha, B. Lothenbach, G. Le Saout, F. Winnefeld, Influence of slag chemistry on the hydration of alkali-activated blast-furnace slag — Part II: Effect of Al2O3, Cement and Concrete Research, 42 (2012) 74-83.
[200] I. Ismail, S.A. Bernal, J.L. Provis, R. San Nicolas, S. Hamdan, J.S.J. van Deventer, Modification of phase evolution in alkali-activated blast furnace slag by the incorporation of fly ash, Cement and Concrete Composites, 45 (2014) 125-135.
[201] A. Schöler, B. Lothenbach, F. Winnefeld, M. Zajac, Hydration of quaternary Portland cement blends containing blast-furnace slag, siliceous fly ash and limestone powder, Cement and Concrete Composites, 55 (2015) 374-382.
[202] M.B. Haha, B. Lothenbach, G. Le Saout, F. Winnefeld, Influence of slag chemistry on the hydration of alkali-activated blast-furnace slag — Part I: Effect of MgO, Cement and Concrete Research, 41 (2011) 955-963.
[203] R. Snellings, Solution-controlled dissolution of supplementary cementitious material glasses at pH 13: The effect of solution composition on glass dissolution rates, J Am Ceram Soc, 96 (2013) 2467–2475.
[204] C. Shi, R.L. Day, Some factors affecting early hydration of alkali-slag cements, Cement and Concrete Research, 26 (1996) 439-447.
[205] J.I. Escalante-García, A.F. Fuentes, A. Gorokhovsky, P.E. Fraire-Luna, G. Mendoza-Suarez, Hydration Products and Reactivity of Blast-Furnace Slag Activated by Various Alkalis, Journal of the American Ceramic Society, 86 (2003) 2148-2153.
[206] S.A. Bernal, R. San Nicolas, R.J. Myers, R. Mejía de Gutiérrez, F. Puertas, J.S.J. van Deventer, J.L. Provis, MgO content of slag controls phase evolution and structural changes induced by accelerated carbonation in alkali-activated binders, Cement and Concrete Research, 57 (2014) 33-43.
[207] I.G. Richardson, J.G. Cabrera, The nature of C□S□H in model slag-cements, Cement and Concrete Composites, 22 (2000) 259-266.
[208] N. Mobasher, S.A. Bernal, J.L. Provis, Structural evolution of an alkali sulfate activated slag cement, Journal of Nuclear Materials, 468 (2016) 97-104.

[209] A.M. Rashad, Influence of different additives on the properties of sodium sulfate activated slag, Construction and Building Materials, 79 (2015) 379-389.
[210] I.G. Richardson, Tobermorite/jennite- and tobermorite/calcium hydroxide-based models for the structure of C-S-H: applicability to hardened pastes of tricalcium silicate, β-dicalcium silicate, Portland cement, and blends of Portland cement with blast-furnace slag, metakaolin, or silica fume, Cement and Concrete Research, 34 (2004) 1733-1777.
[211] I.G. Richardson, G.W. Groves, The structure of the calcium silicate hydrate phases present in hardened pastes of white Portland cement/blast-furnace slag blends, Journal of material Science, 32 (1997) 4793-4802.
[212] E. Tajuelo Rodriguez, I.G. Richardson, L. Black, E. Boehm-Courjault, A. Nonat, J. Skibsted, Composition, silicate anion structure and morphology of calcium silicate hydrates (C-S-H) synthesised by silica-lime reaction and by controlled hydration of tricalcium silicate (C3S), Advances in Applied Ceramics, 114 (2015) 362-371.
[213] M. Vandamme, F.-J. Ulm, P. Fonollosa, Nanogranular packing of C–S–H at substochiometric conditions, Cement and Concrete Research, 40 (2010) 14-26.
[214] K. J. Krakowiak, W. Wilson, S. James, S. Musso, F.-J. Ulm, Inference of the phase-to-mechanical property link via coupled X-ray spectrometry and indentation analysis: Application to cement-based materials, Cement and Concrete Research, 67 (2015) 271-285.
[215] S.P. Pandey, R.L. Sharma, The influence of mineral additives on the strength and porosity of OPC mortar, Cement and Concrete Research, 30 (2000) 19-23.
[216] D.P. Bentz, Modeling the influence of limestone filler on cement hydration using CEMHYD3D, Cement and Concrete Composites, 28 (2006) 124-129.
[217] I. Soroka, N. Stern, Calcareous fillers and the compressive strength of portland cement, Cement and Concrete Research, 6 (1976) 367-376.
[218] I. Soroka, N. Setter, The effect of fillers on strength of cement mortars, Cement and Concrete Research, 7 (1977) 449-456.
[219] V. Bonavetti, H. Donza, G. Menéndez, O. Cabrera, E.F. Irassar, Limestone filler cement in low w/c concrete: A rational use of energy, Cement and Concrete Research, 33 (2003) 865-871.
[220] E.F. Irassar, D. Violini, V.F. Rahhal, C. Milanesi, M.A. Trezza, V.L. Bonavetti, Influence of limestone content, gypsum content and fineness on early age properties of Portland limestone cement produced by inter-grinding, Cement and Concrete Composites, 33 (2011) 192-200.
[221] A.-M. Poppe, G. De Schutter, Cement hydration in the presence of high filler contents, Cement and Concrete Research, 35 (2005) 2290-2299.
[222] M. Nehdi, S. Mindess, P.-C. Aïtcin, Optimization of high strength limestone filler cement mortars, Cement and Concrete Research, 26 (1996) 883-893.
[223] T. Matschei, B. Lothenbach, F.P. Glasser, Thermodynamic properties of Portland cement hydrates in the system CaO–Al 2 O 3–SiO 2–CaSO 4–CaCO 3–H 2 O, Cement and Concrete Research, 37 (2007) 1379-1410.
[224] G. Ye, X. Liu, G. De Schutter, A.M. Poppe, L. Taerwe, Influence of limestone powder used as filler in SCC on hydration and microstructure of cement pastes, Cement and Concrete Composites, 29 (2007) 94-102.

[225] P. Mounanga, M.I.A. Khokhar, R. Hachem, A. Loukili, Improvement of the early-age reactivity of fly ash and blast furnace slag cementitious systems using limestone filler, Materials and Structures, 44 (2011) 437-453.
[226] Y. Zhang, G. Ye, Effect of Limestone Powder on Microstructure of Ternary Cementitious System., Sustainable Construction Materials (2012) 225-234.
[227] W.A. Klemm, L.D. Adams, An investigation of the formation of carboaluminates in: P. Klieger, R.D. Hooton (Eds.) Carbonate Additions to Cement, ASTM STP 1064, American Society for Testing and Materials, Philadelphia, 1990, pp. 60-72.
[228] L. Basheer, J. Kropp, D.J. Cleland, Assessment of the durability of concrete from its permeation properties: a review, Construction and Building Materials, 15 (2001) 93-103.
[229] P.H.R. Borges, J.O. Costa, N.B. Milestone, C.J. Lynsdale, R.E. Streatfield, Carbonation of CH and C–S–H in composite cement pastes containing high amounts of BFS, Cement and Concrete Research, 40 (2010) 284-292.
[230] J.J. Chen, J.J. Thomas, H.M. Jennings, Decalcification shrinkage of cement paste, Cement and Concrete Research, 36 (2006) 801-809.
[231] J. Kim, W.J. McCarter, B. Suryanto, S. Nanukuttan, P.A.M. Basheer, T.M. Chrisp, Chloride ingress into marine exposed concrete: A comparison of empirical- and physically- based models, Cement and Concrete Composites, 72 (2016) 133-145.
[232] U. Balters, U. Ludwig, Influence of cement type on resistance against freezing and thawing, with or without deicing chemicals, of cement mortar, Frost Resistance of Concrete, 34 (2004) 119.
[233] A. Marciniak, W. Grymin, T. Margiewicz, M. Koniorczyk, Influence of freezing-induced damage on the carbonation rate of concrete, European Journal of Environmental and Civil Engineering, (2016) 1-16.
[234] J. Stark, A. Eckart, H.M. Ludwig, Influence of C_3A content on frost and scaling resistance, in: M.J. Setzer, R. Auberg (Eds.) Frost Resistance of Concrete Proceedings of the International RILEM Workshop on Resistance of Concrete to Freezing and Thawing With or Without De-icing Chemicals, E & FN SPON, University of Essen, 1997, pp. 100-109.
[235] H. Toutanji, N. Delatte, S. Aggoun, R. Duval, A. Danson, Effect of supplementary cementitious materials on the compressive strength and durability of short-term cured concrete, Cement and Concrete Research, 34 (2004) 311-319.
[236] G.J. Osborne, Durability of Portland blast-furnace slag cement concrete, Cement and Concrete Composites, 21 (1999) 11-21.
[237] L.J. Parrott, Some effects of cement and curing upon carbonation and reinforcement corrosion in concrete, Materials and Structures, 29 (1996) 164-173
[238] O. Wowra, Effects of carbonation to microstructure and pore solution, in: N.J. Setzer, R. Auberg, I.J. Keck (Eds.) International RILEM Workshop on Frost Resistance of Concrete, 2002, pp. 61 - 68.
[239] T. Grounds, H. Midgley, D. Novell, Carbonation of ettringite by atmospheric carbon dioxide, Thermochimica Acta, 135 (1988) 347-352.
[240] E. Dubina, L. Korat, L. Black, J. Strupi-Šuput, J. Plank, Influence of water vapour and carbon dioxide on free lime during storage at 80 C, studied by Raman spectroscopy, Spectrochimica Acta Part A: Molecular and Biomolecular Spectroscopy, 111 (2013) 299-303.

[241] L. Black, K. Garbev, I. Gee, Surface carbonation of synthetic CSH samples: A comparison between fresh and aged CSH using X-ray photoelectron spectroscopy, Cement and Concrete Research, 38 (2008) 745-750.
[242] Z. Šauman, Effect of CO2 on porous concrete, Cement and Concrete Research, 2 (1972) 541-549.
[243] E. Gruyaert, P. Van den Heede, N. De Belie, Carbonation of slag concrete: Effect of the cement replacement level and curing on the carbonation coefficient – Effect of carbonation on the pore structure, Cement and Concrete Composites, 35 (2013) 39-48.
[244] E.T. Stepkowska, J.L. Pérez-Rodríguez, M.J. Sayagués, J.M. Martínez-Blanes, Calcite, vaterite and aragonite forming on cement hydration from liquid and gaseous phase, Journal of Thermal Analysis and Calorimetry 73 (2003) 247 - 269.
[245] D. Russell, P.A.M. Basheer, G.I.B. Rankin, A.E. Long, Effect of relative humidity and air permeability on prediction of the rate of carbonation of concrete, Proceedings of the ICE - Structures and Buildings, 146 (2001) 319 - 326.
[246] D.W.S. Ho, Q.Y. Cui, D.J. Ritchie, The influence of humidity and curing time on the quality of concrete, Cement and Concrete Research, 19 (1989) 457-464.
[247] Z. Šauman, Carbonization of porous concrete and its main binding components, Cement and Concrete Research, 1 (1971) 645-662.
[248] Z. Hu, M. Shao, Q. Cai, S. Ding, C. Zhong, X. Wei, Y. Deng, Synthesis of needle-like aragonite from limestone in the presence of magnesium chloride, Journal of Materials Processing Technology, 209 (2009) 1607-1611.
[249] P. Pipilikaki, M. Beazi-Katsioti, The assessment of porosity and pore size distribution of limestone Portland cement pastes, Construction and Building Materials, 23 (2009) 1966-1970.
[250] O. Çopuroğlu, A.L.A. Fraaij, J.M.J.M. Bijen, Effect of sodium monofluorophosphate treatment on microstructure and frost salt scaling durability of slag cement paste, Cement and Concrete Research, 36 (2006) 1475-1482.
[251] B. Johannesson, P. Utgenannt, Microstructural changes caused by carbonation of cement mortar, Cement and Concrete Research, 31 (2001) 925-931.
[252] G. Fagerlund, Internal frost attack - State of the art, in: M.J. Setzer, R. Auberg (Eds.) Frost Resistance of Concrete Proceedings of the International RILEM Workshop, Essen, 1997, pp. 321 - 338.
[253] H.-J. Chen, S.-S. Huang, C.-W. Tang, M.A. Malek, L.-W. Ean, Effect of curing environments on strength, porosity and chloride ingress resistance of blast furnace slag cement concretes: A construction site study, Construction and Building Materials, 35 (2012) 1063-1070.
[254] V.T. Ngala, C.L. Page, EFFECTS OF CARBONATION ON PORE STRUCTURE AND DIFFUSIONAL PROPERTIES OF HYDRATED CEMENT PASTES, Cement and Concrete Research, 27 (1997) 995-1007.
[255] M. Pigeon, M. Setzer, ACTION OF FROST AND DEICING CHEMICALS-BASIC PHENOMENA AND TESTING, RILEM PROCEEDINGS 30 FREEZE-THAW DURABILITY OF CONCRETE, (1997).
[256] J.J. Beaudoin, C. MacInnis, The mechanism of frost damage in hardened cement paste, Cement and Concrete Research, 4 (1974) 139-147.
[257] M. Setzer, Action of frost and deicing chemicals: basic phenomena and testing, Freeze Thaw Durability of Concrete, (1976) 3-21.

[258] O. Coussy, P.J.M. Monteiro, Poroelastic model for concrete exposed to freezing temperatures, Cement and Concrete Research, 38 (2008) 40-48.
[259] O. Coussy, P. Monteiro, Unsaturated poroelasticity of freezing water-infiltrated materials with air voids, in: Poromechanics III-Biot Centennial (1905-2005): Proceedings of the 3rd Biot Conference on Poromechanics, 24-27 May 2005, Norman, Oklahoma, USA, CRC Press, 2005, pp. 457.
[260] G.J. Verbeck, P. Klieger, Studies of'salt'scaling of concrete, Highway Research Board Bulletin, (1957).
[261] O. Çopuroğlu, E. Schlangen, Modeling of frost salt scaling, Cement and Concrete Research, 38 (2008) 27-39.
[262] V. Penttala, Surface and internal deterioration of concrete due to saline and non-saline freeze–thaw loads, Cement and Concrete Research, 36 (2006) 921-928.
[263] J.S. Walder, B. Hallet, The physical basis of frost weathering: Toward a more fundamental and unified perspective, Artic and Alpine Research, 18 (1986) 27-32.
[264] D.R. Uhlmann, B. Chalmers, K.A. Jackson, Interaction Between Particles and a Solid-Liquid Interface, Journal of Applied Physics, 35 (1964) 2986-2993.
[265] D.J. Janssen, The influence of material parameters on freeze-thaw resistance with and without deicing salt, in: M.J. Setzer, R. Auberg (Eds.) Proceedings of the Internal RILEM Workshop on Resistance of Concrete to Freezing and Thawing with or without De-icing Chemicals E&FN SPON, University of Essen, 1997, pp. 3-10.
[266] A. Bilodeau, V.M. Malhotra, Deicing salt scaling resistance of concrete incorporating supplementary cementious materials: CANMET Research, in: J. Marchand, M. Pigeon, M. Setzer (Eds.) RILEM PROCEEDINGS 30 FREEZE-THAW DURABILITY OF CONCRETE, E and F Spon Limited, Quebec, Canada, 1997, pp. 121-156.
[267] T.F. Rønning, Freeze-Thaw Resistance of Concrete: Effect of: Curing Conditions, Moisture Exchange and Materials, (2001).
[268] W. Sun, Y.M. Zhang, H.D. Yan, R. Mu, Damage and damage resistance of high strength concrete under the action of load and freeze-thaw cycles, Cement and Concrete Research, 29 (1999) 1519-1523.
[269] Z. Giergiczny, M.A. Glinicki, M. Sokołowski, M. Zielinski, Air void system and frost-salt scaling of concrete containing slag-blended cement, Construction and Building Materials, 23 (2009) 2451-2456.
[270] C. Girodet, M. Chabannet, J. Bosc, J. Pera, Influence of the type of cement on the freeze-thaw resistance of the mortar phase of concrete, Frost Resistance of Concrete, 34 (2004) 34.
[271] P. Taylor, Effect of Clinker Chemistry on Salt Scaling Resistance of Concrete, Transportation Research Record: Journal of the Transportation Research Board, 2113 (2009) 108-113.
[272] H.F.W. Taylor, C. Famy, K.L. Scrivener, Delayed ettringite formation, Cement and Concrete Research, 31 (2001) 683-693.
[273] A. Müller, C. Fuhr, D. Knöfel, Frost resistance of cement mortars with different lime contents, Cement and concrete research, 25 (1995) 809-818.
[274] R. Bleszynski, R.D. Hooton, M.D. Thomas, C.A. Rogers, Durability of ternary blend concrete with silica fume and blast-furnace slag: laboratory and outdoor exposure site studies, ACI Materials Journal, 99 (2002) 499-508.

[275] S.E. Chidiac, D.K. Panesar, Evolution of mechanical properties of concrete containing ground granulated blast furnace slag and effects on the scaling resistance test at 28days, Cement and Concrete Composites 30 (2008) 63-71

[276] M.S. Meddah, M.C. Lmbachiya, R.K. Dhir, Potential use of binary and composite limestone cements in concrete production, Construction and Building Materials, 58 (2014) 193-205.
[277] B. Li, J. Wang, M. Zhou, Effect of limestone fines content in manufactured sand on durability of low- and high-strength concretes, Construction and Building Materials, 23 (2009) 2846-2850.
[278] B. Espion, B. Lebon, C. Pierre, O. Germain, A. Hellebois, Characterisation of new ternary cements with reduced clinker content, in: Proceedings of the First International Conference on Concrete Sustainability, Japan Concrete Institute, 2013, pp. 145-152.
[279] I.K. Battaglia, J.F. Munoz, S.M. Cramer, Proposed behavioral model for deicer scaling resistance of slag cement concrete, J Mater CivEng, 22 (2011) 361-368.
[280] O. Çopuro, L. Fraaij, J. Bijen, Effect of curing conditions on freeze-thaw de-icing salt resistance of blast furnace slag cement mortars, WIT Transactions on The Built Environment, 76 (2004).
[281] R.M. Geiker, Studies of Portland Cement Hydration: Measurements of Chemical Shrinkage and a Systematic Evaluaiton of Hydration Curves by Means of Dispersion Model, in: Technical University of Denmark, Technical University of Denmark, Technical University of Denmark, 1983.
[282] J. Hjorth, J. Skibsted, H.J. Jakobsen, 29Si MAS NMR studies of portland cement components and effects of microsilica on the hydration reaction, Cement and Concrete Research, 18 (1988) 789-798.
[283] A. Bentur, Effect of Gypsum on the Hydration and Strength of C3S Pastes, American Ceramic Society, 59 (1976) 210-213.
[284] D. Ménétrier, I. Jawed, J. Skalny, Effect of gypsum on C3S hydration, Cement and Concrete Research, 10 (1980) 697-701.
[285] I. Pane, W. Hansen, Investigation of blended cement hydration by isothermal calorimetry and thermal analysis, Cement and Concrete Research, 35 (2005) 1155-1164.
[286] I. Wadsö, L. Wadsö, Systematic errors in isothermal micro-and nanocalorimetry, Journal of thermal analysis and calorimetry, 82 (2005) 553-558.
[287] L. Wadsö, Operational issues in isothermal calorimetry, Cement and Concrete Research, 40 (2010) 1129-1137.
[288] S.T. Bergold, F. Goetz-Neunhoeffer, J. Neubauer, Influence of the reactivity of the amorphous part of mechanically activated alite on its hydration kinetics, Cement and Concrete Research, 88 (2016) 73-81.
[289] J.L. Poole, K.A. Riding, K.J. Folliard, M.C. Juenger, A.K. Schindler, Methods for calculating activation energy for Portland cement, ACI Materials Journal, 104 (2007) 86.
[290] A. C1608-12, Standard Test Method for Chemical Shrinkage of Hydraulic Cement Paste, in, ASTM International, West Conshohocken, PA, 2012.
[291] N. Setter, D.M. Roy, Mechanical features of chemical shrinkage of cement paste, Cement and Concrete Research, 8 (1978) 623-634.

[292] T.C. Powers, T.L. Brownyard, Studies of the physical properties of hardened Portland cement paste, in: Journal Proceedings, 1946, pp. 101-132.
[293] H.J.H. Brouwers, The work of Powers and Brownyard revisited: Part 1, Cement and Concrete Research, 34 (2004) 1697-1716.
[294] M. Geiker, T. Knudsen, Chemical shrinkage of portland cement pastes, Cement and Concrete Research, 12 (1982) 603-610.
[295] S. Boivin, P. Acker, S. Rigaud, B. Clavaud, Experimental assessment of chemical shrinkage of hydrating cement pastes, in: Autogenous shrinkage of concrete Spon Press, Proceedings of the International Workshop organized by the JCI (Japan Concrete Institute), 1999, pp. 81-92.
[296] P. Lura, F. Winnefeld, S. Klemm, Simultaneous measurements of heat of hydration and chemical shrinkage on hardening cement pastes, Journal of Thermal Analysis and Calorimetry, 101 (2010) 925-932.
[297] F. Lin, C. Meyer, Hydration kinetics modeling of Portland cement considering the effects of curing temperature and applied pressure, Cement and Concrete Research, 39 (2009) 255-265.
[298] L.J. Parrott, M. Geiker, W.A. Gutteridge, D. Killoh, Monitoring Portland cement hydration: Comparison of methods, Cement and Concrete Research, 20 (1990) 919-926.
[299] H.M. Dyson, I.G. Richardson, A.R. Brough, A Combined 29Si MAS NMR and Selective Dissolution Technique for the Quantitative Evaluation of Hydrated Blast Furnace Slag Cement Blends, J Am Ceram Soc, 90 (2007) 598-602.
[300] L. McCusker, R. Von Dreele, D. Cox, D. Louer, P. Scardi, Rietveld refinement guidelines, Journal of Applied Crystallography, 32 (1999) 36-50.
[301] G. Le Saoût, V. Kocaba, K. Scrivener, Application of the Rietveld method to the analysis of anhydrous cement, Cement and concrete research, 41 (2011) 133-148.
[302] L. Mitchell, P. Whitfield, J. Beaudoin, The effects of particle statistics on quantitative Rietveld analysis of cement, in: 12th International congress on the Chemistry of Cement, Montreal, 2007, pp. 1-12.
[303] R. Snellings, A. Bazzoni, K. Scrivener, The existence of amorphous phase in Portland cements: Physical factors affecting Rietveld quantitative phase analysis, Cement and Concrete Research, 59 (2014) 139-146.
[304] W. Dollase, Correction of intensities for preferred orientation in powder diffractometry: application of the March model, Journal of Applied Crystallography, 19 (1986) 267-272.
[305] N.C. Popa, Microstructural properties: Texture and macrostress effects, Chapter, 12 (2008) 332-375.
[306] R. Von Dreele, Quantitative texture analysis by Rietveld refinement, Journal of Applied Crystallography, 30 (1997) 517-525.
[307] D.L. Bish, S. Howard, Quantitative phase analysis using the Rietveld method, Journal of Applied Crystallography, 21 (1988) 86-91.
[308] H. Rietveld, A profile refinement method for nuclear and magnetic structures, Journal of applied Crystallography, 2 (1969) 65-71.
[309] K.L. Scrivener, T. Füllmann, E. Gallucci, G. Walenta, E. Bermejo, Quantitative study of Portland cement hydration by X-ray diffraction/Rietveld analysis and independent methods, Cement and Concrete Research, 34 (2004) 1541-1547.

[310] D. Jansen, C. Stabler, F. Goetz-Neunhoeffer, S. Dittrich, J. Neubauer, Does Ordinary Portland Cement contain amorphous phase? A quantitative study using an external standard method, Powder Diffraction, 26 (2011) 31-38.
[311] F.H. Chung, Quantitative interpretation of X-ray diffraction patterns of mixtures. I. Matrix-flushing method for quantitative multicomponent analysis, Journal of Applied Crystallography, 7 (1974) 519-525.
[312] F.H. Chung, Quantitative interpretation of X-ray diffraction patterns of mixtures. III. Simultaneous determination of a set of reference intensities, Journal of Applied Crystallography, 8 (1975) 17-19.
[313] D. Jansen, F. Goetz-Neunhoeffer, C. Stabler, J. Neubauer, A remastered external standard method applied to the quantification of early OPC hydration, Cement and Concrete Research, 41 (2011) 602-608.
[314] P.M. Suherman, A. van Riessen, B. O'Connor, D. Li, D. Bolton, H. Fairhurst, Determination of amorphous phase levels in Portland cement clinker, Powder Diffraction, 17 (2002) 178-185.
[315] G. Le Saout, K. Scrivener, Early Hydration of Portland Cement with Corundum Addition, in: 16 Internationale Baustofftagung (ibausil), Weimar, Germany, 2006, pp. 409-416.
[316] A. De La Torre, S. Bruque, M. Aranda, Rietveld quantitative amorphous content analysis, Journal of Applied Crystallography, 34 (2001) 196-202.
[317] I.C. Madsen, N.V. Scarlett, A. Kern, Description and survey of methodologies for the determination of amorphous content via X-ray powder diffraction, Zeitschrift für Kristallographie Crystalline Materials, 226 (2011) 944-955.
[318] B.H. O'Connor, M.D. Raven, Application of the Rietveld refinement procedure in assaying powdered mixtures, Powder Diffraction, 3 (1988) 2-6.
[319] C. Hesse, F. Goetz-Neunhoeffer, J. Neubauer, M. Braeu, P. Gaeberlein, Quantitative in situ X-ray diffraction analysis of early hydration of Portland cement at defined temperatures, Powder Diffraction, 24 (2009) 112-115.
[320] S.T. Bergold, F. Goetz-Neunhoeffer, J. Neubauer, Quantitative analysis of C–S–H in hydrating alite pastes by in-situ XRD, Cement and Concrete Research, 53 (2013) 119-126.
[321] N.C. Collier, J.H. Sharp, N.B. Milestone, J. Hill, I.H. Godfrey, The influence of water removal techniques on the composition and microstructure of hardened cement pastes, Cement and Concrete Research, 38 (2008) 737-744.
[322] J. Zhang, G.W. Scherer, Comparison of methods for arresting hydration of cement, Cement and Concrete Research, 41 (2011) 1024-1036.
[323] K.L. Scrivener, H. Patel, P. Pratt, L. Parrott, Analysis of phases in cement paste using backscattered electron images, methanol adsorption and thermogravimetric analysis, in: Mater Res Soc Symp Proc, Cambridge Univ Press, 1987, pp. 67-76.
[324] P.J. Goodhew, J. Humphreys, R. Beanland, Electron microscopy and analysis, CRC Press, 2000.
[325] H.S. Wong, M.K. Head, N.R. Buenfeld, Pore segmentation of cement-based materials from backscattered electron images, Cement and Concrete Research, 36 (2006) 1083-1090.
[326] X. Feng, E.J. Garboczi, D.P. Bentz, P.E. Stutzman, T.O. Mason, Estimation of the degree of hydration of blended cement pastes by a scanning electron

microscope point-counting procedure, Cement and Concrete Research, 34 (2004) 1787-1793.
[327] T.C. Powers, Structure and physical properties of hardened Portland cement paste, Journal of the American Ceramic Society, 41 (1958) 1-6.
[328] A.B. Abell, K.L. Willis, D.A. Lange, Mercury Intrusion Porosimetry and Image Analysis of Cement-Based Materials, Journal of Colloid and Interface Science, 211 (1999) 39-44.
[329] S. Diamond, Mercury porosimetry: An inappropriate method for the measurement of pore size distributions in cement-based materials, Cement and Concrete Research, 30 (2000) 1517-1525.
[330] P.J. McDonald, V. Rodin, A. Valori, Characterisation of intra- and inter-C–S–H gel pore water in white cement based on an analysis of NMR signal amplitudes as a function of water content, Cement and Concrete Research, 40 (2010) 1656-1663.
[331] H. Elaqra, N. Godin, G. Peix, M. R'Mili, G. Fantozzi, Damage evolution analysis in mortar, during compressive loading using acoustic emission and X-ray tomography: Effects of the sand/cement ratio, Cement and Concrete Research, 37 (2007) 703-713.
[332] E.W. Washburn, Note on a method of determining the distribution of pore sizes in a porous material, Proceedings of the National Academy of Sciences, 7 (1921) 115-116.
[333] C. Gallé, Effect of drying on cement-based materials pore structure as identified by mercury intrusion porosimetry: A comparative study between oven-, vacuum-, and freeze-drying, Cement and Concrete Research, 31 (2001) 1467-1477.
[334] L. Konecny, S. Naqvi, The effect of different drying techniques on the pore size distribution of blended cement mortars, Cement and concrete research, 23 (1993) 1223-1228.
[335] H. Ma, Mercury intrusion porosimetry in concrete technology: tips in measurement, pore structure parameter acquisition and application, Journal of porous materials, 21 (2014) 207-215.
[336] N. Hearn, R.D. Hooton, Sample mass and dimension effects on mercury intrusion porosimetry results, Cement and Concrete Research, 22 (1992) 970-980.
[337] L. Tang, P.-E. Petersson, Slab test-freeze/Thaw resistance of concrete—Internal deterioration, Materials and Structures, 34 (2001) 526-531.
[338] G.W. Scherer, Freezing gels, Journal of Non-Crystalline Solids, 155 (1993) 1-25.
[339] B. Lothenbach, P. Durdzinski, K. De Weerdt, Chapter 5: Thermogravimetric Analysis, a practical guide to microstructural analysis of cementitious materials, Edt Karen Scrivener, Ruben Snellings, and Barbara Lothenbach, to be published byTaylor & Francis Group, (2016).
[340] PDCEN/TR15177, Testing the freeze-thaw resistance of concrete-Internal structural damage, in, 2006.
[341] E. Knapen, O. Cizer, K. Van Balen, D. Van Gemert, Effect of free water removal from early-age hydrated cement pastes on thermal analysis, Construction and Building Materials, 23 (2009) 3431-3438.
[342] M. Whittaker, L. Black, Relationship between, early stage microstructure and long term durability of slag-containing cements, in: M. Russell (Ed.) 32nd

Cement and Concrete Science Conference, Queens University Belfast, 2012, pp. 161-165.
[343] L. Zhang, F. Glasser, Critical examination of drying damage to cement pastes, Advances in cement research, 12 (2000) 79-88.
[344] R.L. Day, B.K. Marsh, Measurement of porosity in blended cement pastes, Cement and Concrete Research, 18 (1988) 63-73.
[345] R.W. Cheary, A.A. Coelho, J.P. Cline, Fundamental parameters line profile fitting in laboratory diffractometers, J Res Natl Inst Stand Technol, 109 (2004) 1-25.
[346] H. Morikawa, I. Minato, T. Tomita, S. Iwai, Anhydrite: a refinement, Acta Crystallographica Section B: Structural Crystallography and Crystal Chemistry, 31 (1975) 2164-2165.
[347] K. Ojima, Y. Nishihata, A. Sawada, Structure of potassium sulfate at temperatures from 296 K down to 15 K, Acta Crystallographica Section B: Structural Science, 51 (1995) 287-293.
[348] H. Schmidt, I. Paschke, D. Freyer, W. Voigt, Water channel structure of bassanite at high air humidity: crystal structure of CaSO4· 0.625 H2O, Acta Crystallographica Section B: Structural Science, 67 (2011) 467-475.
[349] W. Mumme, R. Hill, G. Bushnell-Wye, E. Segnit, Rietveld crystal structure refinements, crystal chemistry and calculated powder diffraction data for the polymorphs of dicalcium silicate and related phases, Neues Jahrbuch fur Mineralogie Abhandlungen, 169 (1995) 35-68.
[350] A. Colville, S. Geller, The crystal structure of brownmillerite, Ca2FeAlO5, Acta Crystallographica Section B: Structural Crystallography and Crystal Chemistry, 27 (1971) 2311-2315.
[351] P. Mondal, J. Jeffery, The crystal structure of tricalcium aluminate, Ca3Al2O6, Acta Crystallographica Section B: Structural Crystallography and Crystal Chemistry, 31 (1975) 689-697.
[352] Y. Takeuchi, F. Nishi, Crystal-chemical characterization of the 3CaO· Al2O3—Na2O solid-solution series, Zeitschrift für Kristallographie-Crystalline Materials, 152 (1980) 259-308.
[353] E. Maslen, V. Streltsov, N. Streltsova, N. Ishizawa, Electron density and optical anisotropy in rhombohedral carbonates. III. Synchrotron X-ray studies of CaCO3, MgCO3 and MnCO3, Acta Crystallographica Section B: Structural Science, 51 (1995) 929-939.
[354] T. Pilati, F. Demartin, C. Gramaccioli, Lattice-dynamical estimation of atomic displacement parameters in carbonates: calcite and aragonite CaCO3, dolomite CaMg (CO3) 2 and magnesite MgCO3, Acta Crystallographica Section B: Structural Science, 54 (1998) 515-523.
[355] G. Renaudin, R. Segni, D. Mentel, J.-M. Nedelec, F. Leroux, C. Taviot-Gueho, A Raman Study of the Sulfated Cement Hydrates: Ettringite and Monosulfoaluminate, Journal of Advanced Concrete Technology, 5 (2007) 299-312.
[356] Á.G. De La Torre, S. Bruque, J. Campo, M.A. Aranda, The superstructure of C 3 S from synchrotron and neutron powder diffraction and its role in quantitative phase analyses, Cement and Concrete Research, 32 (2002) 1347-1356.
[357] T. Runčevski, R.E. Dinnebier, O.V. Magdysyuk, H. Pöllmann, Crystal structures of calcium hemicarboaluminate and carbonated calcium

hemicarboaluminate from synchrotron powder diffraction data, Acta Crystallographica Section B: Structural Science, 68 (2012) 493-500.
[358] M. Bellotto, B. Rebours, O. Clause, J. Lynch, D. Bazin, E. Elkaïm, A reexamination of hydrotalcite crystal chemistry, The Journal of Physical Chemistry, 100 (1996) 8527-8534.
[359] D. Taylor, Thermal expansion data. I: Binary oxides with the sodium chloride and wurtzite structures, MO, Transactions and journal of the British Ceramic Society, 83 (1984) 5-9.
[360] D. Henderson, H. Gutowsky, A nuclear magnetic resonance determination of the hydrogen positions in Ca (OH) 2, in, DTIC Document, 1962.
[361] Y. Le Page, G. Donnay, Refinement of the crystal structure of low-quartz, Acta Crystallographica Section B: Structural Crystallography and Crystal Chemistry, 32 (1976) 2456-2459.
[362] D.C. Creagh, J.H. Hubbell, X-ray absorption (or attenuation) coefficients, International Tables for Crystallography, C (2006) 220-229.
[363] V.S. Ramachandran, R.M. Paroli, J.J. Beaudoin, A.H. Delgado, Handbook of Thermal Analysis of Construction Materials, in, NOYES Publications, 2002, pp. 72-136.
[364] R.S. Barneyback Jr, S. Diamond, Expression and analysis of pore fluids from hardened cement pastes and mortars, Cement and Concrete Research, 11 (1981) 279-285.
[365] P.S. Whitfield, L.D. Mitchell, Quantitative Rietveld analysis of the amorphous content in cements and clinkers, Journal of Materials Science, 38 (2003) 4415-4421.
[366] P. Scardi, Microstructural properties: lattice defects and domain size effects, Powder Diffraction Theory and Practice, (2008) 376-413.
[367] Q. Zhou, F.P. Glasser, Thermal stability and decomposition mechanisms of ettringite at <120°C, Cement and Concrete Research, 31 (2001) 1333-1339.
[368] J.H. Hubbell, Review and history of photon cross section calculationsWork supported by the National Institute of Standards and Technology, Physics in medicine and biology, 51 (2006) R245.
[369] R. Snellings, —X-ray powder diffraction applied to cement, A Practical Guide to Microstructural Analysis of Cementitious Materials, (2016) 107.
[370] A. Arora, G. Sant, N. Neithalath, Ternary blends containing slag and interground/blended limestone: Hydration, strength, and pore structure, Construction and Building Materials, 102, Part 1 (2016) 113-124.
[371] I. Jawed, J. Skalny, Alkalies in cement: A review, Cement and Concrete Research, 8 (1978) 37-51.
[372] L. Opoczky, Grinding technical questions of producing composite cements, Int J Miner Process, 44-45 (1996) 395-404.
[373] A. Kumar, G. Sant, C. Patapy, C. Gianocca, K.L. Scrivener, The influence of sodium and potassium hydroxide on alite hydration: Experiments and simulations, Cement and Concrete Research, 42 (2012) 1513-1523.
[374] T. Vuk, V. Tinta, R. Gabrovšek, V. Kaučič, The effects of limestone addition, clinker type and fineness on properties of Portland cement, Cement and Concrete Research, 31 (2001) 135-139.
[375] K. Vance, M. Aguayo, T. Oey, G. Sant, N. Neithalath, Hydration and strength development in ternary portland cement blends containing limestone and fly ash or metakaolin, Cement and Concrete Composites, 39 (2013) 93-103.

[376] A. Gruskovnjak, B. Lothenbach, F. Winnefeld, B. Münch, R. Figi, S.-C. Ko, M. Adler, U. Mäder, Quantification of hydration phases in supersulfated cements: review and new approaches, Adv Cem Res, 23 (2011) 265-275.
[377] P.Z. Wang, R. Trettin, V. Rudert, Effect of fineness and particle size distribution of granulated blast-furnace slag on the hydraulic reactivity in cement systems, Advances in Cement Research, 17 (2005) 161-166.
[378] J. J. Biernacki, J. M. Richardson, P. E. Stutzman, D.P. Bentz, Kinetics of Slag Hydration in the Presence of Calcium Hydroxide, J Am Ceram Soc, 85 (2002) 2261–2267.
[379] S.C. Pal, A. Mukherjee, S.R. Pathak, Investigation of hydraulic activity of ground granulated blast furnace slag in concrete, Cement and Concrete Research, 33 (2003) 1481-1486.
[380] H. Zhang, Z. Lin, D. Tong, Influence of the type of calcium sulfate on the strength and hydration of portland cement under an initial steam-curing condition, Cement and concrete research, 26 (1996) 1505-1511.
[381] J. Cheung, A. Jeknavorian, L. Roberts, D. Silva, Impact of admixtures on the hydration kinetics of Portland cement, Cement and Concrete Research, 41 (2011) 1289-1309.
[382] D. Rothstein, J.J. Thomas, B.J. Christensen, H.M. Jennings, Solubility behavior of Ca-, S-, Al-, and Si-bearing solid phases in Portland cement pore solutions as a function of hydration time, Cement and Concrete Research, 32 (2002) 1663-1671.
[383] P. Monteiro, P.K. Mehta, Interaction between carbonate rock and cement paste, Cement and Concrete Research, 16 (1986) 127-134.
[384] M.T. Palou, J. Majling, Effects of sulphate, calcium and aluminum ions upon the hydration of sulphoaluminate belite cement, Journal of thermal analysis, 46 (1996) 549-556.
[385] D. Bentz, G. Sant, J. Weiss, Early-Age Properties of Cement-Based Materials. I: Influence of Cement Fineness, Journal of Materials in Civil Engineering 20 (2008) 502–508.
[386] M. Collepardi, G. Baldini, M. Pauri, M. Corradi, The effect of pozzolanas on the tricalcium aluminate hydration, Cement and Concrete Research, 8 (1978) 741-751.
[387] J. Péra, S. Husson, B. Guilhot, Influence of finely ground limestone on cement hydration, Cement and Concrete Composites, 21 (1999) 99-105.
[388] T. Oey, A. Kumar, J.W. Bullard, N. Neithalath, G. Sant, The Filler Effect: The Influence of Filler Content and Surface Area on Cementitious Reaction Rates, J Am Ceram Soc, 96 (2013) 1978 - 1990.
[389] E.H. Oelkers, General kinetic description of multioxide silicate mineral and glass dissolution, Geochimica et Cosmochimica Acta, 65 (2001) 3703-3719.
[390] J.J. Thomas, H.M. Jennings, A colloidal interpretation of chemical aging of the C-S-H gel and its effects on the properties of cement paste, Cement and Concrete Research, 36 (2006) 30-38.
[391] G.J. Stockmann, D. Wolff-Boenisch, N. Bovet, S.R. Gislason, E.H. Oelkers, The role of silicate surfaces on calcite precipitation kinetics, Geochimica et Cosmochimica Acta, 135 (2014) 231-250.
[392] N. Voglis, G. Kakali, E. Chaniotakis, S. Tsivilis, Portland-limestone cements. Their properties and hydration compared to those of other composite cements, Cement and Concrete Composites, 27 (2005) 191-196.

[393] M. Ben Haha, B. Lothenbach, G. Le Saout, F. Winnefeld, Influence of slag chemistry on the hydration of alkali-activated blast-furnace slag — Part I: Effect of MgO, Cement and Concrete Research, 41 (2011) 955-963.
[394] O. Chowaniec, Limestone addition in cement., in: Laboratoire des matériaux de construction, EPFL, 2012.
[395] L. Montanaro, A. Negro, M. Regourd, Action de CaCO3, CaSO4 et CaSO4·2H2O sur l'Hydratation de C3S, Cement and Concrete Research, 18 (1988) 431-437.
[396] A.P. Barker, An electron optical examination of zoning in blastfurnace slag hydrates: Part I. Slag cement pastes at early ages, Advances in Cement Research, 2 (1989) 171-179.
[397] A. Vollpracht, B. Lothenbach, R. Snellings, J. Haufe, The pore solution of blended cements: a review, Materials and Structures, 49 (2016) 3341-3367.
[398] D.-T. Nguyen, R. Alizadeh, J.J. Beaudoin, L. Raki, Microindentation creep of secondary hydrated cement phases and C–S–H, Materials and Structures, 46 (2013) 1519-1525.
[399] EN206:2013, Concrete. Specification, performance, production and conformity, in, 2013.
[400] C. Hall, Water sorptivity of mortars and concretes: a review, Magazine of Concrete Research, 41 (1989) 51-61.
[401] M. Ghirci, S. Kenai, M. Said-Mansour, Mechanical properties and durability of mortar and concrete containing natural pozzolana and limestone blended cements, Cement and Concrete Composites, 29 (2007) 542-549.
[402] V. Bonavetti, V. Rahhal, E.F. Irassar, Studies on the carboaluminate formation in limestone filler-blended cements, Cement and Concrete Research, 31 (2001) 853-859.
[403] DDCEN/TS12390-9:2006, Testing hardened concrete. Freeze-thaw resistance. Scaling, in.
[404] S. Rahman, Z. Grasley, E. Masad, D. Zollinger, S. Iyengar, R. Kogbara, Simulation of Mass, Linear Momentum, and Energy Transport in Concrete with Varying Moisture Content during Cooling to Cryogenic Temperatures, Transport in Porous Media, 112 (2016) 139-166.
[405] H. Cai, X. Liu, Freeze-thaw durability of concrete: ice formation process in pores, Cement and Concrete Research, 28 (1998) 1281-1287.
[406] T. RILEM, L.T. IDC, P. P-E, Final Recommendation of RILEM TC 176-IDC'Internal Damage of Concrete due to frost action', Materials and Structures, 37 (2004) 754-759.
[407] P.A.M. Basheer, # Clam'permeability tests for assessing the durability of concrete, in, Queen's University of Belfast, 1991.
[408] G. Fagerlund, The critical degree of saturation method of assessing the freeze/thaw resistance of concrete, Matériaux et Construction, 10 (1977) 217-229.
[409] Z. Liu, W. Hansen, A hypothesis for salt frost scaling in cementitious materials, Journal of Advanced Concrete Technology, 13 (2015) 403-414.
[410] Z. Liu, W. Hansen, Freezing characteristics of air-entrained concrete in the presence of deicing salt, Cement and Concrete Research, 74 (2015) 10-18.
[411] S. Tsivilis, G. Batis, E. Chaniotakis, G. Grigoriadis, D. Theodossis, Properties and behavior of limestone cement concrete and mortar, Cement and Concrete Research, 30 (2000) 1679-1683.

[412] A. Morandeau, M. Thiéry, P. Dangla, Impact of accelerated carbonation on OPC cement paste blended with fly ash, Cement and Concrete Research, 67 (2015) 226-236.
[413] K. Suzuki, T. Nishikawa, S. Ito, Formation and carbonation of C-S-H in water, Cement and Concrete Research, 15 (1985) 213-224.
[414] F. Sanchez, M.K. Langley White, A. Hoang, Leaching from granular cement-based materials during infiltration/wetting coupled with freezing and thawing, Journal of Environmental Management, 90 (2009) 983-993.
[415] C. Carde, R. François, J.-M. Torrenti, Leaching of both calcium hydroxide and C-S-H from cement paste: Modeling the mechanical behavior, Cement and Concrete Research, 26 (1996) 1257-1268.
[416] C. Gervais, A.C. Garrabrants, F. Sanchez, R. Barna, P. Moszkowicz, D.S. Kosson, The effects of carbonation and drying during intermittent leaching on the release of inorganic constituents from a cement-based matrix, Cement and Concrete Research, 34 (2004) 119-131.
[417] T. Nishikawa, K. Suzuki, S. Ito, K. Sato, T. Takebe, Decomposition of synthesized ettringite by carbonation, Cement and Concrete Research, 22 (1992) 6-14.
[418] A. Hidalgo, C. Domingo, C. Garcia, S. Petit, C. Andrade, C. Alonso, Microstructural changes induced in Portland cement-based materials due to natural and supercritical carbonation, Journal of Materials Science, 43 (2008) 3101-3111.
[419] S.A. Bernal, M.C. Juenger, X. Ke, W. Matthes, B. Lothenbach, N. De Belie, J.L. Provis, Characterization of supplementary cementitious materials by thermal analysis, Materials and Structures, 50 (2017) 26.
[420] L. Divet, R. Randriambololona, Delayed Ettringite Formation: The Effect of Temperature and Basicity on the Interaction of Sulphate and C-S-H Phase 1, Cement and Concrete Research, 28 (1998) 357-363.
[421] J.J. Thomas, J.J. Chen, A.J. Allen, H.M. Jennings, Effects of decalcification on the microstructure and surface area of cement and tricalcium silicate pastes, Cement and Concrete Research, 34 (2004) 2297-2307.
[422] J.E. Rossen, B. Lothenbach, K.L. Scrivener, Composition of C–S–H in pastes with increasing levels of silica fume addition, Cement and Concrete Research, 75 (2015) 14-22.
[423] R.K. Iler, Effect of adsorbed alumina on the solubility of amorphous silica in water, Journal of Colloid and Interface Science, 43 (1973) 399-408.
[424] L. Lam, Y.L. Wong, C.S. Poon, Degree of hydration and gel/space ratio of high-volume fly ash/cement systems, Cement and Concrete Research, 30 (2000) 747-756.

Appendices

A.1.1 Data extraction from Chemical shrinkage images

The steps involved in the extraction of data of shrinkage data from the automatically recorded images are presented in the flow chart shown in

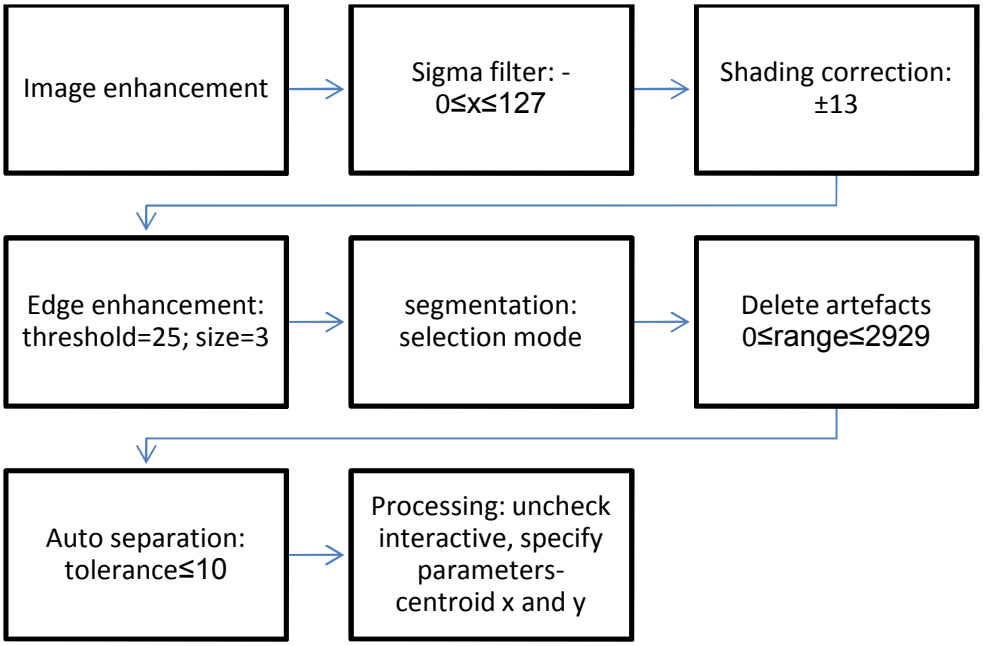

Figure A-1 Steps for automatic extraction of shrinkage data from images

The change in volume was defined by two independent means; the y-centre and the bound bottom. The change in height measured (y_{∇}) is the difference between the initial height at zero time (y_0) and the heights at different hydration times (y_t) as illustrated in equation 1.

$$y_{\nabla} = y_t - y_0 \text{-------- Equation 9-1}$$

A.1.2 Scoping results

The preliminary studies involved measurement of compressive strength, heat of reaction and chemical shrinkage of 22 mixes. Based on these, six mixes were selected for the main investigation.

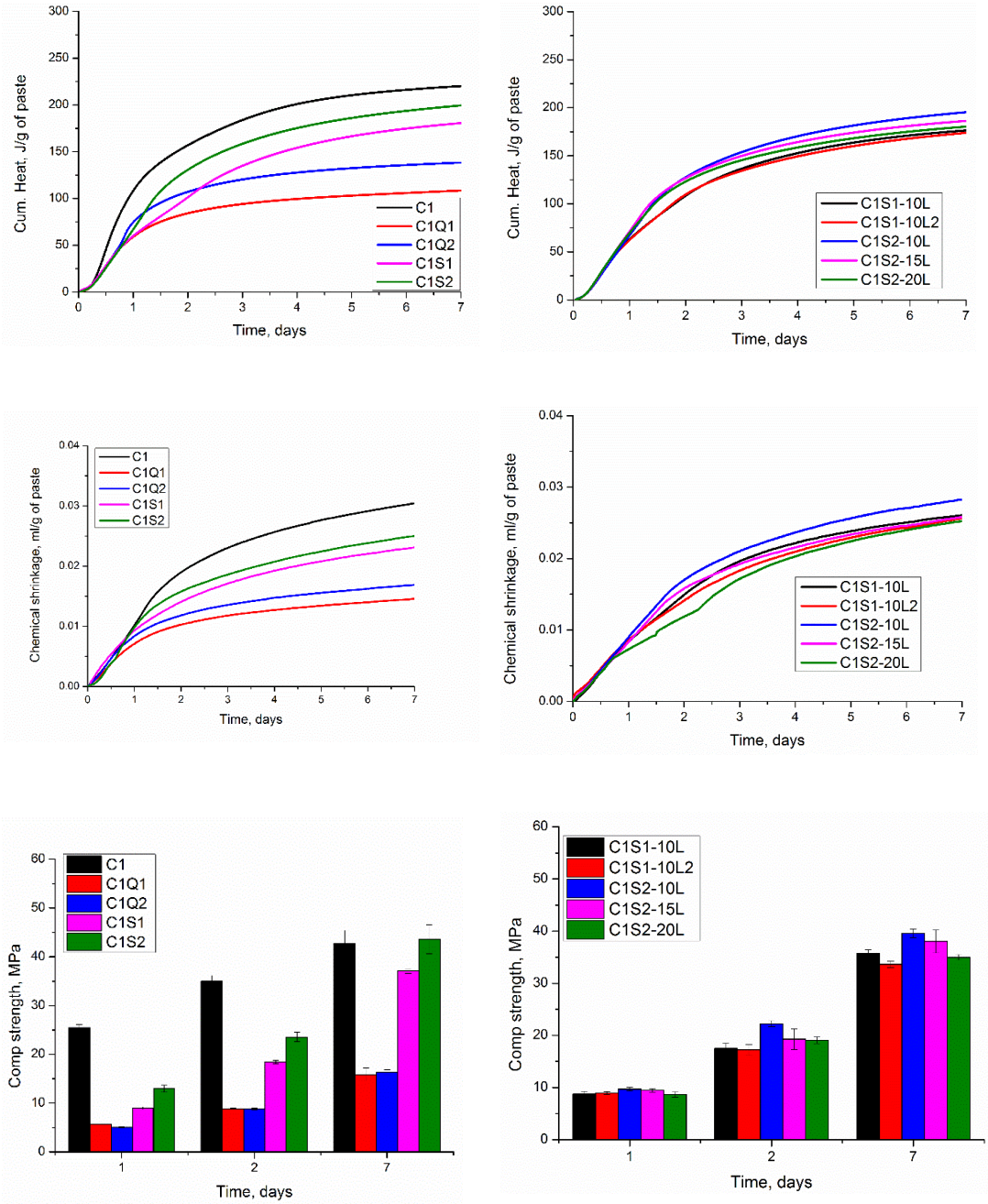

Figure A-2 Cumulative heat, chemical shrinkage and strength development in CEM I 42.5R composite cements.

Showing, effect of slag, filler, limestone content, and fineness

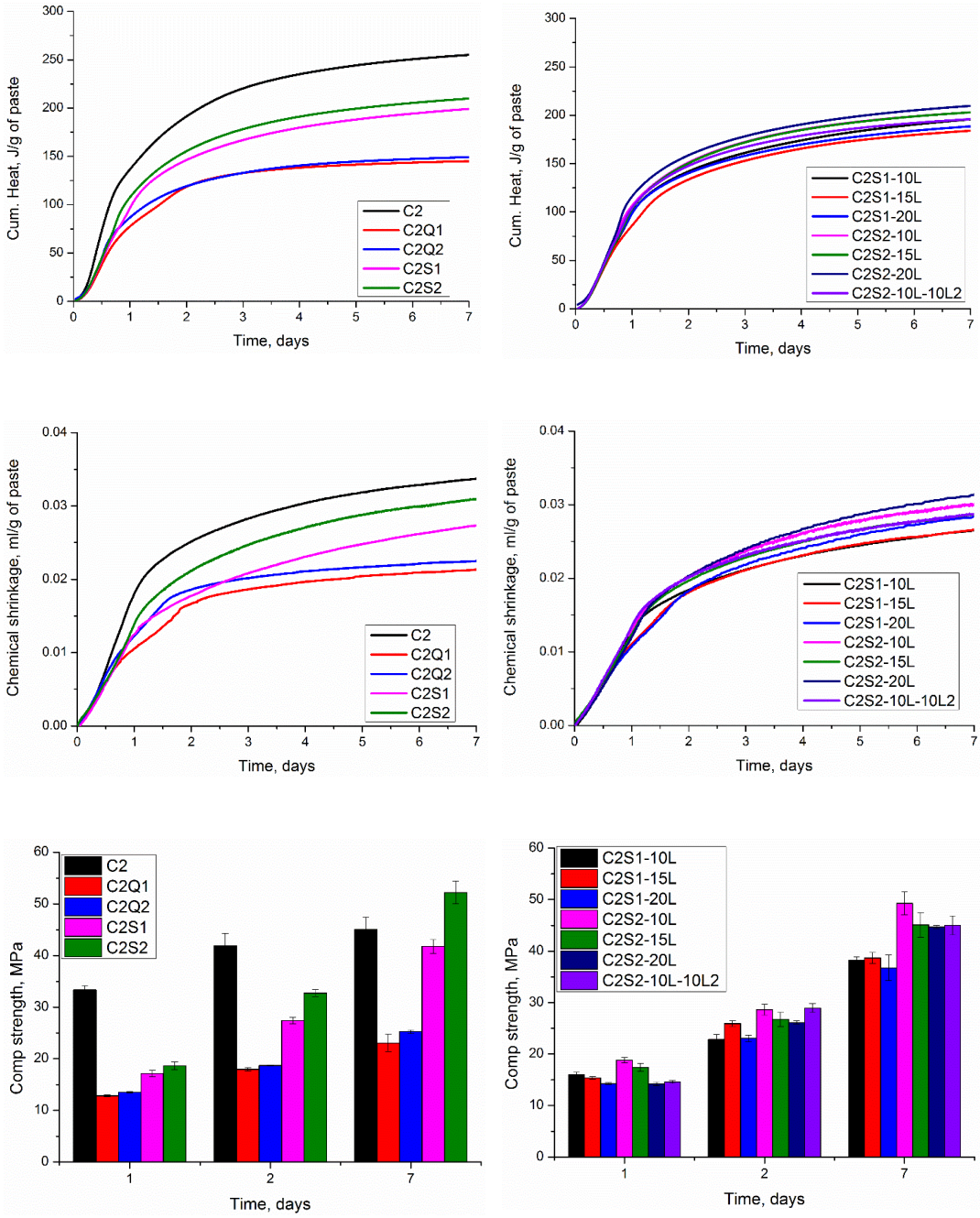

Figure A-3 Cumulative heat, chemical shrinkage and strength development in CEM I 42.5R ternary slag blends as a function of fineness and limestone content

A.1.3 Rietveld Refinement/PONKCS

The output from Rietveld refinement including implementation of the PONKCS phase to extract residual slag and clinker contents plus hydrates are shown here to supplement chapter 5. First, the deconvolution of constituents and hydrates is presented. Following similar procedures, the different cements were analysed and the calculated patterns superimposed on the observed and the background as well as difference plots are shown for each of the five main composite slag cements reported in Chapter 5 and 6. The G-factor, scale factor, MAC of sample and Rwp of refinement also provided for reference.

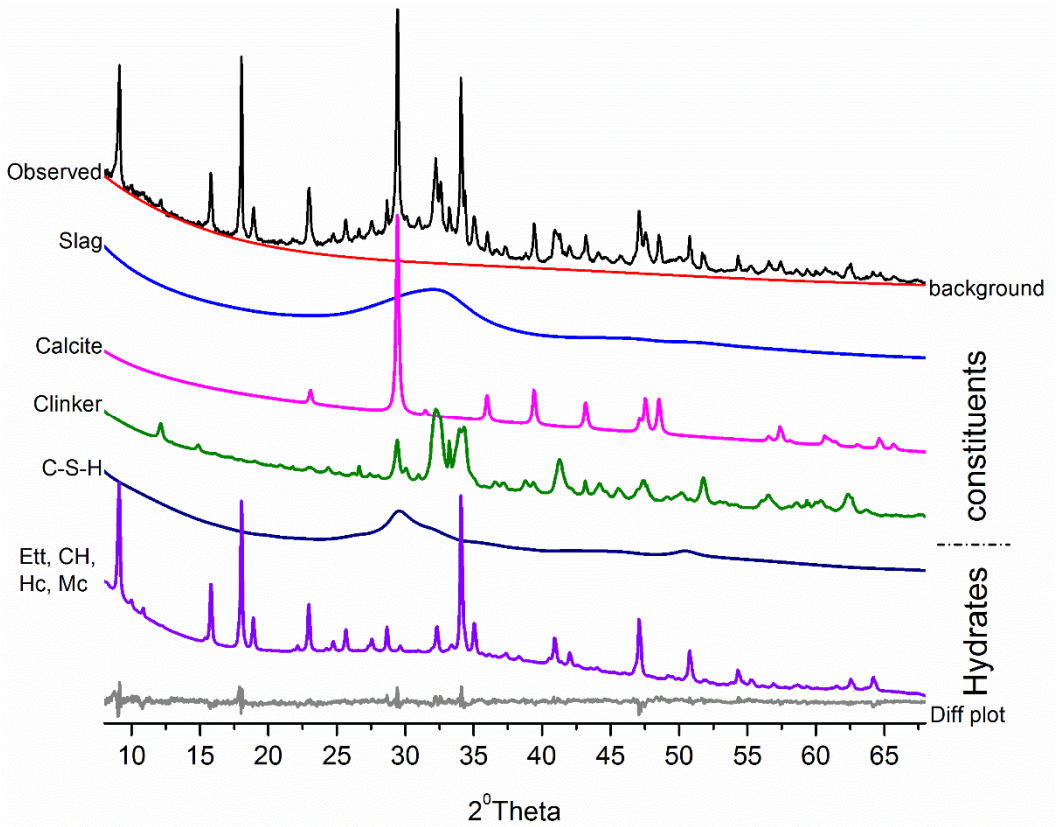

Figure A-4 Observed pattern for mix C2S1-10L hydrated for 1 day.

Deconvoluted into constituents' phases and hydrates, background and difference plot.

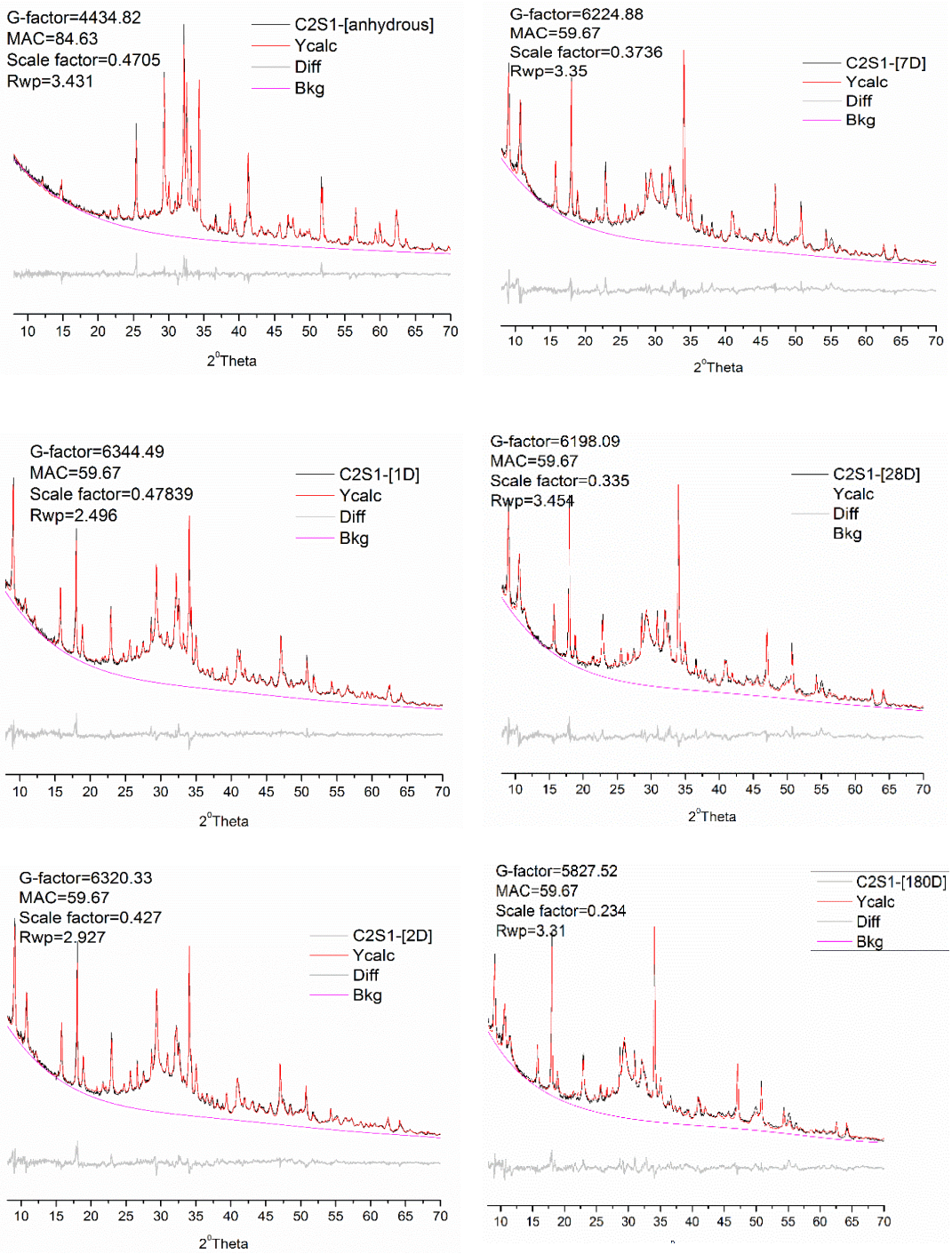

Figure A-5 Refined pattern for mix C2S1

showing , calculated patterns superimposed on observed pattern plus background and difference plot for anhydrous and samples hydrated for 1,2,7, 28 and 180 days.

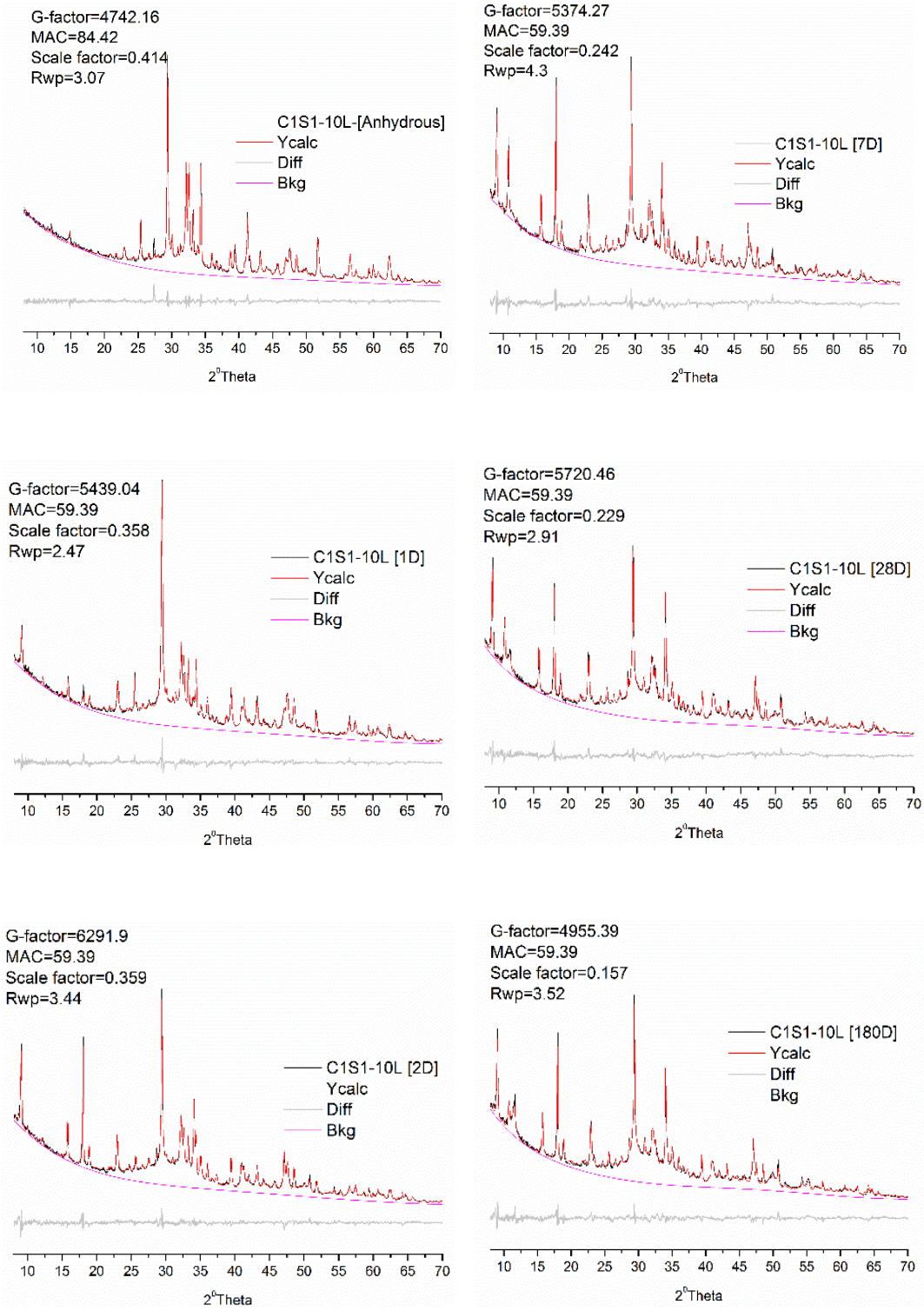

Figure A-6 Refined pattern for mix C1S1-10L

showing , calculated patterns superimposed on observed pattern plus background and difference plot for anhydrous and samples hydrated for 1,2,7, 28 and 180 days.

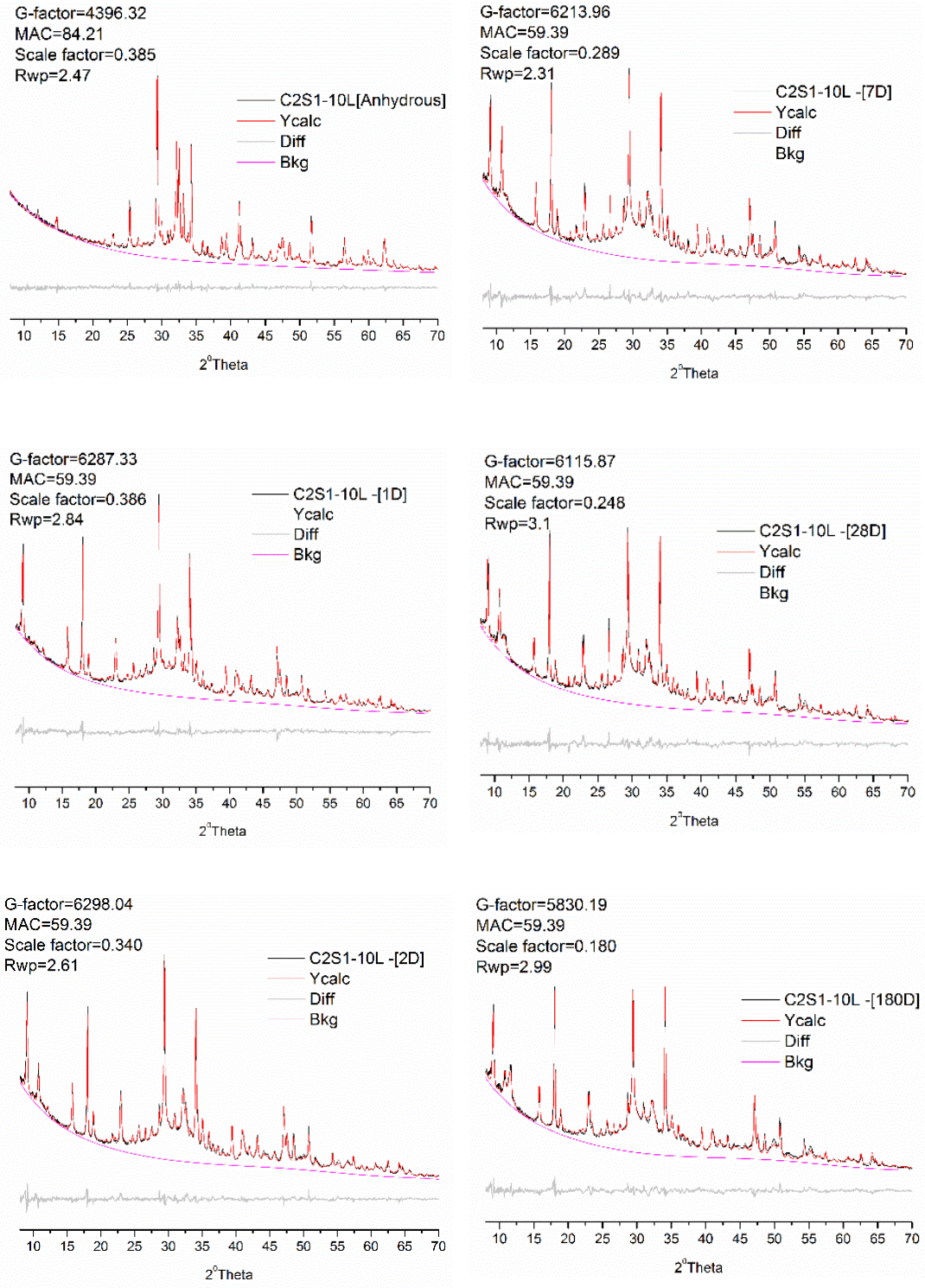

Figure A-7 Refined pattern for mix C2S1-10L

showing , calculated patterns superimposed on observed pattern plus background and difference plot for anhydrous and samples hydrated for 1,2,7, 28 and 180 days.

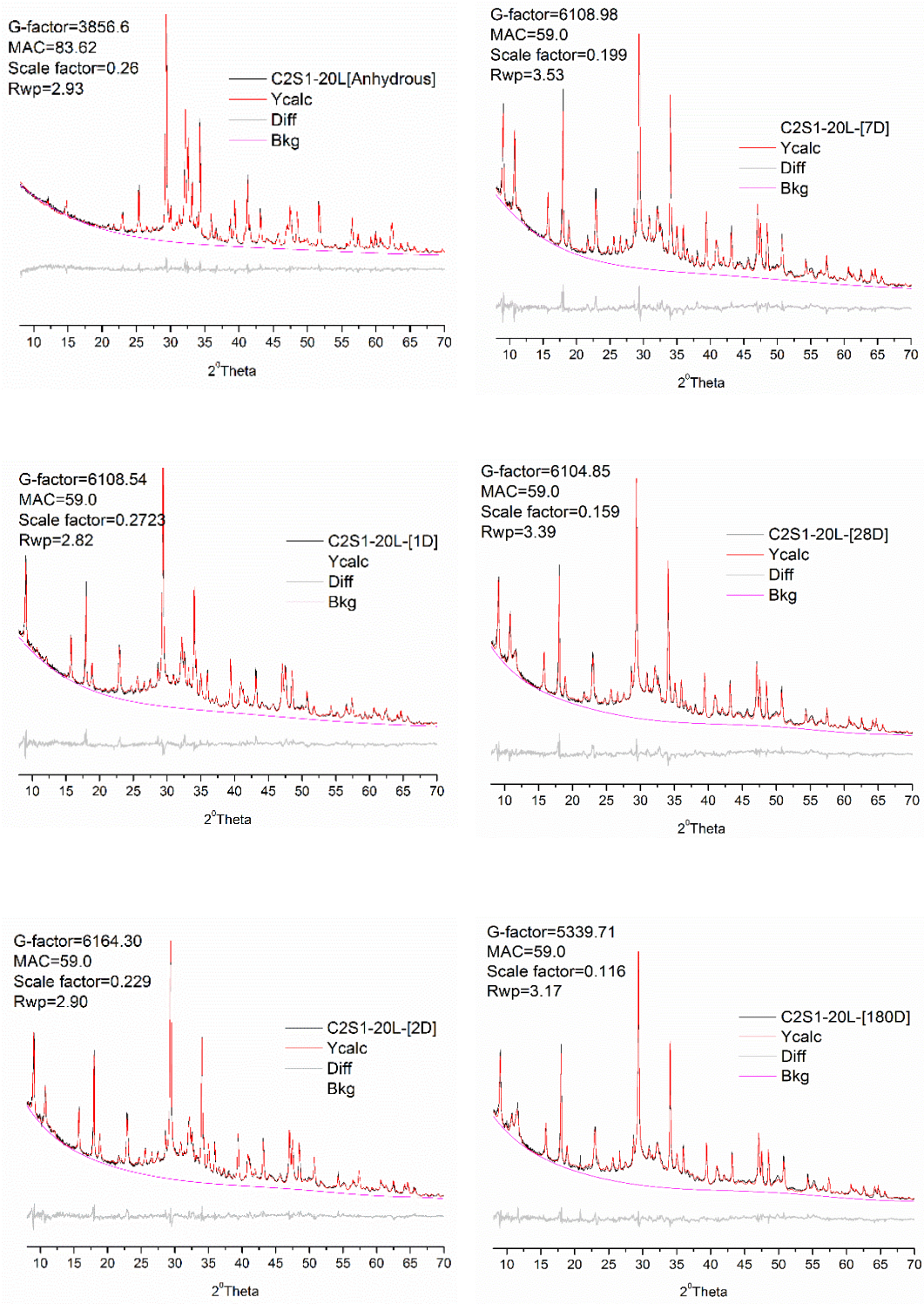

Figure A-8 Refined pattern for mix C2S1-20L

showing , calculated patterns superimposed on observed pattern plus background and difference plot for anhydrous and samples hydrated for 1,2,7, 28 and 180 days.

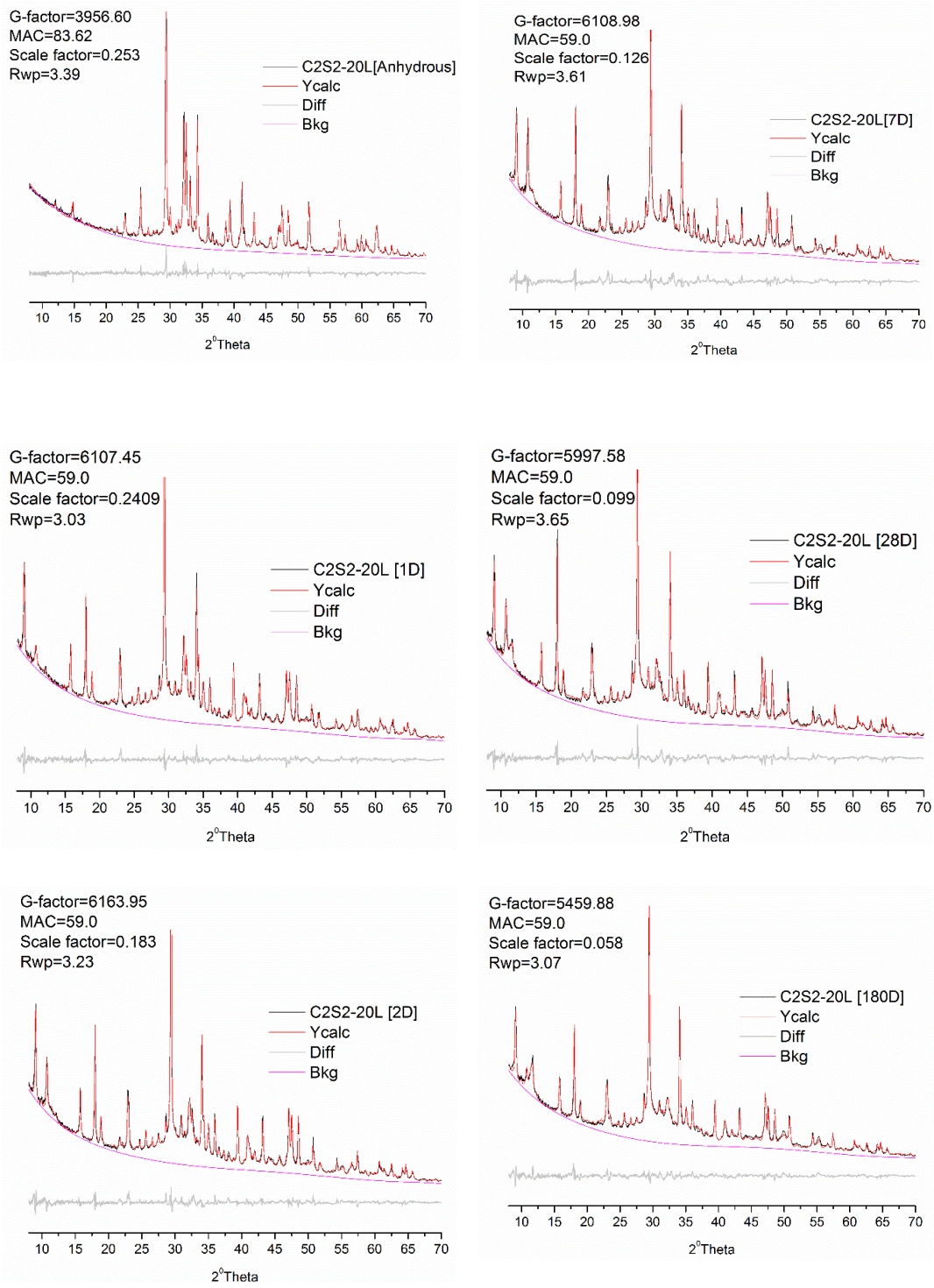

Figure A-9 Refined pattern for mix C2S2-20L

showing , calculated patterns superimposed on observed pattern plus background and difference plot for anhydrous and samples hydrated for 1,2,7, 28 and 180 days.

A.1.4 Backscattered SEM images and thresholding for quantitative analysis

These figures supplement the SEM data reported in Chapters 5 and 6

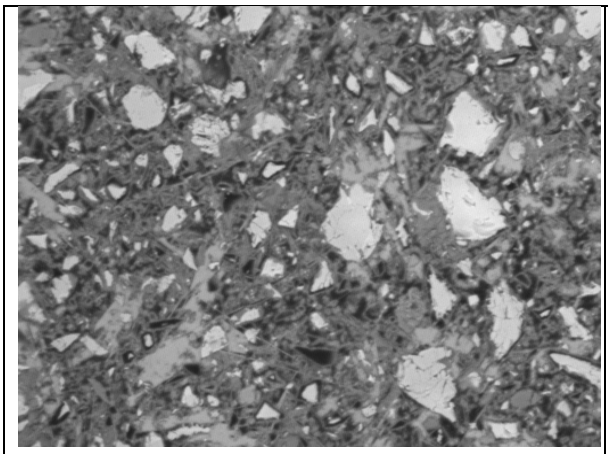	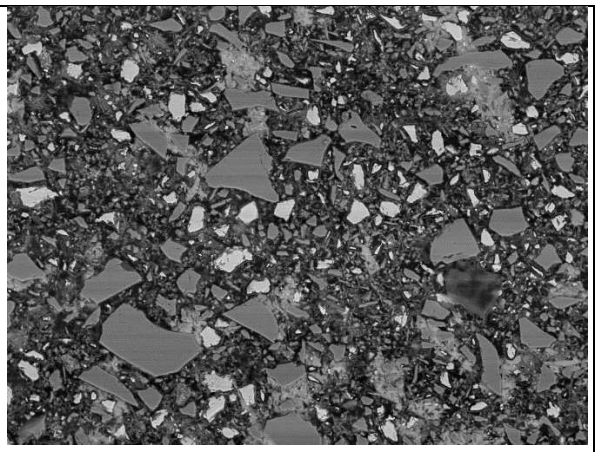
C2- 1 d	C2Q1 – 1d
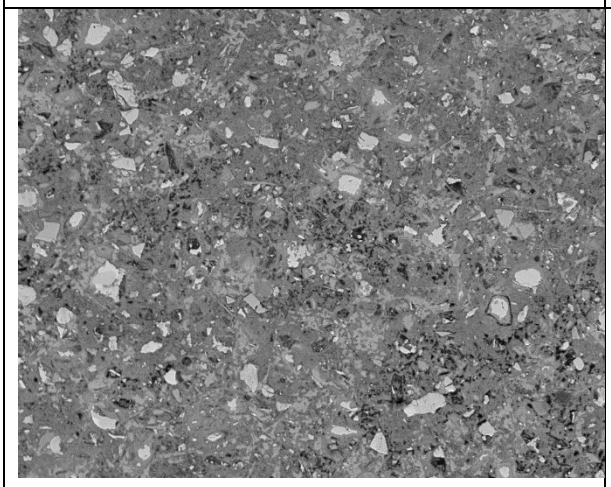	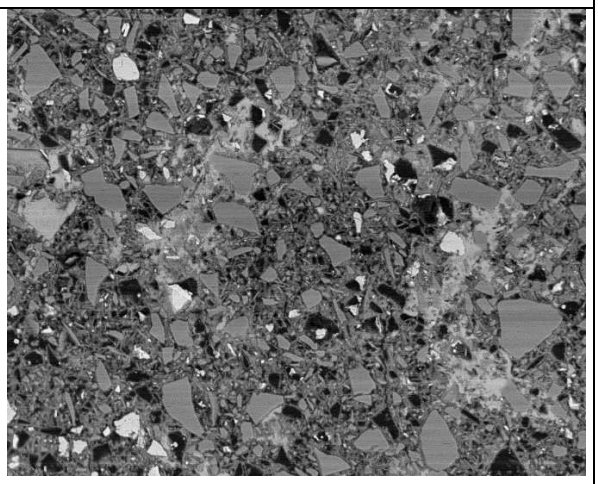
C2 – 7d	C2Q1 – 7d
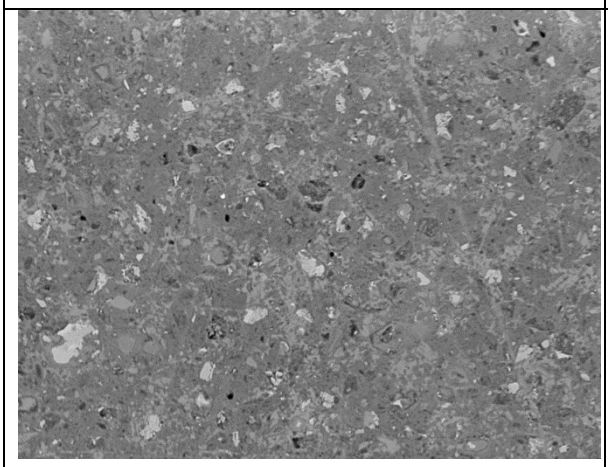	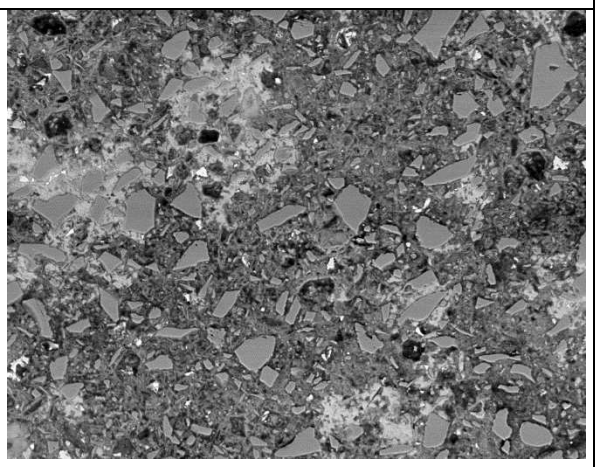
C2-28d	C2Q1 – 28d

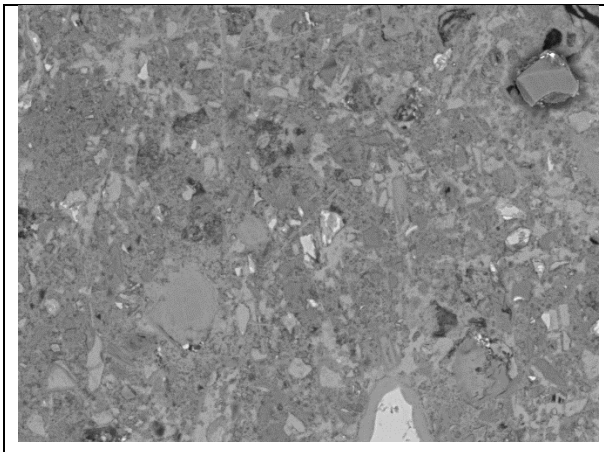

C2-180d

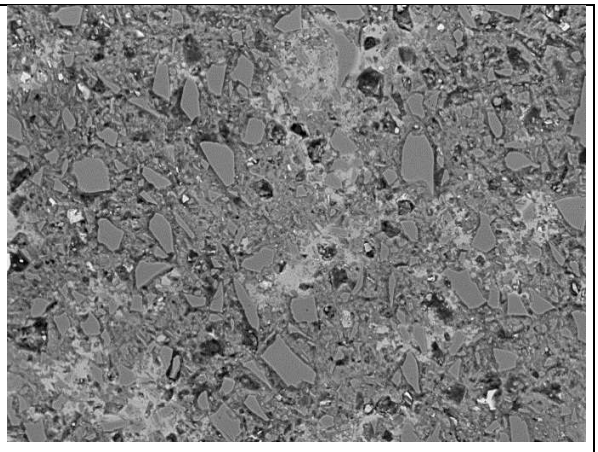

C2Q1 – 180d

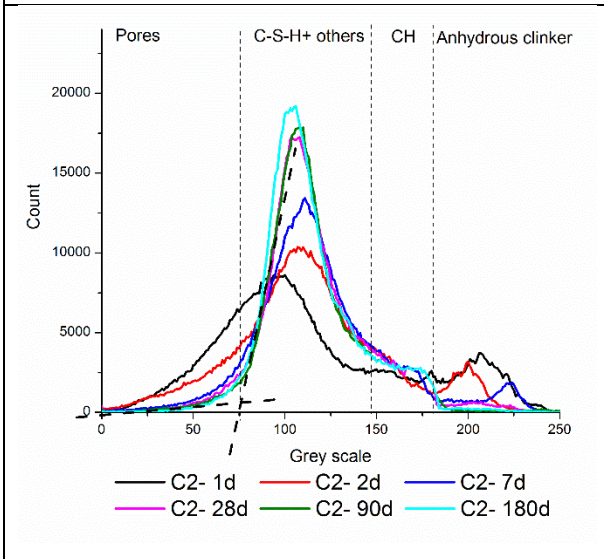

Thresholding for mix C2

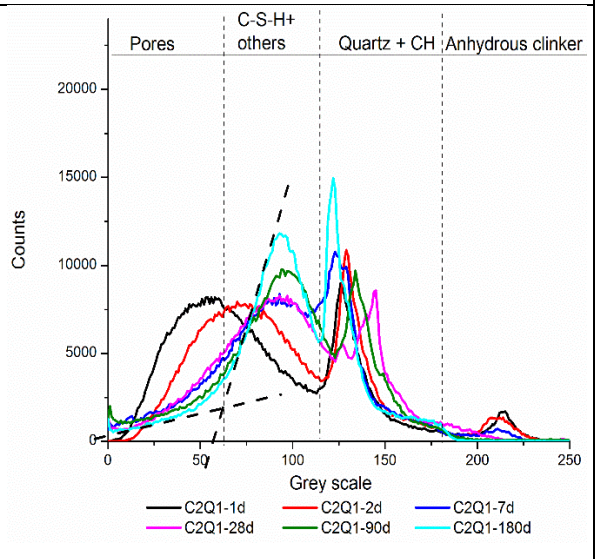

Thresholding for mix C2Q1

Figure A-10 Typical B-SEM images and thresholding for mixes C2 and C2Q1

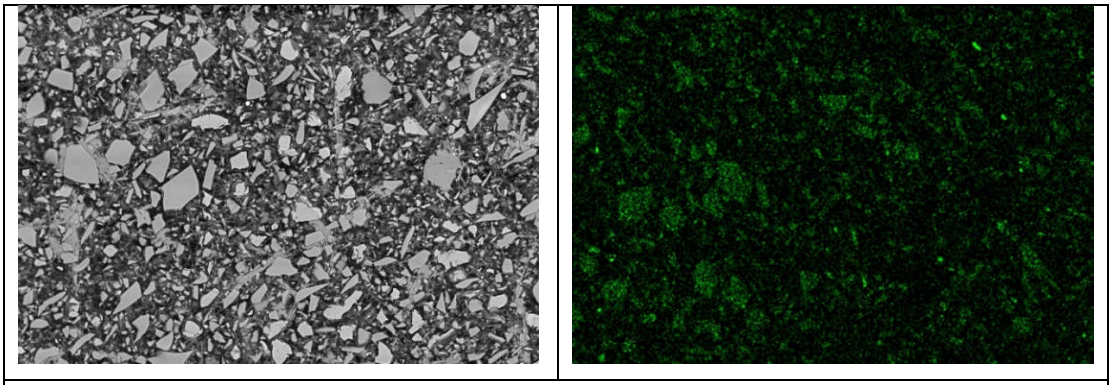

C2S1 - 1 D

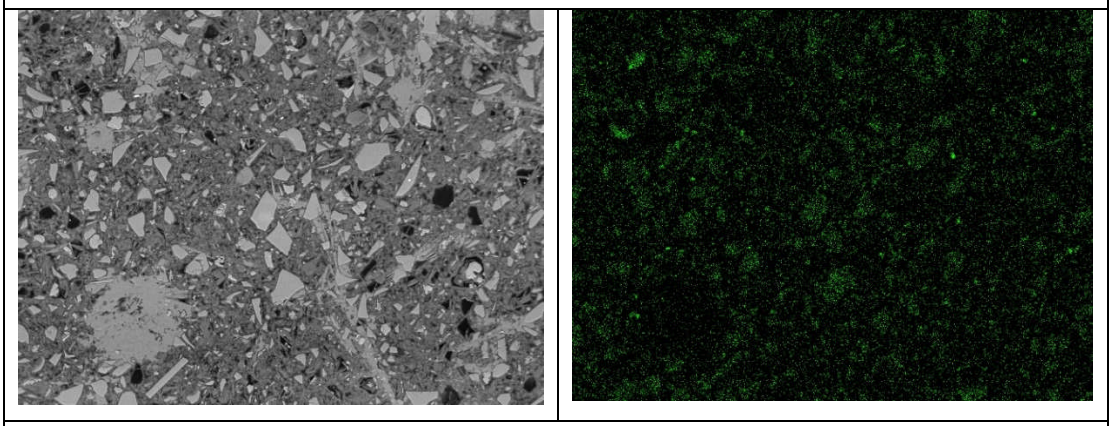

C2S1 - 7 D

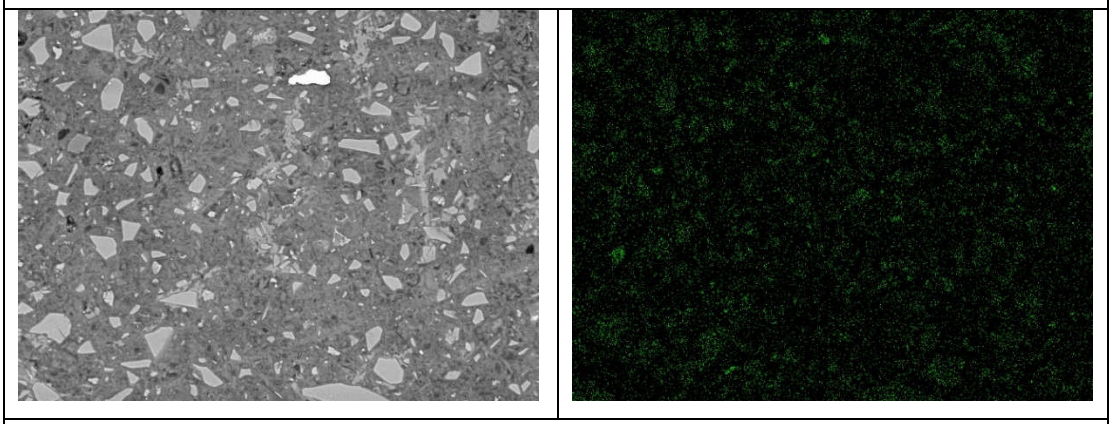

C2S1 - 28 D

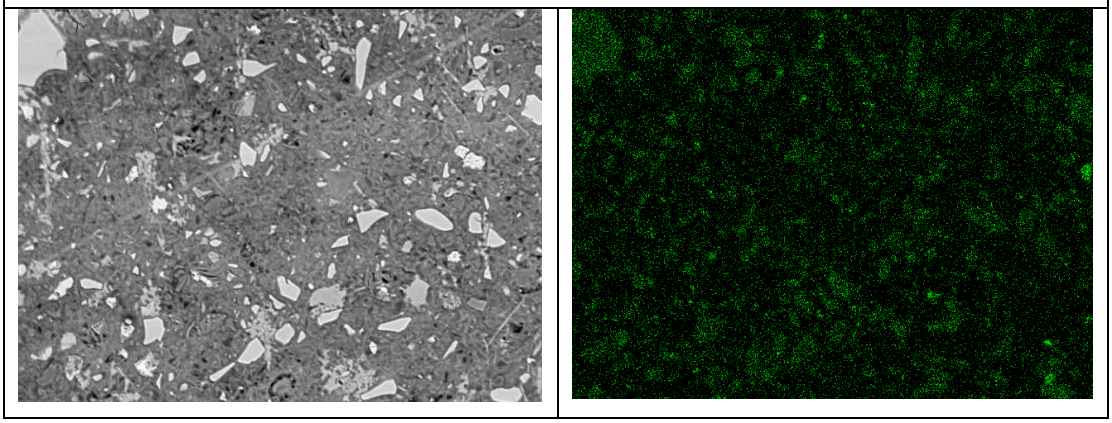

C2S1 -180 D

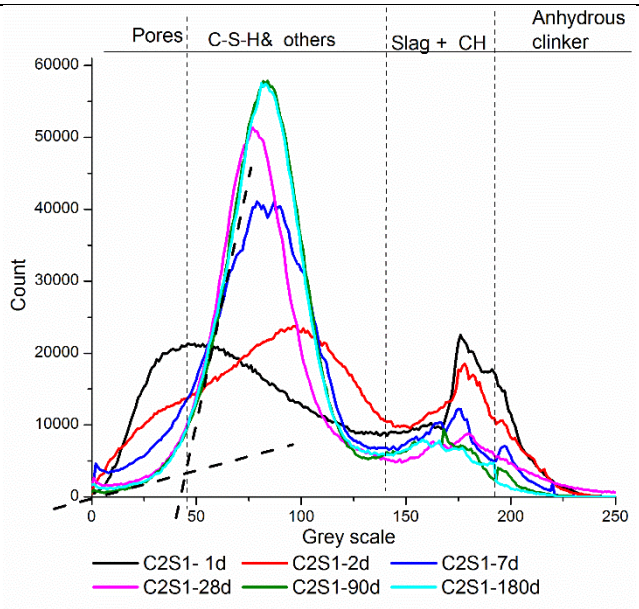

Thresholding for mix C2S1

Figure A-11 Typical B-SEM images and thresholding for mix C2S1

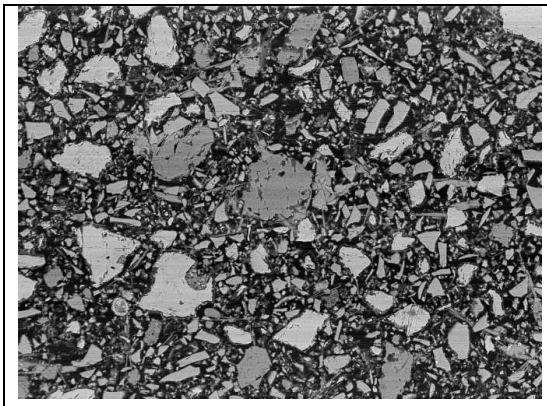

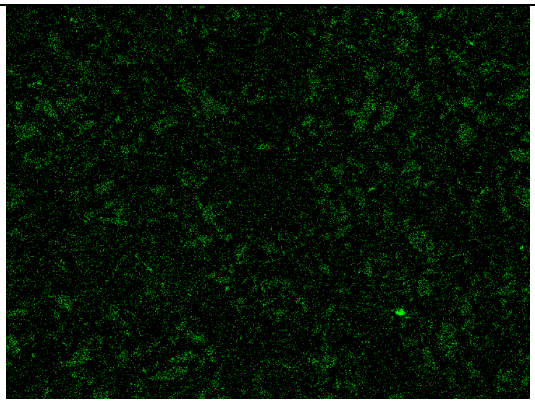

C1S1-10L - 1 D

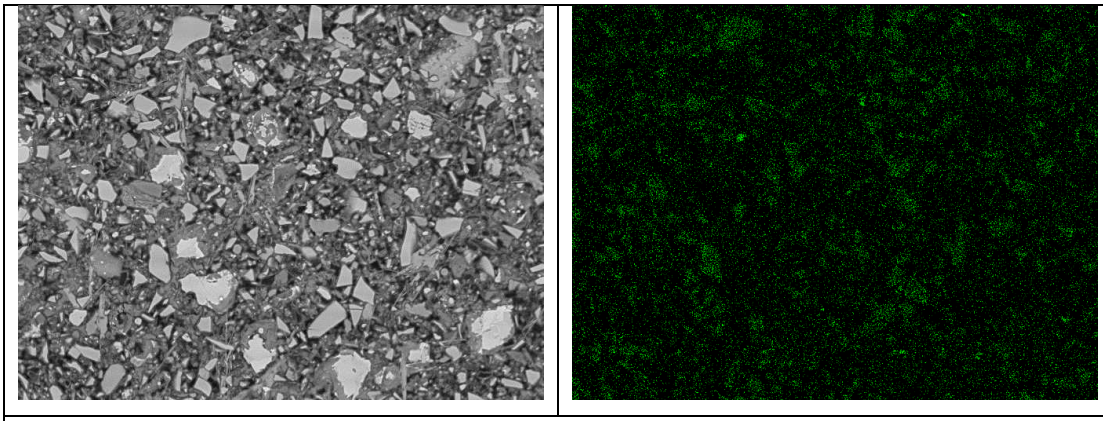

C1S1-10L - 7 D

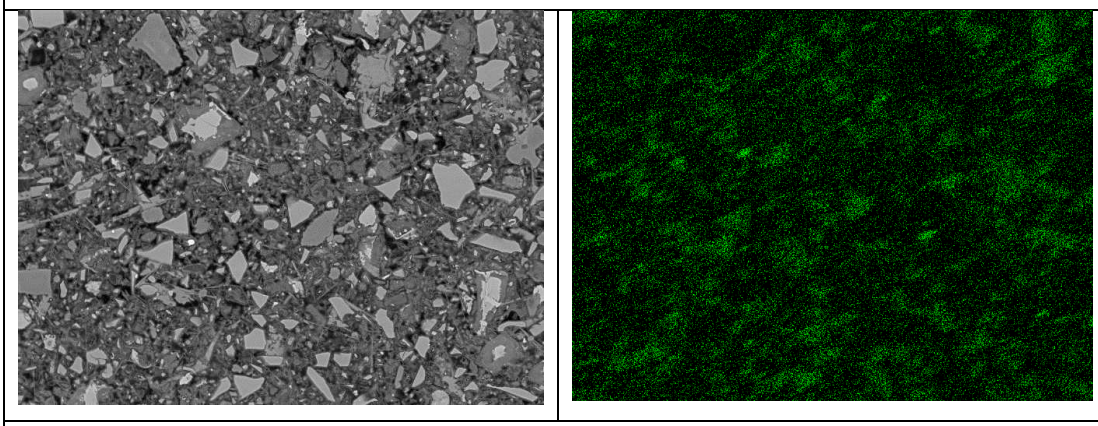

C1S1-10L – 28 D

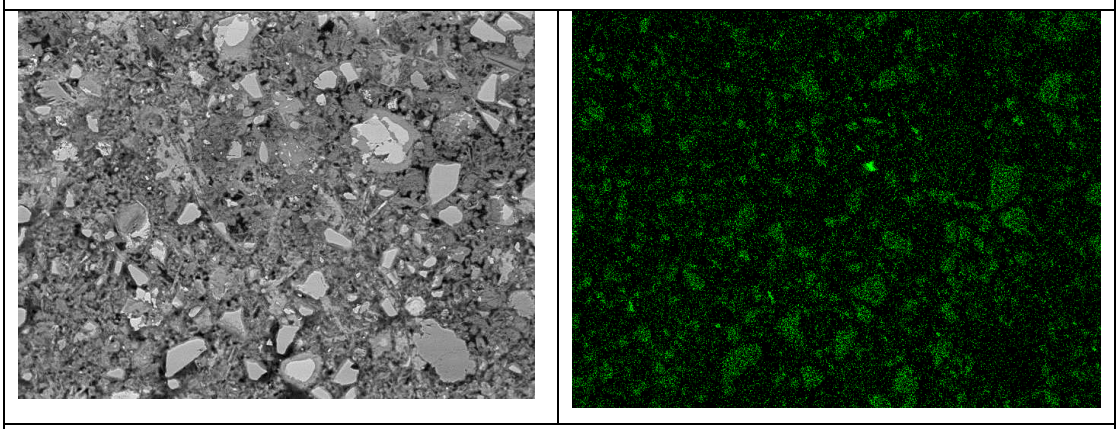

C1S1-10L -180 D

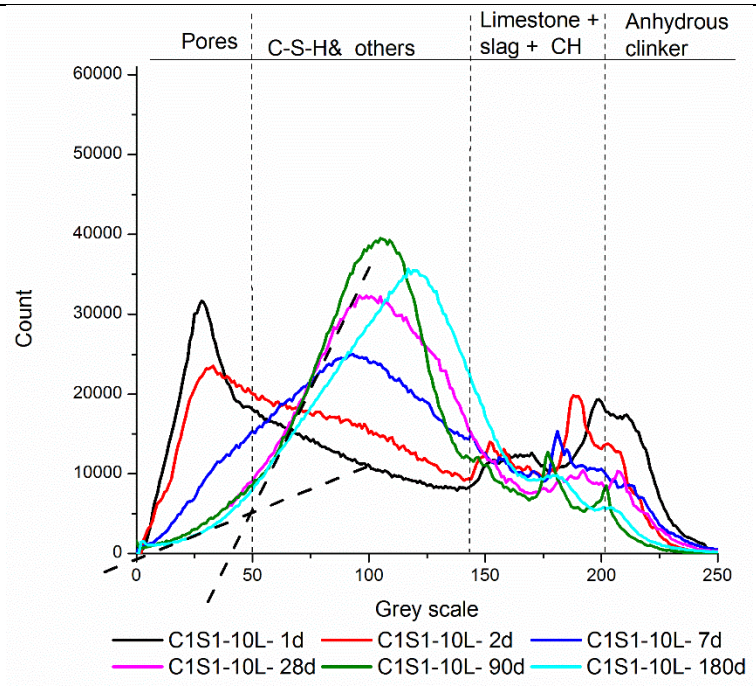

Thresholding for mix C1S1-10L

Figure A-12 Typical B-SEM images and thresholding for mix C1S1- 10L

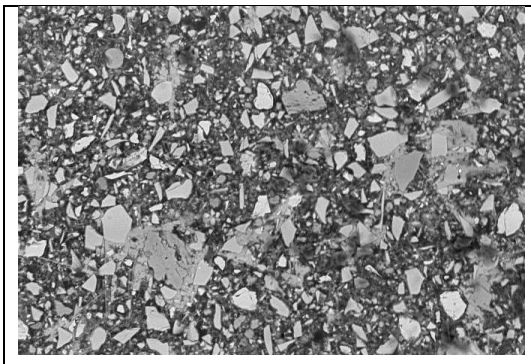

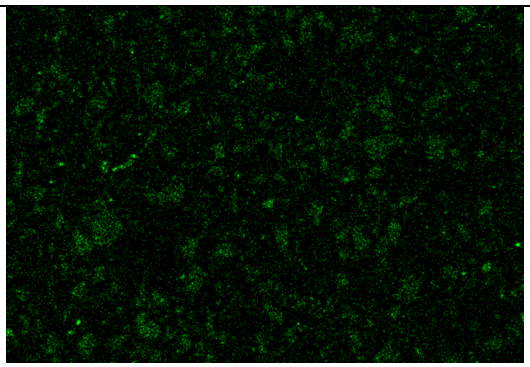

C2S1-10L - 1D

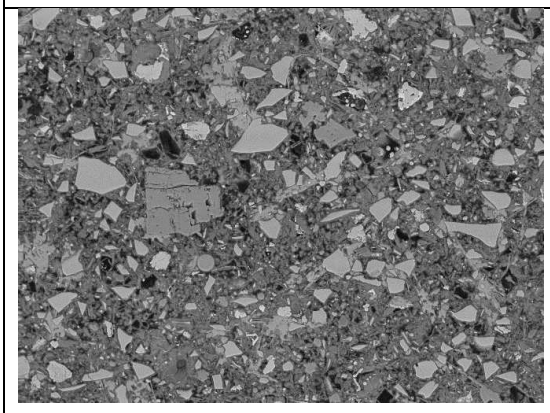

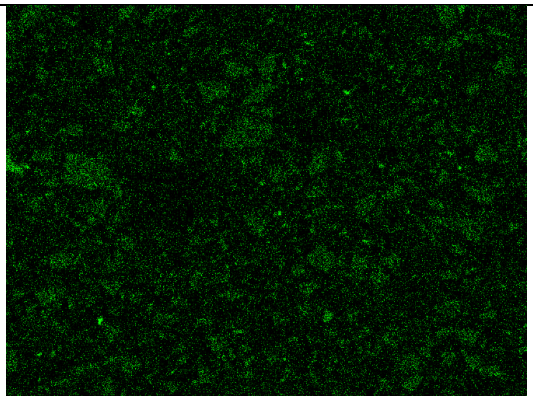

C2S1-10L - 7D

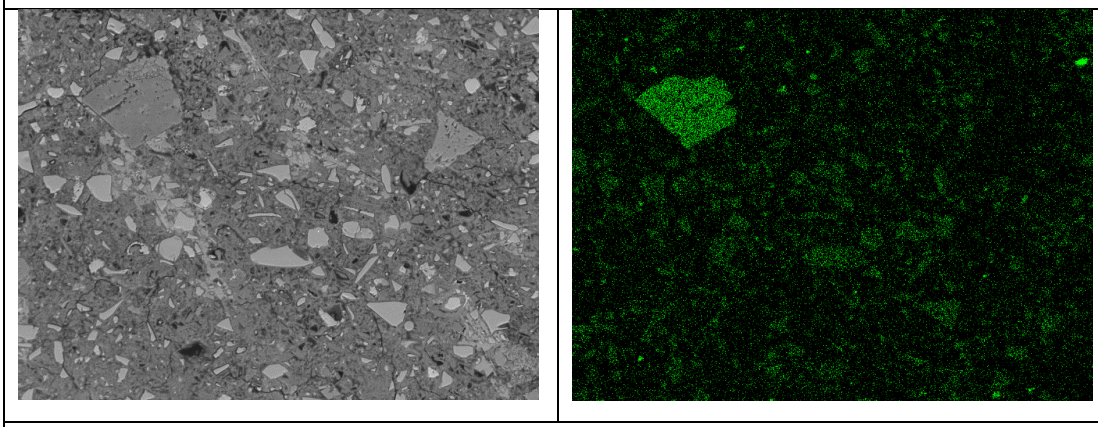

C2S1-10L -28D

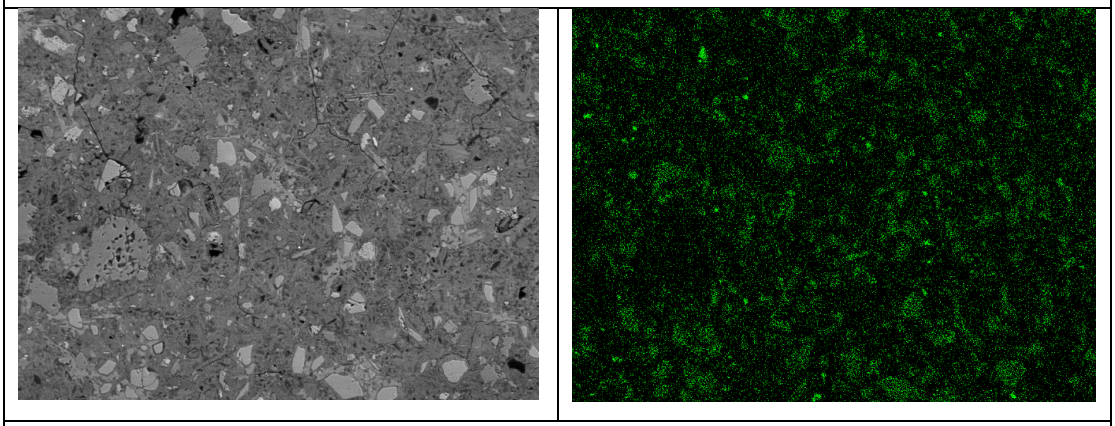

C2S1-10L -180D

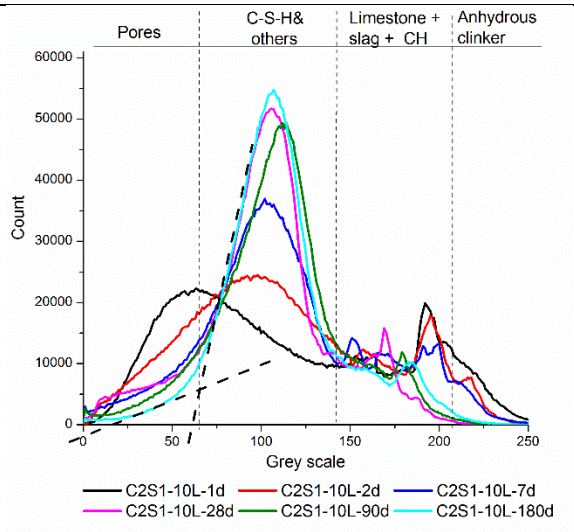

Thresholding for mix C2S1-10L

Figure A-13 Typical B-SEM images and thresholding for mix C2S1-10L

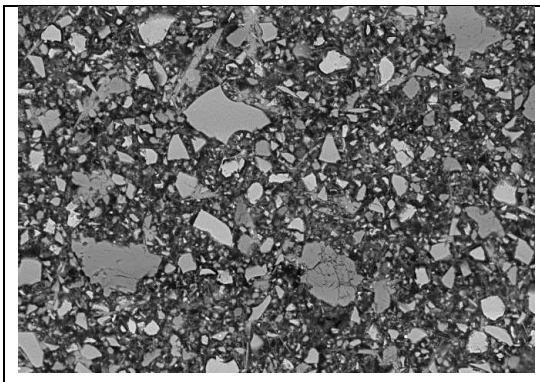
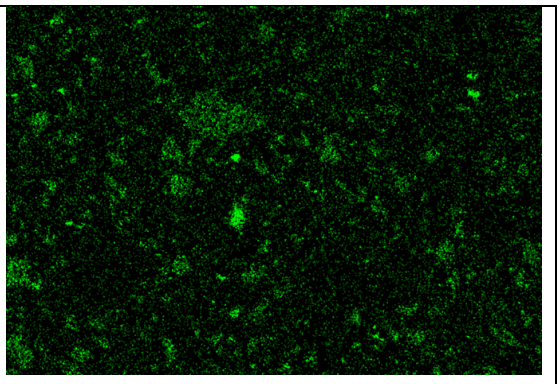

C2S1-20L -1D

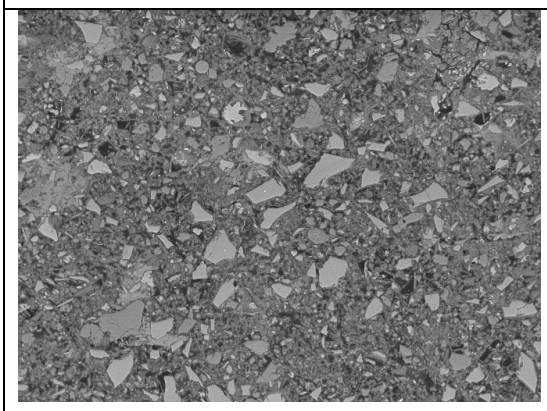
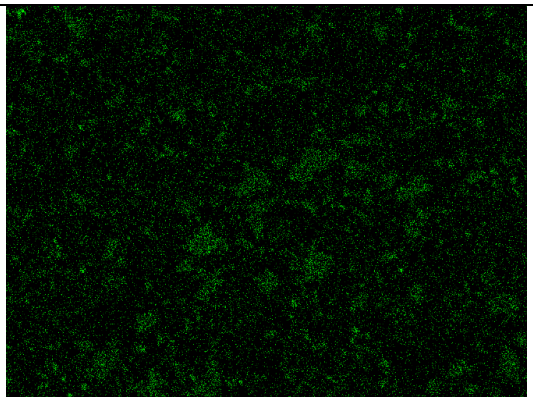

C2S1-20L -7D

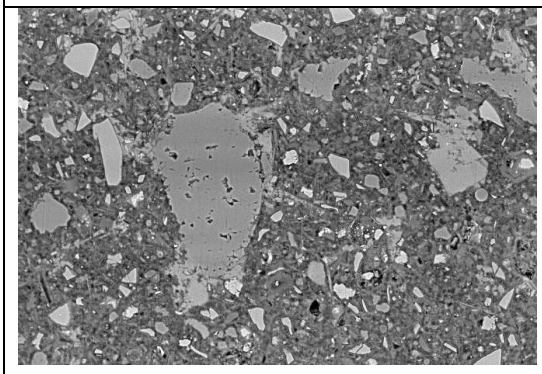
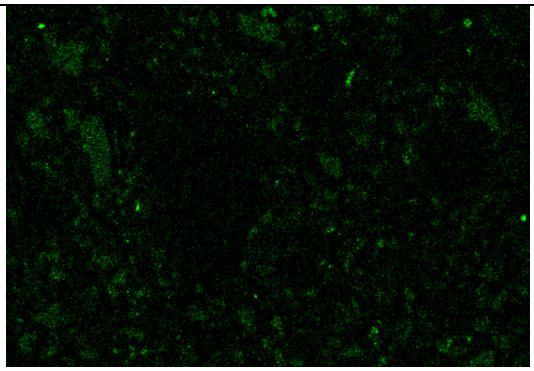

C2S1-20L -28D

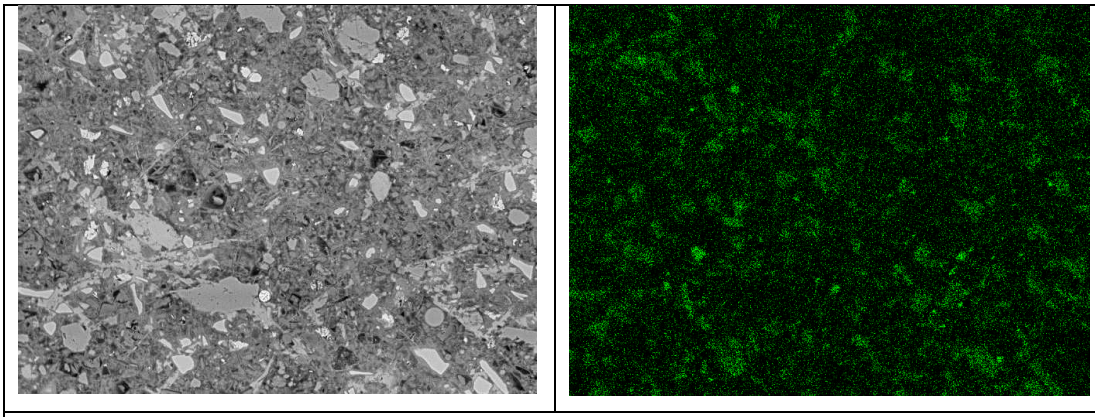

C2S1-20L -180D

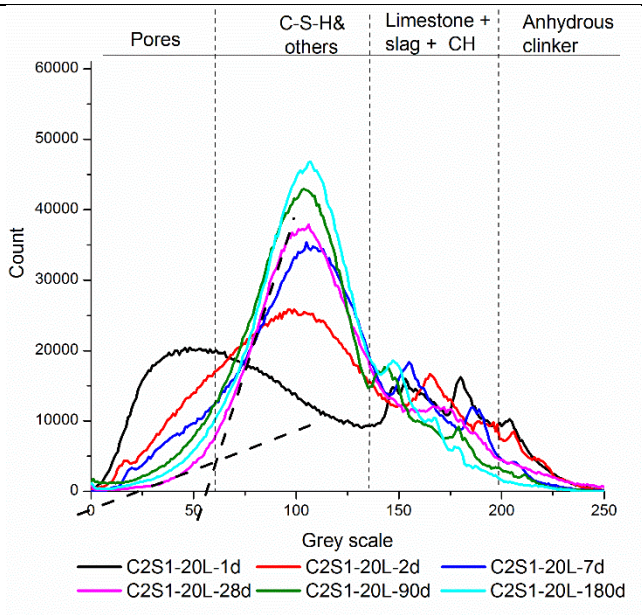

Thresholding for mix C2S1-20L

Figure A-14 Typical B-SEM images and thresholding for mix C2S1-20L

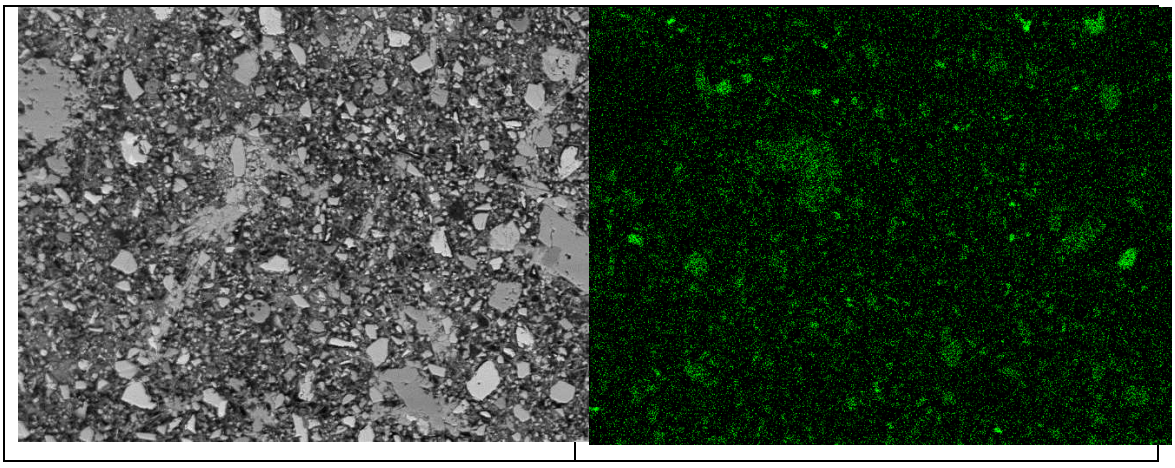

C2S2-20L -1D

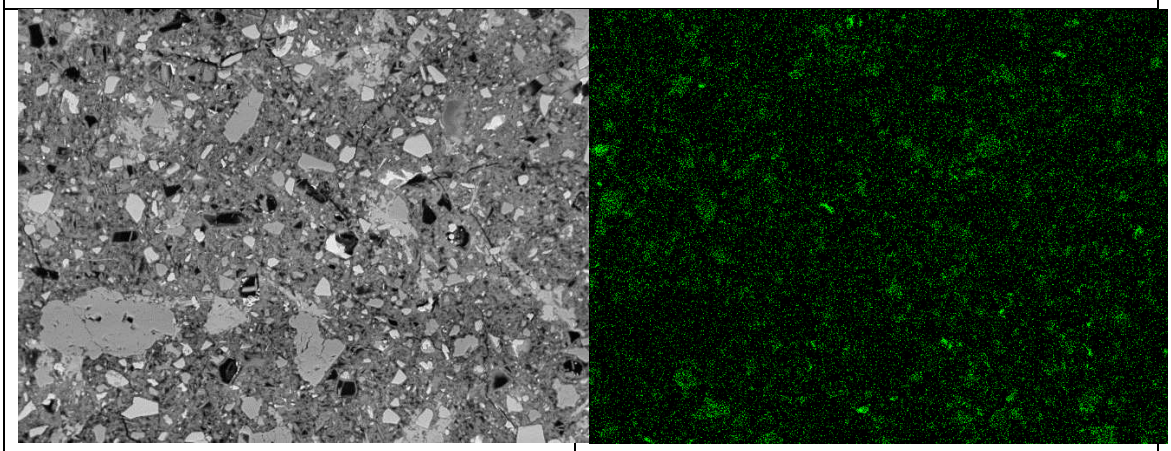

C2S2-20L -7D

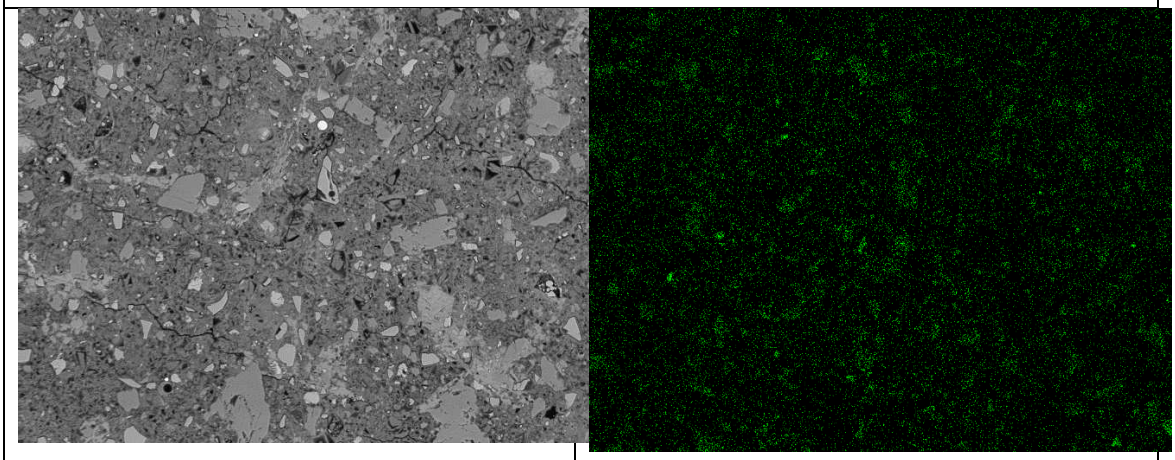

C2S2-20L -28D

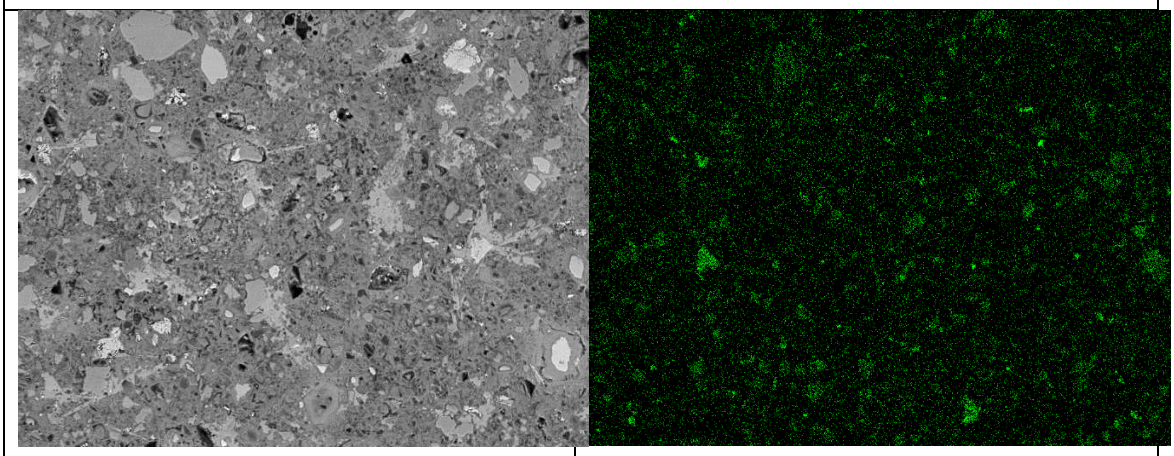

C2S2-20L -180D

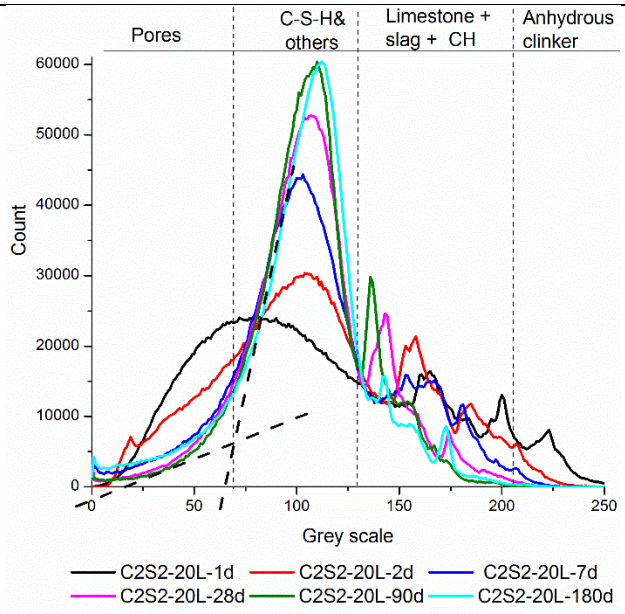

Thresholding for mix C2S2-20L

Figure A-15 Typical B-SEM images and thresholding for mix C2S2-20L

A.1.5 Pore solution composition during hydration

This table supplement Chapter 5.

Table 1-1 Concentrations in the pore solution (mM) with hydration time

Mix ID	Time (d, hr)	Ca	Cl	K	Na	Si	S	OH^-
C2S1	0.003	38.90	-	76	15.2	0.027	46.50	109
	0.02	30.40	-	78	15.5	0.009	31.70	144
	0.04	34.70	-	80	15.8	0.006	29.60	169
	0.08	33.70	-	81	16	0.007	29.10	169
	0.25	28.90	-	85	17.7	0.015	30.20	151
	1.00	5.90	-	141	35.8	0.036	16.60	213
	7.00	1.72	0.49	158	55.31	0.034	1.18	208
	14.00	1.08	0.6	145	53.85	0.054	1.26	204
	28.00	1.28	0.51	143	56.76	0.053	1.34	204
	99.00	1.47	0.51	147	63.2	0.104	0.82	173
C2S1-10L	0.003	35.20	-	75	15.20	0.028	40.90	107
	0.02	32.20	-	79	15.30	0.015	30.90	128
	0.04	35.90	-	78	15.90	0.009	29.00	147
	0.08	33.90	-	79	16.10	0.011	28.60	141
	0.25	29.40	-	83	17.70	0.014	29.40	141
	1.00	8.10	-	103	22.30	0.043	20.80	158
	7.00	1.84	0.61	159	56.29	0.038	1.77	208
	14.00	1.71	0.62	152	54.67	0.038	2.04	204
	28.00	1.34	0.71	140	55.66	0.043	2.45	194
	99.00	1.33	0.82	143	62.81	0.106	1.85	173
C2S1-10Q	0.003	34.30	-	77	15.10	0.027	46.10	81
	0.02	29.60	-	78	15.50	0.011	32.60	107
	0.04	32.10	-	78	15.90	0.004	30.80	102
	0.08	30.60	-	80	16.20	0.005	31.30	107
	0.25	26.10	-	84	17.70	0.009	31.60	93
	1.00	8.20	-	114	33.70	0.011	17.90	186
	7.00	1.55	0.50	162	56.94	0.031	1.08	213
	14.00	1.60	0.48	161	57.24	0.033	1.11	218
	28.00	1.50	0.52	156	59.62	0.038	1.23	218
	99.00	1.25	0.54	144	63.28	0.104	1.04	186
C2S1-20L	0.003	35.60	-	67	15.30	0.038	38.70	74
	0.02	35.40	-	73	15.90	0.020	29.00	93
	0.04	39.80	-	75	16.10	0.014	29.20	107
	0.08	36.60	-	77	16.50	0.017	29.00	104
	0.25	30.70	-	80	17.70	0.020	30.40	97
	1.00	7.00	-	109	23.80	0.067	12.40	166
	7.00	1.80	0.50	158	53.70	0.035	1.60	177
	14.00	0.90	0.70	146	53.00	0.053	2.10	186
	28.00	1.40	0.70	145	54.00	0.036	2.50	186
	99.00	1.60	0.80	157	65.10	0.098	1.80	158

A.1.6 Phase assemblage changes due to freeze-thaw

The images below compare the surface and core samples using DTG and XRD. These supplement the profiles shown in Chapter 6.

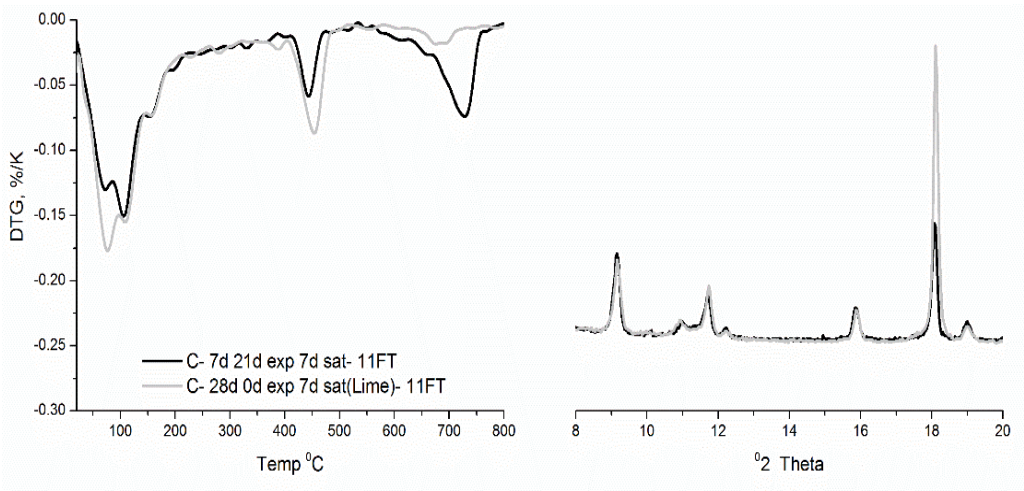

Figure A-16 Comparison between the surface and the core of mix C after 11 freeze-thaw cycles

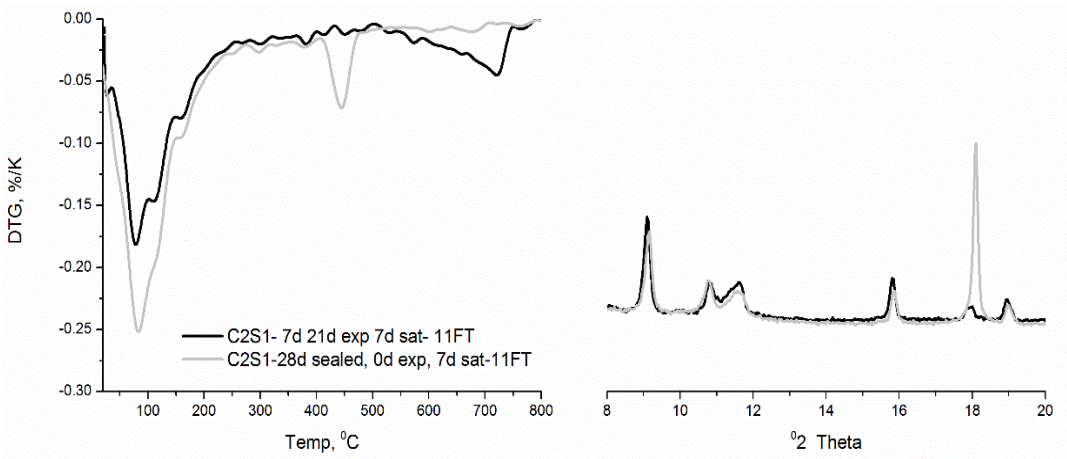

Figure A-17 Comparison between the surface and the core of mix C2S1 after 11 freeze-thaw cycles

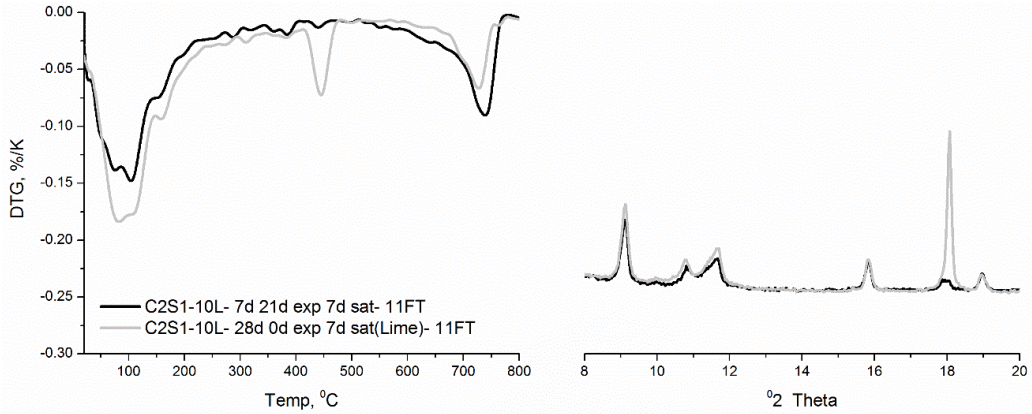

Figure A-18 Comparison between the surface and the core of mix C2S1-10L after 11 freeze-thaw cycles

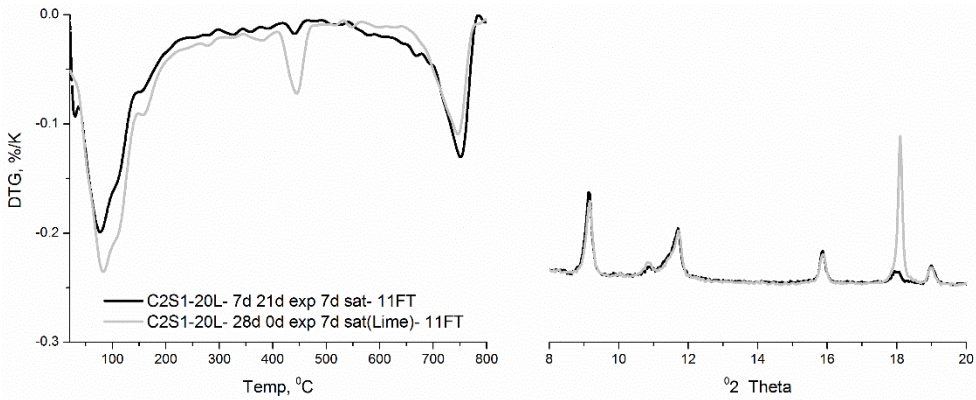

Figure A-19 Comparison between the surface and the core of mix C2S1-20L after 11 freeze-thaw cycles